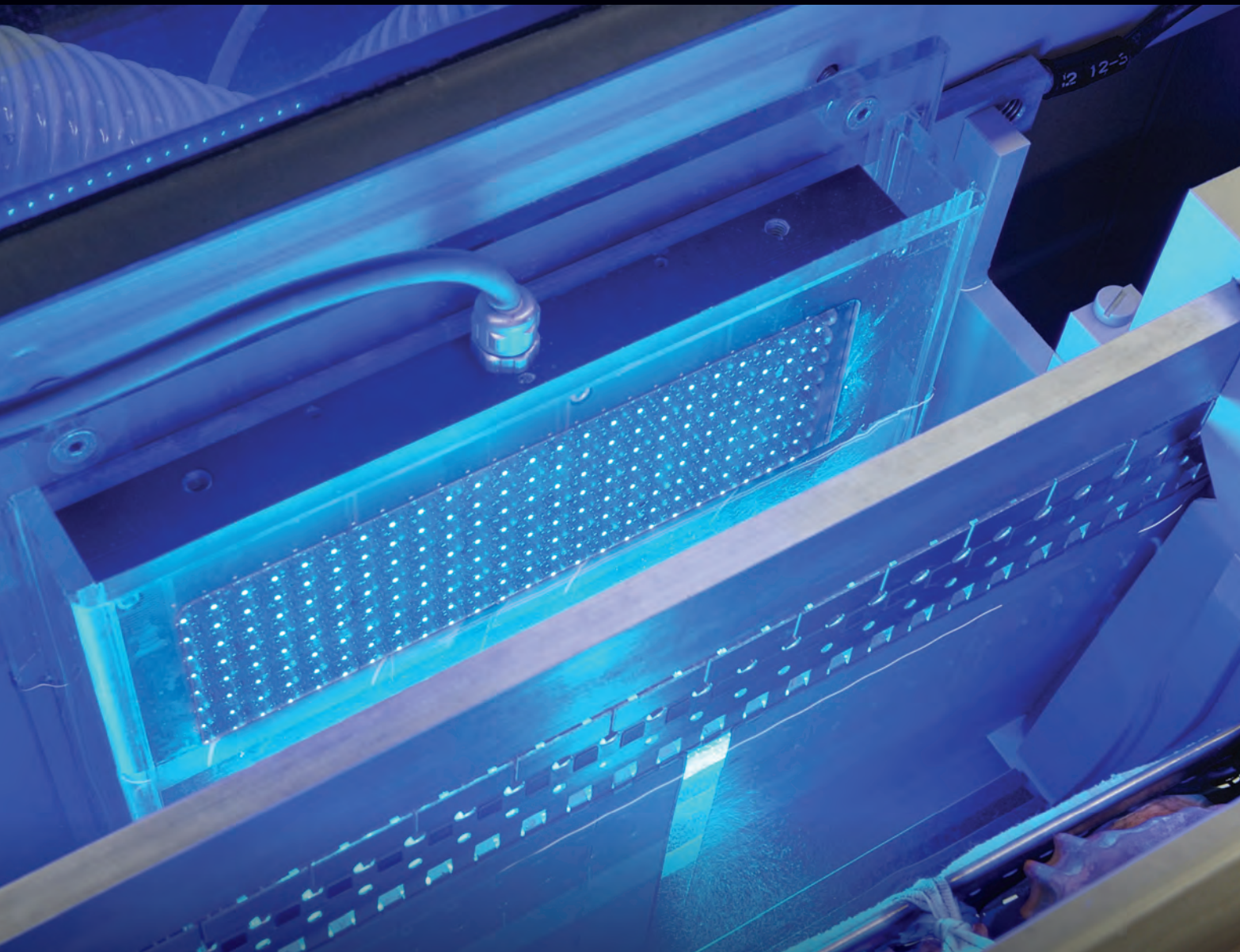


Thirty First Edition

# Photovoltaics

International

THE TECHNOLOGY RESOURCE FOR PV PROFESSIONALS

- 
- SERIS** Cell-to-module power loss/gain analysis of silicon wafer-based PV modules
  - Fraunhofer ISE** Understanding process-related efficiency variations in mc-Si PERC cells
  - NREL-CSM** The present and future silver cost component in crystalline silicon PV module manufacturing
  - Solar Intelligence** PV capital expenditure shifts from polysilicon to cell capacity additions
  - Aurinka** Polysilicon vs. upgraded metallurgical grade silicon (UMG-Si): Technology, quality and costs
  - CEA SOLENNA<sub>(3)</sub>**: The ultimate simplification of bifacial silicon technology, at a competitive cost/Wp

First Quarter, February 2016

[www.pv-tech.org](http://www.pv-tech.org)

**JA SOLAR**

[www.jasolar.com](http://www.jasolar.com)



# Harvest the Sunshine

## Premium Cells, Premium Modules

**JA Solar Holdings Co., Ltd.**

Building No.8, Nuode Center, Automobile Museum East Road, Fengtai District, Beijing

Tel: +86 (10) 63611888 Fax: +86 (10) 63611999 Email: [sales@jasolar.com](mailto:sales@jasolar.com); [market@jasolar.com](mailto:market@jasolar.com)

**Published by:**

Solar Media Ltd.,  
3rd Floor, America House, 2 America Square  
London EC3N 2LU, UK  
Tel: +44 (0) 207 871 0122  
Fax: +44 (0) 207 871 0101  
E-mail: [info@pv-tech.org](mailto:info@pv-tech.org)  
Web: [www.pv-tech.org](http://www.pv-tech.org)

**Publisher:** Chris Riley

**Head of Content:** Ben Willis  
**Deputy Head of Content:** John Parnell  
**Commissioning Editor:** Adam Morrison  
**Sub-Editor:** Steve D. Brierley  
**Senior News Editor:** Mark Osborne  
**Reporters:** Andy Colthorpe, Tom Kenning,  
**Design:** Tina Davidian  
**Production:** Daniel H Brown, Sarah-Jane Lee

**Sales Director:** David Evans  
**Account Managers:** Adam Morrison,  
Graham Davie, Lili Zhu, Colin Michael, Matthew  
Bosnjak

While every effort has been made to ensure the accuracy of the contents of this journal, the publisher will accept no responsibility for any errors, or opinion expressed, or omissions, or for any loss or damage, consequential or otherwise, suffered as a result of any material here published.

Cover image: Light-induced copper plating section in Meco DPL

Image courtesy of Meco Equipment Engineers

Printed by Buxton Press

Photovoltaics International  
Thirty First Edition  
First Quarter, February 2016  
Photovoltaics International is a quarterly journal published in February, May, August and December.

Distributed in the USA by Mail Right International, 1637 Stelton Road B4, Piscataway, NJ 08854.

ISSN: 1757-1197

The entire contents of this publication are protected by copyright, full details of which are available from the publisher. All rights reserved. No part of this publication may be reproduced, stored in a retrieval system or transmitted in any form or by any means – electronic, mechanical, photocopying, recording or otherwise – without the prior permission of the copyright owner.

USPS Information  
USPS Periodical Code: 025 313

Periodicals Postage Paid at  
New Brunswick, NJ  
Postmaster: Send changes to:  
Photovoltaics International,  
Solar Media Ltd., C/o 1637 Stelton  
Road, B-4, Piscataway, NJ 08854, USA

# Foreword

The latest capex cycle in the solar PV industry has been gathering pace since 2013, when the previous two-year period of oversupply came to an end and a degree of upstream confidence was restored. Manufacturers worldwide have since been gearing up to start investing in new production capacity again, with announcements since 2014 now amounting to many tens of gigawatts of putative capacity.

But how much of that announced capacity has been built out? In a detailed piece of analysis for *Photovoltaics International*, our Senior News Editor Mark Osborne, who has been tracking the latest wave of capacity announcements since 2014, seeks to answer this question.

His report (p.11) provides the first full picture of two years' worth of capacity announcements and how those are now being translated into real nameplate capacity. The key takeaway is that although initially the realisation of recent announcements did not happen as quickly as might have been expected, the ramp rate gathered momentum in 2015. How that plays out in 2016 and further ahead will no doubt be the subject of further analysis.

In another special report for *Photovoltaics International*, Finlay Colville, our Head of Solar Intelligence, characterises the nature of the current PV capex cycle as compared to the last one between 2006 and 2011 (p.112). Whereas the previous spending cycle was notable for being what Colville describes as "frantic", the latest one has so far been more measured, with manufacturers focusing on strengthening their positions in specific segments of the value chain rather than seeking to expand across the full c-Si value chain as was the case before.

So far module and more recently cell investments have dominated, with wafer and ingot capex likely to be next in line. Yet to materialise is any significant new surge in polysilicon capex, with investor confidence in this link in the value chain yet to be restored, according to Colville.

Other highlights in this issue include a paper from researchers at the Solar Energy Research Institute of Singapore (SERIS) exploring cell-to-module losses (p.90). Few months pass in the world of solar without a manufacturer or research institute announcing new champion cell efficiency. But what really matters is conversion efficiency at a module level, and this typically lags behind cells by a few percent. The SERIS team look at why such losses are happening, how they can be quantified and, most importantly, how they can be avoided.

Meanwhile, researchers from the Colorado School of Mines (CSM) and US National Renewable Energy Laboratory (NREL) look at the likely future impact of c-Si solar manufacturing on silver prices (p.62). Silver is clearly a key component in c-Si solar cells, and the CSM-NREL team explore how an expansion in production could lead to an increase in manufacturing costs because of a consequent rise in silver prices.

We hope you find this edition of the journal essential reading at what is a pivotal time for the upstream solar industry. Our team will be at the SNEC PV expo in Shanghai in May. We look forward to meeting you there.

**Ben Willis**  
Head of Content  
*Solar Media Ltd*

Photovoltaics International's primary focus is on assessing existing and new technologies for "real-world" supply chain solutions. The aim is to help engineers, managers and investors to understand the potential of equipment, materials, processes and services that can help the PV industry achieve grid parity. The Photovoltaics International advisory board has been selected to help guide the editorial direction of the technical journal so that it remains relevant to manufacturers and utility-grade installers of photovoltaic technology. The advisory board is made up of leading personnel currently working first-hand in the PV industry.



## Editorial Advisory Board

Our editorial advisory board is made up of senior engineers from PV manufacturers worldwide. Meet some of our board members below:



*Prof Armin Aberle, CEO, Solar Energy Research Institute of Singapore (SERIS), National University of Singapore (NUS)*

Prof Aberle's research focus is on photovoltaic materials, devices and modules. In the 1990s he established the Silicon Photovoltaics Department at the Institute for Solar Energy Research (ISFH) in Hamelin, Germany. He then worked for 10 years in Sydney, Australia as a professor of photovoltaics at the University of New South Wales (UNSW). In 2008 he joined NUS to establish SERIS (as Deputy CEO), with particular responsibility for the creation of a Silicon PV Department.



*Dr. Markus Fischer, Director R&D Processes, Hanwha Q Cells*

Dr. Fischer has more than 15 years' experience in the semiconductor and crystalline silicon photovoltaic industry. He joined Q Cells in 2007 after working in different engineering and management positions with Siemens, Infineon, Philips, and NXP. As Director R&D Processes he is responsible for the process and production equipment development of current and future c-Si solar cell concepts. Dr. Fischer received his Ph.D. in Electrical Engineering in 1997 from the University of Stuttgart. Since 2010 he has been a co-chairman of the SEMI International Technology Roadmap for Photovoltaic.



*Dr. Thorsten Dullweber, R&D Group Leader at the Institute for Solar Energy Research Hamelin (ISFH)*

Dr. Dullweber's research focuses on high efficiency industrial-type PERC silicon solar cells and ultra-fine-line screen-printed Ag front contacts. His group has contributed many journal and conference publications as well as industry-wide recognized research results. Before joining ISFH in 2009, Dr. Dullweber worked for nine years in the microelectronics industry at Siemens AG and later Infineon Technologies AG. He received his Ph. D. in 2002 for research on Cu(In,Ga)Se<sub>2</sub> thin-film solar cells.



*Dr. Wei Shan, Chief Scientist, JA Solar*

Dr. Wei Shan has been with JA Solar since 2008 and is currently the Chief Scientist and head of R&D. With more than 30 years' experience in R&D in a wider variety of semiconductor material systems and devices, he has published over 150 peer-reviewed journal articles and prestigious conference papers, as well as six book chapters.



*Jim Zhu, Chief Scientist, Wuxi Suntech*

Jim Zhu has bachelor and master's degrees from Fundan University and a Ph.D. from the Shanghai Institute of Technical Physics of the Chinese Academy of Sciences. In 2007 he joined Suntech as group VP with responsibility for customer service, quality management and R&D. He has been the company's Chief Scientist since 2013.



*Florian Clement, Head of Group, MWT solar cells/printing technology, Fraunhofer ISE*

Dr. Clement received his Ph.D in 2009 from the University of Freiburg. He studied physics at the Ludwigs-Maximilian-University of Munich and the University of Freiburg and obtained his diploma degree in 2005. His research is focused on the development, analysis and characterization of highly efficient, industrially feasible MWT solar cells with rear side passivation, so called HIP-MWT devices, and on new printing technologies for silicon solar cell processing.



*Sam Hong, Chief Executive, Neo Solar Power*

Dr. Hong has more than 30 years' experience in solar photovoltaic energy. He has served as the Research Division Director of Photovoltaic Solar Energy Division at the Industry Technology Research Institute (ITRI), and Vice President and Plant Director of Sinonar Amorphous Silicon Solar Cell Co., the first amorphous silicon manufacturer in Taiwan. Dr. Hong has published three books and 38 journal and international conference papers, and is a holder of seven patents. In 2011 he took office as Chairman of Taiwan Photovoltaic Industry Association.



*Matt Campbell, Senior Director, Power Plant Products, SunPower*

Matt Campbell has held a variety of business development and product management roles since joining the SunPower, including the development of the 1.5MW AC Oasis power plant platform, organized SunPower's power plant LCOE reduction programmes, and the acquisition of three power plant technology companies. Campbell helped form a joint venture in Inner Mongolia, China for power plant project development and manufacturing. He holds an MBA from the University of California at Berkeley and a BBA in Marketing, Finance, and Real Estate from the University of Wisconsin at Madison.



*Ru Zhong Hou, Director of Product Center, ReneSola*

Ru Zhong Hou joined ReneSola as R&D Senior Manager in 2010 before being appointed Director of R&D in 2012. Before joining ReneSola he was a researcher for Microvast Power Systems, a battery manufacturer. His work has been published in numerous scientific journals. He has a Ph.D. from the Institute of Materials Physics & Microstructures, Zhejiang University, China.



We'll help you  
catch more rays

## Unleash the power of silicon chemistry in your business

### PROVEN, RELIABLE AND DURABLE MATERIALS

Dow Corning delivers silicon-based technology and high-performance silicone products that are tested to meet the specific requirements of the solar energy industry. We have solutions that will help you to increase kWh output, lower costs, increase durability and reliability, and ultimately boost profitability.

### COLLABORATION

We're working closely with our customers and partners to create a world in which clean, renewable, solar energy becomes economically competitive with traditional sources.

### A GLOBAL TRACK RECORD

Driven by innovation and fueled by 70 years of talent, expertise and capabilities, our solutions reach across the value chain, from feedstocks to module assembly and installation.

To see how silicones can make your solar applications more reliable and cost effective, visit us at [dowcorning.com/solar](http://dowcorning.com/solar).



Solar  
Solutions

# Contents

## 8 Section 1 Fab & Facilities

+ NEWS

Page 11

### Full-year 2015 PV manufacturing capacity expansion plans and analysis

Mark Osborne, Senior News Editor, *Photovoltaics International*

Page 17

### How facilities can affect energy consumption in PV cell production

Martin Schottler, AVEREM process engineering, Stuttgart, Germany, & Mariska de Wild-Scholten, SmartGreenScans, Groet, The Netherlands



## 23 Section 2 Materials

+ NEWS

Page 25

### Inline diamond wire inspection based on resonant vibrations

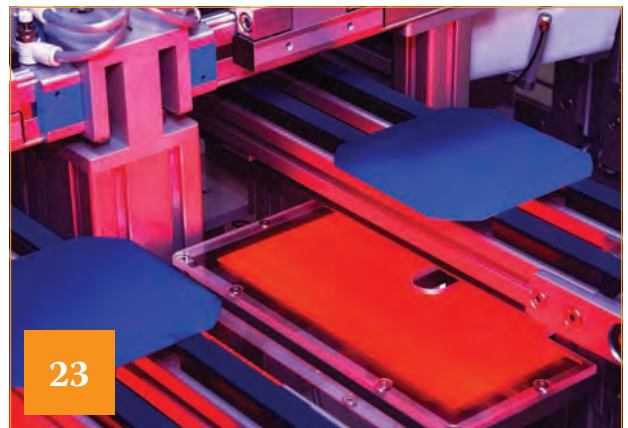
Hubert Seigneur<sup>1,2,3</sup>, Sergei Ostapenko<sup>4</sup>, Igor Tarasov<sup>4</sup>, Chad Rodrigues<sup>4</sup>, Yuriy Zaikin<sup>5</sup>, Kevin Morrow<sup>6</sup> & Winston V. Schoenfeld<sup>1,2,3</sup>

<sup>1</sup>c-Si US Photovoltaic Manufacturing Consortium (PVMC), Orlando, Florida; <sup>2</sup>Florida Solar Energy Center (FSEC), Cocoa, Florida; <sup>3</sup>University of Central Florida (UCF), Orlando, Florida; <sup>4</sup>Ultrasonic Technologies, Inc. (UST), Wesley Chapel, Florida; <sup>5</sup>PetroBeam, Inc., Sweetwater, Tennessee; <sup>6</sup>Niabraz LLC, Tonawanda, New York, USA

Page 29

### Polysilicon vs. upgraded metallurgical-grade silicon (UMG-Si): Technology, quality and costs

Eduardo Forniés, Laura Méndez & Marta Tojeiro, Aurinka PV Group SL, Madrid, Spain



## 40 Section 3 Cell Processing

+ NEWS

Page 43

### Understanding process-related efficiency variations in mc-Si PERC cells

Sven Wasmer, Johannes Greulich, Hannes Höffler, Nico Wöhrle & Stefan Rein, Fraunhofer Institute for Solar Energy Systems ISE, Freiburg, Germany

Page 53

### SOLENN(3): The ultimate simplification of bifacial silicon technology, at a competitive cost/Wp

Raphaël Cabal, Thomas Blévin, Rémi Monna & Yannick Veschetti  
CEA Tech-INES, Le Bourget du Lac, France

Page 52

### The present and future silver cost component in crystalline silicon PV module manufacturing

Michael Redlinger<sup>1</sup>, Michael Woodhouse<sup>2</sup> & Roderick G. Eggert<sup>1</sup>

<sup>1</sup>Division of Economics and Business, Colorado School of Mines (CSM), Golden, Colorado; <sup>2</sup>Strategic Energy Analysis Center, National Renewable Energy Laboratory (NREL), Golden, Colorado, USA



# RENOLIT REFLEXOLAR

*The One-Step Multilayer Backsheet*

DEVELOPING  
PRODUCTS FOR  
TOMORROW

## Reaching new heights in reflection & endurance.

RENOLIT REFLEXOLAR is a totally new class of backsheets in the Solar PV industry. RENOLIT REFLEXOLAR is an engineered, highly white reflective, flexible Polyolefin-Polyamide multilayer construction. It has a synergetic dynamic barrier system, managing low moisture and oxygen concentrations inside the module but allowing the acetic acid to escape, hence offering extended durability to the module. Rely on it.



*Rely on it.*

For further information, visit: [renolit.reflexolar.com](http://renolit.reflexolar.com)

# Contents

## 76 Section 4 Thin Film + NEWS

Page 79

### Damp-heat-induced degradation of layers in CIGS solar cells

Mirjam Theelen, TNO/Solliance, Eindhoven, The Netherlands



## 87 Section 5 PV Modules + NEWS

Page 90

### Cell-to-module power loss/gain analysis of silicon wafer-based PV modules

Jai Prakash Singh, Yong Sheng Khoo, Jing Chai, Zhe Liu & Yan Wang, Solar Energy Research Institute of Singapore (SERIS), National University of Singapore (NUS), Singapore

Page 99

### Double-glass PV modules with silicone encapsulation

Shencun Wang<sup>1</sup>, Xiang Sun<sup>1</sup>, Yujian Wu<sup>2</sup>, Yanxia Huang<sup>2</sup>, Nick Shephard<sup>3</sup> & Guy Beaucarne<sup>4</sup>

<sup>1</sup>BYD, Shenzhen, Guangdong, China; <sup>2</sup>Dow Corning (China) Holding Co. Ltd., Shanghai, China; <sup>3</sup>Dow Corning Corporation, Midland, Michigan, USA; <sup>4</sup>Dow Corning Europe S.A., Seneffe, Belgium



## 108 Section 6 Market Watch + NEWS

Page 112

### PV capital expenditure shifts from polysilicon to cell capacity additions

Finlay Colville, Head of Market Intelligence, Solar Media Ltd.



## 115 Subscription / Advertisers Index

## 116 The PV-Tech Blog



# Fab & Facilities

---



8

Page 8  
News

---

Page 11  
Full-year 2015 PV  
manufacturing capacity  
expansion plans and analysis

Mark Osborne, Senior News Editor,  
*Photovoltaics International*

.....

Page 17  
How facilities can affect  
energy consumption in PV  
cell production

Martin Schottler, AVEREM process  
engineering, Stuttgart, Germany,  
& Mariska de Wild-Scholten,  
SmartGreenScans, Groet, The  
Netherlands

.....



11

### 2016 manufacturing capacity expansion announcements pick up where 2015 left off

PV manufacturing capacity expansion announcements topped 55.19GW in 2015, up from 21GW in 2014. The data, collated by PV Tech, includes thin-film, solar cell, dedicated module assembly and integrated cell and module categories.

The tally includes additions throughout the year and beyond as part of longer-term phased roll outs. It also includes some capacity that was announced and later cancelled, such as that of Hanergy Thin Film Power.

A total of 25GW of expansions were announced in November 2015 alone. 2016 kicked-off with another raft of announcements. January saw 9.5GW of expansions including LG, GCL and 1GW of phased expansions by the Al-Afandi Group in Saudi Arabia.

Around 2.76GW of dedicated c-Si solar cell announcements were made in January, notably with LG Electronics announcing it would expand n-type monocrystalline cell production from 1GW to 3GW by 2020 with capital expenditure of US\$435 million. January also delivered 5.35GW of planned module assembly capacity expansions and 1.5GW of integrated cell and module expansions.



Credit: Hamisha QCELLS

Capacity expansions top 55.19GW in 2015.

### Closures, suspensions and delays

#### SunEdison closes poly plant and puts ingot facility on hiatus

Struggling renewables firm SunEdison is making drastic changes to its upstream manufacturing operations as its financial position remains precarious.

The company announced in February that it would permanently close its Pasadena, Texas polysilicon production facility by the third quarter of 2016. The closure will result in one-time impairment and restructuring charges

of US\$363 million that will be reflected in SunEdison's fourth quarter financial results, and approximately US\$10 million to US\$13 million in restructuring charges that are expected to be reported in 2016. SunEdison said around 180 jobs would be lost from the closure of the plant.

SunEdison also said it would be halting high-volume production of silicon crystal ingot at its facility in Oregon, US, which is expected to reduce operating expenses to optimise cash utilisation, according to the company. Approximately 40 jobs are expected to be affected by the changes.

The facility has been consolidated into an R&D and technology demonstration

and training centre for future licensees of the company's continuous Czochralski silicon crystal ingot manufacturing technology. As a result, SunEdison said one-time impairment and restructuring charges of US\$39 million would also be reflected in its fourth quarter results.

#### Monocrystalline ingot and wafer producer M.Setek halts polysilicon production

Japan-based M.Setek, a subsidiary of Taiwan based flat panel display and PV module manufacturer, AU Optronics Corp (AUO) is to stop production of monocrystalline polysilicon production, due to cost competitive issues.

In a Taiwan Stock Exchange statement, AUO noted that it would incur a one-time impairment charge of M.Setek's equipment and facilities totalling NT\$6.75 billion (US\$203 million).

However, AUO noted that it would continue to operate M.Setek's ingot/wafer slicing operations at the facilities. According to PV Tech's own analysis, M.Setek had less than 10,000MT of direct polysilicon production per annum.

#### Timeline slides on SolarCity's gigafab due to equipment lead times

US installer SolarCity said in its fourth quarter 2015 earnings call that its ambitious 1GW Buffalo Riverbend manufacturing facility had been impacted by longer than expected equipment lead times, pushing some equipment installs into the second-half of 2016.

Construction of the facility was started in September, 2014 with plant



Credit: Flickr/©Gov. Andrew Cuomo

New York Andrew M. Cuomo at an event at the Riverbend facility. Tool deliveries are holding up progress at the site of SolarCity's new fab.

construction including internal facilities guided to be completed by the end of 2015. However, internal facilities were still being installed in January and previous SolarCity management remarks on manufacturing equipment install schedules, meant initial tool installs would slip from the first quarter to the second quarter of 2016.

Lindon Rive, SolarCity's chief executive officer, noted in the latest earnings call that all building work should be completed by the end of the first quarter or probably early second quarter, followed by initial tool install taking place in the second and third quarter of 2016.

Rive also explained that longer than expected equipment lead times than originally expected would have a greater impact on the overall production ramp schedules and delay the purchase of an unidentified amount of the equipment until some time in 2017. "So the building should be completed at the end of this quarter probably early Q2," he said. "We'll then start moving in equipment. As some of the equipment has longer lead time than we originally expected. And so that equipment is going to arriving around Q2, Q3 next year. Because of that it will actually – the effect of that we can delay the purchasing of some of the other equipment and so a lot of the CapEx or probably about half the CapEx are actually moving to 2017."

India MoUs

Essel and GCL explore 5GW India-based module plant

A consortium between India-based integrated utility and solar developer Essel Infra and China-based PV material manufacturer Golden Concord Holdings (GCL) has signed a memorandum of understanding (MoU) with the Andhra Pradesh government to invest US\$2 billion in developing 5GW of module manufacturing capacity by 2020 in the Indian state.

The module facility would cater to both the domestic and overseas PV markets, said and Essel Infra release. The project will also create 15,000 skilled jobs.

Shu Hua, vice chairman of the GCL Group said: "We are very excited to be a part of the 'Make in India' campaign of prime minister Narendra Modi. GCL looks forward to contributing towards the progress of this wonderful country by not only bringing in investments but also the latest available technologies of PV industry."

Subhash Chandra, founder and chairman of Essel Group, said: "Renewable energy is the key for the economic growth of our country. It will aid clean energy initiative of the


government. Taking the lead, Essel Group intends to facilitate India's green energy requirement by delivering sustainable energy and creating value to empower people, communities and businesses."

India's SECI to explore joint solar manufacturing and deployment with Russian Energy Agency

The Solar Energy Corporation of India (SECI) has signed a memorandum of understanding with the Russian Energy Agency (REA) for both entities to develop utility-scale solar PV plants and manufacturing facilities in India between the years 2016-2022.

Under the agreement, a 500MW pilot project would be constructed. The two entities will draw up a roadmap for developing the projects and manufacturing hubs and will also establish a working group to determine future steps. REA will contribute state-of-the-art technology and low-cost financing, while SECI will help to acquire Indian government clearances and permits.


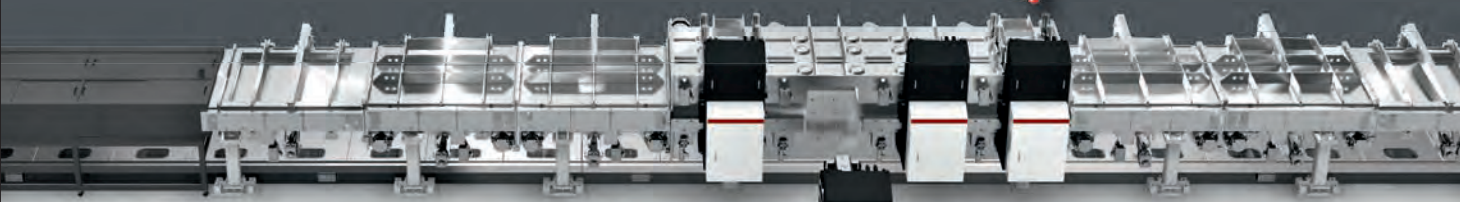
The MoU was signed by REA director general A.V. Tikhonov and SECI managing director Ashvini Kumar. A SECI statement said the plans would boost India's 'Make in India' programme.

**VON ARDENNE** 


[www.vonardenne.biz](http://www.vonardenne.biz)

**HIGH-PERFORMANCE CONTACT LAYERS**

**VACUUM DEPOSITED ON BOTH SIDES**

With our horizontal wafer coating system XEA|nova, even very thin substrates can be coated on both sides without breaking the vacuum or flipping the substrates. The system is designed for both sequenced and simultaneous treatment.



**XEA|nova**  
Wafer coating system



Yingli's Thailand plant will be its first outside of mainland China.

Credit: Hanwha QCELLS

### Module assembly

## Yingli to build first module assembly plant outside mainland China

Struggling Silicon Module Super League (SMSL) member Yingli Green Energy said it was building its first PV module assembly plant outside mainland China in a joint venture partnership with EPC firm, Demeter Power Company.

Yingli Green said that the assembly plant with a nameplate capacity of 300MW would be located in the Pruckdang district in Rayong, Thailand at a cost of around US\$19 million.

The new assembly plant is expected to be operational in the second half of 2016, producing Yingli Green's branded Yingli Solar multicrystalline modules.

However, due to Yingli Green's financial position the company is not taking a majority share or directly funding its share of the new facility.

The company said that its holding subsidiary, Hainan Yingli New Energy Resource Co, had signed the JV agreement with Demeter Power Company, a subsidiary of Demeter Corporation and would only take a 40% shareholding in the new JV.

Liansheng Miao, chairman and CEO of Yingli Green Energy said: "Manufacturing PV panels in Thailand will enable the company to operate more competitively in overseas markets as well as in the emerging markets of Southeast Asia."

## Canadian Solar bags finance for Vietnam assembly plant

The second-largest Silicon Module Super League (SMSL) member, Canadian Solar, has secured US\$70 million in loans and equity investment from the International Finance Corporation to support its plans to establish a 300MW module assembly plant in Vietnam and production plants elsewhere, such as Brazil.

Canadian Solar had previously announced it would allocate around US\$401 million in capital expenditures through the end of 2016 to significantly increase in-house wafer, cell and module production capacity and locate new plants in multiple countries, including 300MW in Vietnam, 30MW in Indonesia, 300MW in Brazil and 400MW in Southeast Asia. However, the major SMSL member has still not publicly provided timelines or plant locations for the expansions in new countries.

### New poly and cell capacity

## Wacker adding new polysilicon capacity as ASPs fall

Major polysilicon producer Wacker Chemie said in early February that its new polysilicon plant in the US had started ramping and existing plants remained at full capacity despite continued price declines that have reached record lows.

Wacker's new 15,000MT plus polysilicon plant in Charleston, Tennessee was expected to start production sometime in the second half of 2015, later revised to year-end.

Wacker's capital expenditures amounted to €835 million in 2015, primarily focused on completing the new polysilicon site in Charleston. Coupled to cost reductions and production improvements at its Burghausen and Nünchritz sites in Germany, Wacker should be able to meet a previous target of 80,000MT in 2017, potentially exceeding China-based GCL-Poly as the leading supplier.

## DMEGC starts construction on 500MW mono plant

Diversified Chinese enterprise Hengdian Group DMEGC Magnetics Co (DMEGC) has started construction of a new 500MW integrated monocrystalline solar cell and module plant in Hengdian, Zhejiang Province, China for subsidiary, DMEGC Solar Energy.

DMEGC, which has also been involved in downstream PV power plant projects, said the capacity expansion was due to a large gap in supply and demand.

The new production facility will be a two-storey construction with a total construction area of 22,000 square metres and cost around US\$106 million. It is expected to be completed in July 2016. The company noted that 100MW would be dedicated to PERC solar cell production with conversion efficiencies targeted at 20.8%. DMEGC also noted that trial operations and production runs were expected to be started in June through July, 2016. DMEGC Solar claims an existing monocrystalline solar cell nameplate capacity of 1GW and over 300MW of module assembly capacity.

# Full-year 2015 PV manufacturing capacity expansion plans and analysis

Mark Osborne, Senior News Editor, Solar Media

Fab & Facilities

Materials

Cell Processing

Thin Film

PV Modules

Market Watch

## ABSTRACT

In this quarterly report a full analysis is given for the first time of two years' worth (2014-15) of PV manufacturers' capacity expansion announcements and assessment of announcements that have or are planned to convert to effective new nameplate capacity through to the end of 2016. The analysis provide the first insight into new capacity ramp profiles of effective capacity expansions over the last two-year period and highlights future ramp profiles so far expected through to the end of 2016.

## Record expansion plans in 2015

According to our analysis, which includes thin film, solar cell, dedicated module assembly and integrated cell and module categories, PV manufacturing capacity expansion announcements in 2015 more than doubled (21GW in 2014) year-on-year to reach 55.19GW.

However, no one should panic that a new cycle of overcapacity is about

to hit the industry in 2016, as it is important to reiterate that this figure is all inclusive. By that we mean that it accounts for actual plans that are expected to become 'effective capacity' over a 12-month period or extended period over several years of phased expansions, as well as memoranda of understanding (MOU) and letters of intent (LOI) that may never happen.

Indeed, in certain cases announcements made in 2015 have

already been cancelled (see below analysis of Hanergy Thin Film), companies have gone bankrupt and previously announced plans (SunPower) re-announced.

As plotted in 2014, announcements by new entrants and start-ups have much longer lead times, primarily due to difficulty in raising finance for production plants, or have simply been dropped.

Specific to 2015 was a ridiculous number of MOUs and LOIs across all



Credit: Hanwha Q CELLS

Announced PV manufacturing expansions doubled in 2015, topping a theoretical 55GW.

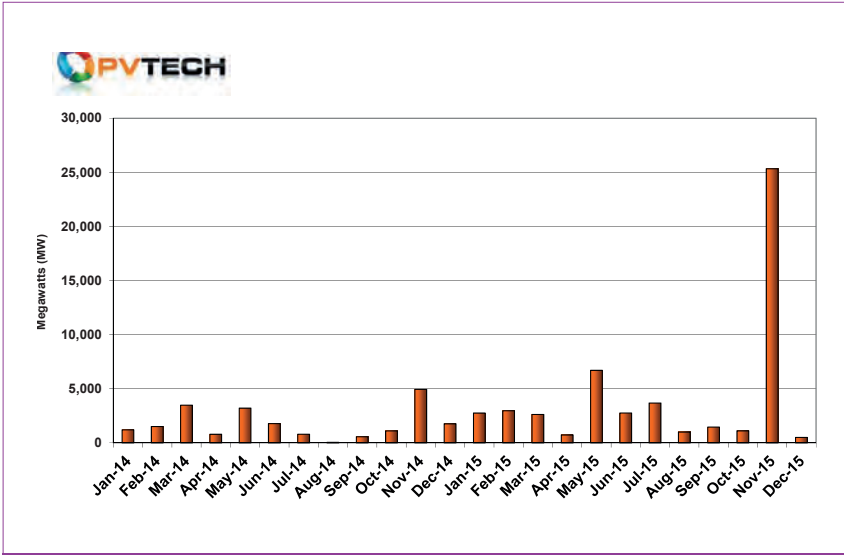


Figure 1. Combined total (c-Si cell/module & thin film) expansion announcements by month (MW)

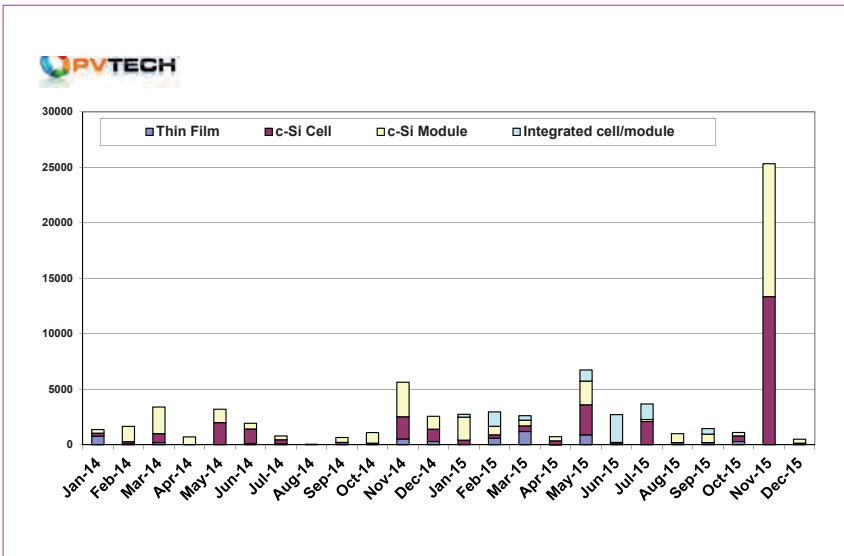


Figure 2. Capacity expansion announcements by product type, monthly (MW)

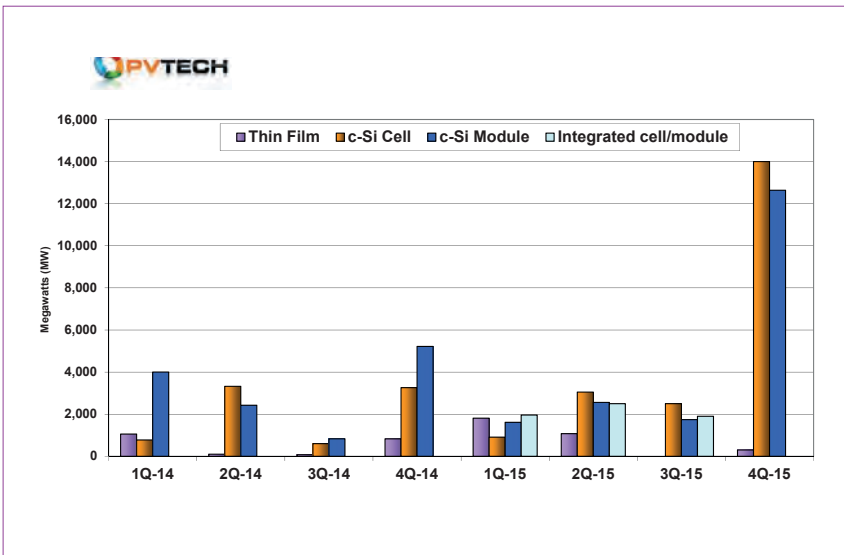


Figure 3. Capacity expansion announcements by product type, quarterly (MW)

segments, including polysilicon, that related to India. The vast majority of these announcements have not been counted, however there are around 6GW of announcements that we have recorded. This is due to the specific companies involved that have a history of good execution as well as those that have finance in place and some plans that have already started to be implemented. However, that still leaves several gigawatts of announcements in India that have yet to progress from paper plans.

Also more specific to 2015 was the scale of many announcements in the 1GW-plus range. However, many of these have more humble initial production capacity ramps than the headline figures. Therefore a complete refresh and reappraisal of all announcements on a monthly basis was undertaken with the intention of providing a more measured headline figure for 2015.

### Effective capacity announcements in 2015

This allowed us to eliminate over 15GW of announcements in 2015 that failed the validity tests, at this time. As a result, a more measured figure for capacity expansion announcements in 2015 is 39.87GW.

Going further and only counting initial-phase capacity expansions as being valid at this time, we can eliminate a further 10.7GW, bringing the most realistic figure of announcements in 2015 that could potentially migrate to effective capacity over the next 12 to 24 months to around 29GW.

We also undertook a specific reappraisal of the record announcements made in November 2015. We had reported preliminary figures for November of over 17GW of new planned capacity expansions, but the reappraisal after the dust had settled revealed an extra 7.7GW of capacity planned, bringing the total to over 25GW.

However, including the validity tests and checks, November stood out for including previously announced capacity expansion plans that would have led to duplication, as well as phantom capacity due to outsourcing and the inclusion of small-scale initial-phase capacity attached to multiple gigawatt future phased expansions with uncertain timescales. As a result November's figures were cut by 11GW, bringing the realistic figure down to 14GW.

Nevertheless, November set several individual benchmarks such as a new

**inter**  
**solar**  
connecting solar business

# DISCOVER THE WORLD OF INTERSOLAR



Intersolar Europe | Munich

Intersolar North America | San Francisco

Intersolar South America | São Paulo

Intersolar India | Mumbai

Intersolar China | Beijing

Intersolar Summits | Worldwide



Discover the World's Leading  
Exhibition Series for the Solar Industry  
[www.intersolarglobal.com](http://www.intersolarglobal.com)

record monthly and subsequently quarterly figure. A key reason for this change was the massive involvement of 'Silicon Module Super League' (SMSL) members (Trina Solar, Canadian Solar, JinkoSolar, JA Solar and Hanwha Q CELLS) announcing significant expansions at existing facilities in China, which remain non-integrated classification, as well as new and further expansions of facilities outside China, namely Malaysia, Thailand and South Korea.

### Thin film

All thin-film type capacity expansions announced totalled around 4.4GW in 2015.

All but 1MW of a-Si thin-film announcements came from Hanergy Thin Film, a total of 2.7GW.

However, all the customers have since cancelled contracts, negating completely these capacity plans, while its 600MW CIGS thin-film plant using acquired company technology from the US and Germany remains a question mark, unless Hanergy TF provides updates that have been absent for almost a year.

More validity exists with other CIGS thin-film plans, which totalled over 1.6GW in 2015. Initial production ramps and expansion phases are only expected to be around 500MW, which includes the odd R&D pilot line. The bulk of the planned CIGS expansion relates to an eventual 1.5GW ramp over multiple years of the Avancis/CNBM plant in China.

Also excluding Hanergy TF from 2014 announcements means thin-film expansions totalled just over 650MW that year, primarily due to First Solar and a lesser extent, Solar Frontier, both notable for executing on those plans and becoming effective capacity additions through 2015.

The relative inactivity in the thin-film segment (excluding First Solar and Solar Frontier) caps several years of thin-film underachievement and underlines the growing dominance of crystalline silicon technologies.

### C-Si solar cells

In that respect, dedicated c-Si solar cell expansion plans topped 20.4GW in 2015, compared to 8GW in 2014. Interestingly, dedicated module assembly announcements failed to exceed those for solar cells, reaching over 18.5GW in 2015, compared to 12.4GW in 2014.

We had highlighted in monthly analysis reports last year that the lack of new cell capacity plans in 2014

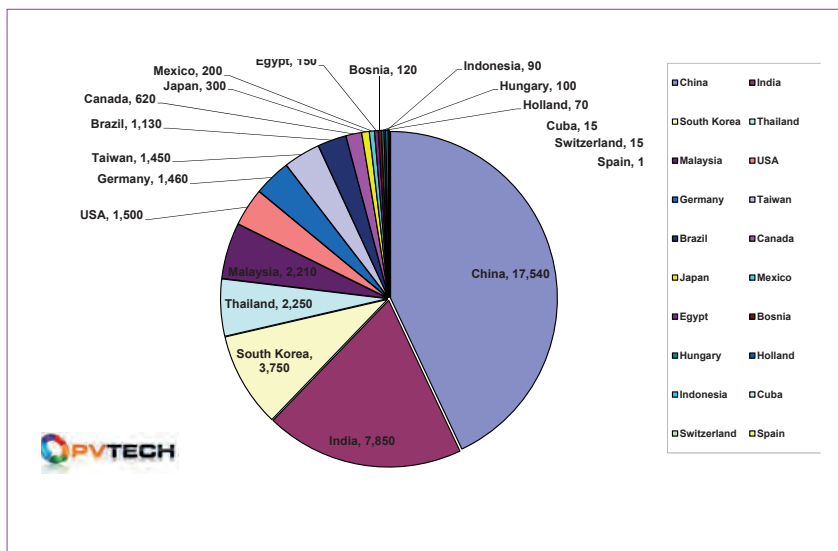


Figure 4. PV manufacturing capacity announcements (cell/module/thin film) by country (MW) in 2015.

compared to module assembly would need to be rebalanced; this is indeed what has happened in 2015.

Another strong trend through the first nine months of 2015 had been the plans for integrated cell and module expansions, a trend not seen in 2014, when dedicated module assembly expansion announcements dominated.

However, the integrated cell and module category gained no further traction in the fourth quarter of 2015, replaced as it was by a much stronger trend of dedicated solar cell capacity and dedicated module assembly capacity expansion announcements.

A full-year breakout highlights that integrated cell and module plans peaked at just over 6.3GW.

### Multi versus mono

The year was also marked by the number and scale of announcements related to n- and p-type monocrystalline cell and module assembly capacity expansion plans, which reached a combined total of nearly 9.4GW, compared to 4.38GW in 2014.

N-type mono cell and module assembly (including heterojunction) announcements topped 2.23GW in 2015, compared to 2.38GW in 2014. However, applying the validity tests we can eliminate 500MW from the 2014 figures and 1.4GW from the 2015 figures at this time, resulting in realistic figures of 1.88GW in 2014 and 830MW in 2015. Clearly, the momentum for mono has built over the last two years but n-type has been in moving at a much slower pace.

That is not the case with multicrystalline solar cell and module assembly capacity expansion

announcements (including integrated cell/module), which topped a combined total of over 41.5GW in 2015. In 2014, multicrystalline announcements stood at over 14GW, and it therefore remains the dominant technology, outstripping monocrystalline technologies' momentum.

### C-Si module assembly

The capacity expansion figures that mean the most relate to c-Si module assembly, which includes integrated and dedicated segments. In 2015 total c-Si module assembly capacity expansion announcements were around 27.5GW.

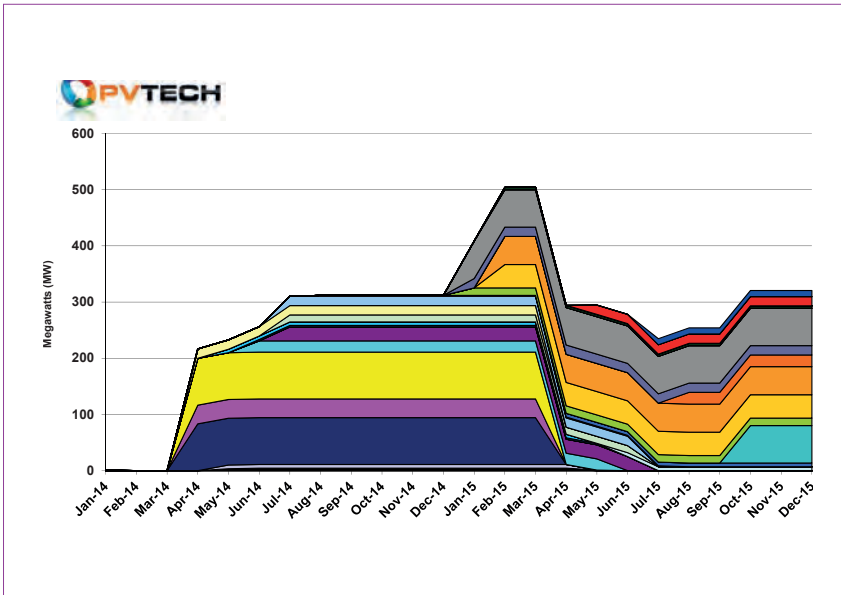
However, validity tests indicate almost 9GW of announcements are highly suspect, based on duplication, financing and past history of companies' execution. This would bring the total down to around 18.6GW, still a sizeable number. Applying analysis undertaken on 2014 announcements to actual effective capacity metrics (see below analysis) suggests it would be prudent at this time to discount a further 30%, simply from an overall execution perspective.

Therefore, around a further 5.58GW could be expected not to materialise from 2015 announcements in the next 24 months. Potential effective expansions of c-Si module assembly capacity from 2015 could be around 13GW.

### Regional shifts

The geographical chart (Fig 4) showing where capacity expansion announcements were targeted in 2015 disguises the fact that the number





**Figure 5. Cumulative c-Si module assembly effective capacity expansions (MW) from 2014 announcements.**

and scale of expansions announced in China in the first half of the year only reached 4.7GW and more than half were related to Hanergy TF.

No major China-based module manufacturer announced expansion plans in China in the first half of the year. Instead, they announced more than 6.7GW of planned capacity expansions in a number of overseas countries, including India, Malaysia, Thailand, South Korea, Brazil and the US.

The lack of new capacity expansions in China contrasts with over 12GW of new announcements in 2015 for other regions across Asia, with Chinese producers accounting for just over half of the capacity announcement figures. The second half of 2015 went a long way to restoring the balance but Southeast Asia remains a hot destination.

New capacity announcements in China increased by over 10GW in the fourth quarter of 2015 alone, resulting in the total reaching over 17.5GW in 2015; as such it remains the destination leader globally, but the figure is below the 19GW announced in the previous year.

Although India is clearly the second largest destination with over 7.8GW of announced plans in 2015, and only 1.4GW in 2014, less than 1GW has moved from the MOU/LOI category. But it is certainly the emerging destination to watch in 2016.

A similar situation exists in relation to Brazil, which has exceeded 1GW of announced capacity plans but again the effective capacity by the end of the year was almost non-existent. Yet, with

gigawatts of PV power plant projects planned, effective capacity activity could move forward in 2016.

One of the surprises for 2015 was South Korea, which generated just over 3GW of capacity expansion announcements. Already in 2016, LG Electronics has built on that momentum with plans to expand n-type monocrystalline cell production from the current 1GW nameplate capacity to 3GW by 2020.

Both Germany and the US did not disappoint with both countries nudging announcements around the 1.5GW mark, and the US beating Taiwan for the second consecutive year.

Interestingly, the figures for Malaysia (2.21GW) and Thailand (2.25GW) may not accurately represent final figures as a number of companies such as Trina Solar, JinkoSolar and SunPower have stated some of their capacity expansion by location but not yet confirmed several gigawatts of planned expansions, all potentially in either Southeast Asia country.

The overriding trend from a location perspective is that manufacturing outside China has seen significant growth and the emergence of a larger global footprint for manufacturing is taking shape.

### C-Si module assembly effective capacity expansion ramp analysis for 2014

As already highlighted, equating capacity expansion announcements with 'effective' capacity is misleading. Understandably, there is a time lag between many announcements and the time when that capacity comes on

stream and potentially meets its annual nameplate figure within the 12-month period from the start of the ramp.

A recent reappraisal of all 2014 c-Si module assembly capacity expansion announcements was made. This was to determine whether plans were realised and to plot the effective ramp rate timelines and the overall effective capacity additions made to the global PV industry from 2014 announcements through to when the final phase of those expansions can be treated as completed effective capacity.

It should be noted that the analysis also includes and adjusts for effective capacity added but for other reasons, such as bankruptcies or sector exits was later shutdown.

Not surprisingly, there was a short period of inactivity from announcements made early in 2014, but an initial momentum phase started in March 2014 and peaked in July. A plateau appeared through the remaining nine months of 2014, due to a stall in further new planned expansions beginning to ramp.

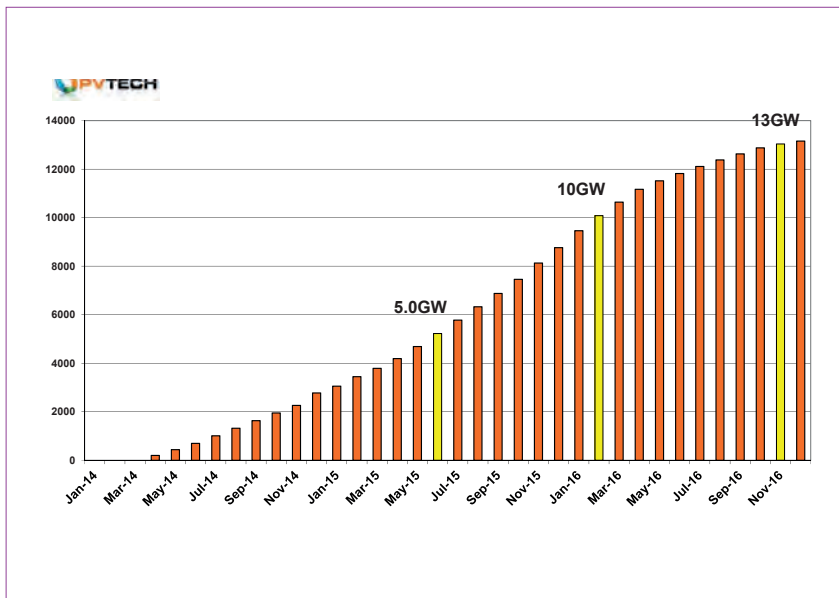
At the end of 2014, a total of around 2.57GW of effective capacity had been added to global c-Si module assembly capacity from 2014 announcements that had totalled 10.7GW. This equated to only a 24% conversion rate. However, significant ramps kicked off again in January 2015 from announcements made in late 2014, with just over 1.4GW added during the first quarter.

However, Q1 2015 announcements picked up momentum faster than those in the same period of 2014, with a further 1GW of cumulative effective capacity added in quarter.

As can be seen in Figure 6, a significant steep ramp developed and by mid-year cumulative effective c-Si module assembly capacity from 2014 and 2015 announcements had reached just over 5.22GW, which had taken 15 months to achieve.

By the end of 2015, the total cumulative effective c-Si module assembly capacity added from 10.7GW of 2014 announcements had reached nearly 6.4GW. Cumulative capacity reached 8.76GW.

Importantly, by mid-2016 all effective c-Si module assembly capacity from 2014 announcements that we know have been ramping will be accounted for, bringing the total effective nameplate capacity to around 7.33GW from the 10.7GW of 2014 announcements. Therefore, around 68.5% of c-Si module assembly capacity expansion announcements from 2014 would have converted to effective nameplate capacity by mid-2016,



**Figure 6. Cumulative C-Si module assembly monthly effective capacity expansions ramps from 2014 & 2015 announcements (MW).**

ending incremental nameplate capacity for that year.

The analysis reaffirms that the headline figures from 2014 get diluted over time (31.5% in that year) while effective nameplate timescales can stretch much longer than many may have expected. However, it should also be noted that several expansion plans from 2014 that have yet to materialise could resurface at any moment so the final conversion figure should not yet be assumed.

Of course effective c-Si module assembly capacity from 2015 announcements has to be included to get the closest realistic picture of completed effective new nameplate capacity for that year.

### 2015 effective capacity expansions

The profile of the capacity additions in 2015 differed considerably from the 2014 ramp profile. More companies added more capacity and kick-started expansions more quickly. Some companies had already started to add capacity before officially announcing plans, which all contributed to the expansion ramp profile divergence.

With the last of 2014 expansions completed in the early part of the fourth quarter of 2015, coupled to the peak in activity from 2015 expansions, a significant drop in expansions happened in the following three months. From a cumulative-capacity-added perspective it is expected to only take eight months (by March 2016) to reach the next 5GW.

From expansions underway from 2015 announcements to date, a total

of just over 13GW of cumulative c-Si module assembly nameplate capacity would have been added since the beginning of 2014.

As Figure 6 shows, effective new capacity, coming on stream in the second half of 2016 looks to be slowing. However, a number of announcements from 2015 have yet to get off the ground for a number of reasons, but meaningful gigawatts could subsequently be added to the ramp profile over the coming months. Therefore, the 13GW figure and slowing ramp curve should be treated as conservative at the current time.

We have also tentatively plotted estimates of global effective nameplate capacity figures from pre-2014 as well as making adjustments for nameplate capacity going offline due to bankruptcies or exits from the sector. As a result, cumulative effective capacity coming on stream from 2014 and 2015 announcements closely match end-market demand growth over the period.

Though further announced capacity from both 2014 and 2015 are expected to become effective capacity at some stage, the nameplate figures do not suggest a swing to any meaningful overcapacity scenario in 2016.

### Tight wafer and polysilicon supply

Looking past 2016 a potential looming shortage of polysilicon and multicrystalline wafers could constrain c-Si cell and module expansions, despite expectations that global end-market demand growth will increase strongly.

Little new ingot/wafer capacity

was announced in 2014, as major suppliers continued to suffer from weak ASPs that were stubbornly below manufacturing costs, providing few commercial reasons to add capacity. Like the polysilicon sector, aggressive expansions before 2014 had come on stream, causing severe overcapacity in both sectors.

However, the key message coming out of REC Silicon's recent fourth quarter financial conference call was the tight supply of both polysilicon and wafers with shortages of polysilicon in China in 2017.

Taking GTM Research's global PV demand forecast data as a 'middle ground' view, REC Silicon highlighted that the global end market demand could reach 64GW in 2016 and climb to 78GW in 2017.

However, with the polysilicon trade war with China yet to be resolved, access to the world's biggest consumer of polysilicon for US-based producers, primarily Hemlock Semiconductor and REC Silicon, is effectively closed.

As PV manufacturing rises to meet end-market demand, excess inventory levels are expected to be depleted but only limited new polysilicon capacity is expected to come on stream. But moving to demand forecasts in 2017, the situation becomes increasingly disconnected, with polysilicon supply markedly below end-market demand to the tune of an estimated 28,000MT.

With Siemens-based polysilicon plants taking an average of four years to build (fluidized bed reactor around 2.5 years), polysilicon supply shortages could be nearly 60,000MT in 2018, based on global PV end-market demand topping 95GW.

Should such conditions develop then this would indeed impact effective capacity expansion plans for c-Si solar cell and module assembly.

### Conclusion

Clearly, the conversion of capacity expansion announcements in 2014 into effective capacity was not as rapid or as high as many would have expected. Momentum clearly built in 2015 and how the tail of those announcements turned into effective capacity could impact on the effective ramp profile for the second half of 2016 and into 2017 remains unclear.

The global manufacturing footprint of the PV industry is set to continue to expand with India and Brazil notable emerging markets. Supply constraints with polysilicon and wafers could impact expansion plans in 2017, yet the impact on the ramp profile also remains uncertain.

# How facilities can affect energy consumption in PV cell production

Martin Schottler, AVEREM process engineering, Stuttgart, Germany, & Mariska de Wild-Scholten, SmartGreenScans, Groet, The Netherlands

Fab & Facilities

Materials

Cell Processing

Thin Film

PV Modules

Market Watch

## ABSTRACT

The production toolset is not the only significant source of power consumption in PV cell production. Cooling water, climatization, pressurized air and, in some cases, clean-room conditions drive up the electrical energy demand. In addition, the geographical location influences the cooling energy demand for air handling, resulting in a non-negligible contribution to electrical power consumption. The extent of this additional consumption over and above the toolset demand depends on whether the structure of the facility systems is 'traditional' or 'smart'. This is demonstrated by a number of quantitative examples in this paper.

## Introduction

This paper examines which portion of the power consumption required for the fabrication of a PV cell is due to facilities, and in particular the options that exist for reducing this consumption. The facilities present a number of significant 'power consumers', because of the requirements of the production toolset: energy supplies of different types (electrical, thermal, pressurized air), gases and chemicals, and services for the disposal of exhaust and waste water or used chemicals. As some cell manufacturing is carried out in clean-room environments, this will also lead to a power consumption related to clean-room operation. All the facility services require power, mostly electrical, for their function.

The parameters of last year's example modelization [1], which was performed mainly to show the interdependencies of water and energy consumption, have been refined in the light of recent total energy consumption data [2]. The aim of this investigation is to enable a ranking of the contributions to be made, and to determine which of these are worth looking at and offer promising optimization potential. Two questions are tackled: 1) to what extent is the range of results determined by assumptions on facility structure?; and 2) what is the relationship of the facility contribution to the electrical power demand of the process equipment toolset? These questions will be restricted to crystalline PV cell production (mono/multicrystalline) and to the choices of facility configuration that actually occur in practice.

## Facility structure for PV cell fabrication

The fraction of electrical power consumed by facility applications is shown in Fig. 1, which is based on the compiled data in de Wild-Scholten [2]

and an estimated breakdown in de Wild-Scholten & Schottler [1]. The absolute numbers are distinctly lower than those given in the ecoinvent 2.2 database and in Schmidt et al. [3]; however, they are based on recent data collection and are expected to reflect the overall advances in PV cell fabrication. It can be seen that a significant part of electrical power consumption is attributable to the production facility, and, as it turns out, substantial variations in this consumption can be induced by varying the design of the facilities.

**“A significant part of electrical power consumption is attributable to the production facility.”**

In general, thermal and electrical energy are provided from sources external to the site. Thermal power usually has three major destinations: office heating, climatization purposes and exhaust treatment. Whether heating is also necessary in wastewater treatment, ultrapure water generation or other facility locations depends on the details, and so this aspect is not taken into

account in the following analysis. Heating for the process equipment, on the other hand, is usually performed electrically. Electrical power is more widespread in its use than thermal power, which means that a variety of end uses have to be considered, and not just a small number as in the case of thermal power.

The main facility consumers of electrical power which will be considered are cooling power production, air handling, bulk gas production and compressed dry air production. These relationships are shown in an overview in Fig. 2, and are independent of the nature (mono/multicrystalline) of the fabricated PV cell. Several scenarios are investigated in the following analysis, which lead to improvements, some with lower power consumptions but others with increased consumptions. The reason for this is to highlight potential influences and their relative importance.

Bulk gas generation, mainly nitrogen in PV fabs, is not shown in Fig. 2; it is also not varied in a dedicated scenario, although its contribution is not negligible. Nitrogen is produced either onsite or offsite. In the latter case it is transported to the site in liquid form and stored there in tanks. In most projects these particular installations are contracted to a company other than the

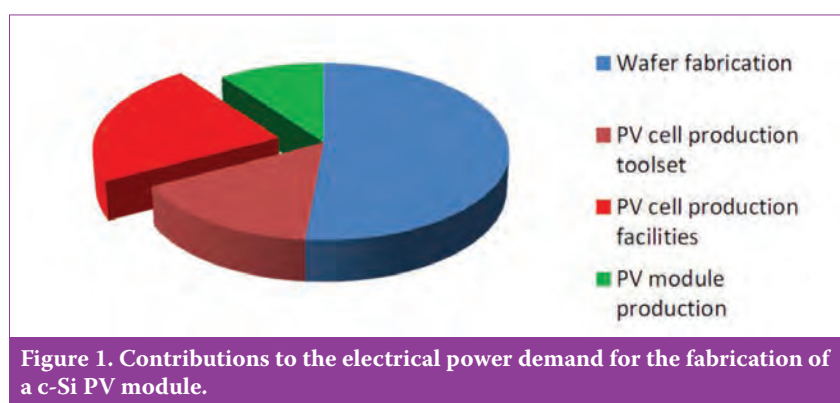


Figure 1. Contributions to the electrical power demand for the fabrication of a c-Si PV module.

fab designer, and energy consumptions are kept strictly separate and confidential, because a manufacturer's production cost is critically dependent on the specific energy consumption during nitrogen production. This energy consumption has been evaluated at 0.75kWh/kg N<sub>2</sub> with the dataset in Schmidt et al. [3], and has been included in the result charts for comparison purposes, but does not undergo any variation.

Facility services, such as ultrapure water generation or treatment of general and corrosive exhaust air streams, that are considered to be minor in terms of electrical power consumption have not been highlighted in detail, in order to keep the breakdown lean. The same is true for office heating and cooling and waste water treatment.

### Scenarios investigated

All the scenarios are based on a production throughput of 9,600 wafers (156mm × 156mm) per hour.

- **Scenarios 1 and 2:** Standard scenarios based on available databases and reports. Scenario 1 showsecoinvent 2.2 data for the sake of comparison; however, they appear outdated and excessively high. Scenario 2 is considered the standard scenario in the following, and is based on the compilation in de Wild-Scholten [2]; it corresponds to the facility structure in Fig. 2. Several design criteria are varied relative to this standard scenario, and the overall results inspected.

- **Scenario 3:** Includes cogeneration.
- **Scenario 4:** Includes cogeneration and an absorption chiller (see Fig. 3).
- **Scenario 5:** As for the standard, but with an additional loop for processing cooling water at a higher temperature than in the coldest loop.
- **Scenario 6:** As for the standard, but uses an ISO class 5 (formerly class 100) clean room.
- **Scenario 7:** As for the standard, but with cold dry winter/hot summer conditions (see Figs. 4 and 5).
- **Scenario 8:** As for the standard, but with constant hot humid outside conditions (see Figs. 4 and 5). A comparison of scenarios 7 and 8 will show how much the influence of climate on the energy required for air handling affects the results.
- **Scenario 9:** As for the standard, but with a biofilter instead of an RTO (regenerative thermal oxidizer) for VOC (volatile

organic compound) exhaust treatment.

- **Scenario 10:** Includes all positive options, as well as the geographical location.

Cogeneration (scenario 3) means the production of electrical power is onsite, which is usually chosen because of the superior stability of the power generated with respect to small or large interruptions. However, it is also beneficial in terms of energy efficiency:

- Transportation losses of electrical power are avoided.
- Power generation is based on natural gas, which has a smaller CO<sub>2</sub> footprint in highly efficient devices than, for example, coal or the power mix in most countries.
- Waste heat from power production can be used for heating purposes, replacing other fuels with natural gas.

The values for assessing CO<sub>2</sub> equivalent emissions are: 1) 500g CO<sub>2</sub>/kWh.el, which is close to the EU power mix with approximately 30% coal in the power mix [4]; and 2) 150g CO<sub>2</sub>/kWh.th for natural gas – a conservative value, including quite substantial escaping methane emissions during gas production [5].

In addition to the advantages of scenario 3, scenario 4 includes the generation of chilled water using the waste heat of power production, thus

eliminating the need for electrical power for the generation of cooling power. This is performed by absorption chillers.

The corresponding schematic block diagram for scenario 4 is shown in Fig. 3. Only natural gas is taken from the environment, with all the rest taking place within the production site.

Scenario 5 is again based on the standard facility structure, but provides three cooling loops instead of two. The coldest loop (usually 6°C, but sometimes less) feeds just the fresh air treatment (and some other, minor, applications), whereas all the other functions – such as return air, process equipment and office climatization – are driven by chillers, yielding 12°C cooling water. In small installations, this loop is often fed by heat exchangers connected to the 6°C system, but separate generation has efficiency advantages, as well as being cost-wise feasible if a certain minimum size of installation is exceeded.

To assess the energy savings possible with three cooling loops instead of two, the coefficient of performance (COP) value of the mechanical chillers needs to be estimated. The COP represents the cooling power in kW (th) that can be generated by 1kWh of electrical power consumed by the compressor of the chiller. It depends on many factors, including the point of operation and the actual supply and return temperatures achieved under certain operating conditions. If the system is not operating at full cooling power, for example, or has been oversized in terms of

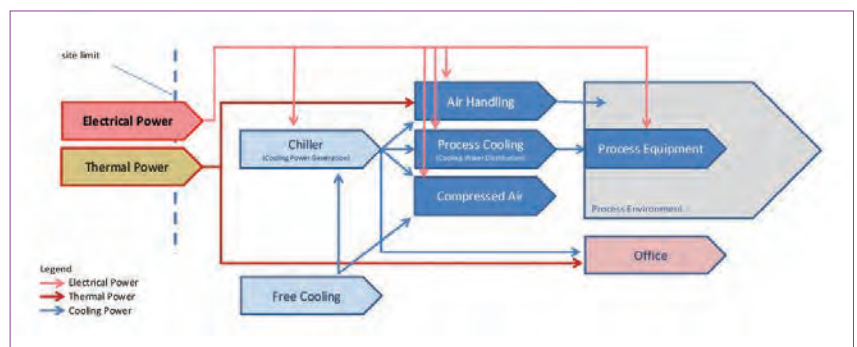


Figure 2. Standard structure of facilities for PV cell production.

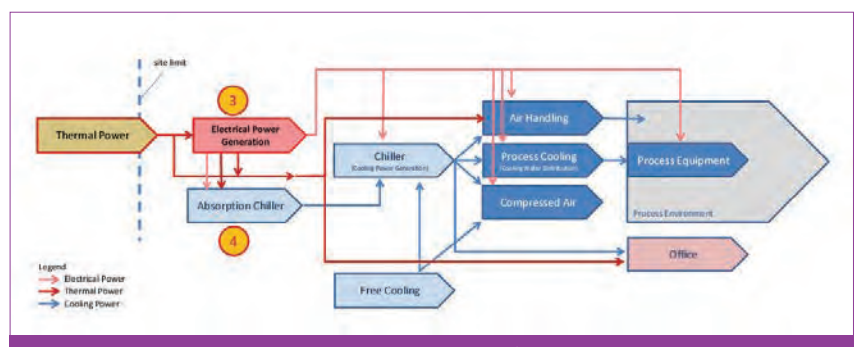


Figure 3. Cogeneration and absorption chiller (scenarios 3 and 4 respectively).

volumetric cooling liquid flow, the supply and return temperature spread decreases, negatively affecting the COP and thus decreasing energy efficiency. Chiller manufacturer data therefore have to be interpreted with care. For the present study, the COP values and their differences for the different chiller types have been set to conservative values in order not to overestimate the energy savings. More details are given in de Wild-Scholten & Schottler [1].

Air handling can in general be divided into fresh air, return air and exhaust air treatment; these are considered in scenarios 6 to 9. Return air is addressed in scenario 6, and fresh air in scenarios 7 and 8. Exhaust air treatment is addressed in scenario 9, but only in part of the VOC treatment, because other types of exhaust are unimportant energy-wise.

Scenario 6 investigates how clean-room conditions for production have an impact on the energy demand and balance. Generally, clean-room conditions affect the power demand of return air management: not only can the demand per m<sup>2</sup> of installed clean-room space be higher than per m<sup>2</sup> of the normal production area, but also the pressure drop of the return air is higher than with normal return air.

It is clear that the settings of non-clean-room return air conditions require some assumptions on the structure and conditions of operation of the air-handling system. The calculations in the scenarios, other than scenario 6, assume some air recirculation, but at lower pressure drops and lower air flow rates than in scenario 6. Certainly more savings in air handling are possible, but this should be the subject of detail engineering in a specific project. Here, it was preferred to produce cautious comparisons without overemphasizing the differences.

The outside air conditions have a major influence on fresh air treatment. This treatment phase consists of process stages for controlling temperature and humidity, and bringing the temperature and humidity of any outside air to within a specification-compliant range by heating/cooling and humidification/dehumidification. A usual process sequence (without filtration stages) is:

- Preheating
- Ventilation
- Humidification
- Dehumidification (by cooling, typically down to 8°C)
- Reheating (typically up to 22°C)

If the outside air is hot (as in scenario 8), the cooling power required for dehumidification purposes is significant, as is the reheating power to reach 22°C in the production environment. More

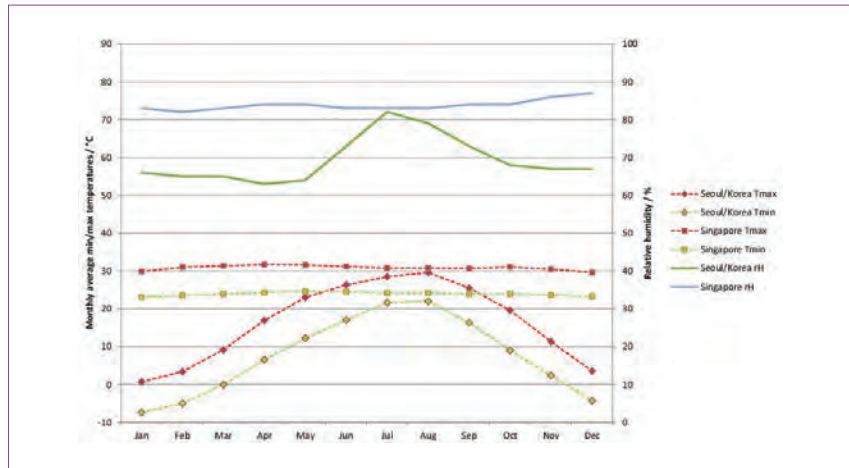


Figure 4. Climatic conditions (monthly averages) for Seoul/Korea and Singapore in 2015.

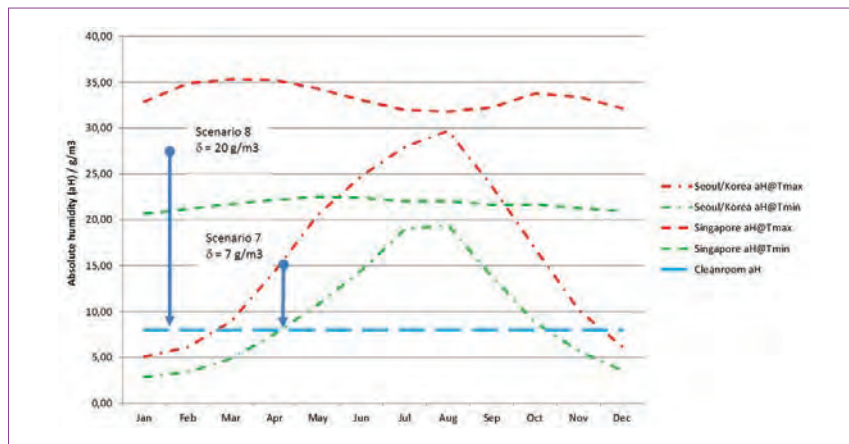


Figure 5. Absolute humidities of the fresh air at the entry to treatment.

important than this use of power, however, is usually the cooling power required for removing water from the outside air if humidity is high, as in the case of scenario 8.

Climatic outside conditions and their impacts on the energy demand are compared using scenarios 7 and 8. Two sample locations were chosen for the comparison: Singapore and Korea. Climate data for 2015 were acquired from the internet [6] and are presented in Figs. 4 and 5. The relative humidity data given were converted to absolute humidities (which are necessary for the calculations) by using the respective minimum/maximum temperatures from the monthly averages and the vapour pressure curve, as taken from ProSim Plus software. For the sample calculations presented here, it was assumed that a yearly average cooling is required from 28 to 8°C in scenario 8, and from 12 to 8°C in scenario 7 (see temperature data in Fig. 4). The absolute humidity, on the other hand, was assumed to have decreased by 20g/m<sup>3</sup> air in scenario 8, and by 7g/m<sup>3</sup> in scenario 7 (see humidity data in Fig. 5).

Although the nearly constant climatic conditions of scenario 8 allow

an easy visual check of temperature and humidity differences, in scenario 7 there is a day/night cycle that needs to be taken into account before assessing the net difference in temperature and humidity. Moreover, in scenario 7 there is no need for dehumidification during three months of the year, but instead humidification is required, as can be seen from Fig. 5. For every month during which the absolute humidity of the outside air is lower than the clean-room specification, humidification is necessary rather than dehumidification. In the months where the absolute humidity of the outside air is lower than the clean-room air specification for the minimum (night-time) temperatures, humidification is also necessary for certain hours during night time. All this makes it impossible to verify straightforwardly the reported 7g/m<sup>3</sup> reduction setting; however, it might be taken as a given and typical value. For a specific project, an analogous evaluation can be run very precisely using climatic data that are available around the world, though not all free of charge. This is the recommended approach for specific projects, because significant differences can even occur in

the same country, and more details of the air-handling system have to be addressed than are reported here.

Scenario 9 considers a special case of exhaust air treatment: whereas exhaust air treatment in general has not much impact on overall energy consumption, the so-called RTO installation for VOC treatment consumes much more thermal power than a biofilter solution. This effect is more pronounced in the VOC exhaust in PV cell fabrication than in other types of production, because a preconcentration cannot take place, as explained in Hottenroth & Schottler [7]. A preconcentrator is an adsorption system, most often based on a turning adsorber wheel; this subjects the VOC to adsorption and desorption, resulting in an air flow with a lower rate than the original one, thus leading to an increase in concentration of the VOC in the air to be treated. Terpeneol, one component of VOC exhaust in PV cell fabrication, would polymerize on the adsorbent media used for preconcentration and thus ruin it in a short time.

The absence of a preconcentrator forces the RTO to operate under suboptimal operating conditions, although these systems usually exhibit a heat recovery rate of 93%. Biofilters are environmentally favourable systems, but require strict technical control of their function in order to obtain satisfactory operational behaviour. Only a strict and efficient growth control of the bacteria in the filter can prevent unpleasant and sudden pressure build-up or unexpected system downtime.

Detailed environmental impact studies, including the power consumption aspect, have already been reported in the literature [8–10], and so scenario 9 is included for the sake of comparison.

Scenario 10 is the best case, combining the most favourable conditions. Since most of the effects found are additive, the savings relative to the standard scenario were added up. Because the favourable cases were cautiously estimated, scenario 10 is considered to be a realistic best case, and not a hypothetical one.

**“Chilled water generation can be clearly identified as the most important contributor to the facility power consumption.”**

## Results

Two main charts were produced in order to highlight the results. First, the electrical power demand of the facility section is given in total and also broken down into major contributors; all are

compared with the electrical power demand of the process equipment toolset (Fig. 6). Here, the chilled water generation can be clearly identified as the most important contributor to the facility power consumption, followed by air handling (in total, i.e. all contributions counted together, except VOC treatment). The bulk gas generation, which was not varied or inspected in detail, is next in importance, and the compressed dry air (CDA) generation after that. The ‘rest’ category encompasses other applications such as office cooling, ultrapure water generation, waste water treatment or simply lighting. This category is calculated from the overall power consumption given by de Wild-Scholten [2] and the sum of the other indicated facility structures; it undoubtedly also exhibits some error or uncertainty. However, it is apparent that most of the major contributions could be identified and ranked.

What the chart in Fig. 6 does not show are thermal power consumptions. The total site CO<sub>2</sub> equivalent emissions were calculated taking into account both thermal and electrical power consumptions (Fig. 7). Here, the VOC treatment, which mainly requires additional thermal power in the case of an RTO, is included in the calculated balance.

It is striking how high the emissions are for the outdated consumption data in scenario 1, and how much scenario 10, the best-of-all combination, is lower than today’s standard value in scenario 2. Clearly visible is the bad influence of hot humid weather (scenario 8), as well as the superior performance of a cogeneration combined with an absorption chiller (scenario 4). The latter is usually combined with several dedicated cooling loops (scenario 5). If an ISO class 5 clean room is necessary (scenario 6), additional power is required compared with scenario 2.

The weather influence (scenarios 7 and 8) has already been discussed in detail and is mainly due to differences in fresh air treatment.

Scenario 9 on the whole consumes less thermal power compared with the standard scenario; this is the benefit of biofiltration.

When the results of Fig. 7 are taken in combination with the production rate of PV cells, the difference relative to the average footprint of the final cell can be expressed in grams of CO<sub>2</sub>/kWh<sub>el</sub> for the best and worst cases:

- Best case (scenario 10): -3g CO<sub>2</sub>/kWh<sub>el</sub>
- Worst case (scenario 6/8): +1.5g CO<sub>2</sub>/kWh<sub>el</sub>

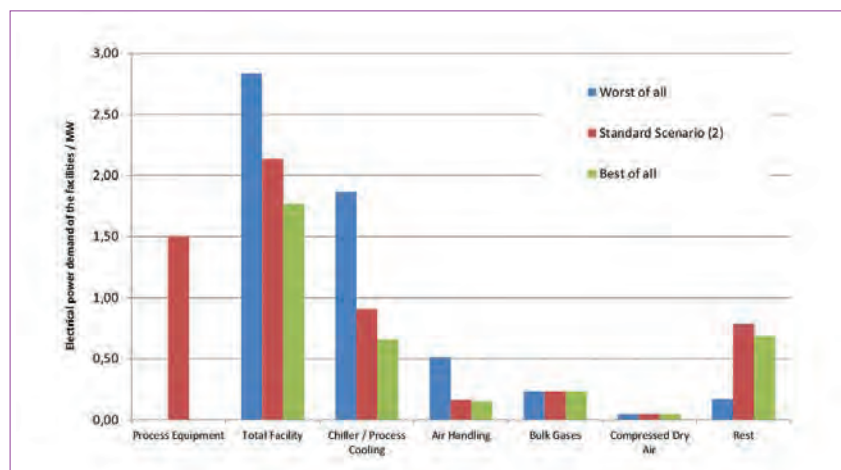


Figure 6. Electrical power consumption per facility installation and scenario.

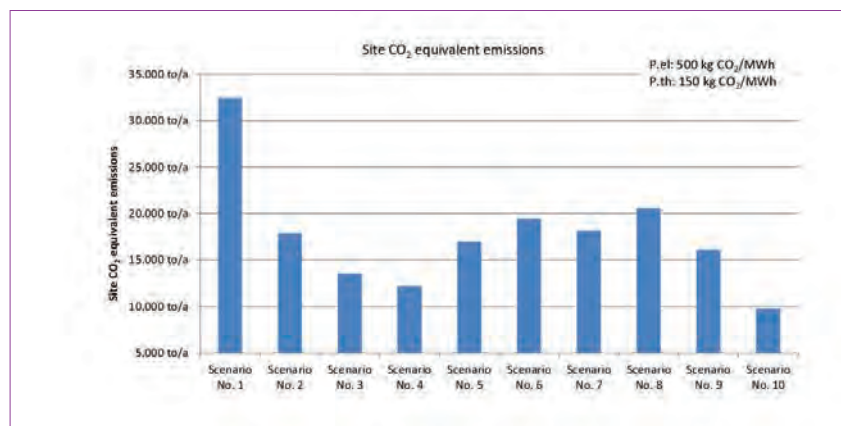


Figure 7. Site CO<sub>2</sub> emissions resulting from the different scenarios.

It is interesting that the 'good' side has more potential than the 'bad' side, at least in the light of the set of scenarios chosen and presented here. When old process and facility designs are used, even higher consumptions/emissions are possible, as can be seen from the older data [2,3]; these data are not incorrect, but rather relate to another generation of production technology.

## Discussion

A general design criterion which improves the CO<sub>2</sub> footprint is the installation of cogeneration with the use of waste heat by absorption chillers. This avoids the direct usage of electrical energy from the network and thus leads to savings in CO<sub>2</sub> equivalent emissions, whenever there is a power mix with significant fossil fuel contribution in the country of consideration. Irrespective of this decision, the cooling power required is one of the major contributions to the facility power demand. Cooling power is required by production tools, but also by air handling; the latter largely depends on the geographical location (local climate) of the production facility. Hot and humid locations drive up the air handling cooling demand.

Exhaust air handling does not usually have a significant impact on energy consumption, except in the case of VOC treatment. The standard VOC treatment systems installed in many PV fabs have considerable natural gas consumptions, and a new design should preferably take into account biofiltration methods. The next most important contribution is nitrogen gas, mainly used for process purposes (flushing) and vacuum pump purging. Any reduction in consumption that is achieved here helps to reduce the overall energy demand. Of lesser importance is CDA production, and of even lesser importance are other facility services (ultrapure water generation, wastewater treatment, lighting, office equipment/heating, etc.) which were excluded from the detailed breakdown shown here.

The best situation is achieved with the production in a country that has cold dry winters and dry summers, installation-wise consisting of a cogeneration with absorption chillers and a minimum of three different cooling loops of chilled water, and a VOC exhaust treatment using biofiltration. This arrangement is highlighted in scenario 10.

Of course, many more variations are possible in the facility engineering of PV cell production; some of the major cases should be analysed in order to determine what part facility design plays in the significant bandwidth

of power consumption. With the particular integrated energy flow model cited [1], every variation can be calculated and assessed. This, however, is usually done within the framework of a specific project. For example, there are ways of overcoming the negative influence of a humid geographical location, but these installations have to be integrated into the design from the very beginning of the project.

## Conclusions

In respect of the large variation between the best and worst scenarios, two conclusions can be drawn. First, a detailed engineering procedure that takes into account the power-saving potentials is mandatory. Second, a PV cell manufacturer should certify its production with regard to specific energy consumption, to turn the engineering efforts made during facility design into a competitive advantage.

**“A PV cell manufacturer should certify its production with regard to specific energy consumption.”**

An energy payback time attributed to a specific type of cell/module without referring to the manufacturer's facility structure or the climate of country of location may provide an indicative figure, but it is not precise enough to support buying and installation decisions from an environmental point of view. The CO<sub>2</sub> footprint of a solar cell produced under the best and the worst conditions can vary by as much as 4.5g CO<sub>2</sub>/kWh, depending on facility structure and geographical location.

## References

- [1] de Wild-Scholten, M. & Schottler, M. 2015, Poster contribution, EU PVSEC, Hamburg, Germany [available online at <http://www.smartgreenscans.nl>].
- [2] de Wild-Scholten, M.J. 2014, "Life cycle assessment of photovoltaics status 2011. Part 1: Data collection", Report, SmartGreenScans, The Netherlands.
- [3] Schmidt, M. et al. 2012, "Life cycle assessment of silicon wafer processing for microelectronic chips and solar cells", *Int. J. Life Cycle Assess.*, Vol. 17, p. 126.
- [4] European Environment Agency 2016, EEA indicators [keyword 'CO<sub>2</sub> emission intensity': <http://www.eea.europa.eu/data-and-maps/daviz>].
- [5] Howarth, R.W., Santoro, R. &

- Ingraffea, A. 2011, "Methane and the greenhouse-gas footprint of natural gas from shale gas formation" (letter), *Climatic Change*, DOI 10.1007/s10584-011-0061-5.
- [6] wetteronline 2016 [[www.wetteronline.de](http://www.wetteronline.de)].
- [7] Hottenroth, H. & Schottler, M. 2009, "VOC reduction in semiconductor and photovoltaic cell production: An ecological assessment", AICHEM congress, Frankfurt, Germany.
- [8] Schottler, M. et al. 2010, "Volatile organic compound abatement in semiconductor and solar cell fabrication with respect to resource depletion", *Chem. Eng. Technol.*, Vol. 33, p. 638.
- [9] Schottler, M., Hottenroth, H. & Schmidt, M. 2010, "VOC Minderung in der Solarzellenfertigung (PV Industrie), Eine Lebenszyklusbetrachtung" (VOC reduction in solar cell production (PV industry): A life cycle assessment), VDI congress Emissionsminderung, Nuremberg, Germany.
- [10] Schottler, M., Hottenroth, H. & Schmidt, M. 2011, "Reduction of hydrocarbon emissions in solar cell fabrication: A life cycle assessment", *Chem. Ing. Tech.*, Vol. 83, p. 1642.

## About the authors



**Martin Schottler** is the managing director of AVEREM process engineering, having previously worked for the design-and-build company M+W in the field of engineering semiconductor and solar cell fabrications. He studied in Saarbrücken and Darmstadt, Germany, and was awarded a Ph.D. for his work on gas phase chemistry in combustion processes.



**Mariska de Wild-Scholten** is the owner of the company SmartGreenScans, having previously worked for the Dutch ECN research centre. She studied geochemistry at Utrecht University and received her M.Sc. degree in 1989. She has been working in the field of life-cycle assessment of PV systems for a number of years.

## Enquiries

Martin Schottler  
 AVEREM process engineering  
 Bismarckstraße 75  
 70197 Stuttgart, Germany

Email: [sho@averem.com](mailto:sho@averem.com)  
 Website: [www.averem.com](http://www.averem.com)

# Materials

Page 23  
News

Page 25  
**Inline diamond wire  
inspection based on resonant  
vibrations**

Hubert Seigneur<sup>1,2,3</sup>, Sergei Ostapenko<sup>4</sup>,  
Igor Tarasov<sup>4</sup>, Chad Rodrigues<sup>4</sup>, Yuriy  
Zaikin<sup>5</sup>, Kevin Morrow<sup>6</sup> & Winston V.  
Schoenfeld<sup>1,2,3</sup>

<sup>1</sup>c-Si US Photovoltaic Manufacturing  
Consortium (PVMC), Orlando,  
Florida; <sup>2</sup>Florida Solar Energy Center  
(FSEC), Cocoa, Florida; <sup>3</sup>University  
of Central Florida (UCF), Orlando,  
Florida; <sup>4</sup>Ultrasonic Technologies,  
Inc. (UST), Wesley Chapel, Florida;  
<sup>5</sup>PetroBeam, Inc., Sweetwater,  
Tennessee; <sup>6</sup>Niabraz LLC, Tonawanda,  
New York, USA

Page 29  
**Polysilicon vs. upgraded  
metallurgical-grade silicon  
(UMG-Si): Technology,  
quality and costs**

Eduardo Forniés, Laura Méndez &  
Marta Tojeiro, Aurinka PV Group SL,  
Madrid, Spain



23

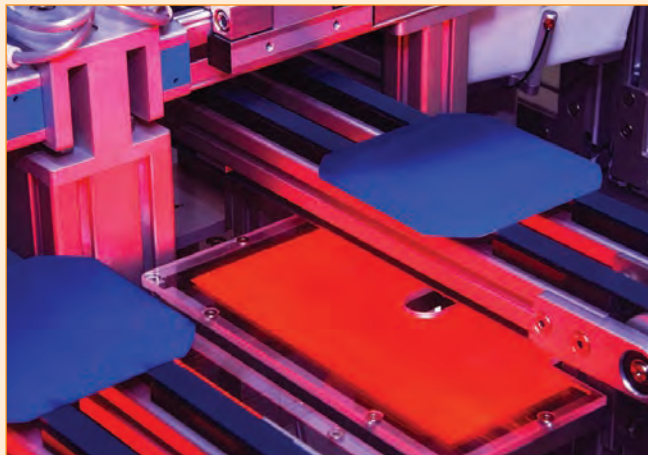


## Analysts offer differing take on 2016 wafer market

Disparity over a potential global shortage of primarily multicrystalline solar wafers has emerged after two market research firms have recently issued contrasting views. IHS Technology had previously warned in October, 2015 of the potential shortage that could emerge in multi c-Si wafers in 2016, while more recently, Taiwan's EnergyTrend said it expected the tight global supply should begin to ease later in the first quarter as around 5GW (see below) of new production capacity starts to come on stream.

However, IHS has reconfirmed its view that due to current wafer capacity levels and end-market growth demand in 2016, wafer supply would continue to remain 'tight in 2016'. The market research firm noted that total wafer (mono and multi) reached 61.9GW in 2015, up from 47.6GW in 2014.

The two firms do agree on the fact that multi c-Si wafer ASPs have increased on tight supply. IHS noted it had estimated that all wafer suppliers were operating at 83% utilisation rates, while major suppliers such as GCL-Poly and GET were operating at utilisation rates of 88%, the highest since 2010. However, with further capacity expansions average utilisation rates are expected to remain high at around 85% on average.



Credit: Flickr/Oregon Dept. of Transport

Analysts disagree on the rate that tight global wafer supply will ease during 2016.

### Wafers

## Multicrystalline wafer supply constraints should ease on 5GW of new capacity - EnergyTrend

EnergyTrend expects the tight global supply of multicrystalline wafers that has led to a spike in prices to ease during the first quarter as new capacity starts to come on stream. EnergyTrend noted that weak pricing in recent years had significantly curtailed capital expenditure for additional capacity, despite growing global end-

market demand for solar modules.

However, around 5GW of new capacity earmarked so far this year should ease constraints and reduce price increases after an expected wind down in demand after the Chinese New Year holidays as the global market stabilises now that demand issues in key markets such as China and US (ITC extension) have eased. Multi-Si wafer prices were set to peak in February, according to the market research firm.

In contrast, EnergyTrend said the monocrystalline wafer market remained in overcapacity, with demand in 2015 totalling around 9.5GW and capacity exceeding 15GW.

## Rising solar wafer prices on tight global supply boon to PV Crystalox

UK-based multicrystalline wafer producer PV Crystalox Solar inferred in a financial statement that it could finally benefit financially from the divergence of polysilicon and wafer prices, after several years of losses.

PV Crystalox acknowledges what other wafer producers such as Taiwan-based Green Energy Technology (GET) had been saying for months, namely that wafer capacity constraints on the back of continued strong demand had pushed ASPs higher and that global wafer capacity constraints existed.

However, due to polysilicon production overcapacity and further new capacity coming on stream in 2016, polysilicon spot prices have fallen to record lows in recent months.

The divergence benefits the likes of PV Crystalox as it sells its wafers on the spot market and with increasing demand could convert more of its stockpiled polysilicon inventory to wafers, rather than limit losses on re-selling its polysilicon on the spot market below its contract purchase prices.

Previously, PV Crystalox had been saddled with fixed-price long-term polysilicon supply contracts but noted that it had concluded obligations under its largest supply contract and taken delivery of the final shipment of polysilicon under that contract in December 2015. The company also noted that shipments under remaining contract were scheduled to continue until late 2018 but the planned quantities were consistent with current production volumes.



Credit: REC Silicon

Expansions at the Moses Lake site were halted in July last year.



Credit: Heraeus

Heraeus has boosted its multi-supplier strategy after a fatal industrial accident at Dowa Hightec impacted silver powder demand.

### Polysilicon

#### REC Silicon halts FBR production at Moses Lake

US-based polysilicon producer REC Silicon is to shut down its Silane IV production unit and remaining fluidized bed reactor (FBR) production at its Moses Lake plant in Washington.

In July, 2015, REC Silicon said it would cut its FBR production 2,000MT and stop planned expansions at the Moses Lake facility. China has imposed import duties of 57% on REC Silicon in retaliation to US anti-dumping duties, sparking a trade war between the countries.

Falling polysilicon spot prices due to overcapacity rather than weak market demand have technically excluded REC Silicon from selling its polysilicon into the Chinese market. Hemlock Semiconductor, one of the largest polysilicon producers, and also based in the US, is also impacted by heavy import duties and has halted construction of a major new production plant.

In the trading update, REC Silicon noted that it expected to shut down the Moses Lake plant in February, undertake preventative maintenance, retaining employees and potentially restart production in June, 2016. The company is also revising previous plans to restart

Silane III production in January, 2016. Excess inventories dictate that the plant will remain closed until a resolution to Chinese import duties is achieved.

#### Tokuyama hit by record low polysilicon prices

Asia-based polysilicon producer Tokuyama Corp said it would take a one-time impairment charge of ¥123.4 billion (US\$1.02 billion) on its two polysilicon plants in Malaysia as ASPs were lower than expected and not in-line with previous business guidance.

Polysilicon spot market prices were said to have dropped below the historical bottom set in December, 2012 when prices reached US\$15.35/kg. Tokuyama had previously expected prices of around US\$16/kg to US\$20/kg in its 2017 business plan, but prices are now set to be in the range of US\$13.5/kg to US\$15/kg in its revised 2017 business plan.

To return to profitability with its polysilicon production, Tokuyama noted that it undertook major maintenance work on the Malaysian plants in October through November, 2015 as well as production cost reduction work, while enabling higher annual production of 11,000MT, though down from previous plans to run 12,000MT per annum in its 2017 business plan.

### Silver linings

#### Heraeus Photovoltaics reacts to silver powder production disruption at Dowa Hightec

PV metallization paste producer Heraeus Photovoltaics says it has bolstered its multi-supplier sourcing strategy for silver powder after an accident in early January 2016 at one of the largest producers, Dowa Hightec, left two workers dead and two injured. The plant was subsequently shut down and could be out of commission for several months, pending investigations.

Heraeus Photovoltaics said the incident had had only a partial impact on its silver paste production and supply, but acknowledged that the impact of the accident revealed that the global PV industry could be "vulnerable to an even short-term interruption of the supply of key raw materials".

To mitigate supply issues to its customers, Heraeus Photovoltaics said that it had expanded its trading partner network to include additional silver powder suppliers, while adopting a new safety-of-stock policy that would mitigate potential supply chain disruptions in the future. The supply disruption of silver powders means that Heraeus releases its newest family of pastes based on different silver powders than before.

# Inline diamond wire inspection based on resonant vibrations

Fab & Facilities

Materials

Cell Processing

Thin Film

PV Modules

Market Watch

Hubert Seigneur<sup>1,2,3</sup>, Sergei Ostapenko<sup>4</sup>, Igor Tarasov<sup>4</sup>, Chad Rodrigues<sup>4</sup>, Yuriy Zaikin<sup>5</sup>, Kevin Morrow<sup>6</sup> & Winston V. Schoenfeld<sup>1,2,3</sup>

<sup>1</sup>c-Si US Photovoltaic Manufacturing Consortium (PVMC), Orlando, Florida; <sup>2</sup>Florida Solar Energy Center (FSEC), Cocoa, Florida; <sup>3</sup>University of Central Florida (UCF), Orlando, Florida; <sup>4</sup>Ultrasonic Technologies, Inc. (UST), Wesley Chapel, Florida; <sup>5</sup>PetroBeam, Inc., Sweetwater, Tennessee; <sup>6</sup>Niabrazee LLC, Tonawanda, New York, USA

## ABSTRACT

Because the wire itself is the dominant cost in diamond wire sawing, economics dictate that the wire life must be prolonged. This paper presents recent progress made in real-time non-contact monitoring of diamond wire using the resonant vibration (RV) characteristics of the wire. This technology was successfully demonstrated on a diamond wire manufacturing line moving at 0.25m/s and showed excellent sensitivity to both plating metal thickness and diamond particle density, despite minor fluctuations in the tension. Additionally, a theoretical framework is presented which shows that the characteristics of the resonance curve do not change at speeds above 500m/s. As a result, this technology is expected to be able to meet the increasing demands of monitoring diamond wire wear during sawing as the wire speed continues to increase in the coming years.

## Introduction

As well as factors such as wire construction, wire management [1], sawing conditions, coolant properties, and material hardness, inline sawing metrology is expected to play a significant role in extending the life of the wire [2]. The need for an effective metrology to monitor diamond wire arises from the high cost of raw materials, and therefore the necessity to avoid waste. For diamond wire manufacturers, the cost/km of raw materials (core wire, diamonds, and plating metal) is the most significant.

To mitigate these challenges, there are optical techniques available for inspecting the diamond wire plating process inline [3,4]. However, these techniques suffer from several limitations:

- The wire is not continuously inspected from start to finish, but rather spot checked at regular intervals.
- The imaged wire profile is used to compute the plating thickness and diamond concentration, even though a large area fraction of the wire remains invisible.
- Since optical approaches provide only

surface diagnostics, it is not possible to detect potential subsurface defects, such as a defective core or plating-metal delamination.

- Because of the sheer amount of data required in image processing, an inline inspection in the case of high-speed applications (i.e. diamond wire sawing) is a serious challenge.
- The ingot cutting process creates a considerable amount of residue; this is harmful for high-resolution optics hardware, potentially requiring substantial tool downtime for cleaning and maintenance.

“The need for an effective metrology to monitor diamond wire arises from the high cost of raw materials.”

If it is assumed that only a fraction of a 250km spool is plated out of specifications, the result could be a loss in the thousands of dollars. In the worst-case scenario, the entire spool would have to be discarded, since the metal and diamond cannot be recovered in a cost-effective way. Similarly, losses for wafer manufacturers can be significant in the event of diamond wire failure during sawing due to wire wear or a structural defect; losses would include scrapped silicon, scrapped wire, and tool downtime to clean up the saw and rewire the web.

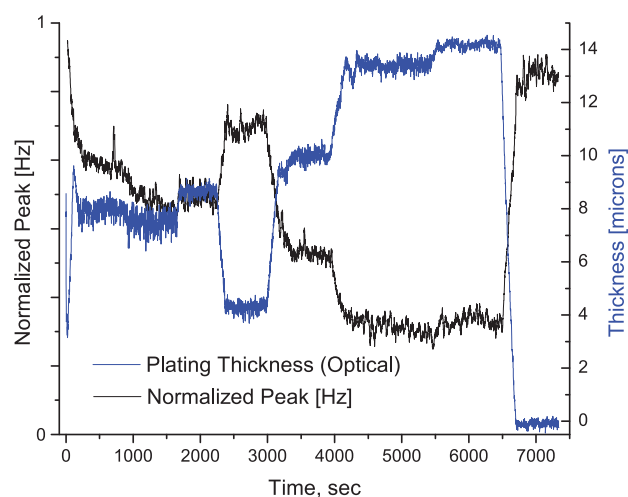


Figure 1. Normalized peak frequency (RV metrology) and plated metal thickness data (optical metrology).

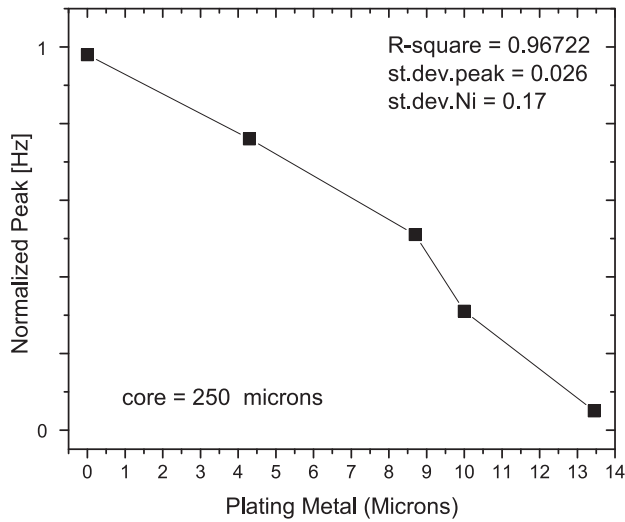


Figure 2. Normalized peak frequency (RV metrology) vs. plated metal thickness data (optical metrology).

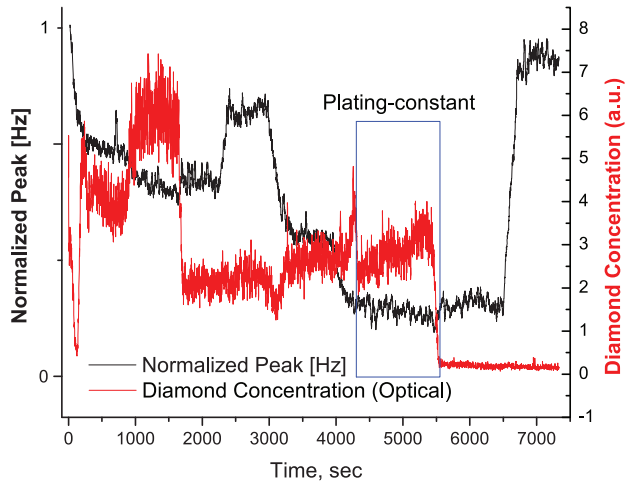


Figure 3. Normalized peak frequency vs. diamond wire concentration.

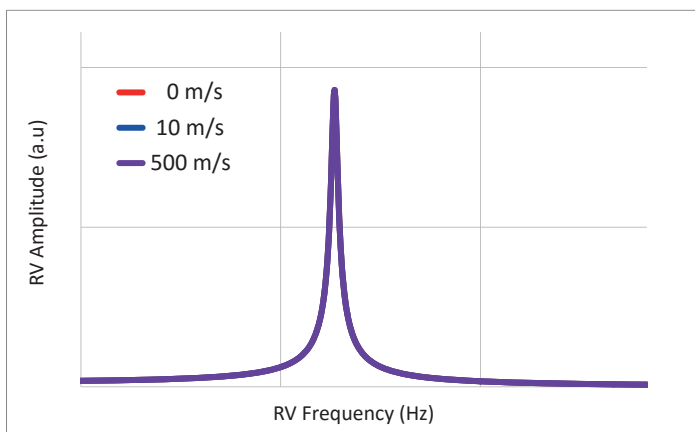


Figure 4. Resonance curve for stationary and moving diamond wire.

Clearly, an effective diamond wire metrology needs to successfully address all these challenges.

### Inline RV metrology on the diamond wire manufacturing line

A novel inline resonant vibration (RV) sensor developed through a c-Si PVMC collaborative programme was installed at the end of a diamond wire manufacturing line, with only minor modification. An additional pulley was introduced before the take-up spool set-up because of the wire moving up and down during spooling and thus causing a lateral force on the pulley adjacent to the sensor. In order to benchmark this new technology with existing optical metrology, computer clocks, sensor position and line speed were used to synchronize the optical and acoustic measurements. The optical data covers approximately 3mm of wire length, taken every 300mm, resulting in 1% of the wire being inspected. On the other hand, the RV data is taken continuously along the entire length of the wire. The core diameter used for this experiment was 250 $\mu$ m.

Fig. 1 shows the normalized peak frequency from RV metrology superimposed on a graph of the plated metal thickness generated from the optical metrology. The RV peak indicates an inverse correlation with the plated metal thickness, despite an estimated 10% variation in the tension on the basis of pre-run data. Nonetheless, the sensitivity to metal thickness is quite pronounced, as seen in Fig. 2.

Next, Fig. 3 shows the normalized peak frequency from RV metrology vs. the diamond concentration data generated from the optical metrology. From 4,500 sec to 5,500 sec (the time window indicated by a blue rectangle), the rate of plating was kept constant, while the diamond concentration was increased. Within that time window, the decrease in the peak frequency (black curve) is the result of an increase in diamond concentration (red curve). Here again, there is an inverse correlation between the peak frequency and the diamond particle concentration. Outside the identified time window, there is no clear correlation between peak frequency and diamond particle concentration, because the plating rate was allowed to change, thus affecting the peak frequency. In order to clearly see the correlation with diamond particle concentration, the effect of the plating would have to be decoupled. Furthermore, the noise in the measured RV peak frequency is much less than in

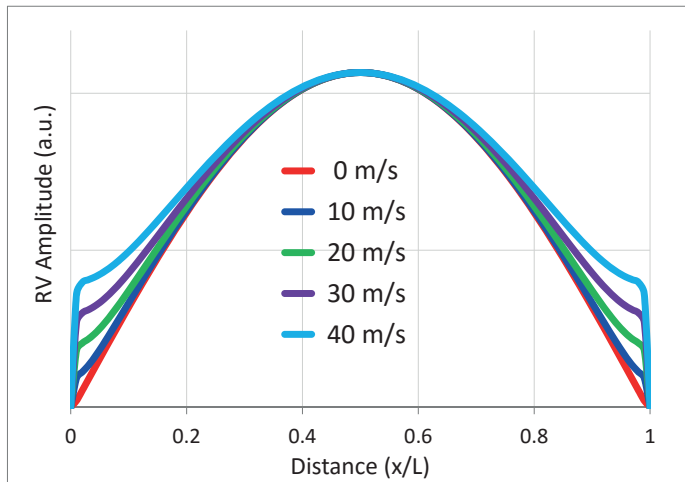


Figure 5. Vibration mode vs. diamond wire speed.

the optical data, even with fluctuations in the tension.

It is expected that the noise in the data can be minimized by correcting the RV sensor data using the real-time measurements of the wire tension. This will be the focus of future work.

### Theoretical framework for high-speed monitoring

The theoretical framework of resonance vibrations of a stationary wire has been developed and subsequently extended

to a moving wire [5,6]. Analytical equations were formulated and solved, and oscillation damping was analysed in Voigt and Maxwell models. Because the wire core diameter is expected to continue decreasing to 70 $\mu$ m within the next two years, the numerical calculations presented below were performed for a core diameter of 70 $\mu$ m and a tension of 10N. The first and most significant result is that resonance frequency is independent of diamond wire speed, which is shown in Fig. 4 by the curves being virtually

indistinguishable. This means that this inline metrology can be used as wire speed continues to increase.

Fig. 5 shows the vibration modes of the diamond wire at speeds of up to 40m/sec. Unlike the peak frequency, the shape of the vibration modes becomes slightly distorted as the speed increases.

Finally considered is the case of a wire moving at a very high speed such that damping occurs on the time scale of the vibration. The vibration mode of the diamond wire is severely distorted, as portrayed in Fig. 6, and even though the resonance damping or bandwidth is slightly affected, the resonance frequency remains unchanged from the stationary case, as shown in Fig. 4. As a result, peak frequency is an ideal metric for diamond wire monitoring as wire speeds increase in wafer manufacturing.

“The proposed new metrology is expected to be a sustainable solution as wire speeds increase.”

### Conclusion

Non-contact monitoring of diamond wire properties using the RV characteristics of the wire has been demonstrated on a diamond wire plating line with wire speeds of up to 0.25m/s. The RV peak shows a



Where: KUALA LUMPUR, MALAYSIA : When: 16 - 17 MARCH 2016

Brand new solar cell manufacturing conference from experienced events organiser  
Solar Media Ltd, parent company of leading solar technology provider PVTECH

- Understand which cell technologies will be used in the next round of capital equipment spending for GW capacity expansions.
- Interact with key stakeholders in c-Si cell manufacturing & processing, including tier 1 cell manufacturers, equipment & materials suppliers.
- Hear about efficiency & cost challenges in upgrading cell production lines, or adding advanced cell concepts in GW scale volume manufacturing.

#### Sponsors:



MEYER BURGER



#### Key Agenda Topics

##### Track 1

- Efficiency & Cost Trade-Off: GW Cell Manufacturing Challenges
- Cell Capex Cyclic Trends - Debottleneck, Upgrade or New Fab?
- Disruptive Approaches to Moving Cell Efficiencies to >20% in Production
- Where Next for Cell Capacity Additions?

##### Track 2

- Advances in Front-End Cell Processing
- PERC - The New Upgrade Cycle
- Metallization Alternatives & Status of Screen-Printing
- Automation, Integration, Inspection, Metrology

To get involved either as a speaker, partner or attendee please contact Sylvester : [sgabriel@solarmedia.co.uk](mailto:sgabriel@solarmedia.co.uk)



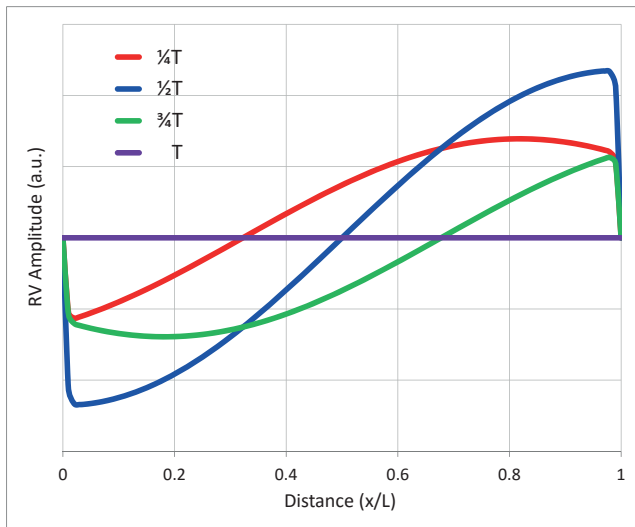


Figure 6. Vibration modes for a fast-moving diamond wire at 150m/s.

clear inverse correlation with plated metal thickness and diamond density when the plating rate is maintained at a constant value. The accuracy of this novel metrology can be further improved by incorporating real-time tension data. Moreover, the theory predicts that the RV peak is independent of the wire speed, unlike the vibration modes and to a lesser degree the damping. As a result, the proposed new metrology is expected to be a sustainable solution as wire speeds increase.

#### References

- [1] Peguiron, J., Heiniger, C. & Habegger, S. 2014, "Reduced-wear equipment for diamond wire wafering", *Proc. 29th EU PVSEC*, Amsterdam, The Netherlands, pp. 386–389.
- [2] Seigneur, H. et al. 2015, "Diamond wire sawing for PV – Short- and long-term challenges", *Photovoltaics International*, 27th edn, pp. 27–39.
- [3] List, E. 2013, "Production monitoring and quality control of thin diamond wire" [[http://www.anglosterling.com/presentation/diamond\\_wire/diamond\\_wire.shtml](http://www.anglosterling.com/presentation/diamond_wire/diamond_wire.shtml)].
- [4] List, E. 2015, "Real-time monitoring of the thin diamond wire manufacturing process", Technical Presentation, Intertech 2015, Indianapolis, Indiana, USA.
- [5] Babakov, N.M. 1968, *Oscillation Theory* [in Russian], Moscow: Nauka.
- [6] Zaykin, Y.A. 2003, "Elastic energy dissipation in radiation-damaged solids", Al Farabi Kazakh National University, Almaty, Kazakhstan.

#### About the Authors



**Dr. Hubert Seigneur** is the manager of the c-Si Feedstock and Wafering Program at US PVMC, where his role involves overseeing the projects and activities of several working groups within that programme relating to new wafering methodologies, thin-wafer platforms and crack mechanics. Over the past 10 years, his research has involved semiconductor device modelling and/or fabrication in the areas of microelectronics, photonics, quantum optics and PV.



**Dr. Sergei Ostapenko** is president and CEO of Ultrasonic Technologies, Inc. He has over 20 years' experience leading R&D projects involving solar silicon, and is the inventor of the resonance ultrasonic vibration method for in-line crack detection in silicon wafers and cells. His primary expertise lies in defect diagnostics and characterization using ultrasonic technology.



**Dr. Igor Tarasov** received his Ph.D. in electrical engineering from the University of South Florida, and is a researcher and software developer at Ultrasonic Technologies, Inc. He has over seven years' experience in solid state photonics, characterization of ceramic substances using ultrasonic technology, and

creation of software for fully automated resonance ultrasonic vibration (RUV) systems.



**Chad Rodrigues** is a member of staff at Ultrasonic Technologies, Inc., specializing in hardware design, prototyping and electronic circuits. He is in charge of the development of customized electromagnets and hardware application.



**Yuriy A. Zaikin** is chief technology officer at PetroBeam, Inc. He received his M.S. in 1971 from Kazakh State University in Almaty, Kazakhstan, and his Ph.D. in physics of condensed matter in 1976 from A.A. Baikov Institute of Metallurgy in Moscow. In 1996 he received his Dr. Sci. in physics of condensed matter from the Institute of Physics and Technology (Almaty). He has published more than 250 articles in various fields, including detailed studies of diffusion and internal friction in irradiated solids.



**Kevin Morrow** is the lead process engineer at Niabrazee LLC, where he is responsible for product research and development, including fixed diamond wire used for slicing in the PV, optics and ceramics industries. He has over 25 years' experience as a controls engineer for automated industrial equipment, including electroplating, material handling and assembly machines.



**Dr. Winston V. Schoenfeld** is currently director of c-Si PVMC and director of the Solar Technologies Research Division of The Florida Solar Energy Center (FSEC) at UCF. He has authored/co-authored more than 110 journal publications in the fields of c-Si PV, MBE growth of oxide semiconductors and devices, solar blind detectors, and quantum entanglement/teleportation in self-assembled quantum dot systems.

#### Enquiries

Hubert P. Seigneur  
PVMC  
12354 Research Pkway Suite 210  
Orlando, FL 32826  
USA  
Tel: +1 (407) 823-6151  
Email: [hubert.seigneur@uspvmc.org](mailto:hubert.seigneur@uspvmc.org)  
Website: [www.uspvmc.org](http://www.uspvmc.org),  
[www.fsec.ucf.edu](http://www.fsec.ucf.edu), [www.ucf.edu](http://www.ucf.edu)

# Polysilicon vs. upgraded metallurgical-grade silicon (UMG-Si): Technology, quality and costs

Eduardo Forniés, Laura Méndez & Marta Tojeiro, Aurinka PV Group SL, Madrid, Spain

## ABSTRACT

Throughout the severe plummet of PV prices that took place during 2008–2012 as a result of overcapacity, the polysilicon sector suffered a major adjustment of costs and capacity to face the reduction in prices and the mismatch between demand and supply. In 2012 that significant drop in prices provoked the bankruptcy of many polysilicon producers, with only the large and efficient players still surviving. However, there was also an impact on the (at that time) promising and immature industry of metallurgical purification of metal silicon, also known as *upgraded metallurgical-grade silicon (UMG-Si)*. The strong selling point of UMG-Si producers – the production costs – was no longer an asset, leaving UMG-Si with nothing but its weakness – the quality. The generation costs for solar energy are currently comparable to those for conventional fuels. The solar industry is self-sustaining and is not dependent on government subsidies. In this current situation, the industry requires an updated comparison between the two main routes of silicon purification and their products, which is the aim of this paper. The first route is the *indirect route (or chemical route)*, in which the metallurgical-grade silicon (MG-Si) is transformed into a silane (typically trichlorosilane TCS, or silane MS), which is refined and finally introduced into a chemical vapour deposition (CVD) reactor where the silicon is deposited. The second route is the *direct route (or metallurgical route)*, whereby the silicon is purified by means of metallurgical processes. The principal technologies within each route, along with their main advantages and challenges, are briefly described in this paper. Subsequently, the inherent quality of the product and the costs associated with each purification route are assessed by compiling the producers' published information and the authors' analyses.

## Introduction

According to PVInsights [1], the spot prices of polysilicon have dropped from \$300/kg in 2006 to \$14/kg in 2015. Because of the high cost of the traditional polysilicon production processes that were industrially available when the demand of silicon started to be significant, back in 2004, a lot of effort in the past ten years has been put into improving costs and quality of materials aimed at the PV industry. The extremely high spot prices reached by polysilicon in the past decade (see Fig. 1) promoted big

investments in solar-grade silicon (SoG-Si), both for commercial production and for R&D activities.

High-purity silicon production processes can be divided in two main groups: the indirect or *chemical* route, and the direct or *metallurgical* route. In the indirect route, silicon is transformed by chemical reactions into a compound that can be purified by conventional chemical techniques, such as distillation. The silicon is then recovered as a pure solid from the selected compound by a chemical vapour deposition (CVD) process,

for which the two predominant technologies are Siemens and fluidized bed reactor (FBR) deposition. In the direct route, a sequence of metallurgical techniques, such as slag treatment or segregation, is applied in order to remove impurities from solid or molten silicon.

The main drawback of the Siemens-type processes for polysilicon production has traditionally been their very high specific energy requirements: typical energy consumption values range between 60 and 120kWh/kg, of which at least 45kWh/kg can be attributed to the CVD process. The use of chlorosilanes and silane as intermediates requires special handling precautions that also need to be considered. Additionally, high capital expenditures are required for establishing a new facility, along with rather long periods of planning, engineering and construction [2].

The direct route can produce different qualities of silicon, all of them called *upgraded metallurgical-grade silicon (UMG-Si)*. However, producers have refused to accept this term because, originally, the quality (99.99%) of UMG-Si was not pure enough and it had to be blended with polysilicon for PV applications. Nevertheless, in the last ten years, important industrial

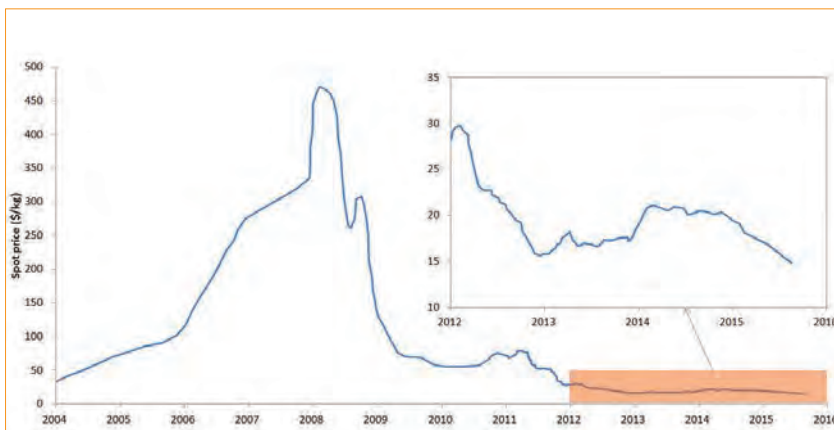


Figure 1. Evolution of polysilicon spot price.

developments in the direct route have led to improvements in silicon quality, resulting in a level of ‘silicon for PV applications’ or solar-grade silicon (SoG-Si > 5N) [3]. On the other hand, in their pursuit to reduce production costs, polysilicon producers have lowered the quality of their electronic-grade silicon (EG-Si), down to that of SoG-Si. Just to differentiate the provenance of SoG-Si, *UMG-Si* refers to the SoG-Si derived from metallurgical cleaning, and *polysilicon* refers to the SoG-Si derived from chemical cleaning. Under the polysilicon denomination, both Siemens-type silicon chunks and granular silicon coming from FBR deposition reactors are included.

“A balance should be established between silicon feedstock cost, maximum allowed impurity concentrations, and cell performance.”

A debate regarding the quality needed for PV applications has been ongoing during the past few years [4]. The specifications of this quality are still not yet defined in an unequivocal manner because of the fact that, excluding the boom period, very high-quality silicon has been available for PV applications, and so no real need to use other materials has arisen. A balance should be established between silicon feedstock cost, maximum allowed impurity concentrations, and cell performance. Since the effect of different chemical elements on cell performance varies, an oversimplification of the specifications leads to the wrong idea that only ultrahigh-purity silicon can be used for all solar PV applications. As the SoG-Si production sector reorganizes, the oversupply situation in recent years will give way to a balanced situation in which this material will not be available in such large quantities as in the past three years; new opportunities will therefore arise for low-cost materials.

Traditionally, the arguments against UMG-Si have been related to quality. It is true that the concentration of metals and dopants is higher in UMG-Si than in polysilicon; nevertheless, this level could be low enough for PV applications. As a result, that lower quality forces UMG-Si producers to sell the silicon at a lower price than polysilicon in order to make it attractive to the rest of the value chain. For example, in their work related to cells manufactured from

UMG-Si and polysilicon, Krause et al. [5] introduced the possibility of implementing a phosphorus gettering step to reduce the effects of some of the typical contaminants present in UMG-Si wafers, especially transition metals [6]. In that study, it was assessed that the price of UMG-Si should be 6 to 18% lower than polysilicon in order to counterbalance the extra cost of the gettering process; this equates to 6% in the case where the efficiencies of the solar cells made of polysilicon and UMG-Si are the same.

## Technology

### Metallurgical route

A variety of purification processes are involved in the metallurgical route [7]. None of them in isolation is efficient enough to achieve an adequate purification of metallurgical-grade silicon (MG-Si); different combinations of them, however, lead to purification sequences that can transform the MG-Si to SoG-Si. The most important processes are:

- Slag treatment of the silicon melt
- Vacuum degassing of the silicon melt
- Plasma treatment
- Acid leaching
- Purification of liquid silicon using gases
- Refining silicon from Al–Si melt
- Segregation during solidification

#### a) Slag treatment of the silicon melt

It is particularly difficult to eliminate boron by directional solidification because of its segregation coefficient in silicon (0.83) [8]. Additionally, its low vapour pressure makes it difficult to evaporate it from the silicon melt in a vacuum degassing process [9]. Consequently, slag treatment is the common method used for boron removal, although it also reduces the concentration of other impurities, such as metals and phosphorus, in the silicon melt.

Also known as *liquid–liquid extraction*, slag treatment is based on the higher solubility of certain impurities in a slag melt than in liquid silicon, or on the reactions of those impurities with some of the slag’s components to form more stable compounds. In this high-temperature process, the slags can be added to the silicon before or after its melting, depending on their composition. Once the slags are melted, they are immiscible with liquid silicon. The impurities are then dissolved in the slags, which, at the end of the process, can be extracted from the molten silicon. There are

different compositions of slags – the ones mostly used are oxides and fluorides.

#### b) Vacuum degassing of the silicon melt

Although phosphorus responds better than boron to directional solidification (segregation coefficient of P is 0.35), it is still difficult to reduce the P concentration to the levels required for the PV industry. Vacuum refining has been demonstrated to be a reliable technique for that purpose, and a large number of publications have contributed to its industrial implementation [10–13]. This technique consists of phosphorus evaporation from the silicon melt, in the form of P(g), P<sub>2</sub>(g) and to a lesser extent P<sub>4</sub>(g) [14]. The stirring of the silicon melt is therefore of major importance in order to allow an optimum transport of phosphorus to the melt surface.

The industrial application of these processes has been already developed with good results [15]. One company that currently uses vacuum degassing as one of the refining steps is Sinosi Group Corporation [16].

#### c) Plasma treatment

Plasma treatment consists of using argon gas to generate plasma, in conjunction with reactive gases that contain oxidizing species. A plasma torch is formed inside a tube and directed onto the melted silicon surface. The silicon purification begins when the reactive gases – oxygen and hydrogen – are injected into the plasma torch. Volatile species, mainly BOH and BO, are produced and extracted, with the consequent reduction of boron in the silicon melt.

The French Photosil consortium uses this process together with different directional solidifications and the selection of the raw material (MG-Si) [17]. One of the difficulties of this technique is the P concentration of the final product, which has to be under 0.6ppm<sub>w</sub>, as the directional solidification processes, by themselves, are not efficient enough for P reduction [18].

#### d) Acid leaching

During silicon solidification, the impurities with lower solubility in solid silicon than in liquid silicon tend to precipitate at grain boundaries and interstitial positions [19]. The addition of CaO and/or CaCO<sub>3</sub> promotes the formation of Ca compounds between the silicon grains; those compounds are also formed by the impurities present in the silicon [20]. The solidified silicon is then mechanically reduced to smaller pieces, which have been broken preferably along the grain



boundaries, exposing the impurities to a subsequent chemical etching with acids (HCl, HF/HNO<sub>3</sub>, etc.).

Acid leaching has been demonstrated to be efficient at removing metals – such as Fe, Al, Ca and Ti – while P has been reduced by as much as 80% [21]. Nevertheless, acid leaching is not an efficient process for boron reduction.

#### e) Purification of liquid silicon using gases

This purification procedure is based on the reaction of certain gases with the impurities in silicon to form slags or volatile species [22]. The gas treatment of the silicon melt is already a common process in MG-Si production. When the MG-Si silicon melt from the submerged arc furnace (SAF) is poured into the ladle, oxygen gas can be introduced, thus promoting the stirring of the melt and oxidizing the silicon to form SiO<sub>2</sub>, which acts as a slag to which the silicon impurities are transferred from the melt.

The same principle has been applied to UMG-Si production. Besides O<sub>2</sub>, other gases (such as chlorine) can be used for silicon refining. A mixture of O<sub>2</sub> and hydrocarbon (oxy-fuel) has been shown to be an effective method for B reduction [23].

#### f) Refining silicon from Al–Si melt

This is a metal–metal extraction process based on the fact that the melting point of Al–Si alloy is lower than that of Si, and that the solubility of Al in Si is low. A mixture of Si and Al melts at a lower temperature than Si, which means the energy needed to make the process is less. After melting in a crucible, the solution is slowly cooled and the silicon precipitates and grows in a flake shape.

In addition, the solubility of impurities in Al–Si alloy is higher than in Si [24]. The Al–Si alloy, which is still in a liquid state, is poured out from the crucible, leaving behind the silicon flakes. The silicon flakes, which are coated with a thin layer of Al, are then etched in chemical baths to remove the coating. To the authors' knowledge, Silcor Materials is the only company that uses this technique.

#### g) Segregation during solidification

The segregation method is based on the impurities' segregation coefficient  $k_i$  during a directional solidification (DS) of silicon; the segregation coefficient is the ratio between impurity concentration in the solid and the concentration of the same impurity in the melt. This means that the further the coefficient is from unity, the more effective is the segregation of

impurities. For example, metals have a very low  $k_i$ ; consequently, during a directional solidification the impurities tend to accumulate at the end of the ingot, and this part of the ingot is discarded. However, B and P have a coefficient close to unity, thus making DS an inefficient process for B and P reduction.

DS is a common technique in all the metallurgical refining processes, and can take place during casting in the SAF furnaces or within the refining process itself. In the next step of the value chain, namely crystal growth, DS is indeed the process used to produce silicon ingots; therefore there is an additional purification in this step [4].

There are a wide range of furnaces and castings that take advantage of the segregation properties of certain elements within silicon. A rapid segregation can be carried out during casting, allowing the silicon melt to cool down naturally while a magnetic stirring of the melt is performed by induction. This stirring promotes the transportation of impurities to the crystallization front and enhances their segregation. In the case of silicon crystallization, there are other examples of directional solidification, such as the use of furnaces quite similar to those used for silicon growth, based on the heat exchange method. However, this is an expensive process, which takes place in a vacuum or inert environment, and serves only for the advanced stages of silicon purification.

#### Other approaches

Other metallurgical processes have not been considered here, because of their poor, or lack of, representation in the industry. Alternative approaches to purifying silicon include the chemical purification of silicon- and carbon-containing compounds that are later transformed into high-purity raw materials used for MG-Si production, specifically silica (SiO<sub>2</sub>) and carbon. A case in point is the ChemArc Process developed by RSI Silicon Products LLC, in which sodium silicate is thoroughly purified by chemical techniques and subsequently reduced with pure carbon in a modified SAF furnace, to yield a solar-grade product.

#### Chemical route

The indirect, or chemical, route for high-purity silicon production has been used since 1950, when the first applications for this material within the semiconductor industry appeared. The evolution of the technology has been slow for several decades, since electronic devices use only a tiny

amount of material. Today, the total demand for electronic-grade silicon (EG-Si) is approximately 30,000 MT/year – one order of magnitude lower than the demand for solar-grade.

Current commercial chemical technologies for the purification of silicon can use trichlorosilane (TCS, SiHCl<sub>3</sub>) or silane (MS, SiH<sub>4</sub>). The processes have in common the fact that the selected silicon compound undergoes a CVD reaction at a high temperature, which can be carried out by means of the traditional Siemens reactors or the less widespread FBR technology [25].

The commercially implemented processes in use today are, in essence, different combinations of precursor synthesis and by-products recycling, together with various deposition alternatives:

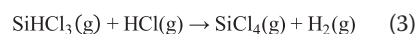
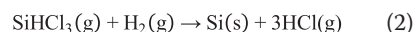
- TCS Siemens with direct chlorination (DC) and silicon tetrachloride thermal conversion
- TCS Siemens with hydrochlorination (HC)
- MS Siemens
- MS FBR

#### a) TCS Siemens with direct chlorination (DC) and silicon tetrachloride thermal conversion (Fig. 2(a))

MG-Si is converted to trichlorosilane (TCS) by a reaction with hydrogen chloride, according to the following equation:



Metallic impurities included in the MG-Si are transformed into their corresponding metal chlorides, remaining in solid phase after the reaction takes place. Boron and phosphorus are also transformed into their chlorides, which are gases in process conditions. TCS is separated from them, and the other chlorosilanes are further refined to the required purity levels, mainly by fractional distillation. The TCS is then mixed with hydrogen and decomposed in the Siemens reactor, yielding solid high-purity silicon and large amounts of silicon tetrachloride (STC, SiCl<sub>4</sub>) as a by-product:



Siemens reactors are hot-filament cold wall reactors in which pure silicon rods are heated up through the Joule effect by means of an electrical power supply with variable current and voltage. As the silicon deposition

reaction takes place in the surface of the rods, their diameter grows, until it reaches a maximum value that depends on reactor geometry.

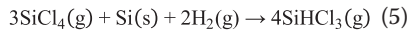
Unreacted TCS and other chlorosilanes present in the Siemens gaseous effluent are condensed and hydrogen is recovered. STC is transformed back to TCS by a high-temperature conversion reaction:



This has been the technology used by incumbent producers for many years, and is still in use by many of them today, their proprietary developments being better than the commercially available alternatives.

#### b) TCS Siemens with hydrochlorination (HC) (Fig. 2(b))

MG-Si and silicon tetrachloride, recovered from the deposition step, react with hydrogen to produce TCS, according to the following overall stoichiometry:



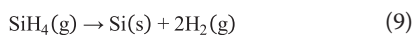
As in the case of the DC process, chlorosilanes are separated and purified by means of a fractional distillation stage. Pure TCS is fed into the Siemens reactor, and STC is recycled to supply the hydrochlorination step. This technology has been adopted by most of the Chinese producers since 2012, following the sharp drop in polysilicon price that came with the oversupply.

#### c) MS Siemens

Only REC Silicon uses the MS Siemens process on a commercial scale. TCS is synthesized by hydrochlorination (Equation 5) and is subject to redistribution reactions to produce silane along with silicon tetrachloride, which is recycled to supply the hydrochlorination step.



The silane, after being purified, is fed into a Siemens-type reactor. Silane decomposition does not yield any by-product apart from hydrogen, which is normally used as a carrier gas in these reactors.



#### d) MS FBR (Fig. 2(c))

This alternative, known as the *Union*

*Carbide Process*, has the same flow diagram as the MS Siemens process, the only difference being that the deposition of solid silicon takes place in an FBR. This reactor has a continuous supply of silane and small beads of pure silicon, which are the seeds for heterogeneous deposition of silicon. Only REC Silicon uses this technology on a commercial scale, although GCL-poly has recently started pilot production. In the case of SunEdison, its plant in Pasadena, Texas, uses an alternative process for silane production, known as the *ethyl corporation process*, in which an alkaline fluorosilicate serves as the starting material instead of MG-Si.

#### e) Other chemical processes

Many processes have been studied and scaled up with different degrees of success. The most important is CVD in the FBR from trichlorosilane, which can be obtained by the procedures described for Siemens technology. Several plants on a pilot scale have been operated by various companies, but their maturity has not yet been sufficiently proved for them to be scaled up to commercial throughputs.

“Many processes have been studied and scaled up with different degrees of success.”

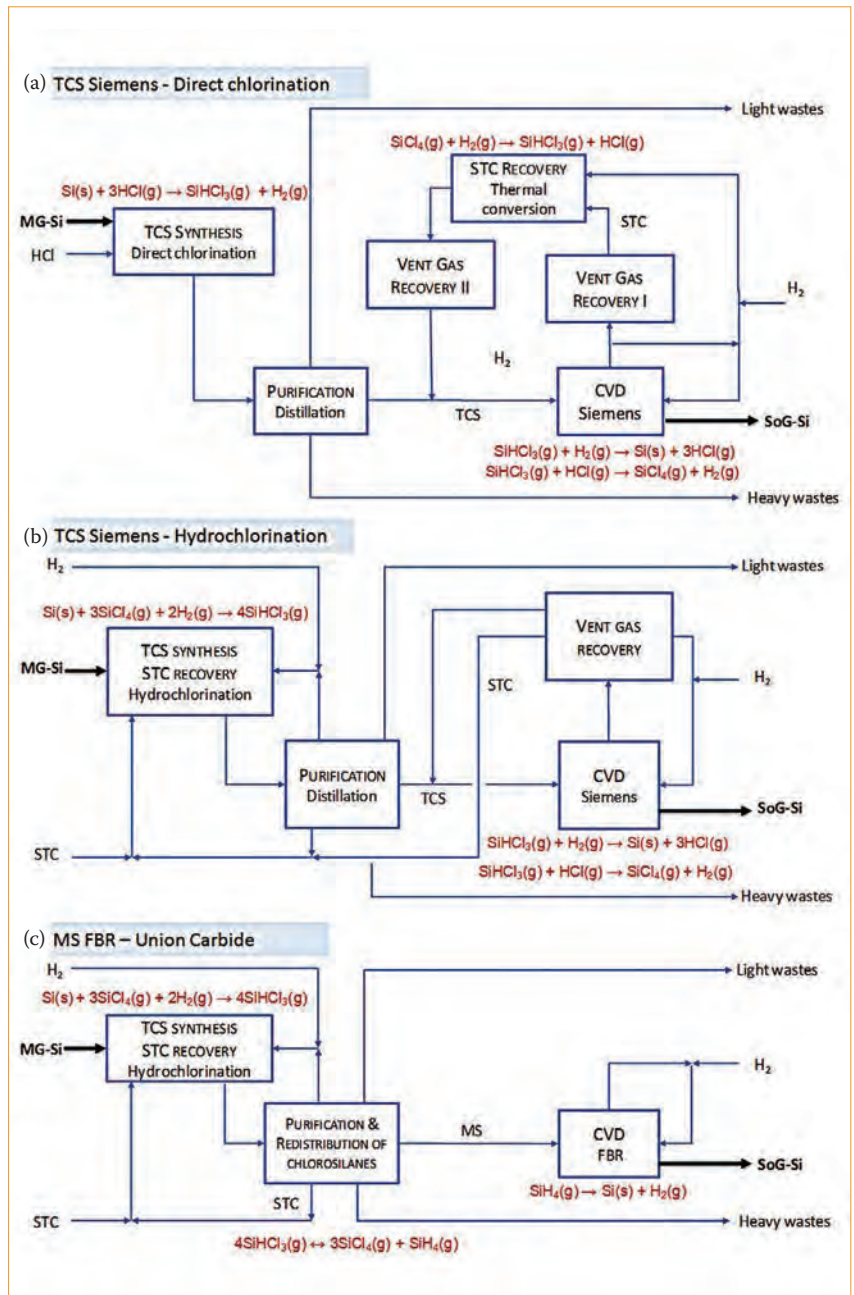


Figure 2. Simplified block diagrams of polysilicon production: (a) TCS Siemens with direct chlorination; (b) TCS Siemens with hydrochlorination; and (c) MS FBR (with hydrochlorination and redistribution).

Of the above-mentioned technologies, two are used industrially for polysilicon production by chemical methods. The first is traditional trichlorosilane Siemens-based silicon deposition, which accounts for around 90% of the total polysilicon production, both by direct chlorination and by hydrochlorination. The second is FBR deposition from silane, responsible for the other 10% of polysilicon production.

## Quality

The global industry association of micro- and nanoelectronics, which includes the PV industry, has issued a standardized specification to classify the different categories of silicon for PV applications [26], that is to say, SoG-Si (see Table 1, in which the values in ppm<sub>w</sub> have also been included, along with the total purity in nines N). This classification includes silicon feedstock purified by the metallurgical route (grades III, IV), as well as polysilicon for PV applications (grades I, II).

The standardization of SoG-Si, however, is not straightforward, since the elements present in the silicon feedstock have different effects on cell performance. For standardization purposes, three different categories of element within silicon can be defined: dopants (B, P, Al, etc.), metallic impurities (Fe, Cr, Ni, Ti, etc.) and non-metal impurities (N, O, C, etc.).

## “The elements present in the silicon feedstock have different effects on cell performance.”

The type of silicon (n or p) is defined by the concentration of dopants (donor or acceptor). In the case of SoG-Si, the material is usually compensated with a significant concentration of donors and acceptors. The compensation ratio  $R_c = (N_A + N_D) / |N_A - N_D|$  is a figure of merit that involves the level of compensation and the total concentration of dopants.

### Dopants

Boron is an acceptor p-type dopant. It has similar properties to silicon, which makes it a difficult element to remove from silicon and its compounds. The SoG-Si producer has to balance the concentration of B in the silicon and the resources needed to reduce its concentration to an acceptable limit. This is also true for P, a donor dopant responsible for the n-type characteristic of silicon. As can be expected from this consideration, the compensation of silicon and its influence on final cell performance have been studied from the point of view of minority-carrier lifetime and mobility [27]. It has been reported that the reduction of minority-carrier mobility because of scattering

in ionized impurities is balanced by the increase in lifetime as a result of free-carrier reduction [28]. Other authors have described a net improvement in solar cell performance when using compensated silicon [29], but this is in contradiction to the results obtained by Hoffmann et al. [30], who showed a linear decrease in efficiency with  $R_c$  in solar cells made of UMG feedstock. Other considerations as well as mobility and lifetime therefore have to be taken into account:

- Compensated silicon presents a low yield in silicon growth. The reason for this is that the high concentration of P tends to change the resistivity of the ingot from positive (in the case of p type) to negative as a result of the accumulation of P in the melt in the final stages of silicon growth. This effect can be mitigated by doping the charge with gallium [31].
- It is known that boron in combination with oxygen has an effect on light-induced degradation (LID). For p-type solar cells made of polysilicon, an LID of 0.5 to 1% has been shown for Cz-Si solar cells, whereas for multicrystalline solar cells the LID has been found to be lower – 0.1 to 0.2%<sub>abs</sub> [32]. However, for solar cells made of UMG, an LID of up to 2.5%<sub>abs</sub> has been reported [33].
- Dopant atoms can themselves form recombination-active centres, such as

	Grade I		Grade II		Grade III		Grade IV	
	ppb <sub>a</sub>	ppm <sub>w</sub>	ppb <sub>a</sub>	ppm <sub>w</sub>	ppb <sub>a</sub>	ppm <sub>w</sub>	ppb <sub>a</sub>	ppm <sub>w</sub>
B	1	0.00038	20	0.01	300	0.12	1000	0.38
C	300	0.12828	2000	0.86	5000	2.14	100000	42.76
Na	10	0.00819	50	0.04	100	0.08	4000	3.27
Al	1	0.00096	20	0.02	300	0.29	1000	0.96
P	1	0.00110	20	0.02	50	0.06	720	0.79
K	10	0.01392	50	0.07	100	0.14	4000	5.57
Ca	10	0.01427	50	0.07	100	0.14	4000	5.71
Ti	10	0.01705	50	0.09	100	0.17	200	0.34
Cr	10	0.01851	50	0.09	100	0.19	200	0.37
Fe	10	0.01989	50	0.10	100	0.20	200	0.40
Ni	10	0.02090	50	0.10	100	0.21	200	0.42
Cu	10	0.02263	50	0.11	100	0.23	200	0.45
Zn	10	0.02328	50	0.12	100	0.23	200	0.47
As	1	0.00267	20	0.05	50	0.13	720	1.92
Mo	10	0.03416	50	0.17	100	0.34	200	0.68
Sb	1	0.00433	20	0.09	50	0.22	720	3.12
	6.7N		5.8N		5.5N		4.3N	

Table 1. SEMI classification of silicon for PV applications [25].

the already mentioned boron–oxygen defect or FeB and CrB [27].

- Although compensation can enhance cell performance because of the increase in carrier lifetime, this applies to already compensated silicon, which has a high concentration of B and P as well as other doping species [29], and should not lead to the conclusion that compensated silicon is better than high-purity silicon. Taking into account ingot yield, LID and cell efficiency, Degoulange et al. [33] suggest the following specifications for UMG-Si:

$$[B] < 0.2\text{ppm}_w, [O_i] < 20\text{ppm}_w \text{ and } [P] < 0.5\text{ppm}_w$$

whereas Hoffmann et al. [30], according to the limiting influence of dopant concentration on solar cell efficiency, propose:

$$[B] < 0.15\text{ppm}_w \text{ and } [P] < 0.3\text{ppm}_w$$

**Metallic impurities**

Metallic impurities introduce deep energy levels in the silicon band gap that act as minority-carrier recombination

centres, provoking a decrease in solar cell performance. Moreover, it is known that interstitial Fe forms pairs with B; this introduces, within the gap, energy levels close to the conduction band, thus reducing the minority-carrier lifetime [34]. The same happens with Cr atoms, but this new energy level is close to the valence band [29]. Metals such as Fe and Ni can form precipitates that also act as recombination centres [34–36].

The impact of some metallic impurities can be reduced by techniques such as gettering [34,37,38] or hydrogenation [39], performed at the solar cell production level. Regarding their behaviour and influence within the solar cell, metal impurities can be divided into two categories: fast-diffusing impurities (e.g. Fe, Cr, Cu and Ni), which are receptive to gettering, and slow diffusers (e.g. Ti, Mo and V) [40]. The latter should be avoided, as they have a significant negative impact on solar cell efficiency because of their insensitiveness to gettering.

Aluminium is also a critical element, since it is an acceptor like boron. As a

consequence, the resistivity and carrier concentration are strongly affected by this metal impurity; moreover, it cannot be reduced by gettering. Owing to the features of the Silicor process, aluminium is an element that can be found at high concentrations in this company’s product. According to studies related to Silicor UMG [38], the performance of cells made of compensated silicon that were intentionally contaminated with Al up to 1ppm<sub>w</sub> showed a 3%<sub>rel</sub> lower efficiency than those without that extra contamination. Aluminium in silicon can also originate from the alumina insulators of directional solidification furnaces as well as from some furnaces used in UMG processes.

**Non-metallic impurities**

Non-metallic impurities consist mainly of C, N and O. The sources of these elements are diverse: for example, carbon can be incorporated into the silicon during its growth, as some of the thermal insulators of furnaces are made of graphite. This is also the case in the

	Siemens						FBR	UMG			Other
	Producers A and B Specs – Low Grade	Producers A and B Specs – High Grade	Producer C Specs – High grade	Producer D Specs – Solar poly	Producer E Specs – Solar poly	Producer F Specs – Solar poly	Producer G Specs – Granular poly	ELKEM Specs – ESS 2015 [46]	Silicor Materials Promotional data 2015	PHOTOSIL Published data 2015 [18]	RSI Promotional data 2015
B	1	0.2	0.04	0.04	0.04	1.92	0.31	200	300	300	81
P	8.5	1.65	0.44	5.51	0.33	5.51	0.88	600	740	600	84
Al						10		150	100	100	18
Ti								80			
Cr				2	1	2					12
Fe				10	10	10		80		100	80
Ni				2	1	2					20
Cu				2	1	2				100	30
Zn				4	2	4					5
Na				15	6	15			50		26
K				10		10					15
Ca								3000			50
Bulk metals (Fe,Cu,Ni,Cr,Zn,Na)			3	15	2	15					
Surface metals total			5	30			30*				
Oxygen	1710	1140									
C	385	214	43	43	107	428	100		15		

\*ppb<sub>a</sub>

**Table 2. Concentrations of impurities (ppb<sub>w</sub>) for different SoG-Si producers. All data are extracted from specifications, promotional data or publications, and are therefore maximum values. (Empty cells represent no available data.)**

metallurgical purification of silicon, which also uses graphite crucibles to perform the silicon casting. In silicon growth, nitrogen is also incorporated from the  $\text{Si}_3\text{N}_4$  coating of the crucibles used in the directional solidification of multi-crystal ingot growth. During Czochralski growth for producing single-crystal ingots, the contamination of silicon with oxygen coming from the silica crucible is also very common.

As a result, the concentration of C, N and O in silicon is about one order of magnitude greater than that of metals. Carbon and nitrogen can form precipitates of  $\text{SiC}$  and  $\text{Si}_3\text{N}_4$  during silicon solidification. Those precipitates are very harmful, as they provoke lattice distortions, shunts in solar cells [41], wire breakage during ingot wafering, crucible damage during MG-Si purification, and so on. In particular, carbon is very detrimental to Czochralski (Cz) growth; silicon for that purpose therefore typically has a C concentration below 1ppm<sub>w</sub>, which makes UMG-Si unsuitable for direct use in single-crystal wafers. Directional solidification for multi-crystal ingot growth, on the other hand, permits up to 30ppm<sub>w</sub> of carbon [4].

The relationship of oxygen, in combination with boron, to LID was mentioned earlier. For granular silicon obtained by FBR deposition, the silicon oxide formed on the surface of the silicon grains as soon as they are exposed to air is very extensive because of the high surface-to-volume ratio. Moreover, during the CVD process, hydrogen is absorbed on the surface of the particles, which can

cause explosions and the splashing of molten silicon during ingot growth. Siemens polysilicon, however, does not exhibit this high O concentration, as it is obtained as large chunks. Graphite pieces are also used in Siemens-type CVD reactors, although the silicon in contact with these pieces is separated from the rods and sold separately as a different grade of polysilicon.

A comparison of the main impurity concentrations for different SoG-Si, including polysilicon, extracted from specification sheets available online and documentation made public by producers, is shown in Table 2. Several studies on the efficiency of solar cells fabricated from UMG-Si [30,38,42–44] or from intentionally contaminated silicon [45] have been conducted; the resulting efficiencies are quite similar to those obtained from polysilicon feedstock, and the outdoor power degradation is low [46].

In Fig. 3 the concentration ranges of boron and phosphorus for different commercial products are compared and classified according to the standard specifications for the four defined grades.

### Technological challenges of reducing cost

#### Chemical route

Although the application of TCS Siemens technology to the industrial production of polysilicon dates back to the 1960s, it is only during the last decade, driven by the pressure of the PV market, that a significant cost reduction has been achieved by process optimization. In this regard,

the replacement of inefficiently designed or nonexistent STC recovery schemes by the proven more cost-effective hydrochlorination technology has put some of the new producers, especially in China, in a position to realise cash operation costs below \$12/kg [4].

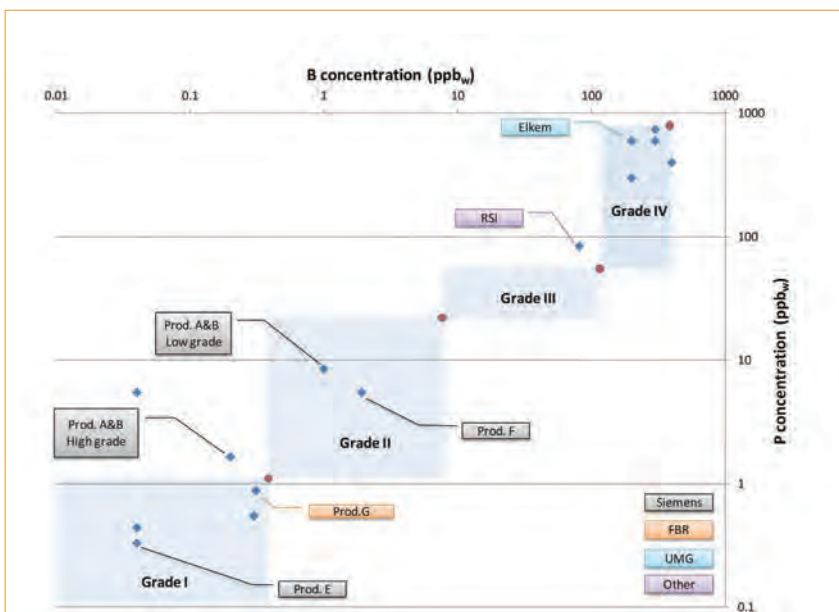
A large part of the cost reduction has been achieved in Siemens deposition reactors. The development of both equipment and recipes that are tailored to solar-grade polysilicon production, and are less demanding in terms of purity than electronic-grade polysilicon, has led to higher silicon deposition velocities and throughput, resulting in lower costs. Energy-saving strategies, mainly the reduction of heat losses and the recovery of part of the supplied electrical power as vapour for heating in other processes of the polysilicon plant (such as the fractional distillation of chlorosilanes), have reduced specific electricity consumption to around 45kWh/kg for state-of-the-art Siemens reactors; of this, over 50% can be recovered.

**“The main strength of silane deposition in FBRs is the very low energy demand of these reactors.”**

On the other hand, the main strength of silane deposition in FBRs is the very low energy demand of these reactors – as low as 5kWh/kg. The low-cost mass production of granular polysilicon is currently taking shape. Two joint ventures have been established by the companies with industrial experience in FBR deposition – SunEdison and REC Silicon – with new plants also employing this technology. In addition, GCL-poly has become a new player in FBR technology, setting up a plant that started its ramp-up in 2014 [25]. Centrotherm SiTec, one of the top polysilicon technology providers, has recently announced that it is developing its own FBR CVD process and reactors [48], which are expected to be available within two years.

Even though at first sight the large difference that exists between electrical power consumptions might suggest that traditional Siemens reactors should be replaced by FBR technology, other important aspects need to be taken into account, such as the quality of the product [49]. Further progress is expected for both technologies.

Although major improvements in



**Figure 3. Concentration ranges of boron and phosphorus in different SoG-Si specifications.**

performance and costs have been achieved during the last decade, research and development is still being carried out regarding the deposition equipment and processes, including studies of CVD in FBRs, for both silane and trichlorosilane [50,51], and of the energy consumption reduction of Siemens reactors.

The precursor synthesis, to produce TCS and MS, has a lower impact on overall polysilicon production costs. Hydrochlorination, because of the advantages of combining TCS synthesis and STC–TCS conversion in one step, has been replacing a significant part of the direct chlorination and thermal conversion capacity during the last few years. While hydrochlorination has advantages over the direct chlorination and thermal conversion combination, it also has some drawbacks, such as the low STC conversion rate and the need to combine pure and impure streams, which result in the need to manage a greater amount of material, especially recycled STC. New reactions are being studied, such as the catalytic hydrodechlorination of STC [52], in order to avoid the introduction of additional impurities into the TCS synthesis, and thus reduce costs associated with purification.

**Metallurgical route**

Unlike the chemical route, the metallurgical route emerged with the clear aim of reducing the costs of producing SoG-Si, which means the margin for further cost reduction is much ‘thinner’. The main challenges of the metallurgical route are the reduction of silicon losses and the recycling of intermediate silicon to obtain satisfactorily refined silicon. Some of the metallurgical processes (described above) are based on the accumulation of impurities in certain small segments of the silicon. Those

parts are rejected (which accounts for silicon losses) or recycled, thus increasing the production costs.

Most of the metallurgical treatments are followed by a block casting in which some kind of directional solidification is performed. The environment during that solidification, the mass transport to the solidification front, and the material of the crucibles or moulds are essential factors that directly influence the yield of purified silicon. As in directional solidification, the purification by vacuum or gas treatment requires a stirring of the silicon melt in order to increase the mass transfer of impurities to the surface, where the refining takes place.

In acid leaching, the optimal size of silicon chunks is of major importance in optimizing the removal of impurities from the grain boundaries and the surface. In this case, the waste treatment of by-products is very important. For slag treatment, it is essential to choose

the correct slags, as well as the contact optimization between slags and silicon. Key steps after the refining are the complete extraction of slags from the melt and their post-processing, as these can contain a high percentage of usable silicon.

In summary, effective processes in terms of silicon yield and reduction of losses are critical in achieving low operational cash costs and energy consumption. The authors consider that, for metallurgical purification, the operational cash costs should be below \$12/kg and the energy consumption below 25kWh/kg, although other considerations, such as capital expenditure, are important.

**Cost analysis**

Some studies have been published in the past regarding polysilicon production costs [53–55], but there is a lack of information about the costs of

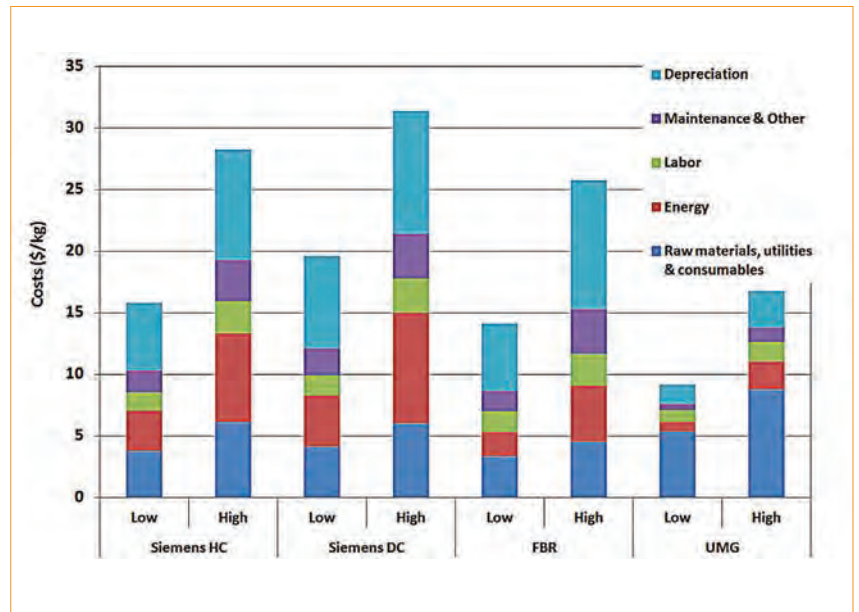


Figure 4. Cost breakdown for different technologies for state-of-the-art facilities and low- and high-cost scenarios.

	Siemens HC		Siemens DC		FBR		UMG	
	Low	High	Low	High	Low	High	Low	High
Raw materials, utilities and consumables	3.8	6.1	4.1	6.0	3.4	4.5	5.4	8.8
Energy	3.2	7.2	4.1	9.0	1.9	4.5	0.8	2.3
Labour	1.5	2.6	1.7	2.8	1.7	2.6	1.0	1.6
Maintenance and other	1.8	3.3	2.2	3.6	1.7	3.6	0.4	1.1
Cash cost	10.3	19.2	12.1	21.4	8.6	15.3	7.5	13.8
Depreciation	5.5	9.0	7.5	10.0	5.5	10.5	1.6	3.0
Manufacturing cost	15.8	28.2	19.6	31.4	14.1	25.8	9.1	16.8

Table 3. Cost breakdown [\$/kg] for different technologies for the best state-of-the-art facilities and low and high scenarios.

the main silicon-refining technologies, namely Siemens, FBR and UMG. Cash costs can be analysed for these cases by taking into account various requirements, such as raw materials, utilities, energy, labour, consumables and maintenance.

It is important to note that there are other aspects, apart from the technology itself, which have a significant impact on the final cash cost figure – electricity price and labour wages at the location of the facility, MG-Si and other raw material prices, the level of automation and scope of the facility (for example, whether or not it manufactures some of the raw materials in-house), and so on. The proposed breakdown, which is useful for comparing different technologies, evaluates a low- and a high-cost scenario for each technology, taking into account appropriate ranges of values for both consumption and unitary cost.

The calculation of the costs is based on the assumption of a nominal capacity of over 15,000MT/year with the use of state-of-the-art technology. The data are presented in Table 3 and shown graphically in Fig. 4. Auxiliary chemicals or waste treatment are included under the category of 'other'.

The manufacturing costs for polysilicon depend on the specific technology. In the case of the chemical route, Siemens with hydrochlorination and FBR can yield costs below \$20/kg. For UMG-Si production, the manufacturing costs can come to just under \$10/kg in a low-cost scenario, characterized by much lower capital costs (around one-third) when compared with the rest of the processes.

## Conclusions

This paper has reviewed the key technological quality vs. cost aspects associated with the chemical and metallurgical approaches to silicon refining. The representative techniques of silicon purification used in both of those approaches have been briefly described. The study of quality, although applicable to any type of silicon, has focused on the metallurgical route because the obtainable purity is lower than that for the chemical route; indeed, a comparison of the concentration of different elements in SoG-Si materials showed a lower presence of impurities and dopants in the silicon obtained by chemical processes. The key question, then, is what the level of purification needs to be achieved in order to strike a good balance between costs and potential cell efficiency.

## “UMG-Si can be considered to be a good alternative to polysilicon.”

Studies referenced in the 'Quality' section, and work carried out by Aurinka, reveal that the solar cell efficiencies obtained from UMG feedstock are close to those obtained from polysilicon, leading to the conclusion that UMG-Si can be considered to be a good alternative to polysilicon. Cell production treatments (gettering, hydrogenation, etc.) that focus on the minimization of the effects of contaminants can offer positive contributions, with further increases in cell efficiency. Finally, the production cash costs of UMG-Si and FBR compared with Siemens HC and Siemens DC make the former alternatives a reasonable choice, especially taking into account that silicon feedstock prices fell to \$14/kg, or even lower, towards the end of 2015 [1,56].

### References

- [1] PVinsights 2016, PV poly silicon prices [www.pvinsights.com].
- [2] Bernreuter, J. 2014, "The 2014 who's who of solar silicon production", Bernreuter Research [http://www.bernreuter.com/fileadmin/user\_upload/silicon\_report/Solar-Silicon-Report-2014-Info.pdf].
- [3] Kohler, D., Seren, S. & Raabe, B. 2011, "Return of UMG-Si: a new hope", *Photovoltaics International*, 12th edn, pp. 42–48.
- [4] Pizzini, S. 2012, *Advanced Silicon Materials for Photovoltaic Applications*. Milan: Wiley & Sons.
- [5] Krause, R. et al. 2010, "Advantages and shortcomings of UMG silicon in photovoltaics device production", *Photovoltaics International*, 8th edn, pp. 38–50.
- [6] Sopori, B.L., Jastrzebski, L. & Tan, T. 1996, "A comparison of gettering in single- and multicrystalline silicon for solar cells", *Proc. 25th IEEE PVSC*, Washington DC, USA.
- [7] Heuer, M. 2013, "Metallurgical grade and metallurgical refined silicon for photovoltaics", *Semiconduct. Semimet.*, Vol. 89, pp. 77–134.
- [8] Hall, R.N. 1953, "Segregation of impurities during the growth of germanium and silicon", *J. Phys. Chem.*, Vol. 57, pp. 836–839.
- [9] Morito, H. et al. 2012, "Low-temperature purification of silicon by dissolution and solution growth in sodium solvent", *Silicon*, Vol. 4, pp. 121–125.
- [10] Yuge, N., Hanazawa, K., Nishikawa,

- K. & Terashima, H. 1997, "Removal of phosphorous, aluminum and calcium by evaporation in molten silicon", *J. Jpn. Inst. Met.*, Vol. 61, pp. 1086–1093.
- [11] Safarian, J. & Tangstad, M. 2010, "Vacuum behaviour of the dissolved elements in molten silicon", *Proc. Silicon Chem. Solar Ind. X*, Ålesund-Geiranger, Norway.
- [12] Pires, J.C.S., Braga, A.F.B. & Mei, P.R. 2003, "Profile of impurities in polycrystalline silicon samples purified in an electron beam melting furnace", *Sol. Energy Mater. Sol. Cells*, Vol. 79, pp. 347–355.
- [13] Zheng, S.S. et al. 2010, "Mass transfer of phosphorous in silicon melt under vacuum induction refining", *Metall. Mater. Trans. B*, Vol. 418, pp. 1268–1273.
- [14] Zheng, S., Engh, T.A., Tangstad, M. & Luo, X.T. 2011, "Numerical simulation of phosphorous removal from silicon by induction vacuum refining", *Metall. Mater. Trans. A*, Vol. 42A, pp. 2214–2225.
- [15] Souto, A., Bullón, J., Ordás, R. & Miguez, J.M. 2014, "Industrial scale vacuum application in the FerroSolar project", *Proc. Silicon Chem. Solar Ind. XII*, Trondheim, Norway.
- [16] Sinosi Group Corp. 2016, "Our facilities" [http://pv.sinosi.com/facilities.htm].
- [17] Fourmond, E. et al. 2004, "Refining of metallurgical silicon for crystalline solar cells", *Proc. 19th EU PVSEC*, Paris, France.
- [18] Cocco, F. et al. 2013, "Photosil UMG silicon: Industrial evaluation by multi-C p-type ingots and solar cells", *Proc. 28th EU PVSEC*, Paris, France.
- [19] Juneja, J.M. & Mukherjee, T. 1986, "A study of the purification of metallurgical grade silicon", *Hydrometallurgy*, Vol. 16, pp. 69–75.
- [20] Schei, A. 1986, "A metallurgical route to solar-grade silicon", *Proc. Flat-plate Solar Array Project Worksh. Low-cost Poly. Terrest. Photovolt. Solar Cell Appl.*, Las Vegas, Nevada, USA.
- [21] Shimpo, T. et al. 2004, "Thermodynamic study of the effect of calcium on removal of phosphorous from silicon by acid leaching treatment", *Metall. Mater. Trans. B*, Vol. 35B, pp. 277–284.
- [22] Khattak, C.P., Joyce, D.B. & Schmid, F. 2002, "A simple process to remove boron from metallurgical grade silicon", *Sol. Energy Mater. Sol. Cells*, Vol. 74, pp. 77–89.
- [23] Leblanc, D. & Boisvert, R. 2008, "Process and apparatus for purifying low-grade silicon material", US Patent US2008/0253955 A1.
- [24] Apel, M., Hanke, I., Schindler, R.

- & Schröter, W. 1994, "Aluminium gettering of cobalt in silicon", *J. Appl. Phys.*, Vol. 76, pp. 4432–4433.
- [25] Bernreuter, J. 2012, "Polysilicon production technologies in a volatile market", *Photovoltaics International*, 18th edn, pp. 29–32.
- [26] SEMI PV17-0611 2011, "Specification for virgin silicon feedstock materials for photovoltaic applications".
- [27] Coletti, G., Macdonald, D. & Yang, D. 2012, "Role of impurities in solar silicon", in *Advanced Silicon Materials for Photovoltaic Applications*, Milan: John Wiley & Sons, pp. 79–125.
- [28] Rougieux, F.E. 2012, "Impact of dopant compensation on the electrical properties of silicon for solar cell applications", Dissertation, Australian National University.
- [29] Dubois, S. et al. 2008, "Beneficial effects of dopant compensation on carrier lifetime in upgraded metallurgical silicon", *Proc. 23rd EU PVSEC*, Valencia, Spain.
- [30] Hoffmann, V. et al. 2015, "Effect of total dopant concentration on the efficiency of solar cells made of CS Silicon", *Proc. 31st EU PVSEC*, Hamburg, Germany.
- [31] Forster, M. et al. 2010, "Doping engineering to increase the material yield during crystallization of B and P compensated silicon", *Proc. 25th EU PVSEC*, Valencia, Spain.
- [32] Sondenå, R. 2015, "Boron-oxygen-related degradation in multicrystalline silicon wafers", *Photovoltaics International*, 28th edn, pp. 22–26.
- [33] Degoulange, J. et al. 2012, "Dopant specifications for P-Type UMG silicon: Mono-C vs multi-C", *Proc. 27th EU PVSEC*, Frankfurt, Germany.
- [34] Peral, A., Míguez, J.M., Ordás, R. & del Cañizo, C. 2014, "Lifetime improvement after phosphorous diffusion gettering on upgraded metallurgical grade silicon", *Sol. Energy Mater. Sol. Cells*, Vol. 130, pp. 686–689.
- [35] Kvande, R. et al. 2008, "Distribution of iron in multicrystalline silicon ingots", *J. Appl. Phys.*, Vol. 104, p. 064905.
- [36] Schön, J. et al. 2015, "Identification of the most relevant metal impurities in mc n-type silicon for solar cells", *Sol. Energy Mater. Sol. Cells*, Vol. 142, pp. 107–115.
- [37] Sopori, B., Jastrzebski, L. & Tan, T. 1996, "A comparison of gettering in single and multicrystalline silicon for solar cells", *Proc. 25th IEEE PVSC*, Washington DC, USA.
- [38] Bartel, T. et al. 2012, "The effect of Al and Fe doping on solar cells made from compensated silicon", *Energy Procedia*, Vol. 27, pp. 45–52.
- [39] Bertoni, M.I. et al. 2011, "Influence of defect type on hydrogen passivation efficiency in multicrystalline silicon solar cells", *Prog. Photovoltaics Res. Appl.*, Vol. 19, No. 2, pp. 187–191.
- [40] Coletti, G. 2011, "Impurities in silicon and their impact on solar cell performance", Dissertation, University of Utrecht, The Netherlands.
- [41] Breitenstein, O., Rakotoniaina, J.P., Rifai, M.H. & Werner, M. 2004, "Shunt types in crystalline silicon solar cells", *Prog. Photovoltaics Res. Appl.*, Vol. 12, pp. 529–538.
- [42] Einhaus, R. et al. 2010, "Purifying UMG silicon at the French PHOTOSIL project", *Photovoltaics International*, 9th edn, pp. 58–65.
- [43] Míguez, J.M. et al. 2012, "UMG-Si based PV materials and devices: Current state and future trends", *Proc. 6th Int. Worksh. Cryst. Si. Sol. Cells*, Aix-les-Bains, France.
- [44] Rougieux, F. et al. 2015, "High efficiency UMG silicon solar cells: Impact of compensation on cell parameters", *Prog. Photovoltaics Res. Appl.*, DOI: 10.1002/pip.2729.
- [45] Meyer, S. et al. 2014, "Influence of the feedstock purity on the solar cell efficiency", *Sol. Energy Mater. Sol. Cells*, Vol. 130, pp. 668–672.
- [46] Sánchez, E. et al. 2011, "Outdoor monitoring of the energy yield and electrical parameters of standard polysilicon based and new umg-Si PV modules", *Energy Procedia*, Vol. 8, pp. 503–508.
- [47] Elkem 2015, "Elkem Solar Silicon-ESS" [<https://www.elkem.com/elkem-solar/elkem-solar-silicon/>].
- [48] Centrotherm SiTec AG 2015, "SiTec GMBH announces new monosilane decomposition technology" [[http://www.centrotherm.de/uploads/media/News\\_SiTec\\_Genesis\\_201509\\_Final.pdf](http://www.centrotherm.de/uploads/media/News_SiTec_Genesis_201509_Final.pdf)].
- [49] Ramos, A. et al. 2015, "Deposition reactors for solar grade silicon: A comparative thermal analysis of a Siemens reactor and a fluidized bed reactor", *J. Cryst. Growth*, Vol. 431, pp. 1–9.
- [50] Wang, C., Wang, T. & Wang, Z. 2012, "Manufacture of granular polysilicon from trichlorosilane in a fluidized-bed reactor", *Chem. Eng. Technol.*, Vol. 35, p. 893–898.
- [51] Li, P., Yu, X., Liu, F. & Wan, T. 2015, "Hydrodynamic behaviors of an internally circulating fluidized bed with wide-size-distribution particles for preparing polysilicon granules", *Powder Technol.*, Vol. 281, pp. 112–120.
- [52] Kwak, D.H. et al. 2015, "Ordered mesoporous carbon nanomaterials for catalytic conversion of silicon tetrachloride to trichlorosilane", *J. Nanosci. Nanotechnol.*, Vol. 15, No. 9, pp. 6714–6718.
- [53] Fu, R., James, T. & Woodhouse, M. 2015, "Economic measurements of polysilicon for the photovoltaic industry: Market competition and manufacturing competitiveness", *IEEE J. Photovolt.*, Vol. 5, No. 2, pp. 515–524.
- [54] Centrotherm SiTec 2012, "Pathways towards light in the dark", *Proc. 10th Photon Solar Silicon Conf.*, Berlin.
- [55] Maurits, J. 2011, "Reducing polysilicon materials costs", *Photovoltaics International*, 13th edn, pp. 41–47.
- [56] Roselund, C. 2015, "Polysilicon prices collapse amid global supply glut", *pv magazine*, 12/2015 edn, pp. 14–15.

#### About the Authors



**Dr. Eduardo Forniés** has a degree and an M.Sc. in applied physics from the Universidad Autónoma de Madrid, and received his Ph.D. from the Universidad de Alcalá in electronic engineering. Since 2001 he has worked in the R&D departments of various companies (BP Solar, Pillar, Silicio Solar, ENSOL and Aurinka) with manufacturing experience across the entire value chain.



**Dr. Laura Méndez** received her Ph.D. in chemical engineering from the Complutense University of Madrid in 2009; her thesis focused on chlorosilane synthesis. She worked as a process engineer and researcher at CENTESIL until 2015, and then joined Aurinka PV Group, where she is involved in activities related to silicon for PV.

**Marta Tojeiro** has worked in the technology department at Aurinka PV Group since 2010. She received her degree in electrical engineering from the Polytechnic University of Madrid and has over 15 years' experience in the PV industry, in which she started out as a quality and production engineer.

#### Enquiries

Dr. Eduardo Forniés  
Aurinka PV Group SL  
R&D Department  
C/ Marie Curie 19  
28521 Madrid, Spain

Tel: +34 914 994 197  
Email: [efornies@aurinkapv.com](mailto:efornies@aurinkapv.com)



# Cell Processing



40

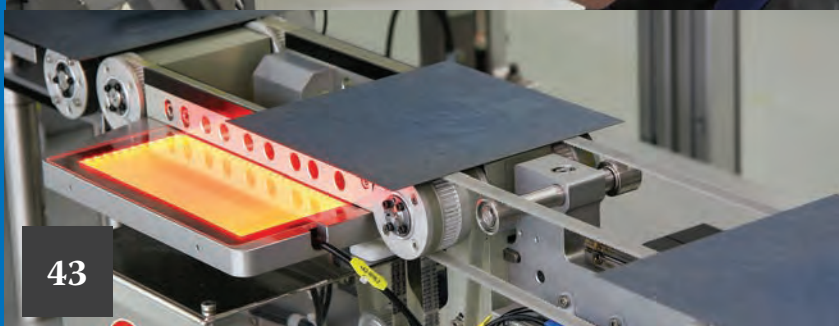
Page 40  
News

Page 43  
**Understanding process-related efficiency variations in mc-Si PERC cells**

Sven Wasmer, Johannes Greulich, Hannes Höfler, Nico Wöhrle & Stefan Rein, Fraunhofer Institute for Solar Energy Systems ISE, Freiburg, Germany

Page 53  
**SOLENNA(3): The ultimate simplification of bifacial silicon technology, at a competitive cost/Wp**

Raphaël Cabal, Thomas Blévin, Rémi Monna & Yannick Veschetti  
CEA Tech-INES, Le Bourget du Lac, France



43

Page 62  
**The present and future silver cost component in crystalline silicon PV module manufacturing**

Michael Redlinger<sup>1</sup>, Michael Woodhouse<sup>2</sup> & Roderick G. Eggert<sup>1</sup>  
<sup>1</sup>Division of Economics and Business, Colorado School of Mines (CSM), Golden, Colorado; <sup>2</sup>Strategic Energy Analysis Center, National Renewable Energy Laboratory (NREL), Golden, Colorado, USA

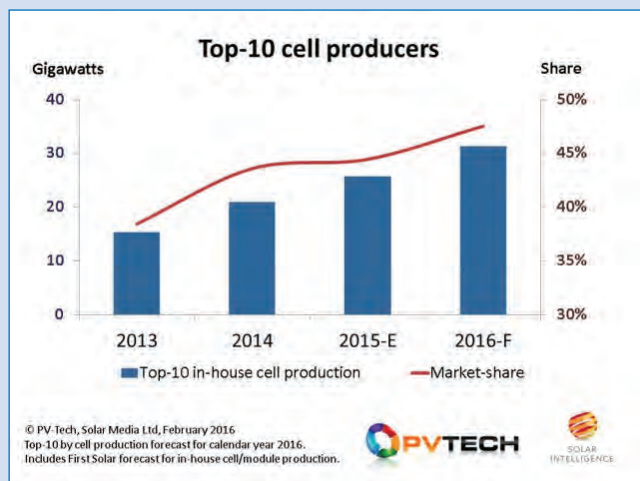
## Solar cell super league for 2016: top 10 approach 50% market share

The top-10 global cell producers are gaining an increasing market share in global cell production, growing from 38% market share in 2013 to 48% in 2016, according to Solar Intelligence. A breakaway of sorts is underway for cell production.

The top-10 cell producers forecast for 2016 are expected to approach 50% of end-market supply this year, with Hanwha Q CELLS set to lead the industry in terms of in-house cell production.

Meanwhile, Solar Intelligence also revealed a continued push from a diverse range of cell architectures, with no sign of any significant push to consolidation across the different n-type or p-type, mono or multi, and standard or advanced cell processes being used in production today.

Company strategies are continuing across different cell substrate types, with growth forecast across the board, and sustained optimism by wafer and cell suppliers to pursue in-house roadmaps and end-market supply tactics.



© PV-Tech, Solar Media Ltd, February 2016  
 Top-10 by cell production forecast for calendar year 2016.  
 Includes First Solar forecast for in-house cell/module production.



## Efficiencies

### NREL and CSEM show future promise of dual-junction stacked cell with new efficiency record

Collaboration by the US Energy Department's National Renewable Energy Laboratory (NREL) and the Swiss Center for Electronics and Microtechnology (CSEM) has set a certified record conversion efficiency of 29.8% for a III-V/Si solar cell.

The mechanically stacked and separately made solar cell was comprised of a silicon hetero-junction base cell with a gallium indium phosphide cell on top, giving it a dual-junction formation that exceeded the theoretical limit of 29.4% for crystalline silicon solar cells.

A new design for the dual-junction

solar cell and contributions from CSEM were said to be key to setting the new record, yet greater efficiencies are possible with closer collaboration, according to the research centres.

Multi-junction cells hold the promise of significantly higher efficiencies than that of conventional silicon cells but have remained extremely expensive to fabricate and confined to niche space markets.

### 'Deep-level' defects can enhance silicon cell efficiency

Certain defects in silicon solar cells appear to improve their performance, according to research by scientists at the NREL.

The findings run counter to conventional wisdom, according to NREL lead researcher Paul Stradins.

So-called deep-level defects in silicon solar cells are generally regarded as

undesirable because they can recombine charge carriers, decreasing the efficiency of the device.

But the NREL research has revealed that defects with deliberately engineered properties can in fact enhance carrier collection out of the cell or improve surface passivation of the absorber layer.

In simulations, the NREL introduced defects within the thin tunnelling silicon dioxide layer, which forms part of the passivated contact for carrier collection, and within the aluminium dioxide surface passivation layer next to the silicon cell wafer.

In both cases, defects with specific energy levels were identified to be beneficial by enhancing the transport of the majority carriers through the cell and/or repelling minority carriers, which could improve overall efficiency.

### SolarWorld reaches 22% efficiency in p-type PERC cell

German manufacturer SolarWorld has achieved 22.04% conversion efficiency in a PERC solar cell.

Verified by research institute Fraunhofer ISE, the figure is a step up from the company's previous best of 21.7%, which it announced in July last year. But it leaves the company short of the current PERC record of 22.13%, which was announced by Trina Solar in December.

SolarWorld said the p-type PERC cells that achieved the new efficiency were made using industrial processes, meaning the technology should be relatively swiftly converted into mass production.

The company has been one of the first to put PERC technology into volume production, with plans underway to migrate its US and Germany production lines to the new technology.



Credit: SolarWorld

SolarWorld's cells can be converted easily into mass production.

Use Discount Code 'PVI15' for a **15% discount\***



# Clean Energy SUMMIT

TWICKENHAM STADIUM  
26 - 28 April 2016



## HUAWEI

Headline Sponsor



**Corporate Energy FORUM**  
*Sponsored by Lightsource*

**Distributed Generation FORUM**



**Clean Energy Summit** brings major energy users together with public sector land and rooftop owners to explore current opportunities in a decarbonising economy

**Solar Summit** - Drivers of demand for solar and storage in the UK - success strategies in a low subsidy environment and new business model

**Corporate Energy Forum** - Energy efficiency updates and clean technology & storage deployment for commercial/industrial energy users.

**Distributed Generation Forum** - Energy efficiency updates and clean technology & storage deployment for public sector energy users.

**Energy Storage Summit** - Exploring the downstream market for Energy Storage across Residential, C&I and Utility Scale

**PARTNERS:**



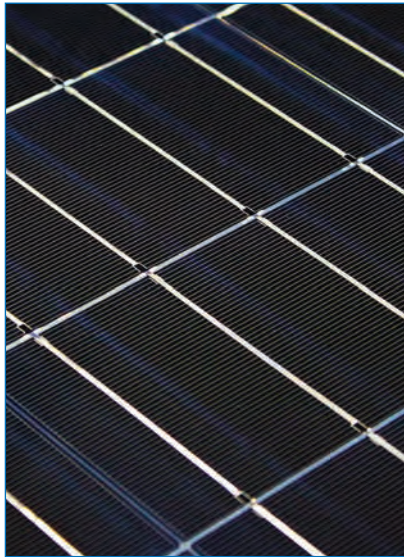
**SPEAKERS:**



[summit.solarenergyevents.com](http://summit.solarenergyevents.com)

For all enquiries please email: [marketing@solarenergyevents.com](mailto:marketing@solarenergyevents.com)

Exclusive to PVI Readers. Offer ends 31/03/2016



Credit: ISFH

Close-up of the PV module with an efficiency of 20.2% developed by ISFH.

### Imec and Total working on n-type PERT bi-facial cell technologies

Nanoelectronics research centre imec and energy giant Total, majority owner of US-based PV energy provider, SunPower, have extended an R&D collaboration to embrace a number of advanced technologies, including n-type PERT bi-facial solar cells and novel low-cost module interconnection concepts.

SunPower will be offering a new 'Performance' (P) Series module developed by US-based Cogenra Solar, which it acquired earlier in 2015.

Total has been supporting SunPower's R&D efforts in a number of ways since its acquisition, including recruiting scientists and engineers to focus on a range of advanced solar cell developments in line with SunPower's 'Maxeon' (IBC) cell and module interconnection technologies.

Research will also be undertaken on smart modules and techniques to more accurately predict the energy production from solar cell and modules under varying weather conditions.

### Previous record for half-cut PERC cells was 19.5%

The Institute for Solar Energy Research Hamelin (ISFH) using half-cut, p-type PERC solar cells in a large-area PV module has achieved a record 20.2% module efficiency and peak power output of 303.2W.

Using half-cut cells with minimum connection distance between the cells had significantly reduced series resistance losses, boosting overall module efficiency levels, beating the previous record of 19.5% for industrial-type modules with p-type silicon solar cells and screen-printed metallization.

The module area without an aluminium frame was 1.501m<sup>2</sup> and it used high-reflective and structured materials for the half-cut cell interconnects to direct further light on to the cell's active surface area.

TÜV Rheinland confirmed the performance results in an independent measurement.

ISFH also noted that the optimized cells had shown no potential-induced degradation, after numerous internal tests using the conditions of 85% relative humidity, a temperature of 85°C, and an applied voltage of 1,000V for 1,000h. This stress test was said to have surpassed the standard test by more than ten times.

## Companies

### Indosolar warns of need to restructure after continued losses in 2015

India-based solar cell producer Indosolar has said in financial filings that continued losses in 2015 have resulted in the need for a second corporate debt restructuring package.

The company had idled production in 2014, but improving market conditions in India and local content requirements on various provincial government tenders for PV power plants had led to a restart of partial production and orders for solar cells of around 75MW in 2015, which the company expects to produce through the first quarter of 2016. Nameplate capacity is around 160MW.

However, having failed to repay a corporate debt last year, the company has a second corporate debt due at the end of March 2016.

The company was exploring the possibility of a sale to an asset restructuring company with the possibility of a change in management.

### Intevac tracking 5GW of n-type mono solar cell capacity expansions

High-tech equipment manufacturer Intevac is tracking around 5GW of high efficiency n-type monocrystalline solar cell capacity expansions that are expected through 2020, providing a market opportunity for its 'MATRIX' platform of around US\$175 million.

The company noted in its fourth quarter 2015 earnings call that with two tier-1 PV manufacturers having adopted its PVD tool as well as completing an ion implant tool process development programme with a partner, demand for high efficiency n-type solar cells was expected to increase significantly.

The company also noted that it had

signed off and received payment for its first MATRIX PVD system order and received an order for a second system from an additional tier-1 customer in 2015.

### Panasonic suspending more than a third of HIT cell and module production

Japanese electronics firm Panasonic has suspended production at its Nishikinohama 'HIT' solar cell and module assembly plant due to weak domestic consumer demand in Japan, reports in February said.

The Nishikinohama plant Ohtsu City, Shiga prefecture, started operations in September 2004, was expanded in 2010 and had a solar cell capacity of 345MW after capacity expansions in 2011. Module assembly nameplate capacity after expansions had only been around 40MW.

However, Panasonic's total HIT production was around 900MW, with the Nishikinohama plant accounting for around 38% of total HIT cell production.

Reports said the plant would stop production at the end of February and remain suspended through the end of October 2016. The workforce would be temporarily dismissed.

## Policy and markets

### Brazil moves one step closer to tax exemption on solar cells and modules

Representatives of Brazil's Chamber of Mines and Energy Committee have approved legislation that includes new solar financing options and tax exemptions for solar cell and module imports, but the proposals must still pass through two more commissions to become law.

The Brazilian legislation 8322 / 2014, which is still under discussion, would introduce an exemption from import taxes for monocrystalline and polycrystalline solar cells as well as PV modules.

Rodrigo Sauaia, executive director of the Brazilian Solar Industry Association, Absolar, said this would be beneficial in supporting the development of a local value chain with more attractive solar prices for the consumer.

However, the exemption applies only as long as there is no national production of these components within Brazil. The country does not currently produce solar cells and Sauaia does not expect solar cells to be manufactured locally before 2020, although he claims this is difficult to predict.

# Understanding process-related efficiency variations in mc-Si PERC cells

Sven Wasmer, Johannes Greulich, Hannes Höffler, Nico Wöhrle & Stefan Rein, Fraunhofer Institute for Solar Energy Systems ISE, Freiburg, Germany

Fab & Facilities

Materials

Cell Processing

Thin Film

PV Modules

Market Watch

## ABSTRACT

This paper introduces and explains a simulation-assisted approach for determining and ranking the most influential causes of variations in experimentally obtained solar cell efficiencies, using the example of an industrially feasible multicrystalline silicon (mc-Si) passivated emitter and rear cell (PERC) process. With the objectives of being independent of material variations and of analysing process-related impacts only, 51 neighbouring high-performance mc-Si wafers are distributed in an experiment in which more than 800 mc-Si PERC cells in total are processed, and this sub-group is comprehensively characterized. The elevated data serve as input for modelling the resulting distribution of cell efficiencies on the basis of numerical 3D simulations, metamodelling and Monte Carlo runs. In order to understand the most detrimental impacts responsible for a widening of this distribution, a variance-based sensitivity analysis is conducted, where the parameters are ranked according to their impact on the total variance of cell efficiencies. In this case, it is possible to explain over 80% of the measured total variance; moreover, the rear-side passivation and a wrap-around during the emitter etch-back process can be identified as responsible for 80% of the variance. The approach presented is especially helpful for ramping up PERC production; however, since it is basically transferable to any solar cell concept, it can also be applied to optimize established production lines.

## Introduction

As of 2014, according to the ITRPV Roadmap [1], almost 90% of the solar cells produced are still based on the conventional concept, namely the solar cell with an aluminium back-surface field (Al-BSF) on the entire rear side. Partly because of the introduction of the so-called *high-performance multi* (HPM) wafers, which allow much higher bulk lifetimes than conventional mc-Si wafers, more and more cell producers are currently switching their production lines to implement the passivated emitter and rear cell (PERC) concept [2], with dielectric passivation layers and local contacting geometries on the rear side. Although this, in principle, permits higher cell efficiencies because of less recombination on the rear side and better light-trapping properties, there are several challenges during the ramping-up phase that have to be dealt with. In this phase, not only the absolute levels of cell efficiencies, which can be analysed, for instance via a loss analysis [3], but also variations thereof have to be considered. An understanding of the causes can reveal the critical processes and parameters that need to be measured more accurately and better tuned, thus leading to an overall improvement in the quality and yield of a production line.

Several works have been published on this topic and will be briefly mentioned here. There are publications dealing with a statistical analysis of wafer process data

and cell data: time series analysis and data manipulation methods are used to detect and understand temporal changes in the final cell characteristics [4,5]. A recent publication [6] analyses, using data mining methods, wafer process data and their correlations with the finished cell characteristics of hundreds of thousands of solar cells, and is able to explain large shares of the measured variance with the data acquired during processing.

Alternatively, methods based on numerical solar cell simulations have been presented. These first deal with the modelling and understanding of the distribution of cell efficiencies of an mc Al-BSF process [7], which is later refined by (to the authors' knowledge) the first application of metamodelling and Monte Carlo simulations in PV research [8]. In the most recent work [9], the approach is transferred to the PERC process, and local derivatives of the metamodel are used as a sensitivity measure to detect the most relevant impacts.

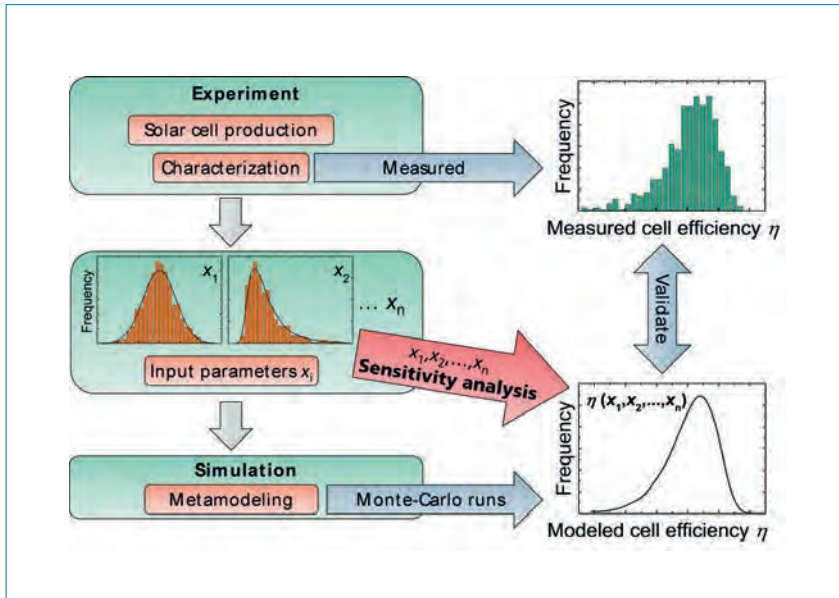
In this paper the approaches mentioned above and in a recent publication [10] are followed and enhanced by using state-of-the-art metamodelling. Then, by means of a variance-based sensitivity analysis, the impacts on a measured distribution of cell efficiencies are globally investigated. The approach presented consists of an overview of the models applied for the numerical 3D device simulations using Sentaurus

TCAD [11], the modelling of the experimentally achieved distribution of cell efficiencies with Monte Carlo runs. This is followed by a variance-based sensitivity analysis, where the input parameters are ranked according to their impact on the total variance. The approach is demonstrated by an example application to an industrially feasible mc-Si PERC process with laser-fired contacts (LFC, [12]).

## Approach

The approach taken here for investigating the impacts of process variations on the distribution of cell efficiencies consists of the following steps:

1. Production and characterization of solar cells.
2. Determination of the relevant input parameters for the simulation, and their distributions.
3. Numerical device simulations and metamodelling thereof.
4. Modelling of the distributions of cell efficiencies via the Monte Carlo method, and validation by measurements.
5. Investigation of the impact of each input parameter in a variance-based sensitivity analysis.



**Figure 1.** Overview of the approach for investigating the impacts of process variations on the distribution of cell efficiencies. In the experiment, the distributions of the cell efficiencies and of the input parameters for the simulations are determined. Monte Carlo runs of a metamodel of the numerical 3D device simulations are carried out, in order to model the distribution of cell efficiencies, which are then validated by the experimentally obtained efficiencies. The input parameters are ranked according to their influence on the total variance in a variance-based sensitivity analysis.

The approach is shown schematically in Fig. 1 and will be explained in detail next. The first two steps basically serve to compile the prevailing variations of cell efficiencies and parameters in a production line via inline and offline characterization methods, and can be assisted by simulations if necessary. The typical steps are discussed in a later section, but first the focus will be on the simulation-based evaluation (steps 3–5) after the data collection.

The numerical 3D device simulations, which are conducted at a device temperature of 25°C, can be divided into: 1) an optical part, in which the spectrally and spatially resolved generation profiles of charge carriers are calculated; and 2) an electrical part, in which these generation profiles are used as input, and the current-voltage ( $I$ - $V$ ) curve is computed.

For the optical part, the Monte Carlo ray tracer of a Synopsys Sentaurus Device is used. The front side is modelled on the assumption of thin  $\text{SiN}_x$  layers of thickness  $d_{\text{ARC}}$ ; these are described by Fresnel's equations using the transfer-matrix formalism [13], on a textured surface, which is described in the case of an isotexture by a characteristic angle  $\omega_{\text{texture}}$  [14,15]. For the silicon bulk with a substrate thickness of  $d_{\text{Si}}$ , Lambert-Beer's law [16] is assumed, and the rear side is modelled by the Phong

model with parameters  $R_0$  and  $\omega_{\text{phong}}$  [17]. Later, the shading of the front side metallization is accounted for by scaling the generation current densities  $j_{\text{ph}}$  by a factor of  $(1-M_{\text{met}})$ , where  $M_{\text{met}}$  is the optical shading ratio. In this case, variations in  $j_{\text{ph}}$  largely depend on variations in texture strength  $\omega_{\text{texture}}$  only, and therefore  $d_{\text{ARC}}$ ,  $d_{\text{Si}}$ ,  $R_0$  and  $\omega_{\text{phong}}$  are kept constant in the subsequent electrical part of the simulation.

In the electrical simulations of solar cell concepts with structured rear sides, as in the case of PERC, it is convenient to assume an effective front side [18] and to account for the shading of the front metallization by scaling  $j_{\text{ph}}$  and by considering an external series resistance  $R_s$  which contains the area-weighted contributions of the emitter, contact and grid resistances. Furthermore, to account for non-ideal recombination at, for instance, the cell edges or the space charge region, a second diode with ideality  $n_2 = 2$  and dark saturation current density  $j_{02}$  is added analytically after finishing the numerical Sentaurus Device simulations. The symmetry element applied in the Sentaurus Device usually has a magnitude of  $d_{\text{Si}}$  in the direction perpendicular to the wafer surface ( $z$  axis), and of half the distance between the contacts on the rear side in the other dimensions ( $x$  and  $y$  axes).

The emitter profile is determined by

means of electrochemical capacitance-voltage (ECV) measurements and imported into the Sentaurus Device, leaving an effective surface recombination velocity  $S_{\text{eff,front}}$  (consisting of a portion  $S_{\text{pass,front}}$  in the passivated area and a portion  $S_{\text{met,front}}$  in the metallized area) as a free parameter. The bulk recombination is modelled by a mid-band gap Shockley-Read-Hall (SRH) defect with defect parameters  $\tau_{n0}$  and  $\tau_{p0}$ ; the recombination at the rear side is modelled by the surface recombination velocities  $S_{\text{pass,rear}}$  in the passivated area and  $S_{\text{met,rear}}$  in the metallized area.

The areas of a local rear contact are usually defined via a contacted and a larger recombination-active region. In the case of the LFC approach, the model of a point contact with a recombination-active area (damaged by the laser pulse) with radius  $r_{\text{LFC}}$  that is twice the size of that of the contacted region  $r_{\text{LFC,cont}}$  is used. The model is implemented for the surface recombination velocity  $S_{\text{met,rear}}$  in the damaged area, introduced by Schwab [19] and applied by Wöhrle et al. [20]. With regard to general models for silicon solar cell simulation, those summarized by Fell et al. [21] are used. For adjusting the density-of-states effective mass of holes for self-consistency of the band gap, effective density of states and intrinsic density at 25°C, the recommendation of Altermatt [22] is followed.

Once the input parameters (e.g. wafer thickness, base doping concentration, texture strength  $\omega_{\text{texture}}$ , emitter doping profile and saturation current density), as well as their minimum and maximum attainable values are known, the next step consists of selecting an adequate experiment design for the numerical simulations, in order to achieve the lowest computation times and the best interpolation properties later. To this end, a space-filling design of experiments (DOE) is chosen, and the design creator available online [23] is utilized for the generation of 300 equidistant sample points in the  $n$ -dimensional input space. The results for the four-cell performance characteristics – short-circuit current density  $j_{\text{sc}}$ , open-circuit voltage  $V_{\text{oc}}$ , fill factor  $FF$  and energy conversion efficiency  $\eta$  – of the numerical device simulations are used for these sample points to train so-called Gaussian process models, which are widely used in computer experiments for interpolation purposes [24]. The advantage of this method compared with, for example,

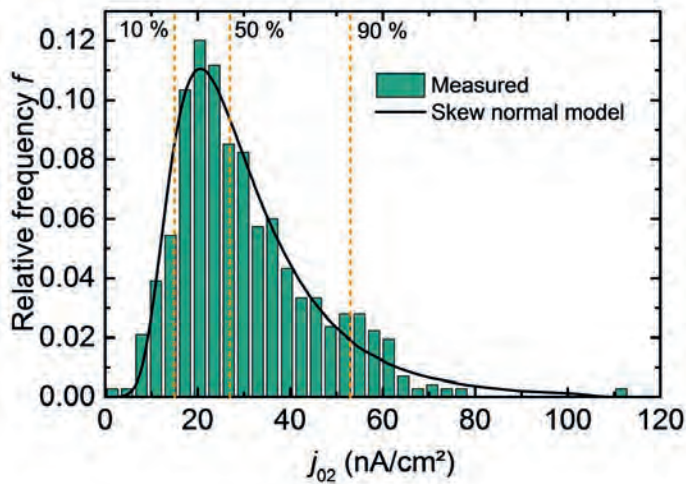


Figure 2. Example of a measured probability density function and the corresponding fitted skew normal model. A good agreement can be seen, despite the use of only three distinct percentiles of the measured distribution for fitting the skew normal model. (Data here taken from a larger experiment.)

inevitable deviations from a strictly symmetric normal distribution. The three distinct percentiles – later referred to as *low*, *medium* and *high* – provide a good estimate of the range of a parameter without being affected by outliers, as would be the case by using, for example, the mean and the variance. Random numbers with values of the order of  $10^5$  are then drawn from these probability density functions for each input parameter, and the aforementioned Monte Carlo runs (step 4) are performed using the Gaussian process model regression. This lowers the computation time for one simulation of  $\eta$  from 1.5 hours for the numerical simulation to 0.3ms for one Gaussian process model prediction, using one core of a standard CPU.

The resulting modelled distribution of cell efficiencies is then compared with the one obtained experimentally; if necessary, it is adjusted so that all three characteristics  $j_{sc}$ ,  $V_{oc}$  and  $FF$  simultaneously match the measured ones. If good agreement is achieved, the model is validated and ready for the most interesting part, the final step – 5.

polynomial regression is the ability to fit any analytic relationship, including asymptotic trends.

The probability density function of each input parameter is then modelled by fitting the three parameters of a

skew normal distribution (Section A.8 in Hosking & Wallis [25]) to the 10th, 50th and 90th percentile of the measured distribution, an example of which is given in Fig. 2. This has the advantage of accounting for the actual

THE WET PROCESSING COMPANY

RENA

# PERC

TOP COMBINATION  
perfect shape & best CoO

## BatchTex

Minimized front side reflection  
Optimized pyramids by monoTEX® additive

## InOxSide<sup>+</sup>

Efficient and faster rear side smoothing



Visit us at  
SNEC 2016  
Booth E3-355

Cells	$\tau_{\text{bulk}}$ samples	$j_{0e}$ samples
p-type mc-Si, 1.7 $\Omega\text{cm}$ , 156 mm		n-type, Cz-Si, 9 $\Omega\text{cm}$ , 156 mm
Acidic texturing		
Phosphorus emitter diffusion		
Chemical emitter etch back on rear side	KOH etching	PSG etching
PECVD AlOx passivation of rear side	SC1/SC2 cleaning	PECVD SiNx on both sides
PECVD SiNx on rear & front	Fast ALD Al <sub>2</sub> O <sub>3</sub> on both sides	Firing
Screen printing Al paste on rear	Annealing	
2x screen printing Ag paste on front	PECVD SiNx on both sides	
Front contact firing		
Local rear contact formation (LFC)		
Forming gas annealing		

Figure 3. Process flows employed for the cells (left), and for the samples used to measure the bulk lifetime  $\tau_{\text{bulk}}$  (middle) and the emitter dark saturation current density  $j_{0e}$  (right).

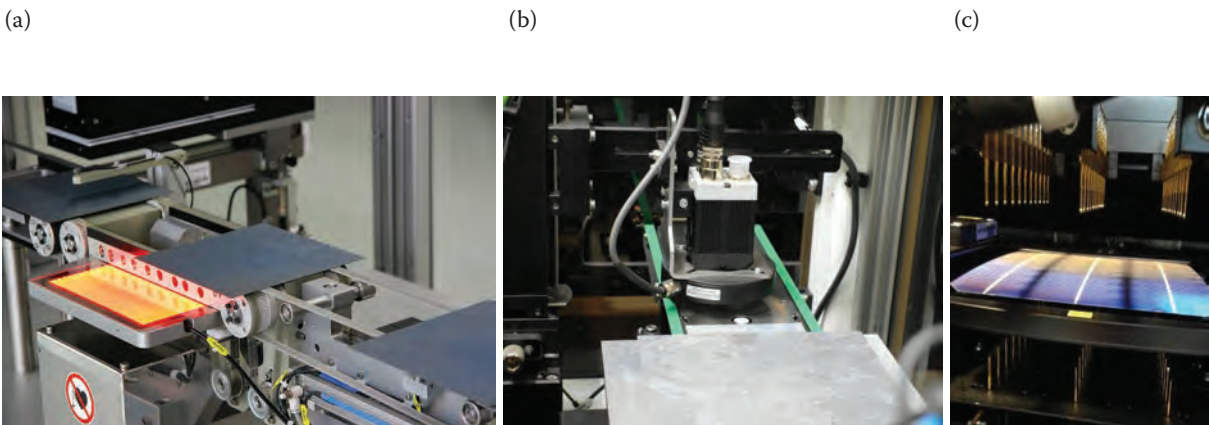


Figure 4. (a) One of the several in-line characterization tools available at Fraunhofer ISE’s PV-TEC for different stages of the solar cell manufacturing process. (b) Wafer-tracking system based on data matrix codes. (c) State-of-the-art in-line automat with a flexible contacting unit, for characterizing the finished cells (which is also suitable for use with back-contact solar cells).

“The variance-based approach takes into account nonlinear responses and considers the interactions between input variables.”

Step 5 ultimately features the investigation of the impact of each input parameter on the variations of cell efficiencies in a sensitivity analysis. Variance is a well-established measure of the variation of a random variable; a variance-based approach [26] is therefore chosen for the sensitivity analysis. An advantage of the variance-based approach is its global character, as

it takes into account nonlinear responses and considers the interactions between input variables. The principal measure of sensitivity of the total variance  $V(y)$  of a random variable  $y$  on the input variable  $x_i$  is known as the main-effect index  $S_i$  and is defined as:

$$S_i = \frac{V(y) - E(V(y|x_i))}{V(y)} = 1 - \frac{E(V(y|x_i))}{V(y)} \quad (1)$$

where  $V(\dots)$  is the variance and  $E(\dots)$  is the mean of a distribution. The term  $E(V(y|x_i))$  is the variance of  $y$  when the  $i_{\text{th}}$  input variable  $x_i$  is given (not varied); it is averaged over all possible values of  $x_i$ . Thus,  $S_i$  is basically a measure of the decrease in total variance  $V(y)$  of  $y$

when  $x_i$  could be fixed and normalized to this total variance. The sum of all the  $S_i$  indices is always less than or equal to unity, where a value of unity would indicate an additive model with no interactions between the input variables. Since for the calculation of the  $S_i$  one would have to consider distributions of distributions, the short-cut proposed in Saltelli et al. [26] is used, which drastically reduces the computational cost compared with the brute-force method.

### Example application

#### Experimental

The discussed investigation is carried out using an example of an industrially



THE FASTEST WAY TO

GET INTO  
PERC!



**C.PLASMA**

The most versatile PECVD system for anti-reflective coatings, passivation and masking layers

- Dielectric AlO<sub>x</sub> / SiN<sub>x</sub> stack with best passivation properties
- More than 5% abs. higher uptime compared to inline systems
- Low cost of ownership due to optimized CAPEX, less maintenance, low TMA consumption and minimum footprint
- Fast and easy upgrade of all centrotherm PECVD systems with minimum space requirements

[www.centrotherm-pv.com](http://www.centrotherm-pv.com)

feasible mc-Si PERC process with LFCs, but basically it could be performed on any solar cell concept. In order to be independent of material variations and to gather just the process-related impacts, 51 neighbouring HPM mc-Si wafers are distributed homogeneously among the batches in a larger experiment, so that approximately every 20th cell is processed on this material. It is assumed that the variation in material properties is insignificant over these 51 wafers. An equivalent approach for the production of PERC cells on monocrystalline Czochralski (Cz) grown wafers could be the distribution of high-quality magnetic-cast Cz-Si wafers in the production line.

An essential requirement for this type of study is the possibility of tracking wafers along the entire value chain as far as the finished solar cell, with the use of, for instance, a wafer-tracking system based on data matrix codes [27,28], which has been implemented on Fraunhofer ISE's PV-TEC research manufacturing line.

A flow diagram of the chosen cell process is given in Fig. 3 (left). After the acidic texturing process, the mc-Si base material is subjected to a phosphorus emitter diffusion, using the process developed by Werner et al. [29]. The phosphosilicate glass (PSG) layer on the front side and the emitter on the rear side are then wet-chemically etched back. After a cleaning step, the rear side is passivated by a stack of plasma-enhanced chemical vapour deposited (PECVD) aluminium oxide and silicon nitride, and the front side is passivated by just silicon nitride. Metallization is applied via screen printing, front-contact formation is then achieved with a firing step in a fast-firing conveyor-belt furnace, and the rear side is contacted using the LFC process. After a forming gas annealing step, the cells are characterized inline on a h.a.l.m. cell tester.

In addition to these cells, three of the 51 HPM mc-Si wafers were processed into samples, with the goal of measuring the bulk lifetime  $\tau_{\text{bulk}}$  (process flux depicted in Fig. 3, middle); highly resistive n-type Cz-Si wafers were also processed into samples, to measure the emitter dark saturation current density  $j_{0e}$  (Fig. 3, right). For measuring  $\tau_{\text{bulk}}$ , it is important that these samples take part in the same emitter diffusion as the cells in order to account for the impacts of gettering and high-temperature steps on the silicon material; the samples also need to be passivated in the best possible manner. Furthermore, every fifth wafer of the HPM cell material is withdrawn after the deposition of the passivation layers and is subjected to a firing step in a fast-firing oven in order to activate the passivation. These samples for measuring the implied open-circuit voltage  $iV_{oc}$  contain valuable information about the front end of the cell process, since they include all recombination effects without any influences due to the metallization.

**Data acquisition**

During the value chain, the versatile inline and offline characterization methods available at the Photovoltaic Technology Evaluation Center (PV-TEC) at Fraunhofer ISE (see also Fig. 4) are utilized.

The inline methods of the front end prior to metallization consist of the following measurements:

- Wafer thickness  $d_{\text{Si}}$  via capacitance.
- Specific resistance  $\rho$  of the silicon wafer, via induction.
- Reflectance  $R_{600\text{nm}}$  at a wavelength of 600nm on a trace of the wafer after texturing, via a spectrometer.
- Imaging of the thickness  $d_{\text{ARC}}$  of the anti-reflection coating layer, via a hyperspectral imaging sensor.

The base doping concentration  $N_{\text{dop}}$  is determined by measuring the resistance in the as-cut state; this value is then compared with the one after the emitter etch-back



UPGRADE SOLUTION OR  
COMPLETE SYSTEM AVAILABLE  
WITH SHORT DELIVERY TIME

process in order to determine the emitter sheet resistance  $R_{sh}$ . In this particular case of an isotexture, the texture strength  $\omega_{texture}$  is determined by fitting the simulated  $R_{600nm}$  to the measurement after the texturing process, as done by Greulich et al. [15]. The finished cells are then characterized using an inline automat. This allows an inspection of the front and rear side metallization, and the measurement of the metal grid resistance and the current-voltage characteristics under illumination, yielding the performance characteristics  $j_{sc}$ ,  $V_{oc}$ ,  $FF$  and  $\eta$ , the current-voltage characteristics in the dark, and the suns- $V_{oc}$  characteristics. It also offers the opportunity to record electroluminescence images under forward bias and thermography images under reverse bias. Furthermore, the parallel and series resistances  $R_p$  and  $R_s$ , as well as the parameters  $j_{01}$  and  $j_{02}$  by fitting the two-diode model to the suns- $V_{oc}$  pseudo  $I-V$  curve, are obtained at the cell level.

The offline methods comprise taking measurements of the spectrally resolved reflectance curves and, using the transfer length method (TLM, [30]), of the metal-semiconductor contact resistance  $\rho_c$  of the finished cells. The reflectance curves are used to measure the finger widths and therefore the optical shading ratio  $M_{met}$ , by repeated subtraction of the reflectance spectrum of the silver fingers until the expected minimum reflectance of the unmetallized part

alone is reached. The parameters  $R_0$  and  $\omega_{Phong}$  of the Phong model are adjusted to match the measured reflectance of the finished solar cells over the 900–1,200nm wavelength range. The emitter dark saturation current density  $j_{0e}$  is determined via a refinement [31] of the Kane-Swanson method [32] applied to quasi-steady-state photoconductance (QSSPC, [33]) measurements of the  $j_{0e}$  samples.

Perhaps the most valuable characterization tool is

photoluminescence (PL) imaging, the particular use of which here will be described next. PL images at 1 sun are acquired before and after the LFC formation process, and the difference in PL intensities is calibrated to a voltage drop  $\Delta V_{oc,LFC}$  because of the additional recombination at the rear contacts. The LFC radius  $r_{LFC}$  in the electrical cell simulations is then adjusted to match this voltage drop in the open-circuit voltage  $V_{oc}$  [10]. QSSPC lifetime calibrated PL images

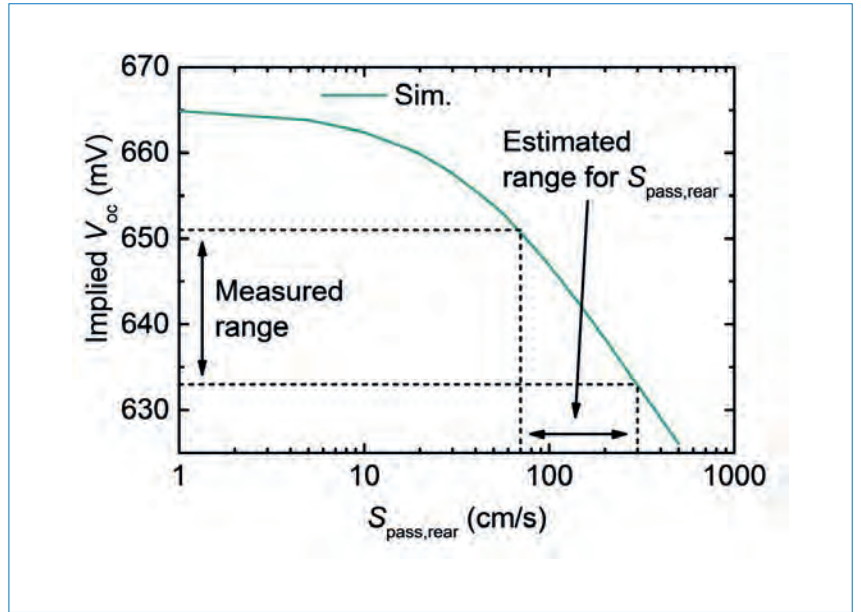


Figure 5. Simulation-assisted estimation of the rear-surface recombination velocity in the passivated area  $S_{pass,rear}$  by comparing the measured range of values for the implied open-circuit voltage  $iV_{oc}$  with the simulated values.

Parameter	Description	Determination	Low	Medium	High
$d_{Si}$ [ $\mu\text{m}$ ]*	Bulk thickness	Measurement	183.7	185.4	186.2
$N_{dop}$ [ $\text{cm}^{-3}$ ]	Bulk doping concentration	Measurement	–	$9 \times 10^{15}$	–
$\tau_{n0}$   $\tau_{p0}$ [ $\mu\text{s}$ ]	Bulk SRH lifetime	$r$ -calibrated PL of $\tau_{bulk}$ samples	–	45   910	–
$\omega_{texture}$ [ $^\circ$ ]	Characteristic texture angle	Adjustments to measured $R_{600nm}$ after texturization	56.5	57.8	61.0
$j_{0e}$ [ $\text{fA}/\text{cm}^2$ ]   $S_{pass,front}$ [ $\text{cm}/\text{s}$ ]	Emitter dark saturation current density	Kane-Swanson method of $j_{0e}$ samples	–	92   $2.5 \times 10^5$	–
$S_{met,front}$ [ $\text{cm}/\text{s}$ ]	Recombination velocity at front metallization	Neglected	–	$S_{pass,front}$	–
$d_{ARC}$ [ $\text{nm}$ ]*	ARC layer thickness	Measurement	77.5	79.6	82.2
$M_{met}$ [%]	Shading ratio front metallization	Measurement	5.04	5.36	5.63
$S_{pass,rear}$ [ $\text{cm}/\text{s}$ ]	Recombination velocity at rear passivation	Adjustments to measured $iV_{oc}$	70	130	300
$S_{met,rear}$ [ $\text{cm}/\text{s}$ ]	Recombination velocity at rear metallization	Model $S_{met}(N_{dop})$ [19,20]	–	2,400	–
$r_{LFC} = 2r_{LFC,cont.}$ [ $\mu\text{m}$ ]	Radius of damaged LFC area	Adjustments to measured $\Delta V_{oc,LFC}$	37	44	51
$d_{LFC}$ [ $\mu\text{m}$ ]	Distance of LFC contacts	LFC target	–	350	–
$R_0$ [-]   $\omega$ [-]	Phong model of reflectance at rear side	Adjustments to measured $R_{>900nm}$ of cell	–	0.935   2	–
$j_{02}$ [ $\text{nA}/\text{cm}^2$ ]	Dark saturation current density of second diode	Adjusted two-diode model to pseudo $I-V$ curve	16.5	23.0	34.5
$R_s$ [ $\Omega\text{cm}^2$ ]	$R_s$ contribution front	Contributions of $R_{sh}$ , $\rho_c$ and $R_{grid}$	0.523	0.547	0.596

\* These parameters are only varied in the optical part of the simulations.

Table 1. Overview of the input parameters, along with their measured ranges and the chosen way of determination. Where just the medium value is given, the parameter variations are neglected in the electrical simulations.



**ASYS  
SOLAR**

A Member of the ASYS Group

# What Awaits Us Beyond Higher Throughput?

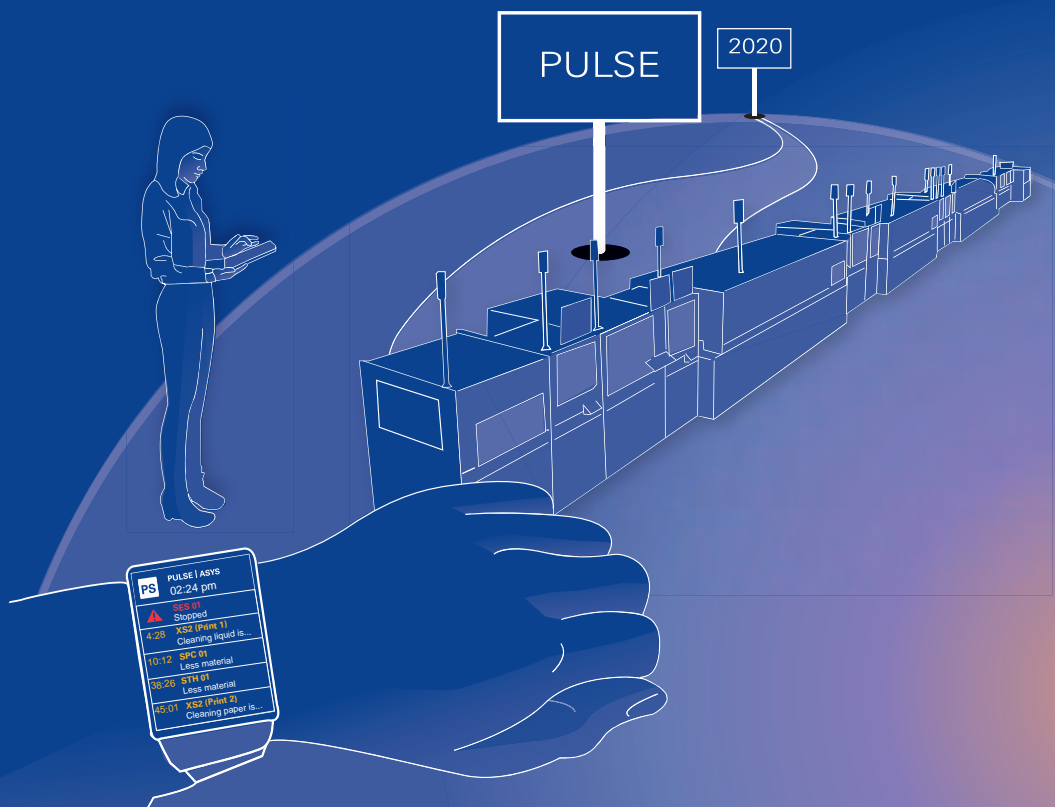
Our vision is really smart production. Self-organized manufacturing with human support for the core tasks. We ensure that the operator will receive more relevant data and that the machines automatically adapt to the product.

Thanks to the award-winning PULSE solution, the most important tasks for the operator are available directly at his wrist. With electro-luminescence inspection in the tester, it is possible to detect micro cracks or breaks in the fingers before the cells are installed in the modules. The motor-driven squeegee head adjusts itself automatically and adapts to the wafer continuously during the printing process. And the integrated inspection system makes it possible to position wafers directly in the screen printer for double printing.

## ASYS Group | Business Unit Solar

ASYS GmbH, Benzstrasse 10, 89160 Dornstadt, Germany

[www.asys-solar.com](http://www.asys-solar.com)



[34] are applied to the samples to measure the implied open-circuit voltage  $iV_{oc}$  and the bulk lifetime  $\tau_{bulk}$ . In the case of the  $iV_{oc}$  samples, the lifetime images acquired at 1 sun are converted to images of the local voltage and averaged over the wafer region. As regards the  $\tau_{bulk}$  samples, an additional image is recorded at 0.04 suns, and the harmonic mean in the diffusion length over the wafer region of the two images is taken; the SRH defect parameters  $\tau_{n0}$  and  $\tau_{p0}$ , required as simulation input to fit the lifetime values at the two different injection conditions, are then adjusted. Along with the use of the measured  $j_{0e}$  and  $\tau_{bulk}$ , the surface recombination velocity  $S_{pass, rear}$  of the passivated area where the damaged LFC area is absent is varied in cell simulations, in order to match the measured range of  $iV_{oc}$ , as depicted in Fig. 5, and to determine  $S_{pass, rear}$ .

In order to reproduce in the model the measured dark saturation current densities  $j_{02, fit}$  derived from the measured  $I-V$  curves with the simulations, the difference  $j_{02} = j_{02, fit} - j_{02, Sent.Device}$ , where  $j_{02, Sent.Device}$  is obtained by fitting the two-diode model to an example Sentaurus Device  $I-V$  curve, is used as the saturation current density of the external second diode. Finally, the series contribution  $R_s$  of the front is calculated by area weighting the single contributions of emitter sheet resistance  $R_{sh}$ , specific contact resistance  $\rho_c$  and grid resistance  $R_{grid}$ .

An overview of the input parameters, along with their

measured ranges and the chosen method of determination, is given in Table 1. Compared with a previous study, the absolute values of  $\tau_{n0}$ ,  $M_{met}$  and  $j_{02}$  are slightly different, but the absolute ranges of these variables remain the same. This is acceptable, since it is primarily the variations in cell efficiencies that are of interest.

“The rear-surface recombination velocity in the passivated area is the dominant origin of efficiency variations.”

### Results

The experimentally obtained distribution of cell efficiencies and the modelled one are given in Fig. 6(a): excellent agreement in both the absolute level and the shape is seen. Note that the solar cells with severe series and parallel resistance issues, represented by the leftmost bar on the chart, were removed prior to determining the mean and the standard deviation. The total standard deviation of the conversion efficiency  $\eta$  in the experiment amounts to 0.23%<sub>abs.</sub>, and more than 80% of the closely related variance in the simulations can be explained. The results of the variance-based sensitivity analysis are given in Fig. 6(b), which shows a breakdown of the various influences. The sum of the aforementioned main-effect indices  $S_i$ , which serve as

sensitivity measures, turns out to be equal to unity within the uncertainties that are due to statistical computation, clearly indicating an additive model  $\eta(x_1, \dots, x_n)$ . It is therefore possible to assign a relative share of the total variance to each of the input parameters  $x_i$ , revealing that the rear-surface recombination velocity in the passivated area  $S_{pass}$  is the dominant origin of variations. Further technological work should focus on improving the stability and the overall quality of the rear-surface treatment and cleaning, and the PECVD of the passivation.

The large process-induced  $j_{02}$  contribution is the second-largest source and is responsible for more than a third of the variation in  $\eta$ . This contribution can be attributed to power losses at the wafer edges, which is underlined by the dark lock-in thermography (DLIT) image at +0.5V for a cell with severe pseudo fill factor problems, shown in Fig. 7. At these distinct edges, a wrap-around of liquid during the emitter etch-back process was visible, even to the naked eye. Subsequent finger printing and firing most likely resulted in the formation of recombination-active defects in the depletion region between the partially etched emitter and the base. For the PERC process utilized, after an optimization of the rear-surface passivation and chemical edge isolation processes (which are responsible for over 80% of the process-induced variations), the next steps to be recommended would include improvements to the optics of the

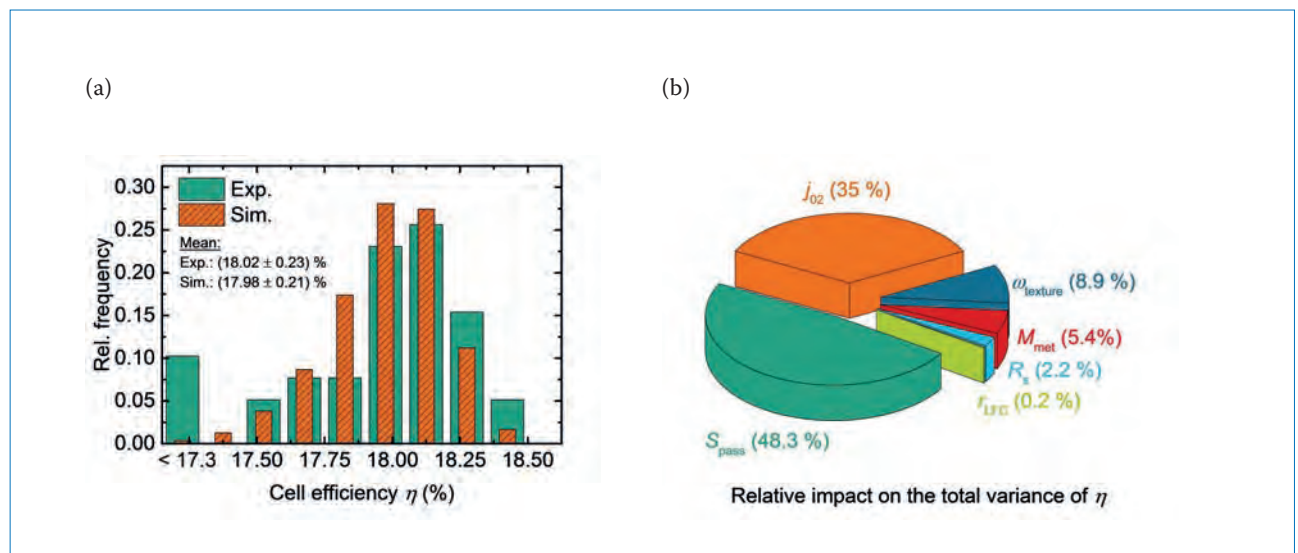
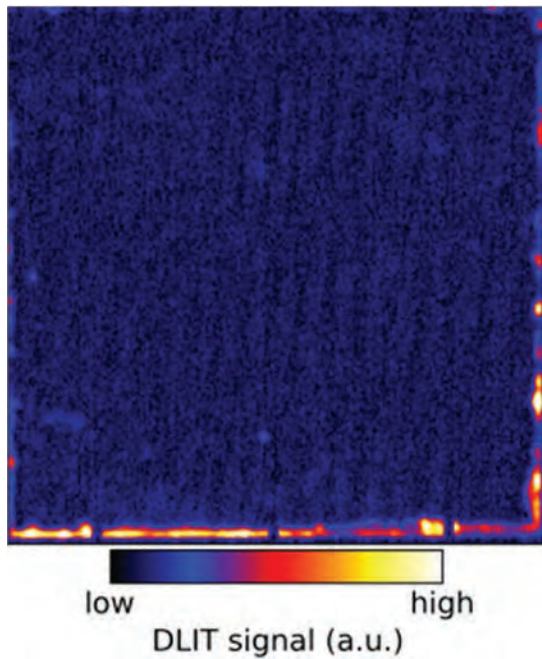


Figure 6. (a) Experimentally obtained (green) and modelled (orange) distributions of cell efficiencies. Prior to determining the mean and the standard deviation in the experiment, the cells with severe series and parallel resistance problems (leftmost bar on the chart) were excluded and a skew normal distribution fitted to the remaining data. (b) Pie chart of the ranked relative impacts of each input parameter on the total variance of cell efficiencies. The variation in rear-surface recombination is the dominant source of variations in energy conversion efficiency  $\eta$ .



**Figure 7.** Dark lock-in thermography (DLIT) image at +0.5V of a cell with severe pseudo fill factor problems ( $pFF = 77.7\%$ ,  $j_{02} = 65\text{nA/cm}^2$ ,  $R_p = 5,162\Omega\text{cm}^2$ ). The power loss which is clearly visible at the bottom and right cell edges was found to be caused by a wrap-around of liquid during the emitter etch-back process. Subsequent finger printing and firing most likely led to the formation of recombination-active defects in the depletion region between the partially etched emitter and the base.

front side, namely the texture strength  $\omega_{\text{texture}}$  and the front metallization shading ratio  $M_{\text{met}}$ .

**“The parameters that lead to the largest variations are often the same ones that offer the greatest potential for optimizing the absolute level of cell efficiencies.”**

## Conclusions

A simulation-based approach for modelling the experimentally obtained distribution of solar cell efficiencies has been introduced. It was shown how to rank the input parameters according to their influence on the total variance of this distribution, thus giving an indication of which processes and parameters need to be measured and better tuned. This approach was illustrated and verified using an example of an industrially feasible mc-Si PERC process with LFC contacts, for which it was possible to explain over 80% of the measured efficiency variation of  $0.23\%_{\text{abs}}$ . In this case, the rear-

surface passivation and a wrap-around during the emitter etch-back process were identified to be responsible for 80% of the efficiency variation. These two processes should therefore be the first to be optimized in the PERC manufacturing process utilized.

This sensitivity analysis can be transferred to other production lines and cell concepts. It is especially helpful for ramping up, for example, PERC production, but can also be used for improving a currently operating production line, since the parameters that lead to the largest variations are often the same ones that offer the greatest potential for optimizing the absolute level of cell efficiencies. Not only is the presented approach basically applicable to every type of solar cell concept, but it can also contribute valuable information towards improving the quality and the yield of any production line, and consequently help in increasing the cost-effectiveness of solar cell manufacturing.

## Acknowledgements

The experiments discussed in this paper were conducted under the framework of the ‘Q-Wafer’ Project (03SF0409A and B), supported by the German Ministry for Education and Research (BMBF).

The authors would like to thank all the team at PV-TEC who helped in the processing and characterization segments, and made this work possible. Sven Wasmer gratefully acknowledges the support by scholarship funds from the State Graduate Funding Program of Baden-Württemberg. Nico Wöhrle gratefully acknowledges the scholarship from the German Federal Environmental Foundation (‘Deutsche Bundesstiftung Umwelt’).

## References

- [1] SEMI PV Group Europe 2015, “International technology roadmap for photovoltaic (ITRPV): 2014 results”, 6th edn (Apr.), Revision 1 (Jul.) [<http://www.itrpv.net/Reports/Downloads/>].
- [2] Blakers, A.W. et al. 1989, “22.8% efficient silicon solar cell”, *Appl. Phys. Lett.*, Vol. 55, No. 13, pp. 1363–1365.
- [3] Greulich, J. et al. 2013, “Numerical power balance and free energy loss analysis for solar cells including optical, thermodynamic, and electrical aspects”, *J. Appl. Phys.*, Vol. 114, No. 20, p. 204504.
- [4] Evans, R. et al. 2014, “Data mining photovoltaic cell manufacturing data”, *Proc. 40th IEEE PVSC*, Denver, Colorado, USA, pp. 2699–2704.
- [5] Evans, R. et al. 2014, “Interpreting manufacturing variance using a data mining approach”, *Proc. 29th EU PVSEC*, Amsterdam, The Netherlands, pp. 406–411.
- [6] Evans, R. et al. 2015, “Multivariate analysis of wafer process data”, *Proc. 31st EU PVSEC*, Hamburg, Germany, pp. 912–917.
- [7] Fischer, G. et al. 2012, “A combined statistical and TCAD model as a method for understanding and reducing variations in multicrystalline Si solar cell production”, *Energy Procedia*, Vol. 27, pp. 203–207.
- [8] Müller, M. et al. 2013, “Understanding and reducing the variations in multicrystalline Si solar cell production”, *Proc. 28th EU PVSEC*, Paris, France, pp. 867–871.
- [9] Müller, M. et al. 2014, “Sensitivity analysis of industrial multicrystalline PERC silicon solar cells by means of 3-D device simulation and metamodeling”, *IEEE J. Photovolt.*, Vol. 4, No. 1, pp. 107–113.
- [10] Wasmer, S. et al. 2015,

- "Investigating the impact of parameter and process variations on multicrystalline silicon PERC cell efficiency", *Proc. 31st EU PVSEC*, Hamburg, Germany, pp. 477–484.
- [11] Synopsis 2013, Sentaurus TCAD.
- [12] Schneiderlöchner, E. et al. 2001, "Laser-fired contacts (LFC)", *Proc. 17th EU PVSEC*, Munich, Germany, pp. 1303–1306.
- [13] Macleod, H.A. 2001, *Thin-film Optical Filters*. Boca Raton, FL: Taylor & Francis.
- [14] Baker-Finch, S.C., McIntosh, K.R. & Terry, M.L. 2012, "Isotextured silicon solar cell analysis and modeling 1", *IEEE J. Photovolt.*, Vol. 2, No. 4, pp. 457–464.
- [15] Greulich, J. et al. 2015, "Optical simulation and analysis of isotextured silicon solar cells and modules including light trapping", *Proc. 5th SiliconPV Conf.*, Konstanz, Germany, pp. 69–74.
- [16] Hecht, E. 2002, *Optics*. Toronto: Addison-Wesley Longman.
- [17] Phong, B.T. 1975, "Illumination for computer generated pictures", *Commun. ACM*, Vol. 18, No. 6, pp. 311–317.
- [18] Rüdiger, M. & Hermle, M. 2012, "Numerical analysis of locally contacted rear surface passivated silicon solar cells", *Jpn. J. Appl. Phys.*, Vol. 51, p. 10NA07.
- [19] Schwab, C. 2013, "Herstellung und Charakterisierung industrieller oberflächenpassivierter p-typ Solarzellen", Dissertation, Fraunhofer ISE, Albert Ludwig University, Freiburg, Germany.
- [20] Wöhrle, N. et al. 2014, "Efficiency potential simulation for an industrially feasible LFC-PERC concept with sensitivity analysis on crucial cell parameters", *Proc. 29th EU PVSEC*, Amsterdam, The Netherlands, pp. 421–426.
- [21] Fell, A. et al. 2015, "Input parameters for the simulation of silicon solar cells in 2014", *IEEE J. Photovolt.*, Vol. 5, No. 4, pp. 1250–1263.
- [22] Altermatt, P. 2011, "Models for numerical device simulations of crystalline silicon solar cells – a review", *J. Computat. Electron.*, Vol. 10, No. 3, pp. 314–330.
- [23] MacCalman, A.D. 2012, DesignCreatorv2 Spreadsheet.
- [24] Sacks, J. et al. 1989, "Design and analysis of computer experiments", *Statist. Sci.*, pp. 409–423.
- [25] Hosking, J.R.M. & Wallis, J.R. 2005, *Regional Frequency Analysis: An Approach Based on L-moments*. Cambridge, UK: Cambridge University Press.
- [26] Saltelli, A. et al. 2010, "Variance based sensitivity analysis of model output: Design and estimator for the total sensitivity index", *Computat. Phys. Comm.*, Vol. 181, No. 2, pp. 259–270.
- [27] Wanka, S. et al. 2011, "Tra.Q – Laser marking for single wafer identification – Production experience from 100 million wafers", *Proc. 37th IEEE PVSC*, Seattle, Washington, USA, pp. 1101–1104.
- [28] Krieg, A., Rajsrima, N. & Rein, S. 2011, "Laser marking of solar cells: Technologies and potential", *Proc. 26th EU PVSEC*, Hamburg, Germany, pp. 2130–2134.
- [29] Werner, S. et al. 2014, "Process optimization for the front side of p-type silicon solar cells", *Proc. 29th EU PVSEC*, Amsterdam, The Netherlands, pp. 1342–1347.
- [30] Mak, L.K., Rogers, C.M. & Northrop, D.C. 1989, "Specific contact resistance measurements on semiconductors", *J. Phys. E: Sci. Instrum.*, Vol. 22, No. 5, pp. 317–321.
- [31] Kimmerle, A., Greulich, J. & Wolf, A. 2015, "Carrier-diffusion corrected  $J_0$ -analysis of charge carrier lifetime measurements for increased consistency", *Sol. Energy Mater. Sol. Cells*, Vol. 142, pp. 116–122.
- [32] Kane, D.E. & Swanson, R.M. 1985, "Measurement of the emitter saturation current by a contactless photoconductivity decay method (silicon solar cells)", *Proc. 18th IEEE PVSC*, Las Vegas, Nevada, USA, pp. 578–583.
- [33] Sinton, R.A., Cuevas, A. & Stuckings, M. 1996, "Quasi-steady-state photoconductance, a new method for solar cell material and device characterization", *Proc. 25th IEEE PVSC*, Washington DC, USA, pp. 457–460.
- [34] Giesecke, J.A. et al. 2011, "Minority carrier lifetime of silicon solar cells from quasi-steady-state photoluminescence", *Sol. Energy Mater. Sol. Cells*, Vol. 95, No. 7, pp. 1979–1982.

#### About the Authors



**Sven Wasmer** studied physics at the University of Freiburg, Germany, and received his diploma in 2013 in collaboration with Fraunhofer ISE, Freiburg. He is currently working towards his Ph.D. at Fraunhofer ISE on the characterization and simulation of

process variations in solar cell production.



**Johannes Greulich** studied physics in Heidelberg and in Freiburg, Germany, and obtained his diploma in 2010. In 2014 he received a Ph.D. in physics from the University of Freiburg for his work on simulation and characterization of novel large-area silicon solar cells. Since 2015 he has headed a research team at ISE working on inline solar cell characterization, device simulation and image processing.



**Hannes Höffler** received his diploma in physics in 2010 from the University of Freiburg, Germany. In 2015 he obtained a Ph.D. in physics from the University of Freiburg for his work on luminescence imaging and its applications in an industrial silicon solar cell processing environment. He is currently responsible for the offline characterization laboratory in the production technology and quality assurance division at Fraunhofer ISE.



**Nico Wöhrle** studied physics at the University of Freiburg, Germany, and received his diploma in 2011 in collaboration with Fraunhofer ISE, Freiburg. He is currently finishing his Ph.D. at Fraunhofer ISE, with a thesis specialization in solar cell device simulation and loss analysis of silicon solar cells.



**Stefan Rein** is head of the inline measurement techniques and laser process technologies/quality assurance group at Fraunhofer ISE. He studied physics at the Albert Ludwig University of Freiburg and received his diploma degree in 1998. He was awarded a Ph.D. in 2004 for his work on lifetime spectroscopy for defect characterization in silicon for PV applications, carried out at Fraunhofer ISE.

#### Enquiries

Sven Wasmer  
Fraunhofer ISE  
Heidenhofstraße 2  
79110 Freiburg  
Germany

Tel: +49 (0)761 4588 5012

Email: sven.wasmer@ise.fraunhofer.de

# SOLENNA<sub>(3)</sub>: The ultimate simplification of bifacial silicon technology, at a competitive cost/Wp

Raphaël Cabal, Thomas Blévin, Rémi Monna & Yannick Veschetti

CEA Tech-INES, Le Bourget du Lac, France

## ABSTRACT

The c-Si PV industry has been historically dominated by the conventional full Al-BSF cell architecture, applied to p-type silicon, because it has so far always yielded the lowest cost at the module level (€/Wp). At the system level (€/kWh), on the other hand, bifacial PV and related reference bifacial n-PERT technology seems to be a better option for cost reduction, but additional cell processing steps (and related costs) are inhibiting bifacial PV growth. This paper first introduces INES' reference 20%-PERT technology 'SOLENN', which is based on a conventional gaseous diffusion process. Passivating/anti-reflective/doping SiO<sub>x</sub>N<sub>y</sub>:B and SiN<sub>x</sub>:P layers have been developed at INES, and the properties of these multifunctional layers are described in detail. Two process simplifications are introduced which provide devices that are both 20%-efficient and co-diffused, and which use to advantage, in the first instance, just the doping properties of the layers. By then capitalizing on the passivating and optical properties of the multifunctional layers, INES' so-called 'SOLENNA<sub>(3)</sub>' technology is presented. This ultimately simplified technology provides large-area (243cm<sup>2</sup>), LID-free, 19.8%-efficient n-PERT cells in only seven processing steps. To the authors' knowledge, this is so far the simplest n-PERT process to be introduced with such a level of performance. Finally, the cost calculation based on a 100MW line capacity and on a comparison of SOLENNA<sub>(3)</sub> with reference technologies (such as Al-BSF, PERC and BBr<sub>3</sub> PERT) was completed, without considering the potential gain from the bifacial properties. Because of its simplicity, SOLENNA<sub>(3)</sub> technology is shown to be clearly competitive with the classical Al-BSF technology in terms of cost per watt at the module level.

## Introduction

Since the c-Si PV industry scaled up to mass production, it has been dominated by the conventional full Al back-surface field (Al-BSF) cell architecture, implemented with p-type silicon. Al-BSF device performance has indeed been steadily improved (with up to 19.5% efficiency achieved for p-type solar cells [1]) and remains today the most suitable option in terms of €/Wp. In the current PV module manufacturing industry, cost reduction and process upgrade are privileged, small modifications of existing production lines being preferred to new investment. As a result, passivated emitter rear contact (PERC) architecture is gaining ground, providing p-type devices with 20–21% efficiency [2] using only a few additional steps (chemical surface preparation, deposition of passivating dielectric layer, local opening of this layer).

On the other hand, the bifacial photovoltaics (bifi-PV) market is soaring, with the passivated emitter, rear totally diffused (PERT) architecture providing 20%-efficient n-type devices that demonstrate no light-induced degradation (LID), but are fabricated using more-complex cell process flows. The PV community is becoming more and more convinced

that the use of bifaciality for future generations of PV systems will allow a significant reduction in the levelized cost of electricity (LCOE). Some direct issues (bankability) are currently being addressed through the installation of large (>1MWp) PV bifacial fields [3] and through the formation of standardization groups.

There is another issue concerning the additional cost incurred in the production of bifacial modules, primarily related to the additional processing steps at the cell level. Indeed, the fabrication of the so-called PERT cell, suitable for bifaciality, meets different specifications, such as single-sided p<sup>+</sup> and n<sup>+</sup> diffusion, B emitter specific passivation and double-sided SiN coating. Over the last few years, academics and manufacturers have made significant R&D efforts in finding ways to simplify the process flow [4]. The use of a hybrid approach combining P-implantation and BBr<sub>3</sub> diffusion is one example of such process simplification [5]. The full implantation process is also very attractive, since the formation of the doped layers can be performed at the same time as the annealing step [6,7]. Finally, the co-diffusion approach involves single-sided deposited doped layers [8,9].

Most of these concepts have in recent years led to solar cells with conversion efficiencies of over 20.0%. Nevertheless, the growth in the production of bifacial cells remains limited, mostly because the economic interest only occurs at the system level (LCOE) when the bifacial gain is considered. The authors believe that a faster growth of bifacial PV requires an even more simplified bifacial cell manufacturing process in order to reduce the initial CAPEX investment, and thus the cost per Wp.

**“A faster growth of bifacial PV requires an even more simplified bifacial cell manufacturing process.”**

## Doping properties of SiO<sub>x</sub>N<sub>y</sub>:B and SiN<sub>x</sub>:P layers

Among the alternative doping techniques considered for simplifying the fabrication of the p<sup>+</sup>/n/n<sup>+</sup> structure, dielectric doped layers are of primary interest, since they open the door to co-diffusion (the formation of the emitter and the BSF in a single step [10–12]). In recent years, the annealing

Fab & Facilities

Materials

Cell Processing

Thin Film

PV Modules

Market Watch

of boron silicate glass (BSG) during  $\text{POCl}_3$  diffusion has led to co-diffused n-PERT devices with 20% efficiency [13]. In this approach, the BSG layer (which is a  $\text{SiO}_x\text{:B}$ -based material) shows both doping properties and a barrier property with regard to phosphorus diffusion. The quality of doping has already been demonstrated at INES, as well as by other teams, with satisfactory doping uniformities (<5%) for a relevant sheet resistance ( $R_{\text{sheet}}$ ) window of 50–100 $\Omega/\text{sq}$ . Since the doping activation is facilitated in the case of boron dopant, it is possible to measure (using a WCT 120 Sinton Lifetime tester) satisfactory B-emitter saturation current densities ( $J_{0e} < 90\text{fA}/\text{cm}^2$  for 70 $\Omega/\text{sq}$ .) on 239 $\text{cm}^2$  Cz textured samples ( $\text{p}^+/\text{n}/\text{p}^+$  structure passivated by thermal  $\text{SiO}_2/\text{SiN}$  stack). In the literature, even lower saturation current density values can be found on polished samples and/or with a higher emitter  $R_{\text{sheet}}$  domain, and/or using an  $\text{AlO}_x/\text{SiN}$  passivating stack [14], offering further evidence of the quality of BSG as a doping source.

At INES, the BSG layer is more precisely a  $\text{SiO}_x\text{N}_y\text{:B}$  material, deposited by low-frequency plasma-enhanced chemical vapour deposition (PECVD), using a mixture of  $\text{SiH}_4$  and  $\text{N}_2\text{O}$ , and  $\text{H}_2$ -diluted  $\text{B}_2\text{H}_6$  as a boron precursor. For this work, various thicknesses of  $\text{SiO}_x\text{N}_y\text{:B}$  were coated on 239 $\text{cm}^2$  Cz(n) wafers (1–4 $\Omega\cdot\text{cm}$ ) and then annealed at 940 $^\circ\text{C}$  (< 1h) under  $\text{N}_2$ . The resulting B-emitter  $R_{\text{sheet}}$  values are plotted in Fig. 1 as a function of  $\text{SiO}_x\text{N}_y\text{:B}$  thickness; it is demonstrated here that the thickness of the layer is not the primary determinant of the final sheet resistance of the emitter. Once the minimum thickness (here 19nm) satisfying the resistance (<100 $\Omega/\text{sq}$ .) and the uniformity (<5%) is reached, any further increase in the thickness of the layer only improves the doping uniformity (< 2%), with no impact on the average sheet resistance value. This quasi-independency of  $R_{\text{sheet}}$  with respect to doping layer thickness is in agreement with studies [15,16] showing stronger dependency on the  $\text{SiH}_4/\text{B}_2\text{H}_6$  ratio. In this case, the gas ratio was chosen below 4%, in order to promote high doping from significantly thinner  $\text{SiO}_x\text{N}_y\text{:B}$  layers (<20nm) than what is usually reported in the literature.

Dielectric doped layers as an alternative  $\text{n}^+$  doping technique to conventional  $\text{POCl}_3$  diffusion are also considered. Here, the aim is to use such a doping layer for the  $\text{n}^+$  BSF of the n-PERT solar cells. PECVD-deposited PSG (phosphorus silicate

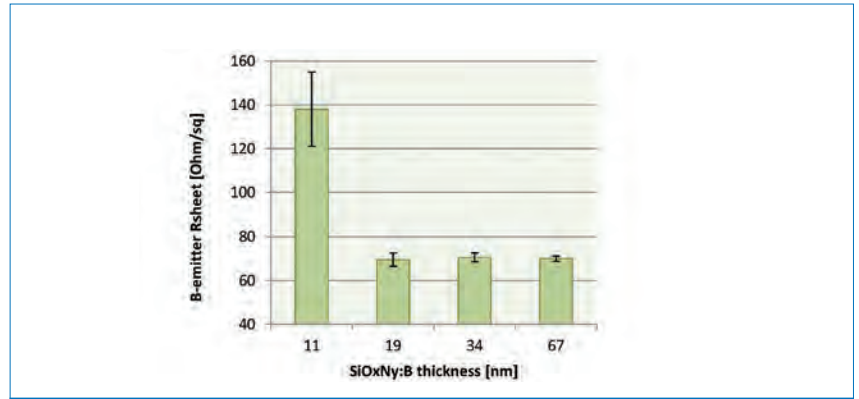


Figure 1. Variation in  $R_{\text{sheet}}$  of the  $\text{p}^+$  emitter for different  $\text{SiO}_x\text{N}_y\text{:B}$  layer thicknesses after the anneal (940 $^\circ\text{C}$ ; <1h).

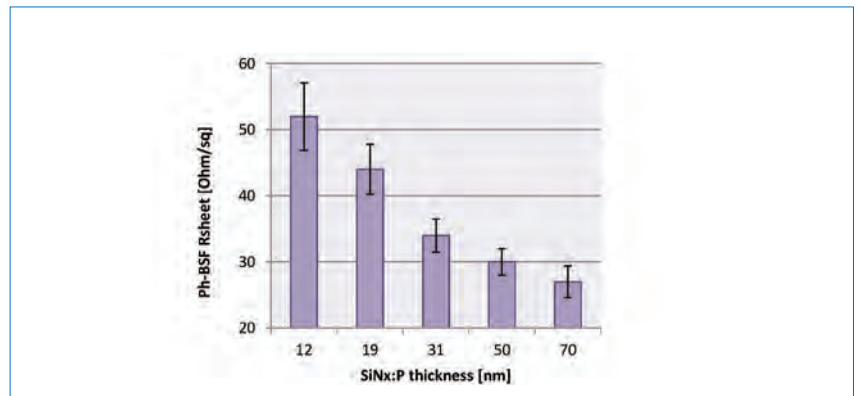


Figure 2. Variation in  $R_{\text{sheet}}$  of the  $\text{n}^+$  BSF for different  $\text{SiN}_x\text{:P}$  layer thicknesses after the anneal (940 $^\circ\text{C}$ ; <1h).

glass) layers have been considered as an option for many years [17,18]. Despite the promising results obtained with PSG on p-type devices [19], no clear benefit of such P-doping sources has been demonstrated up to now. Aside from this most commonly studied P-doped  $\text{SiO}_x$  material, it was preferred to focus on the development of hydrogenated  $\text{SiN}_x\text{:P}$  layers, with the aim of combining doping and passivating properties in one layer.

The use of  $\text{SiN:P}$  as a phosphorus doping source has been investigated in the past for laser-doped selective emitter p-type solar cells fabrication [20], but has yielded high emitter contact resistance. In the present work, the  $\text{SiN:P}$  was deposited by low-frequency PECVD, using a mixture of  $\text{SiH}_4$ ,  $\text{NH}_3$  and  $\text{H}_2$ -diluted  $\text{PH}_3$  as a phosphorus precursor. Various thicknesses of  $\text{SiN}_x\text{:P}$  were coated on 239 $\text{cm}^2$  Cz(p) wafers (2 $\Omega\cdot\text{cm}$ ), which were then annealed at 940 $^\circ\text{C}$  (<1h) under  $\text{N}_2$ . The resulting  $\text{n}^+$  region sheet resistance is plotted in Fig. 2 as a function of  $\text{SiN}_x\text{:P}$  thickness; the  $R_{\text{sheet}}$  of the  $\text{n}^+$  BSF increases steadily as the  $\text{SiN}_x\text{:P}$  thickness decreases. The doping behaviour is consistent with a finite source: the thinner the layer, the higher the  $R_{\text{sheet}}$ . It should be noted that there is no dramatic degradation of doping

uniformity (<8%), even for the thinner layer (12nm).

### Moderately simplified n-PERT solar devices

A first integration of the boron and phosphorus doping layers was performed on 239 $\text{cm}^2$  n-PERT solar cells. As a reference, INES' baseline PERT process was used, which is based on two separate gaseous diffusions. This process is then referred to as the SOLENN process (SOLAR ENHANCED N-type).

#### SOLENN process

The processing sequence for SOLENN solar cells includes alkaline texturing of Cz(n) wafers surfaces,  $\text{BCl}_3$  boron diffusion (940 $^\circ\text{C}$ ) and  $\text{POCl}_3$  phosphorus diffusion (840 $^\circ\text{C}$ ). PECVD-deposited  $\text{SiO}_x$  barriers are coated on the opposite side of the wafer, prior to each diffusion, and removed (by HF-dip + RCA clean) after each diffusion. Once the  $\text{p}^+/\text{n}/\text{n}^+$  structure is obtained, both sides are passivated by thermal oxidation, leading to  $\text{SiO}_2$  growth of less than 10nm in thickness. PECVD deposition of anti-reflective hydrogenated  $\text{SiN}$  is then carried out on both sides. A Ag/Al grid is screen printed on the front, while a Ag grid is



# Metallization Workshop 2016

6<sup>th</sup> Workshop on Metallization and Interconnection  
for Crystalline Silicon Solar Cells

May 2-3, 2016  
Konstanz, Germany

**REGISTER NOW!**  
[www.metallizationworkshop.info](http://www.metallizationworkshop.info)



- ❖ Advance in metallization has been the main technological progress in PV technology over the last 10 years.
- ❖ New solar cell interconnection is likely to become the next key area for PV performance improvement.

Do you want to understand evolutions in those fields and anticipate what it can mean for your activities?

**Join the prime event for experts in Metallization and Interconnection of Crystalline Silicon Solar Cells!**

**NEW! You can choose to attend the event remotely but interactively through a live webinar !**

sponsors



Besi



supporters



media partners



printed on the rear, for contacting the p<sup>+</sup> emitter and the n<sup>+</sup> BSF respectively; the actual contacting is done during the subsequent co-firing step in an IR belt furnace.

**1st simplified approach**

The first way to make the n-PERT process flow shorter is to use the SiO<sub>x</sub>N<sub>y</sub>:B layer as a boron doping source, and benefit from the POCl<sub>3</sub> diffusion step to promote formation of the B emitter: such a co-diffusion combining solid and gaseous doping sources has been widely studied in the literature [21,22], and will therefore not be expanded on too much here. It is just worth recalling the requirement of the B-doped layer to act as a barrier to POCl<sub>3</sub> diffusion. In order to do so, the use of a thick (>100nm) BSG, including optional surface-capping layers, is often reported; for instance, Rothhardt et al. [9] use a ~180nm BSG/SiO<sub>x</sub> stack deposited by APCVD for their 19.9% CoBiN n-PERT cell. Similarly, the aforementioned SiO<sub>x</sub>N<sub>y</sub>:B would not alone ensure good barrier properties, and so SiN<sub>x</sub> was used as a capping layer.

The processing sequence for ‘SOLENNA<sub>(1)</sub>’ devices (i.e. the 1st simplified SOLENN approach) is the following. After alkaline texturing, the wafer front side is coated by the low-frequency PECVD stack (a 30nm-thick SiO<sub>x</sub>N<sub>y</sub>:B capped by 50nm of SiN<sub>x</sub>) prior to the co-diffusion cycle (involving a first plateau at 940°C under N<sub>2</sub>, followed by the POCl<sub>3</sub> injection at a lower temperature). The POCl<sub>3</sub>-induced glass (rear) and B-doped stack (front) are then HF removed, and the wafers surfaces are RCA cleaned. The subsequent passivation and metallization sequence is identical to INES’ reference process (SOLENN).

**2nd simplified approach**

The second way of simplifying n-PERT technology is to co-anneal solid sources only. Solid sources have been studied for decades [23,24]; Das et al. [25], for instance, demonstrated the high potential of B-doped spin-on glass by fabricating 20%-efficient 4cm<sup>2</sup> devices incorporating it. Nevertheless, the significant bifacial

cell results obtained so far have always combined one solid doping source with a more conventional technique (ion implantation or gaseous diffusion). More precisely, what are referred to here as ‘SOLENNA<sub>(2)</sub>’ devices (i.e. 2nd simplified SOLENN approach devices) combine the SiO<sub>x</sub>N<sub>y</sub>:B and SiN<sub>x</sub>:P layers for the p<sup>+</sup> emitter and n<sup>+</sup> BSF formation.

The processing sequence for SOLENNA<sub>(2)</sub> solar cells includes, as always, the alkaline texturing, followed by SiO<sub>x</sub>N<sub>y</sub>:B (front) and SiN<sub>x</sub>:P (rear) deposition. Samples are then co-annealed in a quartz tube furnace (940°C; <1h) under a N<sub>2</sub> atmosphere. Note that the use of a solid P-doped layer instead of POCl<sub>3</sub> allows thin (<40nm) uncapped SiO<sub>x</sub>N<sub>y</sub>:B layers to be employed. Doped dielectrics are then HF removed, and the wafers surfaces are RCA cleaned. The subsequent steps are identical to the previously described processes (see SOLENN and SOLENNA<sub>(1)</sub>).

**Cell results**

The different process flows described so far are depicted in Fig. 3. Batches of 239cm<sup>2</sup> Cz n-type wafers (2–3Ω·cm) were processed into n-PERT screen-printed solar cells, following these different approaches. The best I–V parameters measured on these batches

(in a class A solar simulator, under standard testing conditions – STC) are listed in Table 1.

The poorer FF/PFF values exhibited by SOLENNA<sub>(1)</sub> solar cells are attributed to localized parasitic P diffusion through SiO<sub>x</sub>N<sub>y</sub>:B/SiN porosities; as a result, a lower shunt resistance value (R<sub>p</sub> < 2kΩ·cm<sup>2</sup>) is reached (50kΩ·cm<sup>2</sup> for the reference process). The SOLENNA<sub>(2)</sub> devices are logically excluded from such an R<sub>p</sub> limitation, since they are made via a pure dielectric co-diffusion route.

Both the 1st and 2nd simplifications of the SOLENN process made it possible to obtain 20%-efficiency n-PERT bifacial solar cells, using a reduced number of processing steps compared with the reference process. Both SOLENNA<sub>(1)</sub> and SOLENNA<sub>(2)</sub> processes have also demonstrated good compatibility with industrial n-type mono-like silicon [13]. Nevertheless, further simplification of n-PERT technology would be possible if the doping PECVD layers could also provide proper passivating and optical properties.

**From doping to multifunctional layers**

Different ways of integrating multifunctional dielectric layers into solar devices are proposed in the



**Figure 3. The n-PERT process flow simplifications: gaseous diffusion route (SOLENN), co-diffusion SiO<sub>x</sub>N<sub>y</sub>:B/POCl<sub>3</sub> route (SOLENNA<sub>(1)</sub>) and full dielectric co-diffusion route (SOLENNA<sub>(2)</sub>).**

	Size [cm <sup>2</sup> ]	J <sub>sc</sub> [mA/cm <sup>2</sup> ]	V <sub>oc</sub> [mV]	FF [%]	η [%]	PFF [%]
SOLENN	239	39.3	647	79.9	20.3	83.5
SOLENNA <sub>(1)</sub>	239	39.7	648	77.8	20.0	82.3
SOLENNA <sub>(2)</sub>	239	39.0	648	79.2	20.0	83.5

**Table 1. Best I–V results for n-PERT screen-printed solar cells (measured under STC: 25°C; AM1.5G; 1,000W/m<sup>2</sup>).**

Successive tuning	SiO <sub>x</sub> N <sub>y</sub> :B/SiN passivated p <sup>+</sup> /n/p <sup>+</sup> structure			SiN <sub>x</sub> :P/SiN passivated n <sup>+</sup> /n/n <sup>+</sup> structure		
	Initial	Plasma	Anneal	Initial	Plasma	Anneal
J <sub>0</sub> (fA/cm <sup>2</sup> )	1443	120	85	337	247	180
1sun-iV <sub>oc</sub> (mV)	595	649	667	646	654	658

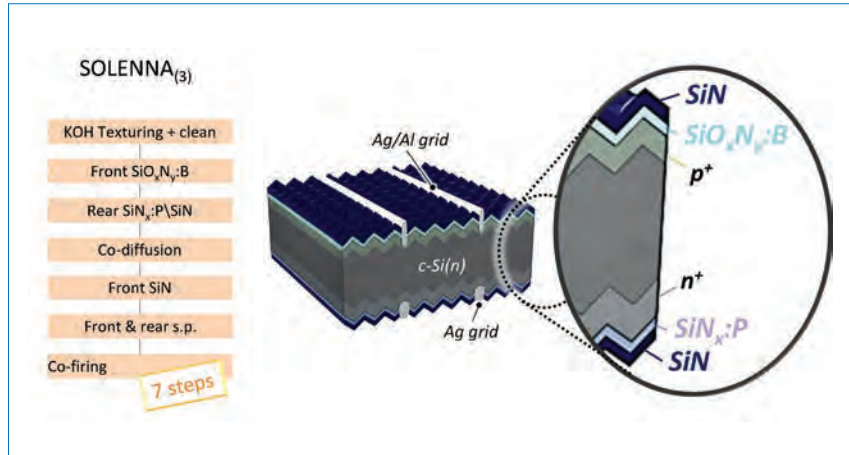
**Table 2.** J<sub>0</sub> and 1sun-iV<sub>oc</sub> values, measured on textured Cz symmetrical structures after successive tuning of the plasma parameters and the co-anneal process.

few papers that can be found in the literature. The PassDop approach uses SiN<sub>x</sub>:P for playing alternatively the role of P-reservoir for laser doping (beneath the contacted regions) and the role of passivating layer between the heavily-doped regions. Reported PassDop n-PERL cell performance is outstanding [26,27], but SiN<sub>x</sub>:P doping and passivating properties are never exploited concurrently in one specific region of the devices.

The quality of passivation offered by existing doped layers has also been reported in the literature. For instance, the passivation of n<sup>+</sup> regions by phosphorus- or boron-doped nitride layers (SiN<sub>x</sub>:P/B) was studied by Gall et al. [28]: in both cases, the introduction of a thermal SiO<sub>2</sub> interfacial layer was required in order to obtain satisfying J<sub>0e</sub>/iV<sub>oc</sub> values. More recently, the passivating potential of 100nm thick SiN<sub>x</sub>-capped BSG layers was reported by Engelhardt et al. [14] with a 1sun-iV<sub>oc</sub> of 675mV obtained on p<sup>+</sup>/n/p<sup>+</sup> FZ samples, with a 60Ω/sq. emitter. Nevertheless, no integration of such a stack in an actual solar device has so far been reported.

Multi-purpose PECVD stacks have been developed, in which each layer ensures one function (anti-reflective, passivating or doping). For instance, 120nm thick PSG/SiN stacks have been reported to provide good n<sup>+</sup> doping and subsequent passivation (65Ω/sq.; 118fA/cm<sup>2</sup>) on shiny-etched FZ [29]. In addition to this, a 300nm-thick dielectric stack made of Al<sub>2</sub>O<sub>3</sub>, capped by an oxidized a-Si:B layer, was used by Seiffe et al. [30] on the back side of LFC solar cells, for p<sup>+</sup> doping (>250Ω/sq.), passivation and optics. Those authors subsequently measured a conversion efficiency of 18.3% on 50mm × 50mm Cz(p) substrates.

At CEA Tech-INES, as suggested previously, PECVD layers were developed with a high doping property, even for thin layers. For instance, as can be seen in Figs. 1 and 2, 20nm-thick SiO<sub>x</sub>N<sub>y</sub>:B and SiN<sub>x</sub>:P layers are sufficient for achieving decent doping targets (in this case, p<sup>+</sup> emitter < 80Ω/sq.; n<sup>+</sup> BSF < 50Ω/sq.). From an optical point of view, the integration of the layers on



**Figure 4.** The ultra-simplified process flow and corresponding cell structure of SOLENNA<sub>(3)</sub>.

both the front and the rear sides of solar devices is thus facilitated. In addition, the decision was taken to develop an hydrogenated nitride layer (SiN<sub>x</sub>:P) to boost the passivating ability of the layer itself, instead of using a SiO<sub>x</sub>:P layer combined with some additional passivating layer.

The passivating properties of the SiO<sub>x</sub>N<sub>y</sub>:B and SiN<sub>x</sub>:P layers were evaluated by means of QSSPC J<sub>0</sub> measurements, on p<sup>+</sup>/n/p<sup>+</sup> and n<sup>+</sup>/n/n<sup>+</sup> sample structures respectively. The thermal budget for the annealing of the layers and the related diffusion of the dopants is still 940°C, for a duration of less than one hour. These samples were created from Cz(n) 4Ω-cm wafers that had previously been alkaline textured, RCA cleaned and double-side coated with the layers under consideration.

The improvement of the initially poor passivating properties of the SiO<sub>x</sub>N<sub>y</sub>:B layer was investigated by capping it first with a typical anti-reflective (and H<sub>2</sub>-reservoir) SiN layer. No significant enhancement of the passivating level was observed (J<sub>0p+</sub> > 1,400fA/cm<sup>2</sup>). Similarly, the initial SiN<sub>x</sub>:P layer was found to exhibit only moderate passivation (J<sub>0n+</sub> > 370fA/cm<sup>2</sup>). Only a marginal improvement was observed when the SiN capping (J<sub>0n+</sub>=337fA/cm<sup>2</sup>) was introduced, but such capping was used as a barrier to out-diffusion of phosphorus.

An enhancement of the passivation

features of the doped layers was made possible by tuning of the plasma deposition conditions as well as of the subsequent co-annealing step. The resulting J<sub>0</sub>/iV<sub>oc</sub> values after firing (800°C) of the samples are given Table 2. The optical indexes (n;k) of the final layers have been measured by ellipsometry. SiO<sub>x</sub>N<sub>y</sub>:B was found to compare quite favourably with stoichiometric silicon oxide (refraction index n < 148 at λ = 633nm), and exhibits decent transparency in the higher wavelength domain (k < 0.0013). At present, further optical tuning is required for SiN<sub>x</sub>:P in order to reduce the high optical indexes caused by a relatively Si-rich stoichiometry.

### Ultra-simplified n-PERT solar devices

#### Process flow and cell results

A batch of 243cm<sup>2</sup> Cz n-type wafers (2Ω-cm) was processed using an ultra-simplified n-PERT approach, in which the doped layers are maintained. With the final front- and rear-surface passivation here being provided by SiO<sub>x</sub>N<sub>y</sub>:B/SiN and SiN<sub>x</sub>:P, it was possible to avoid thermal oxidation as well as chemical removal of the doped layer and subsequent cleaning. Furthermore, the rear PECVD SiN deposition layer was integrated (because of out-diffusion concerns) as

	Size [cm <sup>2</sup> ]	$J_{sc}$ [mA/cm <sup>2</sup> ]	$V_{oc}$ [mV]	FF [%]	$\eta$ [%]	PFF [%]
Average	243	38.6	644	79.1	19.7	82.9
Best cell		38.5	645	79.6	19.8	82.7

**Table 3.**  $I$ – $V$  results for SOLENN<sub>(3)</sub> n-PERT screen-printed solar cells (measured under STC: 25°C; AM1.5G; 1,000W/m<sup>2</sup>). A batch of 10 cells was used.

capping in the SiN<sub>x</sub>:P recipe.

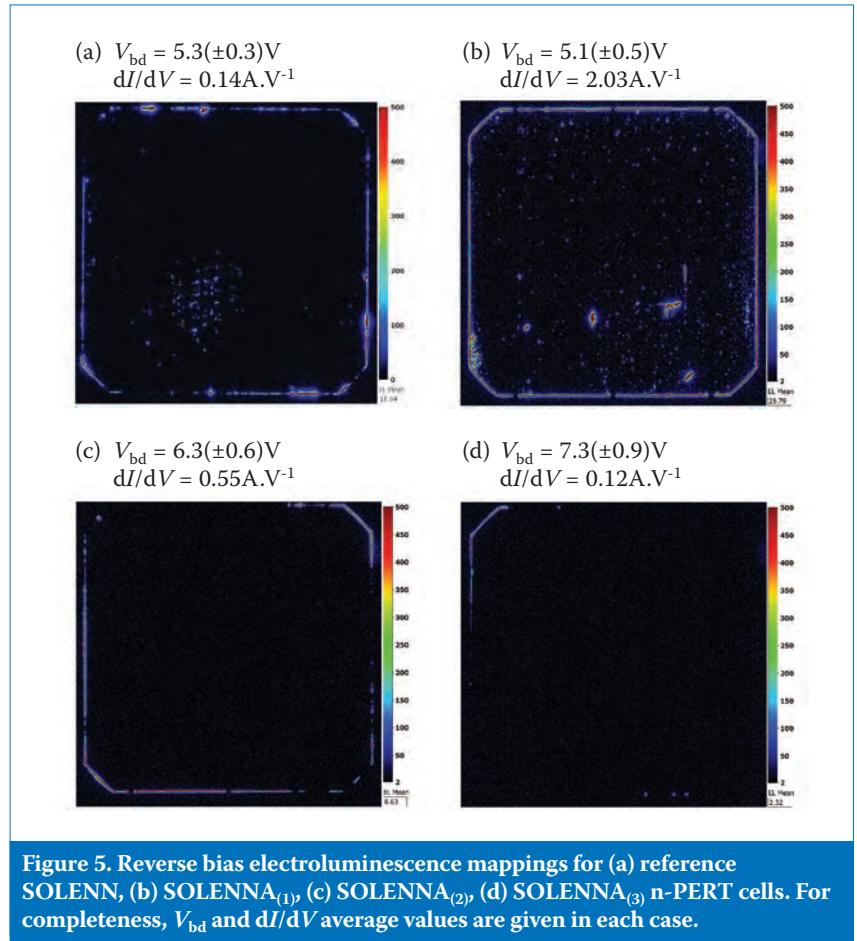
As a consequence, the processing sequence for ‘SOLENN<sub>(3)</sub>’ devices (i.e. the 3rd simplified SOLENN approach) is reduced to seven steps, as depicted in Fig. 4. After alkaline texturing and RCA cleaning of the wafer (1), the SiO<sub>x</sub>N<sub>y</sub>:B layer (2) and the SiN<sub>x</sub>:P/SiN stack (3) are deposited on the front and rear sides. The samples are co-annealed (940°C; <1h) (4), leading to a 70Ω/sq. B emitter and a 35Ω/sq. P BSF. PECVD ARC SiN is deposited on the front (5). The front and rear silver-based grid contacts are screen printed (6) and then co-fired (7).

The average and best  $I$ – $V$  parameters measured on this batch are listed in Table 3. The  $J_{sc}$  value is slightly lower for SOLENN<sub>(3)</sub> solar cells (<38.8mA/cm<sup>2</sup>), because of the non-optimized transparency of the doped layers, and also because of the heavily doped n<sup>+</sup> BSF. A comparison of SOLENN and SOLENN<sub>(3)</sub> spectral responses revealed an average loss of 3%<sub>rel.</sub> in the short wavelength IQE ( $\lambda < 500$ nm), but a more pronounced loss (4.5%<sub>rel.</sub>) in the long wavelength domain ( $\lambda > 950$ nm). The other cell parameters are all competitive with INES’ reference n-PERT devices. The shunt resistance is similar to what was observed for SOLENN<sub>(2)</sub> devices.

“Conversion efficiencies of up to 19.8% were obtained on large-area Cz(n) wafers processed into n-PERT devices using only seven steps.”

Conversion efficiencies of up to 19.8% were obtained on large-area Cz(n) wafers processed into n-PERT devices using only seven steps. To the authors’ knowledge, this is the simplest n-PERT process ever introduced with such a level of performance. As the resulting cell architecture involves layers with high concentrations of dopant impurities, it needs to be verified that no related LID could occur that might alter the cell behaviour.

An initial evaluation of the long-



**Figure 5.** Reverse bias electroluminescence mappings for (a) reference SOLENN, (b) SOLENN<sub>(1)</sub>, (c) SOLENN<sub>(2)</sub>, (d) SOLENN<sub>(3)</sub> n-PERT cells. For completeness,  $V_{bd}$  and  $dI/dV$  average values are given in each case.

term stability of SOLENN<sub>(3)</sub> performance has been carried out: no efficiency degradation occurs after prolonged light exposure (>120h; 0.3sun; 50°C). The cell behaviour under reverse bias was also monitored and compared with that of reference n-PERT cells. Both reverse  $I$ – $V$  curves and ReBEL mappings were compared in order to qualify the ultra-simplified SOLENN<sub>(3)</sub> device as a candidate for PV module integration. As can be seen in Fig. 5, the typical ReBEL mappings obtained under a reverse bias of 10V are quite different, depending on the process flow involved. For each technology, corresponding batches of five solar cells had their reverse  $I$ – $V$  curves measured in order to extract average values of: 1) breakdown voltage ( $V_{bd}$ ), defined by the abscissa of the maximal curvature point; and 2) leakage current slope ( $dI/dV$ ) in the ‘hard breakdown’ domain (i.e. for  $|V| > V_{bd}$ ).

The reference SOLENN and the

SOLENN<sub>(1)</sub> technologies, which involve at least one gaseous diffusion, exhibit both edge and surface defect signatures (see Fig. 5(a) and (b)). Reference SOLENN surface defectiveness is mainly caused by handling (the impact of which is accentuated by process flows involving many steps) [31]. The surface defect signature is nonetheless much more obvious in the case of SOLENN<sub>(1)</sub> and is related to the aforementioned microporosity of SiO<sub>x</sub>N<sub>y</sub>:B/SiN to POCl<sub>3</sub>, which leads to noticeable micro-shunts spread over the entire wafer surface. The corresponding cell electrical behaviour is degraded under reverse bias, as evidenced by a much steeper  $dI/dV$  slope (>2A.V<sup>-1</sup>) compared with the average value obtained for SOLENN cells. On the other hand, SOLENN<sub>(2)</sub> and SOLENN<sub>(3)</sub> devices (Fig. 5(c) and (d)), which exploit exclusively dielectric layer doping sources, show only edge defectiveness and a slightly improved  $V_{bd}$ . Of course,

Technology	Wafer	Status	Average efficiency [%]	No. of processing steps
Al-BSF	Cz	Standard technology	19.0	5
PERC	Cz	Next p-type generation	20.0	8–9
Industrial PERT	Cz	In production – BBr <sub>3</sub>	20.0	8–11
SOLENN <sub>(3)</sub>	Cz	Lab scale	20.0	7

Table 4. Summary of the cell technologies considered for the cost study.

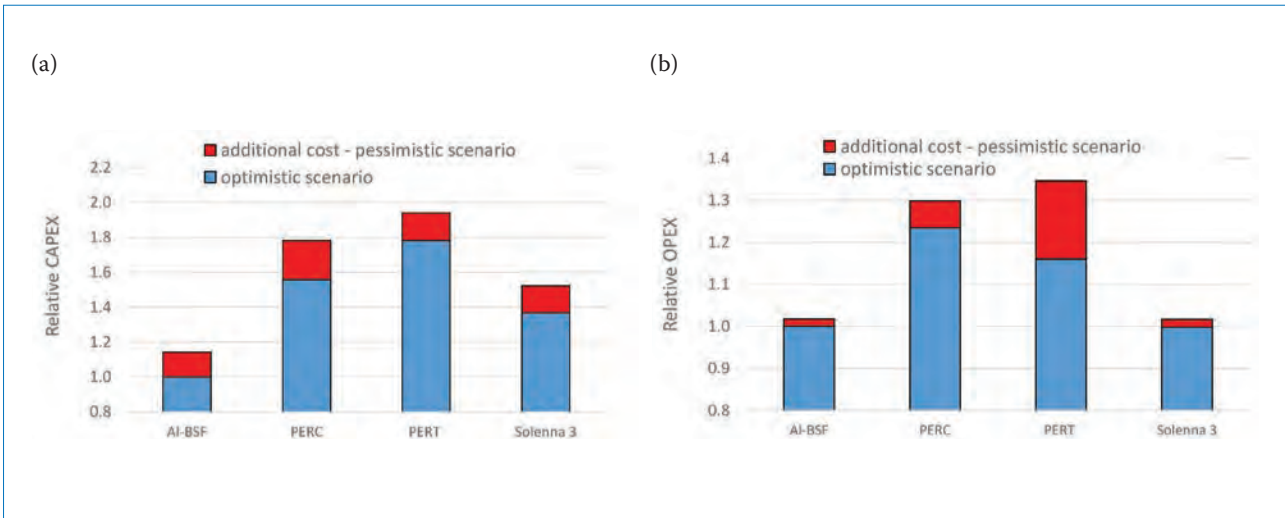


Figure 6. CAPEX (a) and OPEX (b) for PERC, PERT and SOLENN<sub>(3)</sub>, compared with the Al-BSF process.

the edge defect contribution can be removed by conventional laser edge junction opening. Such edge isolation is required in the case of the n-PERT cell architecture in order to meet PV module requirements ( $I < 1A$  at  $-12V$ ).

### Cost calculation

A cost study was performed to assess the economic advantage of SOLENN<sub>(3)</sub> technology over the reference technologies listed in Table 4. The calculation addresses the cell process cost (CAPEX and OPEX), as well as the total cost of ownership (CoO) in €/W<sub>p</sub>, including wafer and module contributions. The scenario of a production line in Europe with an annual capacity of 100MW was used. Parameters such as yield, uptime, manpower, building and facilities were adjusted with the number of process steps. Depreciations of 5 years for the equipment, 10 years for the facilities and 20 years for the building were fixed. No bifacial gain was considered in the study.

All the investigated processes were based on two scenarios: optimistic and pessimistic. This variation depends on the process complexity (number of steps) or on the characteristics of the equipment (throughput and cost). For the PERC process, additional steps – such as Al<sub>2</sub>O<sub>3</sub> and rear SiN deposition, and laser opening – were added to the standard Al-BSF. Although this

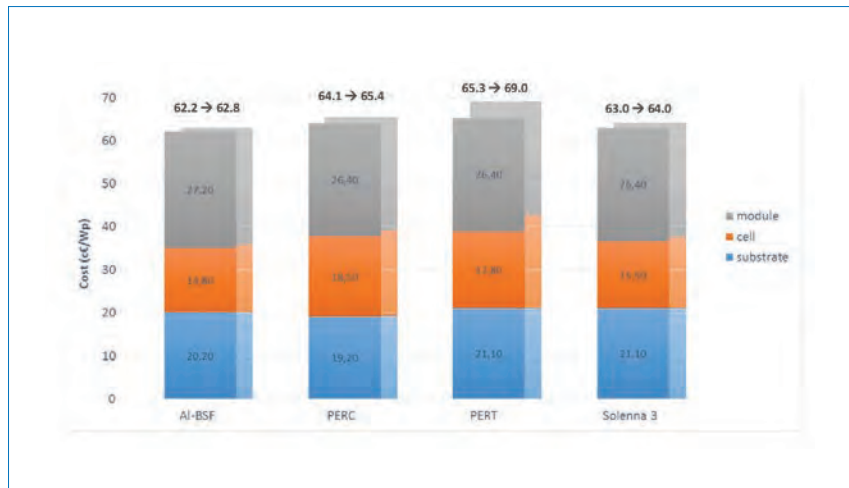
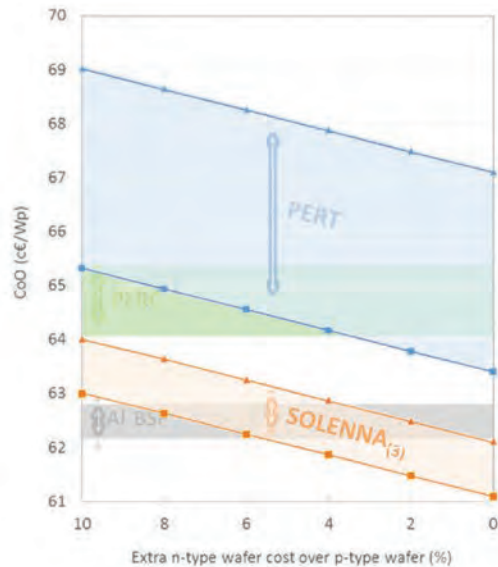


Figure 7. Contribution of wafer (blue), cell (orange) and module (grey) to the total CoOs, including optimistic (dark shades) and pessimistic (light shades) scenarios, and assuming a 10% higher price for n-type wafers. Total technology CoO ranges are indicated at the top of each bar.

technology currently sets lab records of close to 22%, an average production efficiency of 20%, including possible LID losses, was considered for this study.

The PERT BBr<sub>3</sub>-based process can be performed in different ways, resulting in the number of processing steps ranging from 8 (so-called PERT+) to 11 (so-called PERT-). At the very least, the PERT process requires additional equipment, such as a BBr<sub>3</sub> tube furnace, wet bench for glass removal, and PECVD tool for the rear SiN layer.

The relative CAPEX for a standard Al-BSF production line is given in Fig. 6(a). For all the high-efficiency technologies investigated, a higher initial investment is required. PERC and PERT technologies show similar CAPEX ranges, corresponding to, in the best case, between 1.6 and 1.8 times the cost of a standard Al-BSF line. The pessimistic scenario of the PERT gaseous approach shows a more pronounced investment, because of the use of a diffusion barrier and specific emitter passivation by thermal oxide.



**Figure 8.** Total CoO ranges (€/Wp) as a function of the n-type wafer additional cost relative to p-type, for the various cell technologies under consideration ('+' and '-' refer to the optimistic and pessimistic scenarios respectively).

As expected, the required CAPEX for SOLENNA<sub>(3)</sub> is more favourable (about 1.4 times the cost of an Al-BSF line), because of the process simplicity. As regards the OPEX, presented in Fig. 6(b), SOLENNA<sub>(3)</sub> technology clearly outperforms PERC and gaseous PERT technologies, and is even equivalent to Al-BSF for both the optimistic and pessimistic scenarios. This is also explained by the reduced number of processing steps.

The CoO at the module level is shown Fig. 7 for the optimistic and the pessimistic scenarios. Both of the n-type technologies (PERT and SOLENNA<sub>(3)</sub>) are penalized by the additional cost of the n wafer (considered here to be 10% higher than p-type), which leads to a more expensive PERT gaseous process than in the case of Al-BSF and PERC. Nevertheless, the very low cell process cost of SOLENNA<sub>(3)</sub> compensates for this weakness, thus allowing a very competitive technology at the module level. Indeed, the corresponding CoO remains slightly higher than that for Al-BSF, but clearly outperforms both PERC and gaseous PERT.

A comparison of the CoOs was then made, taking into consideration a reduction of 10% to 0% in the extra cost of n-type wafers compared with p-type wafers (Fig. 8). The validity of such an assumption increases with n-type market volume. Assuming the cost of n-type wafers is the same as p-type wafers, the CoO cost of 20%-efficient SOLENNA<sub>(3)</sub> technology

would be in a range of 61.1–62.1€/Wp; this is even cheaper than 19%-efficient Al-BSF technology (62.2€/Wp).

## Conclusion

The potential of dielectric doping layers for simplifying the manufacture of PERT solar cells was discussed, and the doping properties of the PECVD-deposited SiO<sub>x</sub>N<sub>y</sub>:B and SiN<sub>x</sub>:P layers were presented. The status of the recent developments made at CEA-INES in 20%-efficient n-PERT was given via a description of following approaches: SOLENN (corresponding to INES' lab reference process based on BCl<sub>3</sub> and POCl<sub>3</sub> gaseous diffusions), SOLENNA<sub>(1)</sub> (mixing SiO<sub>x</sub>N<sub>y</sub>:B with POCl<sub>3</sub>), SOLENNA<sub>(2)</sub> (pure dielectric co-diffusion route).

Finally, SOLENNA<sub>(3)</sub> technology was introduced for a simplified fabrication of n-type bifacial PERT cells in seven steps. This technology relies on the opportunity to combine doping, passivating and optical properties in the SiO<sub>x</sub>N<sub>y</sub>:B and SiN<sub>x</sub>:P layers, which allows these layers to be retained in the final device architecture, with no detrimental effect on conversion efficiency: SOLENNA<sub>(3)</sub> devices achieving 19.8% efficiency have already been obtained on 243cm<sup>2</sup> Cz(n) wafers. Further improvements regarding cell efficiency (new generation of pastes, five to six busbars, passivation improvements) could collectively lead to a very high-efficiency, low-cost technology.

**“On the basis of possible n-type wafer cost reductions, SOLENNA<sub>(3)</sub> could become the most competitive technology.”**

At an industrial level, the cost study indicates that SOLENNA<sub>(3)</sub> technology can clearly compete with the classical Al-BSF technology in terms of cost per watt. A particular feature is that only a limited initial investment for new production lines, or additional investment for upgrading production lines, is necessary. Furthermore, the SOLENNA<sub>(3)</sub> processing sequence requires only one chemical (texturing) step, thus opening the door to significant reductions in facility costs, which is of interest in both economic and environmental terms. In addition, the potential extra power output (linked to device bifaciality) was not taken into account in this study. At the module level (CoO), SOLENNA<sub>(3)</sub> outperforms PERC, even with the higher wafer cost. On the basis of possible n-type wafer cost reductions, SOLENNA<sub>(3)</sub> could become the most competitive technology.

## References

- [1] SEMI PV Group Europe 2015, “International technology roadmap for photovoltaic (ITRPV): 2014 results”, 6th edn (Apr.) [http://www.itrpv.net/Reports/Downloads/].
- [2] Metz, A. et al. 2014, “Industrial high performance crystalline silicon solar cells and modules based on rear surface passivation technology”, *Solar Energy Materials & Solar Cells*, Vol. 120, pp. 417–425.
- [3] Kopeček, R. et al. 2014, “Bifaciality: One small step for technology, one giant leap for kWh cost reduction”, *Photovoltaics International*, 26th edn.
- [4] Lim, B. et al. 2014, “Simplifying the fabrication process flow of n-type PERT solar cells: Recent progress at ISFH”, *Photovoltaics International*, 26th edn.
- [5] Wang, J. et al. 2015, “Modeling and mass-production high efficiency n-type solar cells with ion-implanted selective back surface field”, *Proc. 31st EU PVSEC*, Hamburg, Germany.
- [6] Bösccke, T.S. et al. 2014, “Fully ion implanted and coactivated

- industrial n-type cells with 20.5% efficiency”, *IEEE J. Photovolt.*, Vol. 4.
- [7] Rothardt, P. et al. 2014, “Characterization of  $\text{POCl}_3$ -based codiffusion processes for bifacial n-type solar cells”, *IEEE J. Photovolt.*, Vol. 4, No. 3.
- [8] Blévin, T. et al. 2014, “Development of industrial processes for the fabrication of high efficiency n-type PERT cells”, *Sol. Energy Mater. Sol. Cells*, Vol. 131, pp. 24–29.
- [9] Rothardt, P. et al. 2014, “19.9 % efficient bifacial n-type solar cell produced by co-diffusion-CoBiN”, *Proc. 29th EU PVSEC*, Amsterdam, The Netherlands, pp. 653–655.
- [10] Cabal, R. et al. 2009, “Investigation of the potential of boron doped oxide deposited by PECVD – Application to advanced solar cells fabrication processes”, *Proc. 24th EU PVSEC*, Hamburg, Germany, pp. 1605–1608.
- [11] Blévin, T. et al. 2014, “Development of industrial processes for the fabrication of high efficiency n-type PERT cells”, *Sol. Energy Mater. Sol. Cells* [<http://dx.doi.org/10.1016/j.solmat.2014.06.022i>].
- [12] Frey, A. et al. 2014, “n-type bi-facial solar cells with boron emitters from doped PECVD layers”, *Proc. 29th EU PVSEC*, Amsterdam, The Netherlands, pp. 656–660.
- [13] Cabal, R. et al. 2014, “20% PERT technology adapted to n-type mono-like silicon: Simplified process and narrowed cell efficiency distribution”, *Proc. 29th EU PVSEC*, Amsterdam, The Netherlands, pp. 648–652.
- [14] Engelhardt, J. et al. 2015, “Passivating boron silicate glasses for co-diffused high-efficiency n-type silicon solar cell application”, *Appl. Phys. Lett.*, Vol. 107, p. 042102.
- [15] Keding, R. et al. 2012, “Silicon doping performed by different diffusion sources aiming codiffusion”, *Proc. 27th EU PVSEC*, Frankfurt, Germany, pp. 1906–1911.
- [16] Wehmeier, N. et al. 2015, “21.0%-efficient co-diffused screen printed n-type silicon solar cell with rear-side boron emitter”, *physica status solidi (RRL)*, Vol. 1–5.
- [17] Keding, R. et al. 2011, “Diffusion and characterization of doped patterns in silicon from prepatterned boron- and phosphorus-doped silicate glass”, *Proc. 26th EU PVSEC*, Hamburg, Germany, pp. 1385–1389.
- [18] Fallisch, A. et al. 2012, “Analysis of phosphorus doped silicon oxide layers deposited by means of PECVD as a dopant source in diffusion processes”, *IEEE J. Photovolt.*
- [19] Benick, J. et al. 2006, “PECVD PSG as a dopant source for industrial solar cells”, *Proc. 21st EU PVSEC*, Dresden, Germany, pp. 1012–1015.
- [20] Paviet-Salomon, B. et al. 2011, “Laser doping using phosphorus-doped silicon nitrides”, *Energy Procedia*, Vol. 8, pp. 700–705.
- [21] Wehmeier, N. et al. 2013, “Boron-doped PECVD silicon oxides as diffusion sources for simplified high-efficiency solar cell fabrication”, *Proc. 28th EU PVSEC*, Paris, France, pp. 1980–1984.
- [22] Engelhardt, J. et al. 2014, “Boron emitters from doped PECVD layers for n-type crystalline silicon solar cells with LCO”, *Energy Procedia*, Vol. 55, pp. 235–240.
- [23] Lachiq, A. et al. 1996, “Simultaneous dopant diffusion and surface passivation in a single rapid thermal cycle”, *Prog. Photovolt. Res. Appl.*, Vol. 4, pp. 329–339.
- [24] Barth, S. et al. 2014, “19.4 efficient bifacial solar cell with spin-on boron diffusion”, *Energy Procedia*, Vol. 38, pp. 410–415.
- [25] Das, A., Ryu, K. & Rohatgi, A. 2011, “20% efficient screen-printed n-type solar cells using a spin-on source and thermal oxide/silicon nitride passivation”, *IEEE J. Photovolt.*, Vol. 1, No. 2.
- [26] Barsch, J. et al. 2014, “21.8% efficient n-type solar cells with industrially feasible plated metallization”, Presented at 4th SiliconPV 2014, *Energy Procedia*, Vol. 55, pp. 400–409.
- [27] Jäger, U. et al. 2015, “Industrial n-type PERL cells with screen-printed front side electrodes approaching 21% efficiency”, *Proc. 31st EU PVSEC*, Hamburg, Germany, pp. 390–393, 2015.
- [28] Gall, S. et al. 2012, “High quality passivation scheme combined with laser doping from  $\text{SiN}_x(\text{P})$  and  $\text{SiN}_x(\text{B})$  layer for silicon solar cell”, *Energy Procedia*, Vol. 27, pp. 467–473.
- [29] Trogus, D. et al. 2011, “Phosphoric anti-reflective coatings as dopant source and front-side passivation for industrial silicon solar cell manufacturing”, *Proc. 26th EU PVSEC*, Hamburg, Germany, pp. 1361–1364.
- [30] Seiffe, J. et al. 2013, “Multifunctional PECVD layers: Dopant source”, *IEEE J. Photovolt.*, Vol. 3, No. 1, pp. 224–229.
- [31] Dauzou, F. et al. 2012, “Electrical behaviour of n-type silicon solar cells under reverse bias: Influence of the manufacturing process”, *Sol. Energy Mater. Sol. Cells*, Vol. 104, pp. 175–179.

#### About the Authors



**Raphaël Cabal** studied semiconductor physics at the Grenoble Institute of Technology, France, where he graduated with an engineer degree in microelectronics and a master’s in material science in 2007. Since receiving his Ph.D. from CEA Grenoble in 2011, he has been working as a project leader at CEA Tech INES on homojunction n-type solar cells.



**Thomas Blévin** received his engineer degree in materials sciences in 2012 and his Ph.D. in 2015 from the University of Lille, France. For his Ph.D., which he earned while working with the homojunction silicon solar cells team at CEA Tech INES, he developed innovative boron doping solutions for n-type solar cells.



**Rémi Monna** received his Ph.D. degree in solar cells in 1997 from the University of Strasbourg, France. After a period of employment with Photowatt-EDF Company, he joined the silicon solar team at the National Institute of Solar Energy in 2003, and currently works as a project leader on n-type PERT solar cells.



**Dr. Yannick Veschetti** obtained his Ph.D. in physics, specializing in crystalline silicon PV, from Strasbourg University, France. After joining CEA-INES in 2005, he contributed to the development of high-efficiency silicon crystalline solar cells, and was responsible of the homojunction silicon solar cells laboratory from 2013 to 2015. His main R&D work concerns the development of solar cell technology on n-type silicon.

#### Enquiries

Email: [raphael.cabal@cea.fr](mailto:raphael.cabal@cea.fr)

# The present and future silver cost component in crystalline silicon PV module manufacturing

Michael Redlinger<sup>1</sup>, Michael Woodhouse<sup>2</sup> & Roderick G. Eggert<sup>1</sup>

<sup>1</sup>Division of Economics and Business, Colorado School of Mines (CSM), Golden, Colorado; <sup>2</sup>Strategic Energy Analysis Center, National Renewable Energy Laboratory (NREL), Golden, Colorado, USA

## ABSTRACT

The purpose of this paper is to determine how increased c-Si PV module production might affect future silver demand and prices, as well as the impacts on total c-Si module manufacturing costs. A bottom-up estimation of the current and potential material intensity (tonnes of silver per GW) for silver in c-Si PV cell fabrication is presented. Partly because of concerns about material intensity, and also because of the changing economics of manufacturing, there is some interest in shifting away from the traditionally higher material intensity approach of screen printing with silver paste to alternative metallization techniques, such as electroplating, which uses substantially less silver. To evaluate how PV's changing demand for silver might affect future silver prices, and the impact in terms of manufacturing costs, some scenarios of silver's contribution to c-Si PV cell manufacturing costs are compiled on the basis of projected changes in demand and price as a result of changes in material intensity. The analysis indicates that an expansion of c-Si production from 55GW/year to 250GW/year results in a 0.05–0.7¢/W increase in manufacturing costs because of higher silver prices. As an illustration of this, the current estimates of the manufacturing costs for the two contrasting methods – silver screen printing and nickel–copper–silver electroplating – are presented.

## Introduction

With the growing demand for PV modules, it is natural to raise questions about potential material-availability constraints. Material availability for many of the thin-film PV technologies has received considerable attention, as their semiconductor materials require the relatively rare elements gallium, indium and tellurium. By contrast, it may seem to be of no concern for crystalline silicon (c-Si), since the semiconductor base material in this case is made from the world's second-most abundant crustal element. However, c-Si technologies still have a potential raw-material availability weak link: silver (Ag), which is typically used in the front- and back-side electrical contacts. Ag has a crustal abundance that is comparable to that of indium but lower than that of gallium [1]. It has a long history of use in currencies, jewellery and ornaments, partly because it is so rare. Moreover, silver markets (including the recent emergence of related exchange-traded funds that invest in physical silver assets) are price volatile by nature and have been vulnerable to speculative trading. The economics of silver are driven by these historical roles and characteristics, and the resulting price fluctuations affect c-Si cell manufacturing costs.

Solar electricity generation

technologies make up a small but increasing share of total global silver use. From 2004 to 2014 the global silver demand from the solar PV industry grew from 0.4% to 7%; it is expected that the demand will have surpassed that from the photography industry in 2015, and that PV will become the third-largest end user of silver behind jewellery/silverware and electronics [2]. If the PV industry continues its growth trajectory, and if c-Si maintains a heavy reliance upon silver metal contacts, the increase in demand for silver could affect future silver prices [3]. In the available literature one can find evaluations of how c-Si PV module production may be *physically* constrained by existing silver resources, yet to the authors' knowledge no rigorous analysis has been done of how the reliance on silver may impact the future costs of c-Si PV module production.

**“From 2004 to 2014 the global silver demand from the solar PV industry grew from 0.4% to 7%.”**

The purpose of this paper is to determine how c-Si PV module production on an increased scale might affect silver prices and, in

turn, have an impact on silver's contribution to total module manufacturing costs. Several scenarios of silver demand in PV module manufacturing are first derived using silver's material intensity (i.e. tonnes of silver required per GW of c-Si manufacturing production) and the projections of solar electricity generation by the International Energy Agency (IEA) and other organizations. Next, a partial equilibrium model of the silver market is constructed, and the effect of different silver demand scenarios on silver prices is simulated. Finally, PV cell manufacturing costs at different silver price levels are compared for the standard silver screen-printing metallization approach and the alternative method of electroplating, which typically requires much less silver.

Section 2 ('Literature review') discusses the available literature concerning silver availability and supply risks. Section 3 ('Scenarios for silver use in PV modules') develops some scenarios for future silver use in c-Si PV modules. Section 4 ('Method') describes the method and the data for the silver market simulation analysis. Section 5 ('Results') presents the results, and section 6 ('Comparison with Ni–Cu electroplating') compares the cost of silver screen printing with that of the alternative metallization



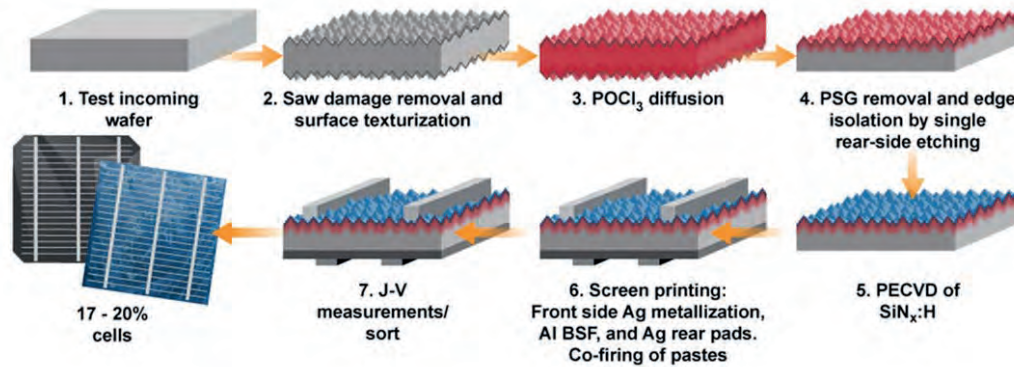


Figure 1. Process flow for the fabrication of a standard entirely screen-printed c-Si solar cell. For multicrystalline or monocrystalline cells, in commercial production using this standard process the projected cell efficiencies are estimated to be 17 to 20%.

approach of electroplating, in which the amount of silver required is significantly lower. Finally, section 7 ('Conclusion') states the implications and limitations of the analysis.

### Literature review

Several articles discuss the raw-material constraints associated with c-Si PV module production, but they focus primarily on the *physical* limitations of silver resources [4–7]. Feltrin and Freundlich [4], Tao et al. [5] and Jacobson and Delucchi [6] find that, of all the elements used in c-Si PV modules, silver is ultimately the material that could constrain growth. Using the United States Geological Survey (USGS) estimates of US silver resources and the amounts of silver required in different solar technologies, Grandell and Thorenz [7] construct upper bounds for annual solar electricity generation: they estimate an upper bound of 530 terawatt-hours per year (TWh/year) for the electricity generation capability of c-Si solar cells. For comparison purposes, total global electricity generation in 2012 (from all fuel types) was 22,721 TWh [8].

Numerous studies evaluate the 'criticality' of various minerals, including silver, but the definition of what is considered critical differs between studies. Generally, a mineral's criticality is determined by: 1) its importance, either to an economy or to a specific sector of the economy; and 2) its supply risks. Supply risk has a slightly different meaning in each study, but typically relates to the vulnerability of production to decline or disruption. Erdmann and Graedel [9] review ten major criticality studies,

	Mid <sup>a</sup>	Low	High
Silver paste for front [mg/cell]	115	110	120
Silver paste for back [mg/cell]	45	40	50
Silver weight for front [%]	88	88	88
Silver weight for back [%]	58	55	60
<b>Monocrystalline</b>			
Wafer area [cm <sup>2</sup> ]	239	239	239
Power rating [W/m <sup>2</sup> ]	210	240	180
Market share [%] <sup>b</sup>	24	24	24
<b>Multicrystalline</b>			
Wafer area [cm <sup>2</sup> ]	243	243	243
Power rating [W/m <sup>2</sup> ]	195	220	170
Market share [%] <sup>b</sup>	65	65	65
<b>Material intensity</b>			
Monocrystalline <sup>c</sup> [tonnes/GW]	25.3	20.7	31.5
Multicrystalline <sup>c</sup> [tonnes/GW]	26.8	22.2	32.8
Weighted average <sup>b</sup> [tonnes/GW]	26.4	21.8	32.4

<sup>a</sup> Mid values are the average of high and low values.

<sup>b</sup> The weighted-average material intensity is weighted by the monocrystalline and multicrystalline market shares: 24% and 65% of global PV module production respectively, with thin films making up 11% [16].

<sup>c</sup> Material intensity is calculated by taking the total of silver paste usage on the front and back, adjusting for the paste's silver weight percentage, and converting from mg/cell to tonnes/GW using the wafer area and power rating. Note that material intensity is inversely related to solar cell power conversion efficiency.

Table 1. Material intensity of silver in c-Si modules.

only four of which analyse silver. Many of these studies were conducted by (or on the behalf of) governmental bodies and departments, such as the European Commission or the U.S. Department of Energy [10–13]. More recently, Graedel et al. [14] analyse the criticality of over 60 metals and metalloids, including silver, and use geological, technological, economic, social and regulatory, and geopolitical factors to assess supply risk. These studies regarding criticality do not have identical conclusions about silver's supply risk, partly because they differ in their purposes and methodologies. Nonetheless, some broad conclusions can be drawn from the literature. First, silver mine production is not concentrated in any one country, or even in a small group of countries; it is well distributed across the globe [10,12]. Second, a sizeable amount of silver is recycled from end-of-life products, although the efficiency of recycling varies across end uses [10]. Third, there is difficulty in substituting other materials for silver in electrical and electronic applications, which make up about a quarter of total silver use [10,12]. While these findings are useful for a qualitative evaluation of how increased silver demand could affect the silver market, they do not allow a quantitative assessment of the impact of an increased demand on prices.

This paper makes three primary contributions to the literature. First, it provides a recent bottom-up estimation of the material intensity (i.e. tonnes/GW) of silver used to make c-Si PV cells, along with an overview of how material intensity is projected to change. Second, to the authors' knowledge this is the first paper to estimate how a rise in silver demand from PV might affect future silver prices and the corresponding cost of silver usage in PV manufacturing. Several studies have looked at how silver resources can physically limit c-Si module production, but they have not analysed how silver prices might have an impact on manufacturing economics. Third, this paper compares the raw-material cost of screen-printed silver with that of the alternative metallization process of electroplating. A comparison of the costs of silver screen printing and electroplating is particularly relevant to c-Si PV module manufacturers that are considering either of these approaches in future manufacturing facilities.

## Scenarios for silver use in PV modules

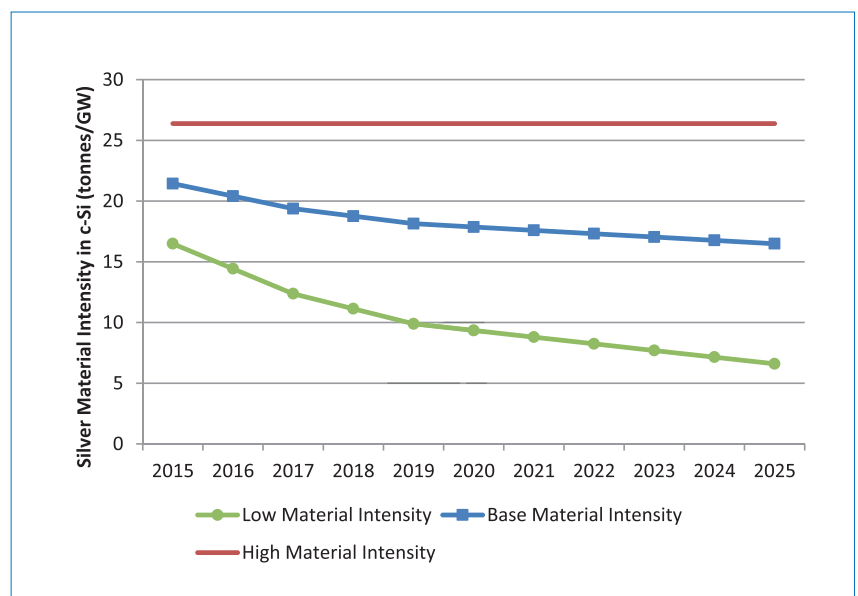
The metallization of a solar cell is necessary for collecting electrical current from the cell. The most ubiquitous approach used for c-Si solar cell metallization involves screen printing a silver paste onto a series of gridlines on the front, screen printing another full-area aluminium paste onto the back, and then screen printing a different composition of silver paste over the Al back, to make contact pads for eventual soldering into cell strings. This is broadly represented as step six in Fig. 1, and has been described in more detail elsewhere [3].

After the three-stage printing process, the entire cell is typically annealed in order to solidify the paste into solid metal. Also during the annealing step, additives of glass frit within the paste serve to melt through the hydrogenated silicon nitride ( $\text{SiN}_x\text{:H}$ ) front-side anti-reflection coating, so that the silver can partially alloy with the underlying silicon wafer. Executing the screen-printing process in its entirety is very simple and predictable, and this process offers high yields in commercial production. If made correctly, screen-printed cells are also quite durable over many years of outdoor deployment. These are the primary reasons why the screen-printing approach currently enjoys a market share greater than 95% [15], and why it remains a formidable opponent of any alternative metallization technology.

The data from industry that are used to calculate the material intensity of

silver in c-Si solar cells are given in Table 1. Using the weight percentages shown for the front- and back-side pastes, the estimate of the total amount of silver for each cell ranges from 119 to 136mg (with a midpoint of 127mg). For a monocrystalline wafer area of  $239\text{cm}^2$  and power ratings of  $180\text{--}240\text{W/m}^2$ , the silver requirement per GW of manufacturing ranges from 20.7 to 31.5 tonnes (with a midpoint of 25.3 tonnes/GW). For multicrystalline cells, with a slightly greater wafer area of ( $243\text{cm}^2$ ) and a lower power rating ( $170\text{--}220\text{W/m}^2$ ), the material intensity is 22.2 to 32.8 tonnes per GW (with a midpoint of 26.8 tonnes per GW). The weighted-average silver material intensity for monocrystalline and multicrystalline, using their respective shares of global c-Si production (27%/73% split for monocrystalline/multi [16]), is 21.8–32.4 tonnes per GW (with an average of 26.4 tonnes per GW).

Few other recent estimates of silver material intensity are available for comparison. A 2013 report by the Silver Institute estimates that the silver material intensity in c-Si PV cells was 65 tonnes per GW in 2012, and notes that manufacturers had been reducing their overall silver usage [17]. Grandell and Thorenz [7] state that current silver use is about  $10\text{g/m}^2$ , which translates to a material intensity of 47.6 and 51.3 tonnes per GW for monocrystalline and multicrystalline cells respectively, if using the midpoint module power ratings in Table 1. The data in Table 1 reflect the most recent 2015 guidance provided to NREL by

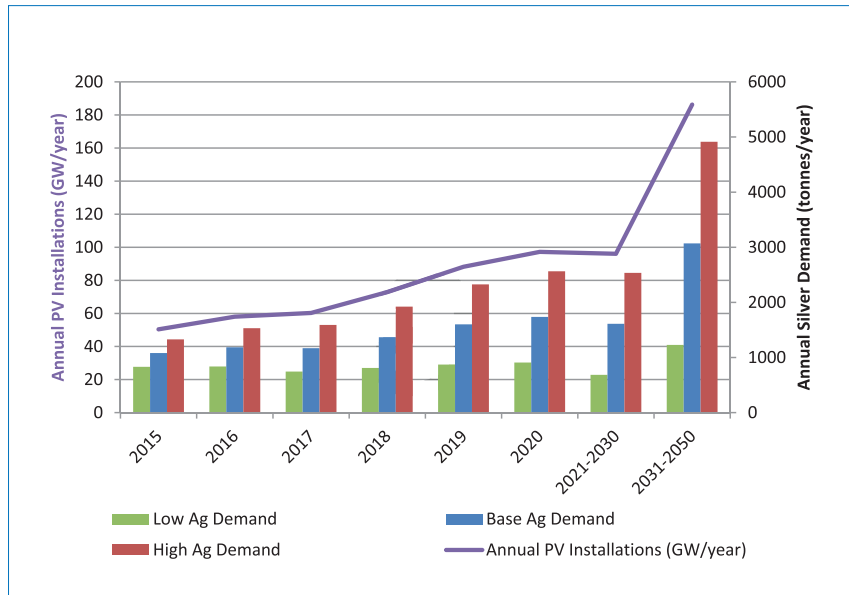


**Figure 2. Silver material intensity (tonnes/GW) in c-Si cells. The low material intensity case estimates are derived from the 2015 ITRPV, the high material intensity case is equal to current material intensity estimated in Table 1, and the base material intensity case is the average of the low and high cases.**

relevant industry players, including paste suppliers and equipment vendors.

There are, however, also multiple pathways to lowering the material intensity even further: these include the options of electroplating, stencil printing, inkjet or aerosol printing, or multiwire approaches (in which a mesh of base metals is overlaid onto a much smaller amount of printed silver). There is also the possibility to retain the screen-printing process but lower the material layout (for example, by using smaller screen line widths in order to reduce the amount of silver present in each finger). For these and other reasons, the 2015 International Technology Roadmap for Photovoltaic (ITRPV) anticipates that the recent declines in silver material intensity in c-Si cells will continue in the coming years. On the basis of the most recent survey, silver paste usage per cell is projected to fall from 130mg per cell in 2014 to 40mg per cell in 2025 [15].

**“Silver paste usage per cell is projected to fall from 130mg per cell in 2014 to 40mg per cell in 2025.”**



**Figure 3. Annual PV installations and silver use in PV cells derived from industry analyst reports (2015–2020) and IEA projections of solar PV generation capacity (2021–2050). The estimates assume that 90% of global PV module production is c-Si modules.**

To account for the current and potential future reductions in silver material intensity, three future scenarios have been developed and are presented in Fig. 2. The low material intensity case in Fig. 2 is derived from the 2015 ITRPV projections of

silver paste required per c-Si cell, and shows the material intensity declining from 16.5 tonnes per GW in 2015 to 6.6 tonnes per GW in 2025. The high material intensity case assumes that silver material intensity makes no progress from 2015, staying constant

# Meco Plating Equipment

## Copper metalization for high efficiency solar cells

- HIT, IBC, bifacial
- PERC plating:
  - > 20.5% on p-type
  - > 22.5% on n-type
- > 65% reduction of metalization costs
- Inline process up to 30 - 100 MW tool capacity
- IEC61215 certified
- Eco-friendly processes with maximum material recycling
- Over 35 years of plating experience
- More than 800 plating tools installed
- Installed base at leading PV manufacturers



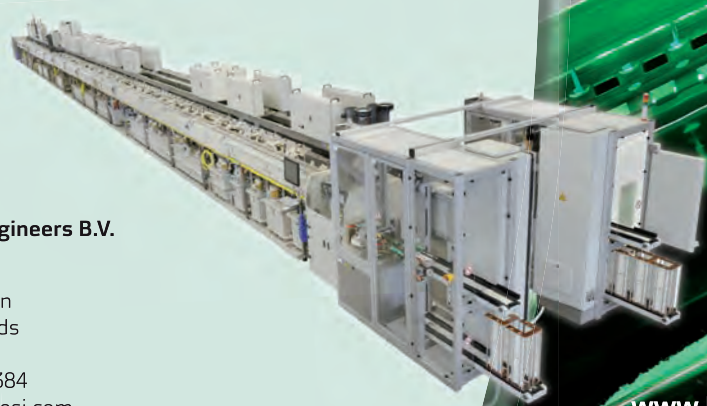
**Besii**

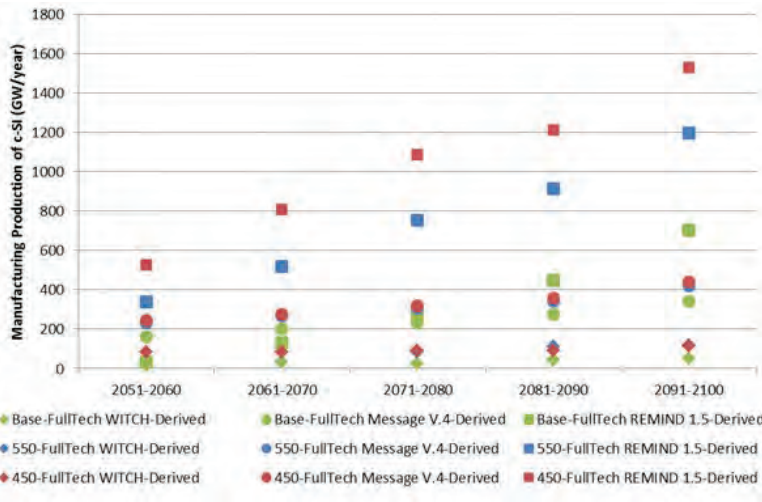
Meco Equipment Engineers B.V.

Marconilaan 2  
5151 DR Drunen  
The Netherlands

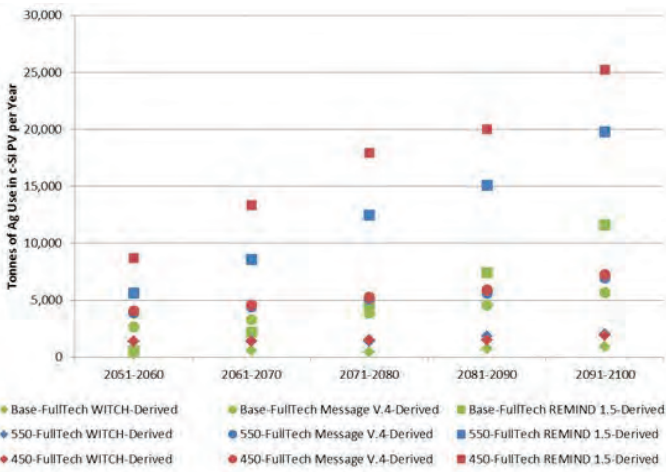
T: +31 416 384 384  
meco.sales@besii.com

[www.besii.com](http://www.besii.com)





**Figure 4. Global c-Si manufacturing (GW/year).** All scenarios are derived from models reviewed in the Fifth Assessment Report of Working Group III of the IPCC. *Base*, *550* and *450* refer to no climate policies and policies enacted to limit greenhouse gas concentrations to 550ppm CO<sub>2</sub> and 450ppm CO<sub>2</sub> respectively. *FullTech* means that all technologies are available, and it contrasts with other cases (not shown here) which limit certain technologies.



**Figure 5. Scenarios of average annual silver usage in PV cells, derived from projections of solar electricity generation.**

at 26.4 tonnes per GW (see Table 1). The base material intensity case is the average of the low and high cases.

Using the three silver material intensity cases in Fig. 2, and the projections of solar PV deployment from various industry analysts and the IEA, three scenarios of silver demand for c-Si PV cells have been constructed: low demand, base demand and high demand (Fig. 3). The industry analyst projections are the median of forecasts made in 2015 by Bloomberg, Cowen and Company, Deutsche Bank, GTM and Navigant Consulting. In the

base demand scenario, annual silver demand increases from 1,080 tonnes in 2015 to 1,736 tonnes in 2020, as annual global c-Si PV installations increase from 50 to 97GW but silver material intensity falls from 21.4 to 17.9 tonnes/GW. On the basis of IEA projections of cumulative installed solar electricity generation capacity [18], the silver demand averages 1,611 tonnes/year from 2021 to 2030 in the base demand scenario, as c-Si PV installations average 96GW/year. From 2031 to 2050, on the basis of IEA projections c-Si PV installations could

average 186GW/year, which would correspond to an average silver use of 3,071 tonnes/year in the base demand scenario.

The IEA projections do not extend past 2050. For the years beyond 2050, solar electricity generation scenarios from the Fifth Assessment Report (AR5) of Working Group III of the IPCC are used to derive estimates of future silver use through 2100. The AR5 reviewed over a thousand different scenarios from 31 integrated assessment models (IAMs), which incorporate scientific and economic dimensions of climate change to evaluate its impact and the effects of various policies. Moss et al. [19] provide a comprehensive discussion of these models. Fig. 4 presents scenarios of c-Si manufacturing (GW/year) based on three scenarios (referred to as *Base-FullTech*, *550-FullTech* and *450-FullTech*) from three of the models (called *WITCH*, *Message V.4* and *REMIND 1.5*) that were reviewed in the AR5 and illustrate the range of potential silver demand by the PV sector. Details of these scenarios and the models can be found in Weyant et al. [20].

These scenarios do not detail how much solar electricity comes from PV versus concentrated solar power (CSP) technologies. In the IPCC-reviewed IAMs, the projected share of solar electricity generation from PV and CSP applications is initially split 90/10 and gradually changes to 60/40 by 2100 [21]. In estimating silver use in c-Si PV modules, it is assumed that PV constitutes 90% of solar electricity generation during the period 2021 to 2030, and that this share falls by 5% per decade until 2090, when it then remains at 60% in accordance with models reviewed by the IPCC. Of the total estimated PV module electrical generation capacity, 90% is assumed to come from c-Si modules, with the remaining 10% coming from thin-films. Fig. 5 shows scenarios of silver usage from 2050 to 2100, which are derived from the projections of annual installed solar electricity generation capacity in Fig. 4.

There is a wide range of potential silver use across different scenarios and models. From 2051 to 2060, the average annual silver use ranges from 274 to 8,670 tonnes; for comparison, the global silver use in PV was 1,950 tonnes in 2014 [2]. From 2091 to 2100, the average annual silver use ranges from 886 to 25,210 tonnes, where the latter figure represents more than 80% of the total global silver mine production in 2014 of 31,007 tonnes.

The scenarios in Fig. 5 demonstrate

efficiency



**Wisdom creates efficiency.**



Our Research and Development team is constantly thinking about paste. We are committed to developing leading-edge solutions, which improve the power output and performance of solar cells at a lower cost per watt. We are always mindful of the current and future technology needs of our customers, and are driven to deliver results. So when you think of paste...think of Heraeus.

Leadership through R&D. Breakthroughs via innovation.  
Achievement by tradition.

Visit us at:  
SNEC 2016 | Booth W3-660 | May 24<sup>th</sup> - 26<sup>th</sup>

Heraeus Photovoltaics Business Unit  
[www.pvsilverpaste.com](http://www.pvsilverpaste.com)  
China | Singapore | Taiwan | Europe | America | Japan

Zero-profit condition	Quantity variable	Complementarity
$MC_S(S) = (S/A_S)^{1/\varepsilon_S} \geq P$	$S \geq 0$	$MC(S) \times S = 0$
$MC_R(R) = (R/A_R)^{1/\varepsilon_R} \geq P$	$R \geq 0$	$MC(R) \times R = 0$
Market clearance condition	Price variable	Complementarity
$D(P) \geq R + S$	$P \geq 0$	$D(P) \times P = 0$

Notes:

- $MC_S(S)$  and  $MC_R(R)$  denote the marginal cost of primary and old scrap silver supply respectively.
- The zero-profit conditions can be derived by solving  $P$  in Equations 1 and 2, then setting price equal to marginal cost. Alternatively, one can derive the zero-profit conditions from a producer profit maximization problem with a Cobb-Douglas production function.
- This table is based on the concise and intuitive 'Energy Supply Model' in Böhringer and Löschel [25].

**Table 2. MCP formulation of silver market equilibrium conditions.**

Data input/parameter	Value	Source
2014 average price [\$/tonne]	614,079	World Bank (2015)
2014 fabrication demand [tonnes]	26,914	CPM (2015)
2014 primary supply [tonnes]	31,007	CPM (2015)
2014 old scrap supply [tonnes]	6,687	CPM (2015)
2014 net investment demand [tonnes] <sup>a</sup>	10,780	Calculation
Price elasticity of primary supply ( $\varepsilon_S$ )	0.342	Table 4
Price elasticity of old scrap supply ( $\varepsilon_R$ )	0.343	Table 4
Price elasticity of industrial demand ( $\varepsilon_D$ )	-0.453	Table 4

<sup>a</sup> Net Investment is calculated as the difference between total supply and fabrication demand.

**Table 3. Silver market simulation model inputs.**

$$\ln S_{it} = \beta_{Ag}^S \ln AgP_t + \beta_{Cu}^S \ln CuP_t + \beta_{Pb}^S \ln PbP_t + \beta_{Zn}^S \ln ZnP_t + \lambda_i^S + \varepsilon_{it}^S \quad (4)$$

$$\ln R_{it} = \beta_{Ag}^R \ln AgP_t + \lambda_i^R + \varepsilon_{it}^R \quad (5)$$

$$\ln D_{it} = \beta_{Ag}^D \ln AgP_t + \gamma \ln GDP_{it} + \lambda_i^D + \varepsilon_{it}^D \quad (6)$$

where

- $\ln S_{it}$  is the natural log of primary supply for country  $i$  in year  $t$
- $\ln R_{it}$  is the natural log of old scrap supply for country  $i$  in year  $t$
- $\ln D_{it}$  is the natural log of demand for country  $i$  in year  $t$
- $\ln AgP_t$ ,  $\ln CuP_t$ ,  $\ln PbP_t$  and  $\ln ZnP_t$  are the natural logs of Ag, Cu, Pb and Zn prices in year  $t$
- $\ln GDP_{it}$  is the natural log of GDP for country  $i$  in year  $t$
- $\lambda_i$  is the time-invariant or fixed effect for country  $i$
- $\varepsilon_{it}$  is the idiosyncratic error for country  $i$  in year  $t$

**Equations 4, 5 and 6.**

that, while there is much uncertainty about the levels of silver use in PV modules, there are several scenarios in which future use is substantially higher than current use. If such high levels of demand for silver were to occur, it is unclear how the silver market would respond and how overall global silver prices would be impacted. The remainder of this paper explores how such increases in demand from the PV sector might affect silver prices and, in turn, the cost of using silver in PV module manufacturing.

**Method**

To determine how a rise in silver demand from PV module manufacturing could affect future silver prices, a partial equilibrium model of the global silver market is developed, and different scenarios of silver demand are simulated. The partial equilibrium model for the silver market and the model inputs are described first.

**Model of the silver market**

The partial equilibrium model assumes that the silver market is perfectly competitive; that is, producers and consumers are price takers and no single agent is able to influence the market price. This assumption is reasonable, given the large number of silver end users and old scrap suppliers and the relatively low Herfindahl-Hirschman Index score of 700–800 for global company-level silver mine production [22]. The Herfindahl-Hirschman Index is a measure of market concentration, ranging between zero and 10,000; a score below 1,500 generally implies the market supply is not concentrated.

To construct the partial equilibrium model, its dimensions are established first: one market (global silver market), one commodity (silver), one representative supplier of primary silver, one representative supplier of old scrap silver and one representative consumer of silver.

Second, the functional forms for primary supply, old scrap supply and silver demand are constant elasticity, as described by Equations 1–3:

$$S(P) = A_S P^{\varepsilon_S} \quad (1)$$

$$R(P) = A_R P^{\varepsilon_R} \quad (2)$$

$$D(P) = A_D P^{\varepsilon_D} \quad (3)$$

The primary silver supply ( $S$ ), shown in Equation 1, is a function of the price of silver ( $P$ ), and  $\varepsilon_S$  is the own-price elasticity of primary silver supply. Note

that the price elasticity of supply is defined as the ratio of the percentage change in quantity supplied and the percentage change in price. Old scrap silver supply ( $R$ ) is also a function of the price of silver, and  $\varepsilon_R$  denotes the own-price elasticity of old scrap silver supply. Silver demand ( $D$ ) is shown in Equation 3, where the parameter  $\varepsilon_D$  is the price elasticity of silver demand. The price elasticity parameters in Equations 1–3 are estimated through the regression analysis described in the next section ('Regression estimation'). The method for determining the values of the coefficients  $A_S$ ,  $A_R$  and  $A_D$  is also discussed.

Third, the standard market supply and demand equilibrium conditions are expressed in Table 2 as a mixed complementarity problem (MCP), which is commonly used in partial equilibrium modelling (see Lanz, Rutherford and Tilton [23] and Zhuang and Gabriel [24] for examples). The zero-profit conditions, where  $MC_S(S)$  and  $MC_R(R)$  denote the marginal cost of silver produced from primary and old scrap respectively, ensure that if supply is strictly positive, then marginal cost equals price. The market clearance condition requires that if the price of silver is strictly positive, then market demand equals market supply.

A solution to the MCP satisfies all equilibrium conditions in Table 2.

Fourth, the model is calibrated using 2014 data for silver supply, demand and price, as well as estimates of the elasticity parameters. In calibrating the model, the values for the coefficients  $A_S$ ,  $A_R$  and  $A_D$  are chosen so that supply, demand and price outputs are consistent with baseline quantities, which are the actual levels of silver supply, demand and price observed in 2014. The price elasticity parameters  $\varepsilon_S$ ,  $\varepsilon_R$  and  $\varepsilon_D$  are estimated through the regression analysis.

Table 3 presents the data inputs used in the silver market simulation model. The levels of global silver primary supply, old scrap supply and fabrication demand in 2014 are sourced from the CPM Group 2015 Silver Yearbook [2], and the average silver price during 2014 is taken from the World Bank Global Economic Monitor database [26]. The level of net investment demand is calculated as the difference between total silver supply and fabrication demand; this represents the net addition or withdrawal of silver from inventories. While investment demand has become a larger share of total silver demand in recent years, the development of a comprehensive model that

incorporates the behaviour of silver investment demand and inventories is outside the scope of this analysis.

With the model calibrated and the baseline values for 2014 replicated, the impacts of various scenarios of silver demand from the PV sector are estimated. Given the wide range of potential future silver demand from the PV sector (see Figs. 3 and 5), PV module production ranging from 100GW/year to 500GW/year is considered. This range falls within the levels of future c-Si production projected in Figs. 3 and 4, which are derived from scenarios of solar electricity generation estimated by the IEA, industry analysts and models that were reviewed in the Fifth Assessment Report of Working Group III of the IPCC. The market is allowed to reach an initial equilibrium based on 2014 levels of supply, demand and price. New demand for silver from the PV module sector is then introduced using a new assumed level of PV module production (e.g. 100GW/year) and the estimates of material intensity of silver in c-Si PV modules (see Table 1).

#### Regression estimation

The price elasticity parameters of silver supply and demand required in the simulation analysis are estimated

## A NEW SOLAR CELL WITH HIGH VOLTAGE AND LOW CURRENT

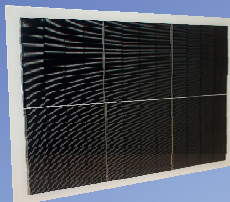
### S'Tile launches the production of the i-Cell in June 2016

30 % cost reduction\*  
10% gain in relative performance and power output

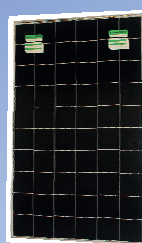
High efficiency solar cell without busbars  
Reduction of resistive losses  
Increase of the useful surface of the module

#### i-Cell: the ideal solution for

Custom modules with  
high voltage output



Standard modules with  
high efficiency



#### INVESTORS

S'Tile is looking for investment  
to support its mass production

S'Tile  
3 rue Raoul Follereau  
86 800 Poitiers, France  
Tel: +33 (0)579 796010  
E-mail: alain.straboni@silicontile.fr



A new concept of Photovoltaic Solar Cells

\* in comparison with the high efficiency modules in the market

using a seemingly unrelated regression (SUR) model with annual country-level data. The SUR model – as opposed to equation-by-equation ordinary least squares (OLS) – is applied, because it will yield more efficient estimates when error correlations exist between equations. The model consists of equations for primary supply, old scrap supply and fabrication demand, as described by equations 4–6. Consistent with the conditions of a perfectly competitive market, each country is considered a price-taker on both the supply and demand sides, so that no country is able to influence silver market prices.

In Equation 4, the dependent variable is primary silver supply, and the independent variables are the logged prices of silver (Ag), copper (Cu), lead (Pb) and zinc (Zn). The world prices (in real terms) for copper, lead and zinc are included in the primary supply regression, because silver is often mined as a co-product with these minerals; thus, changes in the prices of these minerals may influence the level of silver supply. According to the 2014 World Silver Survey [27], 29% of primary silver supply was mined as the main product; 58% was mined along with copper, lead or zinc; and the remaining 13% was mined as a co-product of gold. In general, metal prices tend to move together; over the sample period, the price of silver is correlated with the prices of gold, copper and lead. For this reason, and because the supply of silver as a co-product of gold represents the smallest share of total primary silver supply, the price of gold is excluded from Equation 4. To account for time-invariant differences in primary silver supply across countries, country-level dummy variables are included in Equation 4. The primary coefficient of interest is  $\beta_{Ag}^S$ , the own-price elasticity of silver primary supply, and is expected to be positive.

Equation 5 has old scrap silver supply as the dependent variable, and the price of silver and country dummy variables as the regressors. The coefficient of interest is  $\beta_{Ag}^R$ , which is the own-price elasticity of old scrap silver supply, and is expected to be positive. In Equation 6, silver fabrication demand is the dependent variable; the logged price of silver, the logged country-level gross domestic product (GDP) and the country dummy variables are the regressors. GDP is included as a regressor because demand for silver is expected to increase with income. The coefficient of interest in Equation 6 is  $\beta_{Ag}^D$ , which is the own-price elasticity

Regressor	Equation		
	Primary supply	Old scrap	Demand
LnAgP	0.342* (0.156)	0.343** (0.057)	-0.453** (0.036)
LnCuP	0.197 (0.263)		
LnPbP	-0.310 (0.231)		
LnZnP	-0.192 (0.174)		
LnGDP			1.241** (0.078)
Observations	189	189	189

Notes:  
 1. \* and \*\* denote significance levels of 5% and 1% respectively. Standard errors are shown in parentheses.  
 2. LnAgP = log of silver price, LnCuP = log of copper price, LnPbP = log of lead price, LnZnP = log of zinc price, LnGDP = log of actual GDP.  
 3. Equations include dummy variables for each country. Ten countries are included in the sample (Australia, Brazil, Canada, China, India, Italy, Japan, Mexico, Thailand and the USA).

**Table 4. Regression results for silver supply and demand equations.**

of silver demand, and is expected to be negative.

Data for the annual quantities of silver primary supply and old scrap supply by country for 1994 to 2013 are sourced from the Silver Institute’s world silver surveys [27]. The annual fabrication demand for silver is taken from the CPM Group’s 2015 Silver Yearbook [2], and data for the actual country-level GDPs and the annual average world metal prices (in real terms) are sourced from the World Bank World Development Indicators and Global Economic Monitor databases.

Table 4 shows the estimation results for the SUR model in Equations 4–6: these results are consistent with expectations of the response of silver supply and demand to silver price changes. The first and second equations show that the responses of primary and old scrap supply to changes in silver prices are positive and significantly different from zero, with significance levels of 5% and 1% respectively. The coefficient for the logged silver price variable in the fabrication demand equation is negative and is statistically different from zero at the 1% significance level.

**“The responses of primary and old scrap supply to changes in silver prices are positive and significantly different from zero.”**

On the basis of the parameter estimates in Table 4, the own-price elasticity values for primary supply, old scrap supply and demand are estimated to be 0.342, 0.343 and -0.453 respectively. These estimates imply that both short-run elasticity of silver supply and short-run elasticity of demand are inelastic, which is consistent with the views of silver market experts [28,29,16]. Few studies have attempted to estimate silver supply and demand elasticities for comparison. Åstrom [30] offers estimates of US silver supply and demand elasticities of 0.179 and -0.105, while Evans and Lewis [31] estimate world silver demand price elasticity at -0.856. Given the uncertainty about the price elasticity estimates, a sensitivity analysis of the results is performed in the next section, to allow for a range of price elasticity values.

## Results

Because of the wide range of potential future silver use scenarios shown in Figs. 3 and 5, the results of the simulation analysis are presented in Fig. 6 for an annual c-Si PV module production ranging from 100GW to 500GW. In the 2014 baseline, an estimated 1,950 tonnes of silver were used by the PV module sector [2]. Total silver use in other industries was 35,744 tonnes, which was a combination of fabrication demand (24,964 tonnes) and net investment demand (10,780 tonnes). The price of



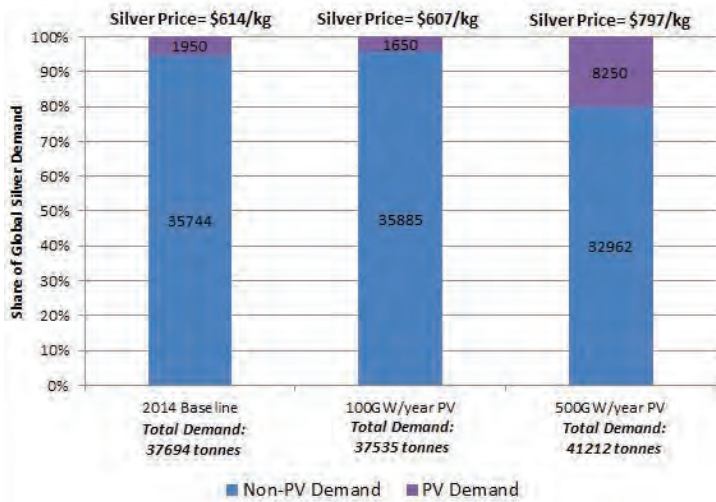


Figure 6. Effects of 100GW/year and 500GW/year c-Si PV module production on the silver market.

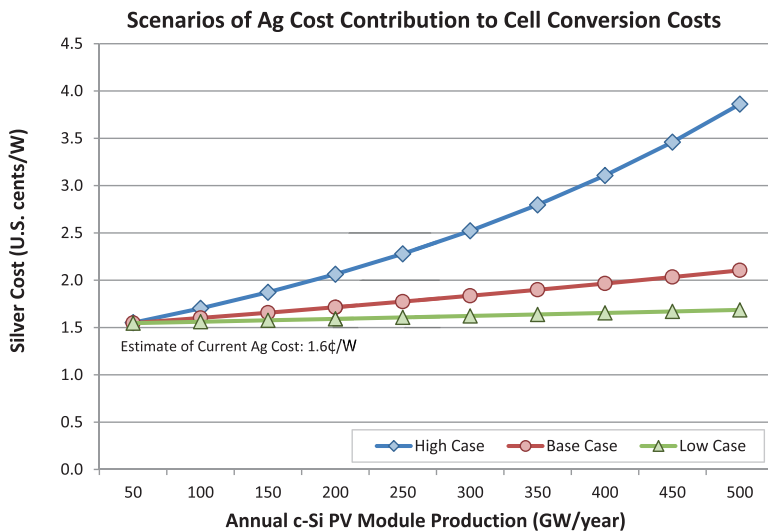


Figure 7. Simulation results for the effects of increased c-Si PV module production on silver costs as a result of increased demand. The high case assumes no reductions in silver intensity from 2015 (26.4 tonnes per GW), and the low case assumes gradual reductions according to the ITRPV projections (down to 6.4 tonnes per GW by 2025). The differences in material intensity affect projected supply and demand (and therefore pricing) scenarios.

silver averaged \$614/kg in 2014.

With 100GW/year of c-Si PV module production, the price of silver is actually predicted to decline slightly, despite the rise in PV production, because the material intensity is projected to be lower than in the 2014 baseline. This reflects the fact that, while there may be growth in c-Si PV production, reductions in material intensity could mitigate growth in demand for silver by the PV sector.

The scenario of 500GW/year c-Si PV module production has a noticeable effect on the silver market: the price of

silver increases to \$797/kg as demand from the PV sector rises by 6,300 tonnes from the 2014 baseline. To accommodate this new demand, total silver supply increases by 3,518 tonnes and non-PV fabrication demand declines by 2,781 tonnes.

The major determinant of how increased demand from the PV module sector could affect future silver prices is the response of supply and demand to a change in price (i.e. the own-price elasticities of silver supply and demand). For example, if silver supply could easily expand to

meet greater demand from PV module manufacturing, the impact on price could be modest. Similarly, if other end uses of silver (e.g. electronics, jewellery) substitute another material for silver, then greater demand from the PV sector may have a limited effect on silver prices. Alternatively, if it is difficult for silver supply to ramp up to meet the increased demand, and if non-PV end uses of silver do not replace the silver with something else, prices could significantly increase.

To demonstrate how different supply and demand price elasticity estimates have an effect on the results, the simulation results are presented for different elasticity estimates in Fig. 7. The high case uses estimates of 0.09, 0.25 and -0.39 for primary supply, old scrap supply and demand price elasticities respectively. The low case uses the estimates of 0.60, 0.44 and -0.51 for primary supply, old scrap supply and demand price elasticities respectively. These values correspond to the bounds of the 90% confidence interval for the own-price elasticity estimates in Table 4.

Fig. 7 shows annual c-Si PV module production and the corresponding silver cost contributions for the high, low and base cases. The high case represents silver costs when silver material intensity is relatively high (using the high material intensity case of 26.4 tonnes per GW in Fig. 2), and when silver supply and silver demand from non-PV end uses are relatively unresponsive to changes in silver prices. The low case in Fig. 7 shows silver costs when silver material intensity is relatively low (using the 6.6 tonnes per GW for the low material intensity case in Fig. 2) and when both silver supply and silver demand from non-PV end uses are relatively responsive to changes in silver prices. The base case presents silver costs when the base material intensity estimate of 16.5 tonnes per GW from Fig. 2 is used, along with the point estimates for price elasticities from Table 4 (i.e. the base case price elasticity estimates).

In the base case, for example, Fig. 7 shows that 250GW/year of c-Si production leads to a silver cost contribution of about 1.77¢/W. In the low and high cases, 250GW/year of c-Si production leads to silver costs of 1.61¢/W and 2.28¢/W respectively.

For comparison, at approximately 50GW of annual module production, the silver cost contribution of screen printing to total cost-of-ownership is currently estimated to be around 1.56¢/W; this figure is based upon the average 2014 silver price of \$614/kg

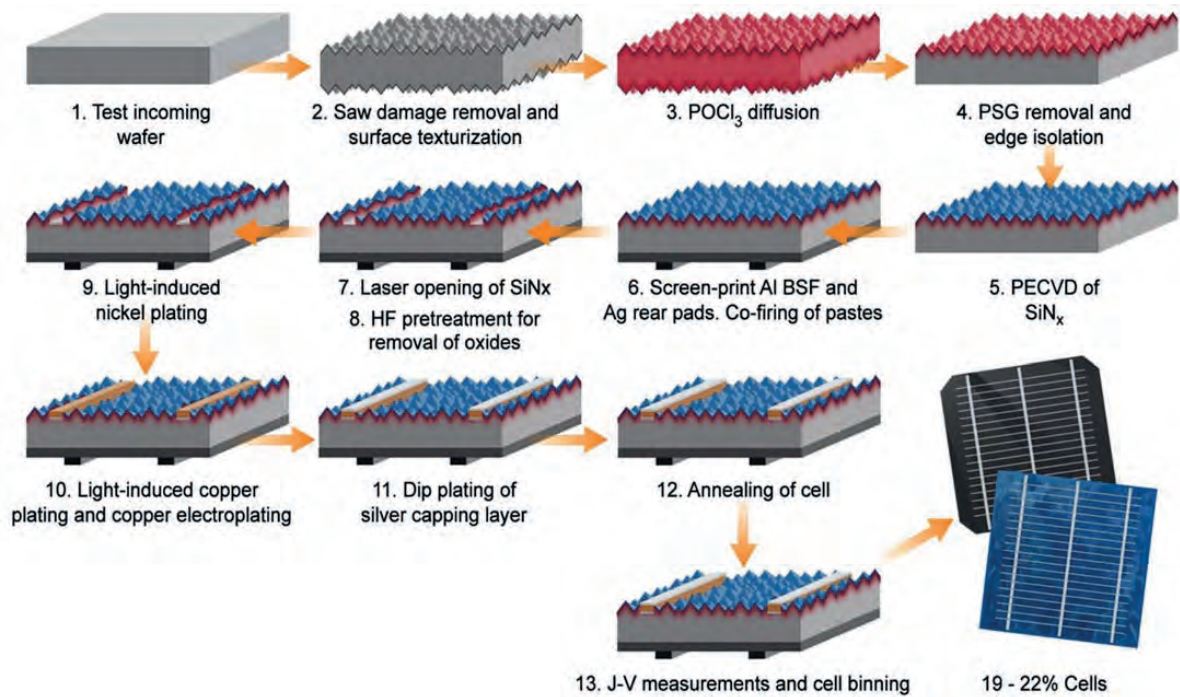


Figure 8. Process flow for fabricating a typical c-Si solar cell by electroplating.

and the usage rates detailed in Table 1. The current c-Si cell manufacturing costs under the standard screen-printing process are estimated to be around 35¢/W (see Fig. 9).

### Comparison with Ni–Cu electroplating

One alternative metallization approach to screen printing is electroplating. The simplest and most widely discussed application of this process, for the short term at least, is front-side metallization, which is illustrated in Fig. 8. Here, a copper grid is deposited on top of a nickel seed layer that is formed by light-induced plating. In high-throughput production (of the order of thousands of wafers per hour per tool), the grid patterns can be defined through the use of lasers. The resulting  $\text{SiN}_x\text{:H}$  anti-reflection layer openings provide the appropriate channels for nickel deposition.

Primarily to inhibit oxidation, a very thin silver-capping layer is additionally applied on top of the copper. The silver requirement for this capping layer is around 8.0mg per cell, substantially less than the estimates of Table 1 (between 95 and 105 net mg per cell). To provide a counter electrode for the front-side electroplating process, the

back-side aluminium and silver pastes can be printed and co-fired as usual.

There are several potential advantages of the electroplating process over screen printing. If done correctly, electroplating may allow higher aspect ratio gridlines, which can lead to improved cell efficiencies by reducing the amount of front-side shading by metals. Furthermore, there is the ability to contact higher-ohmic emitters formed within the underlying silicon, and solid copper is more conductive than silver paste after the co-firing process. These factors translate to lower emitter recombination and  $I^2R$  losses within the solar cell. In total, the efficiency benefit of electroplating over screen printing may be of the order of 0.5% [32].

The electroplating process nevertheless has its drawbacks. There is more cell breakage, and there are additional chemical handling and waste considerations (and therefore costs) associated with handling the electroplating electrolytes. Moreover, the capital expenditures and maintenance costs for electroplating equipment are higher than for screen printing. Electroplating also requires pinhole-free silicon nitride layers; without them, copper will be deposited within the pinholes, and the solar cell

efficiency will drop precipitously, as a result of light being blocked and also because of electrical shunts.

By limiting the amount of silver required to just the back-side pads and the capping layer, a transition to front-side electroplating reduces the total amount of silver per cell from 120–140mg to 30–40mg. This reduction in silver usage would lower the material intensity from today's 21–33 tonnes per GW to 5–10 tonnes per GW. With certain solar cell architectures it is also possible to employ electroplating in such a way that the silver intensity is 0mg per cell; at least two large-scale cell manufacturers already have proprietary processes that employ such techniques.

Fig. 9 compares the manufacturing costs of standard screen-printed cells and electroplated cells at current silver prices. The figure is assembled from cost-of-ownership estimates provided by relevant equipment and materials suppliers. In comparison to the base case, the total direct metallization materials costs are lower for electroplating than for screen printing (0.5–1.5¢/W savings, including the expense of regular replacement of screens for printing). However, the use of electroplating equipment rather than screen printers requires an

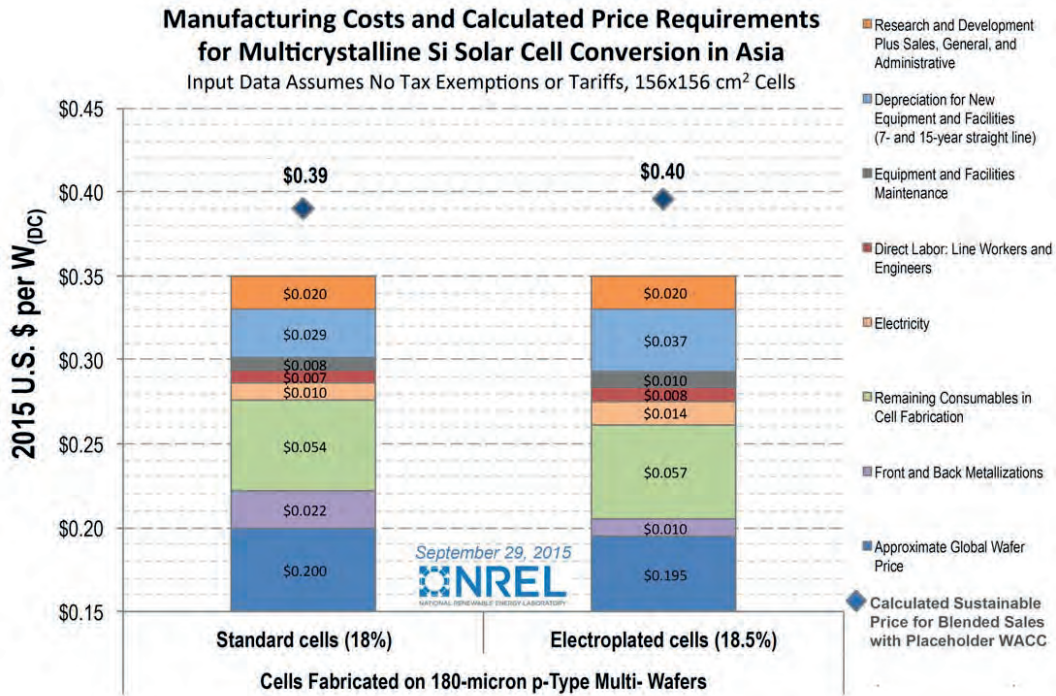


Figure 9. Comparison of manufacturing costs for standard and electroplated cells, based upon cost-of-ownership estimates provided by relevant industry players. The numbers beneath each bar correspond to the assumed cell efficiencies.

initially higher capital expenditure as well as greater maintenance costs. In total, from cost-of-ownership estimates these additional expenses are of the order of 1.0¢/W. Electroplating also entails higher waste water handling costs (0.1–0.3¢/W) than screen printing, and there are slightly higher yield losses (translatable to around 0.1¢/W estimated cost penalty). Utilizing more equipment in the electroplating case also carries with it greater electricity needs (with higher associated costs calculated to be 0.4–0.8¢/W).

### Conclusion

Silver has long been considered the ‘Achilles heel’ of megascale c-Si manufacturing. While the PV sector currently represents a small share of global silver demand, at slightly less than 10% of the total, if c-Si solar cell production continues to grow, the PV industry could become a significant end user of silver. The impact on total silver demand and prices could have relevance for the cost competitiveness of traditional silver screen-printed cells vs. electroplated cells, as well as for developing concepts such as multiwire, stencil printing and inkjet printing. In this paper the effects of a greater

silver demand from the PV industry on silver prices was investigated, as well as the resultant effects on manufacturing costs. For the low to high scenarios, the analysis results indicate a 0.05–0.7¢/W impact on cell manufacturing costs when production is expanded from 55GW to 250GW, depending on the material requirements for metallization. Initial indications are that the cost competitiveness of electroplating may be approaching that of traditional screen printing at current silver prices.

“Initial indications are that the cost competitiveness of electroplating may be approaching that of traditional screen printing at current silver prices.”

Moreover, from NREL’s cost models, an additional efficiency benefit of 0.5–1.0%<sub>abs</sub> (if enabled by a process such as electroplating) would correspond to savings of roughly 0.5–1.2¢/W and 4.0–7.8¢/W at the module level and the utility-scale balance-of-systems level respectively. On a levelised

cost of electricity (LCOE) basis, this would correspond to approximately 0.20–0.36¢/kWh for a moderate solar resource in the USA [33].

From a total life cycle economics perspective, however, an important issue is whether the long-term outdoor reliability (and notably the metal adhesion) of electroplated cells is in general equal to that of screen-printed cells. All of these questions will influence whether, and by how much, the demand for silver may or may not concurrently grow with the PV industry.

### References

- [1] Haxel, G.B., Hedrick, J.B. & Orris, G.J. 2002, “Rare earth elements – Critical resources for high technology” [http://pubs.usgs.gov/fs/2002/fs087-02/fs087-02.pdf].
- [2] CPM Group 2015, *The CPM Silver Yearbook 2015*, New York: CPM Group.
- [3] Goodrich, A. et al. 2013, “A wafer-based monocrystalline silicon photovoltaics road map: Utilizing known technology improvement opportunities for further reductions in manufacturing costs”, *Sol. Energy Mater. Sol. Cells*, Vol. 114, pp. 110–135.
- [4] Feltrin, A. & Freundlich, A.

- 2008, "Material considerations for terawatt level deployment of photovoltaics", *Renew. Energy*, Vol. 33, pp. 180–185.
- [5] Tao, C.S., Jiechao, J. & Tao, M. 2011, "Natural resource limitations to terawatt-scale solar cells", *Sol. Energy Mater. Sol. Cells*, Vol. 95, pp. 3176–3180.
- [6] Jacobson, M.Z. & Delucchi, M.A. 2011, "Providing all global energy with wind, water, and solar power. Part I: Technologies, energy resources, quantities and areas of infrastructure, and materials", *Energy Policy*, Vol. 39, pp. 1154–1169.
- [7] Grandell, L. & Thorenz, A. 2014, "Silver supply risk analysis for the solar sector", *Renew. Energy*, Vol. 69, pp. 157–165.
- [8] IEA 2014, "IEA world energy outlook 2014" [<http://www.worldenergyoutlook.org/publications/weo-2014/>].
- [9] Erdmann, L. & Graedel, T.E. 2011, "Criticality of non-fuel minerals: A review of major approaches and analyses", *Environ. Sci. Technol.*, Vol. 45, pp. 7620–7630.
- [10] European Commission (2014), "Report on critical raw materials for the EU" [[http://ec.europa.eu/enterprise/policies/raw-materials/files/docs/crm-critical-material-profiles\\_en.pdf](http://ec.europa.eu/enterprise/policies/raw-materials/files/docs/crm-critical-material-profiles_en.pdf)].
- [11] Willis, P., Chapman, A. & Fryer, A. 2012, "Study of by-products of copper, lead, zinc, and nickel", Report prepared for Int. Lead and Zinc Study Group, Int. Nickel Study Group and Int. Copper Study Group.
- [12] Morley, N. & Eatherley, D. 2008, "Material security: Ensuring resource availability for the UK economy" [[http://www.oakdenhollins.co.uk/pdf/material\\_security.pdf](http://www.oakdenhollins.co.uk/pdf/material_security.pdf)].
- [13] U.S. DOE 2011, "Critical materials strategy" [[http://energy.gov/sites/prod/files/DOE\\_CMS2011\\_FINAL\\_Full.pdf](http://energy.gov/sites/prod/files/DOE_CMS2011_FINAL_Full.pdf)].
- [14] Graedel, T.E. et al. 2015, "Criticality of metals and metalloids", *Proc. Natl. Acad. Sci.*, Vol. 112, No. 14, pp. 4257–4262.
- [15] SEMI PV Group Europe 2015, "International technology roadmap for photovoltaic (ITRPV): 2014 results" [<http://www.itrpv.net/Reports/Downloads/>].
- [16] NREL 2014, "2013 renewable energy data book" [<http://www.nrel.gov/docs/fy15osti/62580.pdf>].
- [17] Silver Institute 2013, "World silver survey 2013" [[http://share.thomsonreuters.com/assets/forms/gfms\\_silver\\_survey\\_2013.pdf](http://share.thomsonreuters.com/assets/forms/gfms_silver_survey_2013.pdf)].
- [18] IEA 2014, "Technology roadmap solar photovoltaic energy" [[https://www.iea.org/media/freepublications/technologyroadmaps/solar/TechnologyRoadmapSolarPhotovoltaicEnergy\\_2014edition.pdf](https://www.iea.org/media/freepublications/technologyroadmaps/solar/TechnologyRoadmapSolarPhotovoltaicEnergy_2014edition.pdf)].
- [19] Moss, R.H. et al. 2010, "The next generation of scenarios for climate change research and assessment", *Nature*, Vol. 463, No. 7282, pp. 747–756.
- [20] Kriegler, E. et al. 2014, "The role of technology for achieving climate policy objectives: Overview of the EMF 27 study on global technology and climate policy strategies", *Climatic Change*, Vol. 123, No. 3–4, pp. 353–367.
- [21] Luderer, G. et al. 2013, "The role of renewable energy in climate stabilization: Results from the EMF27 scenarios", *Climatic Change*, Vol. 123, No. 3–4, pp. 427–441.
- [22] Chapman, A. et al. 2013, "Study on critical raw materials at EU level" [[http://ec.europa.eu/enterprise/policies/raw-materials/index\\_en.htm](http://ec.europa.eu/enterprise/policies/raw-materials/index_en.htm)].
- [23] Lanz, B., Rutherford, T.F. & Tilton, J.E. 2013, "Subglobal climate agreements and energy-intensive activities: An evaluation of carbon leakage in the copper industry", *World Econ.*, Vol. 36, No. 3, pp. 254–279.
- [24] Zhuang, J. & Gabriel, S.A. 2008, "A complementarity model for solving stochastic natural gas market equilibria", *Energy Econ.*, Vol. 30, No. 1, pp. 113–147.
- [25] Böhringer, C. & Lösche, A. 2006, "Promoting renewable energy in Europe: A hybrid computable general equilibrium approach", *Energy J.*, Vol. 27, pp. 135–150.
- [26] World Bank 2015, "Global economic monitor" [<http://data.worldbank.org/data-catalog/global-economic-monitor>].
- [27] Silver Institute 2014, "World silver survey 2014" [<https://www.silverinstitute.org/site/publications/>].
- [28] Cross, J. 2009, "Prospects for silver supply and demand" [[http://www.lbma.org.uk/assets/alc57\\_prospects\\_silver\\_supply.pdf](http://www.lbma.org.uk/assets/alc57_prospects_silver_supply.pdf)].
- [29] GFMS Ltd 2011, "The future of silver industrial demand" [<https://www.silverinstitute.org/site/wp-content/uploads/2011/07/futuresilverindustrialdemand.pdf>].
- [30] Åstrom, M. 2013, "Supply and demand of the silver market" [<https://pure.ltu.se/ws/files/67780553/LTU-EX-2013-62059944.pdf>].
- [31] Evans, M. & Lewis, A. 2002, "Is there a common metals demand curve?", *Resour. Policy*, Vol. 28, No. 3, pp. 95–104.
- [32] Russell, R. et al. 2013, "Cost-effective and reliable Ni/Cu plating for p- and n-type PERC silicon solar cells yielding efficiencies above 20.5%", *Photovoltaics International*, 21st edn, pp. 62–69.
- [33] Jones-Albertus, R. et al. 2015, "Technology advances needed for photovoltaics to achieve widespread grid price parity", Submitted to *Prog. Photovoltaics Res. Appl.*

#### About the Authors



**Michael Redlinger** is a Ph.D. candidate in the Mineral and Energy Economics Program at CSM. His research interests include material constraints on solar deployment, economics of thin-film PV cell recycling, and mineral scarcity and price volatility.



**Dr. Michael Woodhouse** is a member of NREL's Strategic Energy Analysis Center, and the Clean Energy Manufacturing Analysis Center, where his analysis activities are focused on solar energy technologies, economics and policy.



**Roderick G. Eggert** is a professor of economics and business at CSM, and deputy director of the Critical Materials Institute, an energy innovation hub created in 2013 by the U.S. DOE to accelerate innovation in energy materials. His research and teaching focus on mineral economics and public policy.

#### Enquiries

Michael Redlinger  
Division of Economics and Business  
Colorado School of Mines  
816 15th Street  
Golden  
Colorado 80401  
USA

Tel: +1 (907) 433-9177

Email: [mike.redlinger@gmail.com](mailto:mike.redlinger@gmail.com)

# Thin Film

---



Page 76  
News

---

Page 79  
Damp-heat-induced  
degradation of layers in CIGS  
solar cells

Mirjam Theelen, TNO/Solliance,  
Eindhoven, The Netherlands

---

## First Solar pushes CdTe cell efficiency to record 22.1%

Leading cadmium-telluride (CdTe) thin-film producer First Solar has set a new world record research cell conversion efficiency of 22.1%, certified at the Newport Corporation's Technology and Applications Center (TAC) PV Lab.

According to First Solar, this is the ninth major update to CdTe record efficiency since 2011. The new cell record has also been documented in the US Department of Energy's National Renewable Energy Laboratory (NREL) "Best Research Cell Efficiencies" reference chart.

Raffi Garabedian, First Solar's chief technology officer, said: "We are tracking very closely to a technology roadmap we first presented in 2013 and revised upward in March 2014. At that time, we said we'd hit a 22% research cell efficiency milestone by the end of 2015. We've delivered on that promise."

The record cell was said to have been produced at First Solar's Perrysburg, Ohio manufacturing factory and Research & Development Center using processes and materials applicable to commercial-scale manufacturing. First Solar noted that in the fourth quarter of 2015 its lead manufacturing lines were producing PV modules with 16.4% conversion efficiency.



Credit: First Solar

First Solar said it achieved the record using "processes and materials applicable to commercial-scale manufacturing".

## First Solar lowers 2016 guidance after record 2015

Cadmium-telluride (CdTe) thin-film producer First Solar has lowered revenue guidance slightly for 2016, while solar module shipments guidance of 2.9GW to 3.0GW remains unchanged.

The company reported record annual net sales of US\$3.6 billion for 2015, while its fourth quarter net sales were US\$942 million, slightly higher than market expectations.

However, sales were down US\$329 million from the third quarter of 2015, due to Desert Stateline project revenue recognition happening a quarter earlier. In addition, sales of third-party module and module plus offerings also decreased quarter-on-quarter.

"We exit 2015 with record annual revenues, record new bookings and earnings per share of over five dollars," said Jim Hughes, CEO of First Solar. "As we look back to the 2015 targets first provided to investors at our analyst day nearly three years ago, we recognise that we have achieved the efficiency, cost per watt and earnings targets outlined at that time. We enter 2016 with tremendous technology, a strong pipeline and an ongoing commitment to achieve the long-term objectives we have communicated to our investors."

In January, Baird Equity Research analyst, Ben Kallo said that as a direct consequence of the US ITC extension there could be

a slowdown in PV project completions by key US-centric photovoltaic energy roviders, notably First Solar. Kallo said that he was lowering revenue expectations for First Solar in 2016 to US\$3.74 billion, down from previous estimates of US\$3.975 billion as the rush to complete projects, due to the previously expected ITC reduction had eased. In actual fact, the company shifted from US\$3.9-4.1 billion to US\$3.8-4.0 billion.

### Hanergy latest

## Hanergy's financial controller resigns

Li Guangim, the financial controller and an executive director of troubled Chinese manufacturer Hanergy Thin Film Power has resigned from the company.

Hanergy announced Li's departure in a statement to the Hong Kong stock exchange, at the time of writing the company is suspended from trading following its share price collapse in 2015.

In its statement, Hanergy said Li's resignation was due to his "personal career development" and that he had "no disagreement with the board and there are no matters relating to his resignation that needs to be brought to the attention of The Stock Exchange of Hong Kong."

Hanergy has brought in three new

directors. Huang Songchun has been appointed financial controller and as an executive. Si Haijian and Zhang Bo have both also been appointed as executive directors of the company

Li's departure caps a difficult year for Hanergy, in which it has gone from being largest biggest company by market capitalisation to ignominy.

Since its share price tumbled in the middle of the year, Hanergy's woes have deepened. Shortly after trading of its shares was suspended, the Hong Kong Securities and Futures Commission revealed it was investigating the company. It has subsequently been forced to cancel a number of large contracts, and recent reports suggested it was being sued for unpaid rent and utility bills.

## Hanergy accused of not paying office rent

There were fresh woes for Hanergy Thin Film Power (HTFP) as reports surfaced that the company was accused of not paying rent on an office in Hong Kong.

According to a report in the *Financial Times*, an unnamed HTFP executive said that outstanding rent of HK\$1.035m (US\$133,544) had actually been paid on 3 December, 2015.

However, a Hong Kong High Court writ filed that same day alleged that the amount owed was HK\$1.7 million, with no explanation forthcoming from the HTFP

Credit: Hanergy



**Hanergy has faced a difficult start to 2016.**

executive on the discrepancy between the two amounts. The company had been accused of not paying rent, management charges and “other fees,” the *FT* said.

According to the report, another high-rise office rented by the company on the 77th floor of the Hong Kong Centre skyscraper has been left empty.

### Hanergy subsidiary eyes European BIPV market

Flexible CIGS thin-film producer MiaSolé, a subsidiary of struggling Hanergy Thin Film Power Group, is offering its BIPV products in Nordic countries including Denmark, Finland, Norway and Sweden through a sales agreement with Finnish firm, Virte Solar.

Virte Solar, a subsidiary of Virte Metal Corporation that builds metal roofing systems, will use MiaSolé’s flexible substrates for BIPV applications, such as commercial and agricultural rooftops.

Last year, Germany-based CIGS module manufacturer Solibro, another Hanergy subsidiary, was reported to have severely curtailed production due to its parent company’s financial issues.

#### Solar Frontier latest

### Solar Frontier ran 900MW Kunitomi CIS plant near full-capacity in 2015

Solar Frontier has reported that its main manufacturing plant ran at almost full

capacity in 2015.

The company also started production at its new Tohoku Plant in April, 2015 with a nameplate annual production capacity of 150MW. The plant was said to have added around 100MW of overall capacity by year-end.

The plant is the company’s fourth solar module production facility and is tasked with demonstrating the commercialization of new technologies and significant cost reductions. The company also noted that it had started the plants transition to commercial production in 2015.

As part of the energy solutions business unit of Showa Shell, the energy solutions business unit reported 2015 sales of 119.4 billion yen (US\$1.06 billion), down 13.8% from the previous year.

The revenue decline was partly due to module ASPs decline and currency impacts. The company noted that the domestic Japanese residential solar market declined significantly in 2015, due to FiT reductions.

Focus on international sales and downstream PV project development in countries such as the US and UK, were designed to offset the weaker Japanese residential market. The company is also developing utility-scale and commercial PV power plants in Japan.

### Solar Frontier and Goldman Sachs-affiliate to develop 300MW of PV projects in Japan

Solar Frontier believes it could make some of Japan’s as-yet-unbuilt utility-scale

solar projects economically viable, as the company’s collaboration with Goldman Sachs-affiliate Japan Renewable Energy prepares to take on 300MW of projects within the next five years.

It has been widely reported that Japan’s support schemes for renewable energy have led to vast and rapid deployment of solar, especially ‘mega solar’ at the multi-megawatt scale. With around 20GW in total deployed for the FiT, there is also a 57GW pool of projects that have been awarded the FiT since 2012, but have not yet been built.

A joint venture formed by Mitsubishi UFJ Financial Group, Mitsubishi Research Institute and Morgan Stanley said in January that it will take on already-built plants that are not performing as well as expected. Meanwhile Japanese newspaper Nikkei has reported that a “business collaboration” between Japan’s Solar Frontier and Goldman Sachs-affiliated Japan Renewable Energy plans to execute up to 300MW of large-scale projects together, which could include some of the unbuilt projects.

The pair claim the partnership will enable them to reduce the project cost of large-scale PV plants by as much as 30%.

Selling electricity from the plants at fixed rates for 20 years, the pair’s projects will utilise Solar Frontier panels, subcontracting the construction work to a number of parties while reducing construction times. Solar Frontier will also be acquiring balance of systems components, mounting racks and other related items.



Credit: Solar Frontier

Solar Frontier has been looking to offset a slow domestic market with project work overseas.

### Tool makers

#### Rescue plan for Singulus takes shape in early 2016

German PV equipment specialist Singulus has cleared several hurdles in its financial restructuring process.

In February, shareholders approved a proposed debt-equity swap the company is looking to implement to stave off likely insolvency just a few days after bondholders had also given their approval to the deal.

Singulus said that although the latest vote meant the main prerequisites for the restructuring had now been met, some shareholders had filed objections to the plan, as had some of its bondholders the previous day.

The company said it would have to wait to see whether this would result in the filing of voidance actions, but reiterated previous assertions that it was "confident" it could override these in a fast-track proceeding. Singulus' debt restructuring had become necessary after it recorded heavy losses in the 2014 financial year.

More encouragingly, Singulus says it has a strong order book, particularly in its solar business, which is expected to account for around 70% of sales in the coming year, according to the company. It secured a €20 million order from India in late 2015.

#### 4JET spins off PV thin-film laser system business

Laser equipment and systems solutions specialist 4JET Technologies said it had spun-off its laser micro-machining technology that included PV thin-film technology into a separate company, 4JET microtech GmbH & Co KG.

4JET Technologies had been known for developing laser-based edge deletion systems for all types of thin-film solar cells as well as flexible, roll-to-roll thin film processing systems.

The new business will remain located at 4JET Technologies' existing facility in Alsdorf, Germany and retain its existing management and staff.

New capacity expansions in thin-film companies has been limited to less than a handful in the last five years, primarily driven by upgrades and small increases in capacity at companies such as First Solar and Solar Frontier.

The last major laser systems order in the PV thin-film market was made by First Solar, placing a large single order with LPKF Laser & Electronics in early 2014.

### Organic thin-film

#### Heliatek pushes OPV lab cell to record 13.2% conversion efficiency

Dresden-based OPV thin-film producer, Heliatek has set a new conversion efficiency record of 13.2% using a multi-junction lab-sized (1.37 cm<sup>2</sup>) sample cell with its small molecule, vacuum deposition process on a plastic film substrate.

Heliatek noted that the results support an in-house roadmap towards 15% efficient organic solar cells and the development of new absorber molecules (green, red or near-infrared light of the wavelength range between 450nm and 950nm) and optimizing the device architecture.

Dr. Martin Pfeiffer, CTO of Heliatek said: "This success is based on our chemical research for new organic absorber

materials. Key to this success is the close cooperation of our physics and chemistry R&D teams, which leads to an optimal combination of the properties of this new solar cell design."

The new record cell efficiency was said to have been independently measured at simulated AM 1.5 illumination by Fraunhofer CSP.

#### Ascent Solar raises US\$7 million; de-lists from NASDAQ

Flexible CIGS thin-film consumer product producer Ascent Solar Technologies raised US\$7 million through a Series F 7% convertible preferred stock placement with existing investor, Redwood Management LLC.

The loss-making company ended the third quarter of 2015 with cash and cash equivalents of only US\$619,000.

Ascent Solar noted in an SEC filing related to the share issue that it did not expect to be cash positive in 2016 and would not expect sales revenue levels and cash flows to be sufficient to support its operations and cash requirements until its consumer business product strategy had been successful.

The company warned that additional capital would be needed in order to continue its current level of operations throughout 2016.

In February it was de-listed from the NASDAQ, as expected.

The lost making thin-film producer's stock price had been below the US\$1.0 dollar minimum requirement for a second time, having undertaken a reverse stock split in August, 2014.

Ascent Solar's stock were scheduled to be transferred to the OTCQB Venture Market on February 25, 2016.



# Damp-heat-induced degradation of layers in CIGS solar cells

Mirjam Theelen, TNO/Solliance, Eindhoven, The Netherlands

## ABSTRACT

Investors require a guarantee of a minimum lifetime for PV installations. It is tempting to provide such a guarantee for a longer lifetime simply by specifying test conditions that are more and more severe. In this paper it is argued that, with a more detailed understanding of the basic mechanisms determining cell material behaviour under specific exposure conditions, not only can the inherent lifetime of solar cells and modules be improved, but also the predictive value and effectiveness of lifetime testing. An overview of the literature contributions regarding the influence of damp-heat exposure of the layers in  $\text{Cu(In,Ga)Se}_2$  (CIGS) solar cells is presented. The material changes, as well as their potential influence on solar cell and module performance, are described. For the molybdenum back contact, it was observed that damp-heat exposure leads to a decrease in conductivity and reflectivity, most likely caused by molybdenum oxidation. The presence of a selenized-molybdenum ( $\text{MoSe}_2$ ) top layer, in combination with the use of low sputtering pressure, resulted in more stable molybdenum films. For the transparent conductive front contact, a comparison of reports in the literature revealed that indium tin oxide (ITO) films are more stable in damp heat than  $\text{ZnO:Al}$  films. It was also observed that  $\text{ZnO:Al}$  films degraded as a result of the ingress of water and  $\text{CO}_2$  via the grain boundaries, thereby lowering the conductivity of the material. The results of damp-heat studies of CIGS absorbers and buffers were difficult to quantify and varied between cases. In many instances, absorber exposure gave rise to the formation of spots on the surface, as well as to sodium migration, whereas buffer exposure often led to interdiffusion and reactions with the absorber and front contact. Literature reports also demonstrated that the  $\text{Mo/ZnO}$  stack in the P2 scribe is a vulnerable location in CIGS modules.

## Reliability of thin-film PV

Thin-film PV modules based on  $\text{Cu(In,Ga)Se}_2$  (CIGS) technology have shown themselves to be very promising. CIGS technology allows lightweight, low-cost PV products, and leads to the highest efficiencies among the various types of thin-film PV; the highest-performing CIGS solar cells today have yielded conversion efficiencies of up to 22.3% [1], thus even outperforming multicrystalline silicon cells.

For the large-scale market introduction of CIGS modules, solid performance stability, along with low initial costs and high efficiency, is an important prerequisite (Fig. 1). Besides the lower electricity costs afforded by reliable, long-lifetime modules, the predictability of performance is also important: financiers, home-owners, utilities, planners and especially producers need to be able to predict when their modules will no longer function, so that the risks can be evaluated. Performance reliability is therefore very important in order to obtain the lowest and most predictable electricity costs.

“For the large-scale market introduction of CIGS modules, solid performance stability is an important prerequisite.”

In cases where the field performance of CIGS modules has been studied, large differences were observed: many modules were very stable (e.g. no degradation after seven years), but field failures were also seen [2,3]. Because of the relatively limited field experience of CIGS modules, combined with the multitude of techniques used for module production, the lifetime prediction for CIGS modules in general is a challenge. More information about

the degradation behaviour of CIGS modules is therefore required in order to decrease degradation rates and make those rates more predictable, and thus to improve long-term performance. Studies have yielded the following observations regarding less stable modules in the field:

- Field exposure mainly affects the fill factor and the voltage, while the current is mostly relatively stable.

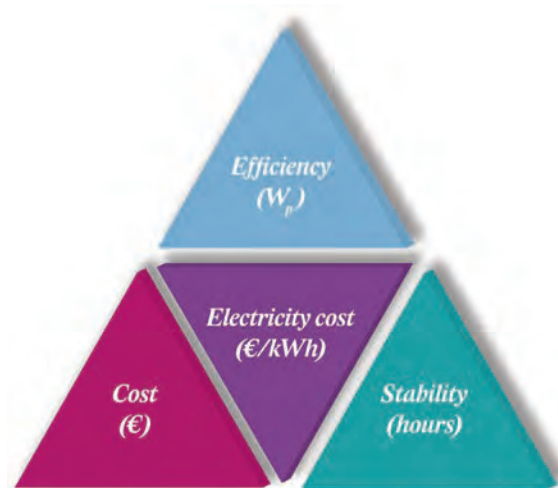


Figure 1. The three main parameters determining the cost competitiveness of electricity generated from PV modules.

- Degradation in the field is often related to the ingress of moisture into the CIGS modules, thereby affecting the CIGS cell material (Fig. 2) inside the module.

Since moisture ingress, often combined with elevated temperatures, has a negative impact on CIGS solar cells, modules are provided with water barriers. For rigid modules, glass is an excellent barrier choice; however, for flexible modules, expensive organic-inorganic multilayer coatings are often required. Therefore CIGS cells

that are intrinsically more stable can help to minimize the barrier costs and facilitate the large-scale market introduction of flexible CIGS modules. Fig. 3 shows the various ways in which intrinsically more stable and predictable solar cells can help lower electricity costs with PV modules.

Knowledge of the stability of CIGS solar cells and modules is often obtained by the simulation of degradation phenomena in accelerated lifetime tests (ALT). In order to study the effect of moisture ingress at elevated temperatures, the IEC procedure 61646

for thin-film PV includes 1,000 hours' exposure to 'damp heat' (85°C/85% relative humidity (RH)).

In learning about the stability of CIGS solar cells and modules, many aspects should be considered, including:

- The damp-heat stability of the individual layers in the CIGS solar cells and modules.
- The interaction between these layers and between the stack and the module package material.
- The influence of biases, such as illumination [3,4].

Although none of these aspects in isolation can be used to predict the failure mechanisms occurring in CIGS modules in the field, they can give an indication of the vulnerable materials and interfaces, and allow improvements to the various parts of the module. In this paper the results of damp-heat exposure of individual layers, and of the interconnection areas within CIGS solar cells and modules, are summarized.

A short overview of the data previously published in Theelen [3] (and in the paper by Theelen & Daume [4], submitted for publication) will be given. In these cited works, more extensive literature references can also be found (in particular for the data used for Figs. 5 and 7).

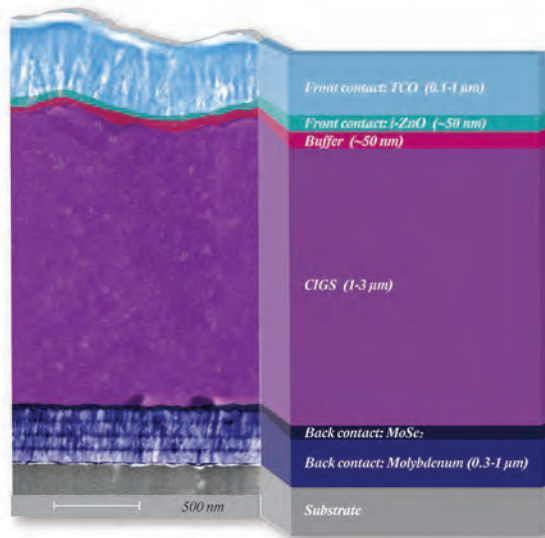


Figure 2. Cross section of the make-up of a typical CIGS solar cell.

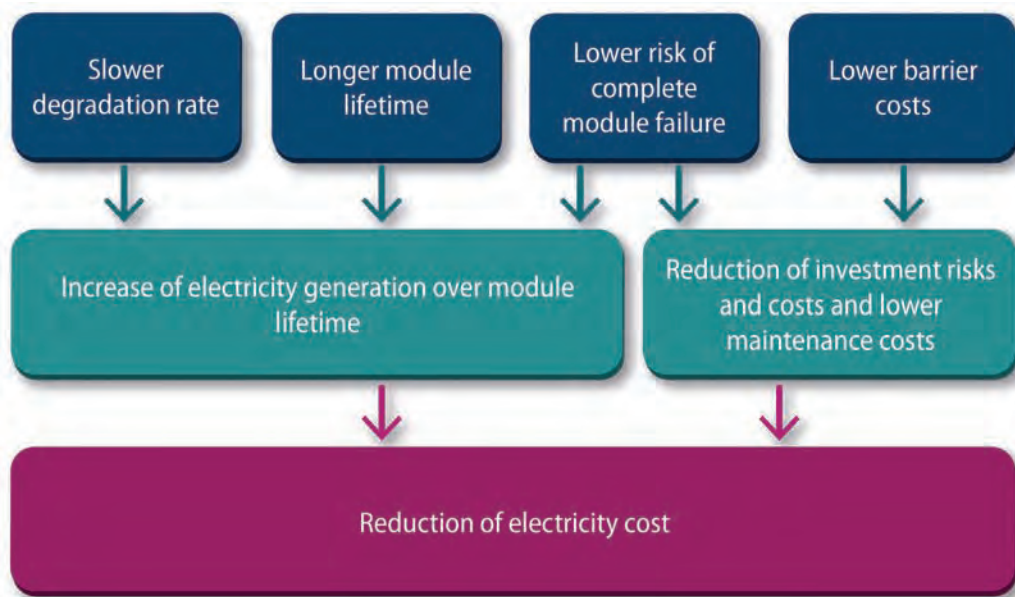


Figure 3. Routes by means of which more intrinsically stable and predictable solar cells can reduce the cost of electricity generated by PV modules. 'Slower degradation rate' and 'longer module lifetime' are naturally related: the former refers to the real non-linear loss of output power in the field ('stability'), while 'lifetime' is the economic lifetime (e.g. maximum 20% efficiency loss) as defined before installation and on which the electricity cost calculations, installation planning and risks assessments are based ('predictability').

## Molybdenum back contact

Sputtered molybdenum (Mo) is used as the back-contact material for CIGS solar cells and modules by nearly every research group and manufacturer. The main requirements for a functional molybdenum back contact are good conductivity and reflectivity, the latter especially when thin absorber layers are used. Molybdenum films within CIGS cells and modules are normally covered by a thin layer of MoSe<sub>2</sub>, while the molybdenum is uncovered between the molybdenum and CIGS deposition steps.

## Stability of the Mo back contact

The degradation of molybdenum can occur at two points in time [5]:

1. Degradation of bare metallic molybdenum in storage. Molybdenum which is not immediately used for further processing can be stored, but exposure of bare molybdenum to the atmosphere can affect the electrical properties of the later-processed CIGS solar cells and modules.
2. Long-term stability of the molybdenum back contact in CIGS

cells and modules. These layers are covered, in most places, by a thin MoSe<sub>2</sub> layer (Mo/MoSe<sub>2</sub> stack), as well as by the rest of the cell stack. These molybdenum layers are therefore mostly vulnerable in the P2 and P3 scribes (see scribe section later). An assessment of the stability of this material should be based on the actual composition of the molybdenum in these particular areas.

In many cases, exposure to elevated temperatures and humidity and oxygen levels leads to oxidation of the films: this is often visible as black and blue stains on both molybdenum and selenized-molybdenum (Mo/MoSe<sub>2</sub>) films, as shown in Fig. 4. These stains contain molybdenum oxide (MoO<sub>2</sub>/MoO<sub>3</sub>), which is generally poor in terms of conductance and reflectance. The molybdenum oxide layers sometimes even show cracks and needles on the surface.

The formation of a thick layer of non-conductive molybdenum oxide can lead to a very rapid decrease in conductivity when measured from the top. Prior to this plummet, most films exhibit a slow decline in conductivity: an overview of the decrease in conductivity for various types of molybdenum films is shown in Fig. 5.

Differences in degradation rate are caused by the presence of the MoSe<sub>2</sub> top layer: selenized molybdenum degrades more slowly than bare molybdenum films, most likely because it is easier to oxidize metallic molybdenum than MoSe<sub>2</sub>. Another factor that influences the degradation rate is the sputter pressure. Degradation effects are the most severe for molybdenum deposited at high pressures during sputter deposition, thereby forming more porous molybdenum layers, which are more susceptible to the ingress of, among other things, water and oxygen [5].

Various references have reported on the presence of sodium, which probably plays a role in molybdenum degradation. Sodium can occur, for example, in the form of needles on the molybdenum surface, but it can also intercalate via a reduction reaction into MoO<sub>3</sub>, thereby forming Na<sub>x</sub>MoO<sub>3</sub> [6].

## Influence on module stability

The presence of molybdenum oxide in the scribes is discussed in the scribe section, and so only the effect of oxidation of the Mo/CIGS interface will be described here. Oxidation can, on the one hand, simply increase the series resistance and decrease the fill factor of a solar cell or module; on the

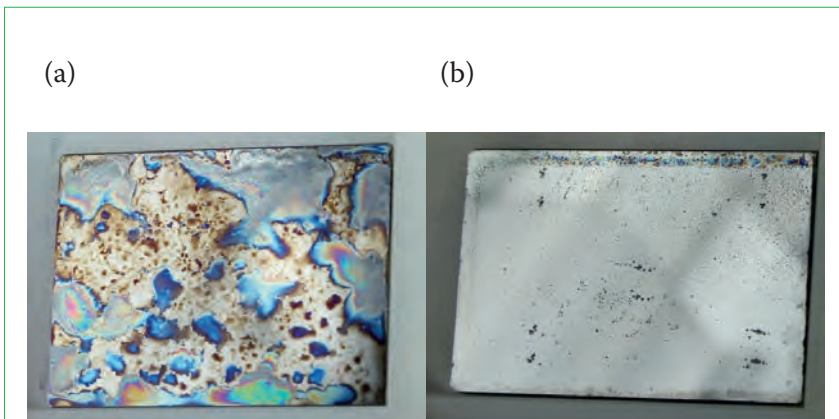


Figure 4. Photographs of two porous molybdenum samples (~30mm × 25mm) after 17 hours' exposure to damp heat: (a) bare molybdenum; (b) molybdenum covered by MoSe<sub>2</sub>. (Taken from Theelen et al. [5].)

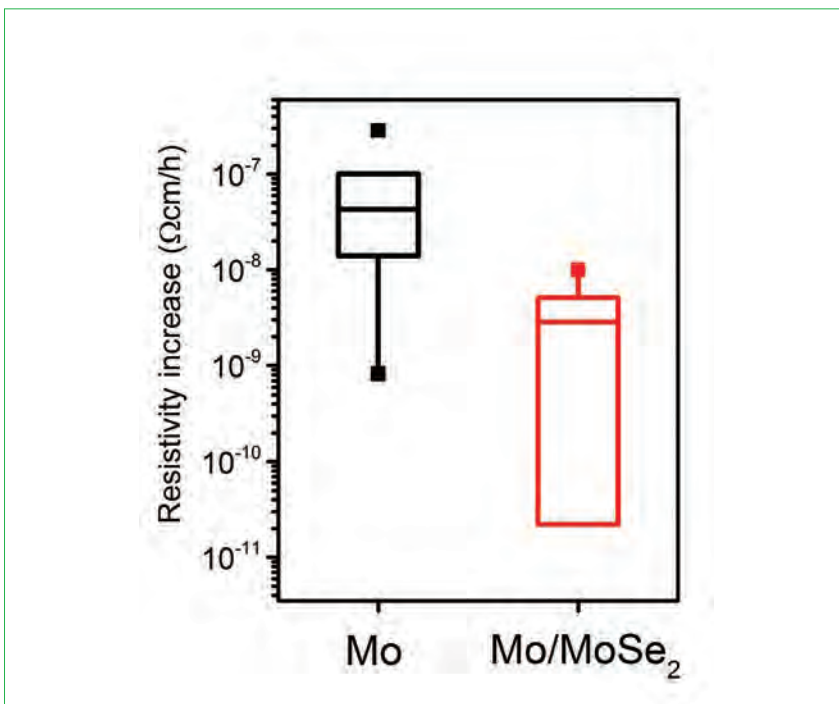


Figure 5. Box plot showing the degradation rate per hour (assumed to be linear) under damp-heat exposure of molybdenum (including Mo alloyed with Al or with a Cr bilayer) and of molybdenum with a MoSe<sub>2</sub> top layer. The resistivity change for MoSe<sub>2</sub> was negative in one case ( $-1 \times 10^{-9} \Omega \text{cm/h}$ ) (not shown on the graph) [3].

other hand, it can change the ohmic behaviour at the Mo/CIGS region, thereby influencing various electrical parameters. It should be noted that oxidation is not always detrimental to cell or module performance; mild oxidation could actually even result in slightly improved efficiency [7].

### The CIGS absorber and the buffer layer

The CIGS absorber and the buffer layer form the p and n parts of CIGS solar cells and modules. A study of the damp-heat stability of these individual layers is complicated, since their interaction with each other and with the front and back contacts greatly influences the stability of the layers. Consequently, these layers are mainly tested as part of the complete solar cell stack, while measurements for the individual layers are scarce, and the interpretation of the effect of the observations on the solar cell or module output is especially complicated.

#### Stability of the CIGS absorber

The CIGS absorber has a variety of point defects with complex interactions that determine their benign electronic behaviour. The CIGS absorber is an impurity-tolerant material with radiation hardness, and it can be stated that CIGS grains themselves are thus intrinsically stable, irrespective of their complicated structure [8]. Changes in the CIGS absorber due to extrinsic influences, such as damp heat, are therefore often caused by changes around the grain boundaries within the polycrystalline absorber film and the interfaces with the back contact and buffer.

It has been observed that the exposure of bare CIGS absorbers to even ambient conditions has led to a rapid reduction in carrier lifetime [9]. This degradation process can be prevented by buffer deposition on top of the CIGS absorber. Another source [10] has reported that when bare CIGS absorbers were exposed to damp heat, spots were formed on the surface. These spots exhibited low concentrations of gallium, copper and selenium, but high sodium content, caused by, for example, hydrolysis or oxidation. Furthermore, the formation of sulphate has been reported as a result of damp-heat-induced oxidation of sulphur in  $\text{Cu}(\text{In,Ga})(\text{Se,S})_2$  solar cells [11].

Sodium has been found to have a very large impact on CIGS absorber stability: oxidation of CIGS absorbers occurs in the presence of sodium and

water. Experiments have shown that this oxidation, catalysed by water, promoted an enhanced removal of selenium from the absorber layer via the formation of  $\text{Na}_2\text{Se}_x$  compounds, leading to severe efficiency loss, mainly because of reduced shunt resistance [12]. Additionally, the presence of a large sodium content due to a porous molybdenum back contact even leads to physical distortions in the CIGS absorber layer [13].

Damp-heat stability is also influenced by the gallium content. Experiments with complete solar cells with CIGS absorbers containing different levels of gallium have shown that for a medium concentration of gallium, the degradation rate was the lowest, whereas cell degradation was more intense in the case of pure CIS or CGS absorbers [14].

#### Stability of the buffer

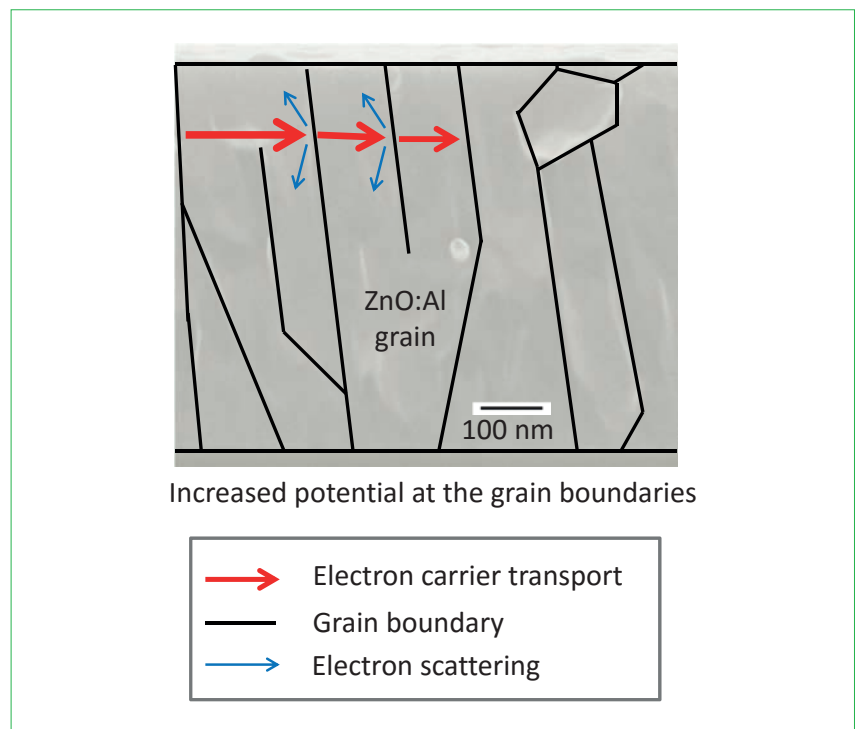
As a buffer in CIGS solar cells, CdS has often been the material of choice. However, because of the toxicity of cadmium and the use of a wet-chemical deposition technique, other materials are being used more and more [15]. The buffer has always been studied in terms of its contact with the other layers.

The stability of the buffers CdS,  $\text{Zn}(\text{O,S,OH})_x$  and  $\text{In}_2\text{S}_3$  under damp-heat conditions has been widely

reported in the literature. It has been found that the CdS buffer can diffuse into the CIGS and ZnO layers under damp-heat conditions. Possible reaction products are  $\text{ZnSO}_4$  or some other sulphate [11], and  $\text{Cd}_{1-x}\text{Zn}_x\text{S}$  and  $\text{ZnO}_{1-x}\text{S}_x$  [16]. The interaction between CdS and the doped ZnO front contact can possibly lead to an increase in the sheet resistance of this contact. An interaction between the buffer and the front contact has also been found when  $\text{Zn}(\text{O,S,OH})_x$  is used as a buffer, which quite likely resulted in the hydration and dehydration of ZnO into  $\text{Zn}(\text{OH})_2$ , and vice versa [17]. When  $\text{In}_2\text{S}_3$  is used as an alternative buffer, no major differences in stability behaviour from that of CdS-based solar cells have been found [18].

### TCO front contact

The transparent conductive oxide (TCO) functions as a front contact of CIGS solar cells or modules. It should be transparent in order to allow the influx of photons into the CIGS layer, while conductivity is required of it for the transport of the produced electrons. The main requirements for a TCO in a solar cell or module are therefore conductivity and transparency. Several types of TCO are possible candidates for the front contacts of CIGS solar cells



**Figure 6.** The presence of grain boundaries in doped zinc oxide can lead to grain boundary scattering, thereby reducing the electron carrier transport (on the basis of Theelen et al. [19,21]). The presence of unwanted species due to damp-heat exposure can increase this effect, leading to a decrease in conductivity of the film.

and modules; of these, the cost-effective sputtered ZnO:Al is the most frequently used, but sputtered indium tin oxide (ITO) is also implemented.

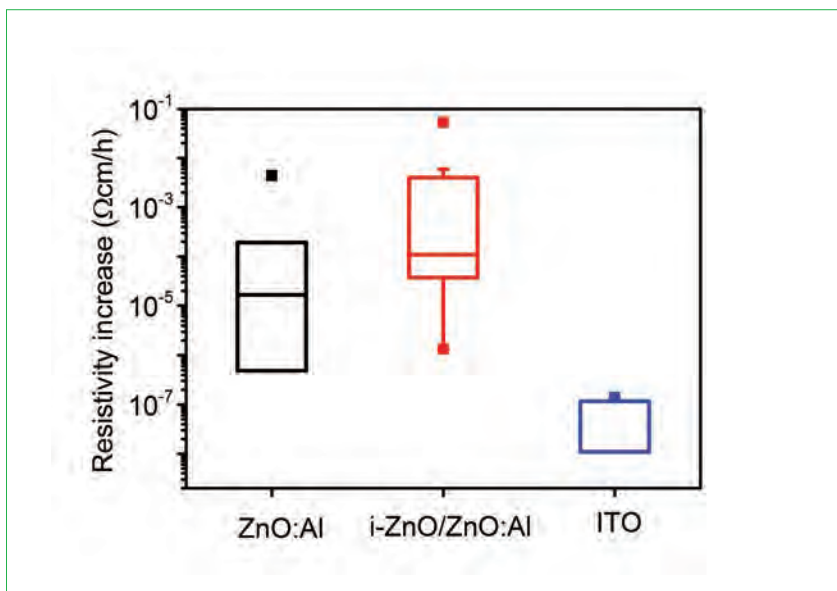
**“An increased resistivity of ZnO:Al films is often found to be the main cause of efficiency losses in solar cells and modules.”**

#### Stability of the TCO front contact

An increased resistivity of ZnO:Al films is often found to be the main cause of efficiency losses in solar cells and modules. This increased resistivity is primarily driven by a decrease in mobility and is typically caused by the diffusion of species from the atmosphere into the grain boundaries. The migration of, among others, water and CO<sub>2</sub> can lead to the formation of molecules such as Zn(OH)<sub>2</sub> and Zn<sub>5</sub>(CO<sub>3</sub>)<sub>2</sub>(OH)<sub>6</sub> [19,20], while the adsorption of atmospheric species in the grain boundaries might also occur. The presence of these species can lead to the formation of a potential barrier at the grain boundaries, resulting in grain boundary scattering (Fig. 6) and thus increased resistivity. Additionally, spot formation has been observed [19], but large changes in the transparency of the ZnO:Al due to damp-heat exposure have not been reported.

More stable ZnO:Al films have been obtained by thicker layers [22], higher deposition temperatures [19] and higher doping concentrations [22]. Furthermore, it has been found that ZnO:Al on rough substrates shows a faster increase in resistivity than on smooth substrates, as a result of damp-heat exposure. Rough underlying absorber and buffer layers can therefore also negatively impact the damp-heat stability of the ZnO:Al film [23]. Increases in resistivity can be largely reversed by annealing in a vacuum or in a reducing atmosphere at elevated temperatures [22,24], but the feasibility of high-temperature annealing of ZnO:Al on the top of complete CIGS solar cells or modules needs to be further investigated.

The more expensive ITO is generally more stable than ZnO:Al in the presence of humidity and elevated temperatures (Fig. 7). The conditions that favour the deposition of damp-heat-resistant ITO films are higher deposition temperatures [25] and lower partial pressures of oxygen [26]. The damp-heat exposure of ITO also often results in the formation of spots [25].



**Figure 7. Box plots showing increase in resistivity per hour (assumed to be linear) for ZnO:Al, ITO and i-ZnO/ZnO:Al films exposed to damp-heat conditions. The resistivity changes for ITO in particular, and in one case for ZnO:Al, can be zero or negative (not shown in the logarithmic graph).**

#### Influence on module stability

There are various ways to determine the impacts of the TCO on the stability of a complete CIGS solar cell or module. The first of these impacts is the one that is mainly addressed in this paper:

1. The impacts of increasing resistivity and decreasing transmission. The effect of an increase in resistivity, as often observed, can mainly be seen in a series resistance increase and thus in a fill factor decrease. A decrease in transmission, on the other hand, reduces the current of the solar cell or module. On the basis of damp-heat experiments, the effect of a transmission change is not expected to be large.
2. Changes in TCO properties due to chemical reactions between TCO and, for example, the encapsulation material, such as ethylene vinyl acetate (EVA). Similarly to point 1, these effects can be found by changing resistivity and transmission values.
3. Water barrier properties of the TCO itself (e.g. i-ZnO and ITO are reported to function as water barriers [27]).
4. The changes in carrier concentration in both the TCO and the CIGS layer can lead to changes in the Fermi level, which will induce a change in voltage.
5. The possibility of atmospheric species diffusing through the TCO,

thereby allowing the underlying CIGS/buffer layers to react with these atmospheric species, leading to a change in the absorber or buffer properties, which can impact, for example, the voltage.

The use of the more expensive ITO instead of the cost-effective ZnO:Al can be considered. Because of the higher stability of the ITO films, the barrier costs in flexible modules can thus be reduced, which can lead to a module with a lower total cost price.

#### Scribe degradation

The monolithic interconnection scheme of a CIGS module plays an important role in module degradation. Fig. 8 shows a scribe area, where the degradation risks are indicated [28]:

- An increase in absorber conductivity around the P1 scribe, which can decrease the shunt resistance. A similar effect has been reported by Allsop et al. [18], but it was not observed very often.
- A series resistance increase in P2, where a Mo/ZnO:Al contact is responsible for the current transport between the solar cells. Possible reasons are the introduction of an oxide layer at the Mo/ZnO:Al interface, deteriorating the contact, or the increased resistivity of ZnO:Al films. This effect has been observed in model systems, such as in Klaer et al. [29].
- Degradation of P3, due to oxidation

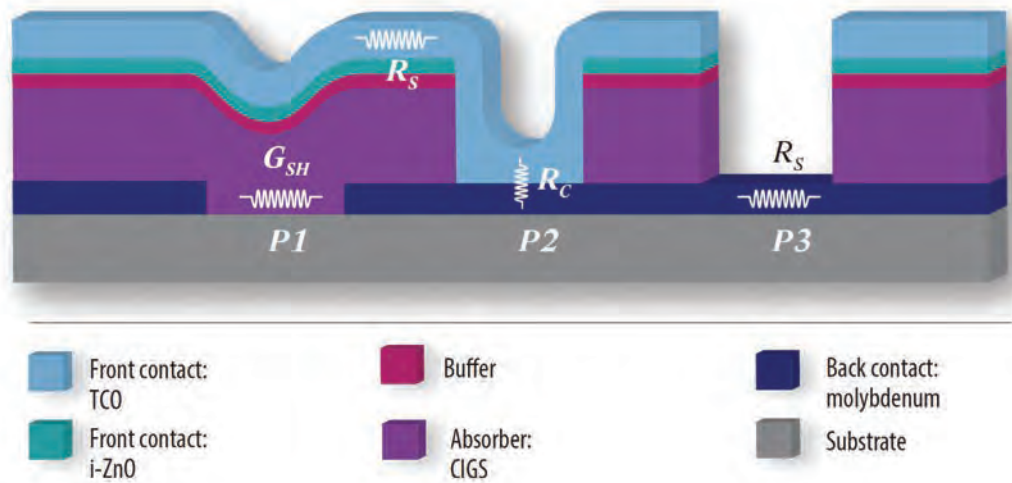


Figure 8. A monolithic interconnection structure for CIGS modules. Functional parts that may degrade and therefore lead to a reduction in conversion efficiency are indicated. (Adapted from Heske et al. [11].)

of molybdenum, for example in locations that have been damaged by the scribing process. This could lead to an increase in series resistance. However, the metal molybdenum has a high conductivity, which means its degradation will only impact module efficiency when the molybdenum layer is almost completely oxidized [6]; this will most likely happen only after harsh exposure.

Furthermore, the increased resistivity of the TCO also has an additional impact on modules in the case where the molybdenum resistivity remains constant: this leads to the creation of a difference in voltage drops at different locations, which can result in local heating in solar cells [30].

## Conclusions and outlook

On the basis of these observations, some practical changes that might lead to more stable solar cells and modules could be implemented. It should be noted that these recommendations are based on the experience of the author with specific CIGS cell fabrication approaches, in combination with literature data; small variations in the composition might lead to other dependencies. The suggested changes are:

- Use molybdenum with a low deposition pressure, especially near the Mo/CIGS interface.
- If possible, keep the selenized-molybdenum film intact in P2 and P3.
- Use ITO films instead of ZnO:Al films.

- Use thicker layers, higher deposition temperatures or doping concentrations, or post-deposition treatments for the ZnO:Al deposition.
- Implement minor changes in, for example, the absorber, which can have a major influence on cell stability.
- Recognize that sodium is often involved in degradation processes, while the role of potassium is still unknown.

**“Future lifetime studies need to focus more on understanding the degradation mechanisms, instead of simple go/no-go judgments being made on the basis of IEC tests.”**

## Future studies

Since moisture ingress is often the reason for degradation, many CIGS-specific degradation problems can be prevented by an adequate water barrier; however, since intrinsically stable CIGS solar cells are preferred, more knowledge is undoubtedly required in this area. In order to expand the current level of knowledge, future lifetime studies need to focus more on understanding the degradation mechanisms, instead of simple go/no-go judgments being

made on the basis of IEC tests.

A better understanding of the degradation can even help to lower the required test loads. Currently, investors might ask for damp-heat tests lasting more than 1,000 hours (IEC test) in order to be certain about the stability of CIGS modules. However, the calculations by Coyle [31] indicate that the current 1,000 hours' damp-heat exposure can simulate between 1.1 and 110 actual years in Miami, depending on the composition of the CIGS solar cells, but also on the nature of the package material. Simply increasing the damp-heat exposure time is therefore only relevant in cases where degradation phenomena with a relatively low acceleration factor are the dominant mechanisms.

To conclude, it is very important to compare accelerated lifetime effects with field test results; this comparison allows the appropriate accelerated tests to be selected. It is therefore of interest (particularly to this author) to always examine modules that have failed in the field and make comparisons with laboratory test results.

## Acknowledgements

The author would first like to acknowledge F. Daume (formerly of Solarion and Leipzig University) for the extensive discussions on the topic of CIGS degradation. Furthermore, for their contribution to the scientific experiments described in this paper, many people are due thanks, especially Z. Vroon (TNO/Solliance), N. Barreau (University of Nantes) and M. Zeman (Delft University). I. Schrauwers (IS design) is acknowledged for the design of Figs. 1, 2, 3 and 8, and F. Ruske (Helmholtz Zentrum Berlin)

for the idea behind Fig. 3. Finally, the author is grateful to F. van den Bruele and A. Kuypers (TNO/Solliance) for proofreading this manuscript.

## References

- [1] Solar Frontier 2015, "Solar Frontier Achieves World Record Thin-Film Solar Cell Efficiency: 22.3%", News Report [http://www.solar-frontier.com/eng/news/2015/C051171.html].
- [2] Jordan, D. & Kurtz, S. 2013, "Photovoltaic degradation rates – An analytical review", *Prog. Photovoltaics Res. Appl.*, Vol. 21, pp. 12–29.
- [3] Theelen, M. 2015, "Degradation of CIGS solar cells", Ph.D. dissertation, Ipskamp Drukkers [www.cigsdegradation.com].
- [4] Theelen, M. & Daume, F. 2016, "Stability of Cu(In,Ga)Se<sub>2</sub> solar cells: A literature review", submitted to *Sol. Energy*.
- [5] Theelen, M. et al. 2014, "Influence of deposition pressure and selenisation on damp heat degradation of the Cu(In,Ga)Se<sub>2</sub> back contact molybdenum", *Surf. Coat. Technol.*, Vol. 252, pp. 157–167.
- [6] Theelen et al. 2016, "Degradation mechanisms of the molybdenum back contact for CIGS solar cells", submitted to *Thin Solid Films*.
- [7] Salomé, P. et al. 2014, "The effect of Mo back contact ageing on Cu(In,Ga)Se<sub>2</sub> thin-film solar cells", *Prog. Photovoltaics Res. Appl.*, Vol. 22, No. 1, pp. 83–89.
- [8] Guillemoles, J. 2002, "The puzzle of Cu(In,Ga)Se<sub>2</sub> (CIGS) solar cells stability", *Thin Solid Films*, *Proc. Thin Film Mater. PV*, Vol. 403–404, pp. 405–409.
- [9] Metzger, W. et al. 2009, "Recombination kinetics and stability in polycrystalline Cu(In,Ga)Se<sub>2</sub> solar cells", *Thin Solid Films*, Vol. 517, pp. 2360–2364.
- [10] Pern, F. et al. 2009, "A study on the humidity susceptibility of thin-film CIGS absorber", *Proc. 34th IEEE PVSC*, Philadelphia, Pennsylvania, USA, pp. 287–292.
- [11] Heske, C. et al. 2002, "Damp heat-induced sulfate formation in Cu(In,Ga)(S,Se)<sub>2</sub>-based thin film solar cells", *Appl. Phys. Lett.*, Vol. 81, pp. 4550–4552.
- [12] Braunger, D. et al. 1998, "Na-related stability issues in highly efficient polycrystalline Cu(In,Ga)Se<sub>2</sub> solar cells", *Proc. 2nd WCPEC*, Vienna, Austria, pp. 511–514.
- [13] Sakurai, K. et al. 2003, "Properties of CuInGaSe<sub>2</sub> solar cells based upon an improved three-stage process", *Thin Solid Films*, Vol. 431–432, pp. 6–10.
- [14] Malmström, J. et al. 2003, "A study of the influence of the Ga content on the long-term stability of Cu(In,Ga)Se<sub>2</sub> thin film solar cells", *Thin Solid Films*, Vol. 431–432, pp. 436–442.
- [15] Naghavi, N. et al. 2010, "Buffer layers and transparent conducting oxides for chalcopyrite Cu(In,Ga)(S,Se)<sub>2</sub> based thin film photovoltaics: present status and current developments", *Prog. Photovoltaics Res. Appl.*, Vol. 18, pp. 411–433.
- [16] Ramanathan, K. et al. 1996, "Effects of heat treatments and window layer processing on the characteristics of CuInGaSe<sub>2</sub> thin film solar cells", *Proc. 25th IEEE PVSC*, Washington DC, USA, pp. 837–840.
- [17] Kushiya, K. et al. 2006, "Improved stability of CIGS-based thin-film PV modules", *Proc. 4th WCPEC*, Waikoloa, Hawaii, USA, pp. 348–351.
- [18] Allsop, N. et al. 2006, "The dry and damp heat stability of chalcopyrite solar cells prepared with an indium sulfide buffer deposited by the spray-ILGAR technique", *Thin Solid Films*, Vol. 511–512, pp. 55–59.
- [19] Theelen, M. et al. 2014, "Physical and chemical degradation behavior of sputtered aluminum doped zinc oxide layers, for Cu(In,Ga)Se<sub>2</sub> solar cells", *Thin Solid Films*, Vol. 550, pp. 530–540.
- [20] Theelen, M. et al. 2014, "Influence of atmospheric species water, oxygen, nitrogen and carbon dioxide on the degradation of aluminum doped zinc oxide layers", *Thin Solid Films*, Vol. 565, pp. 149–154.
- [21] Liu, H. et al. 2010, "Transparent conducting oxides for electrode applications in light emitting and absorbing devices", *Superlattices Microstruct.*, Vol. 48, pp. 458–484.
- [22] Minami, T. et al. 2007, "Effect of thickness on the stability of transparent conducting impurity-doped ZnO thin films in a high humidity environment", *physica status solidi (RRL)*, Vol. 1, No. 1, pp. R31–R33.
- [23] Greiner, D. et al. 2009, "Influence of damp heat on the optical and electrical properties of Al-doped zinc oxide", *Thin Solid Films*, Vol. 517, pp. 2291–2294.
- [24] Owen, J. et al. 2009, "Damp-heat treatment effects on sputtered Al-doped ZnO films", *Proc. 24th EU PVSEC*, Hamburg, Germany, pp. 2774–2778.
- [25] Xu, J. et al. 2014, "Effect of growth temperature and coating cycles on structural, electrical, optical properties and stability of ITO films deposited by magnetron sputtering", *Mater. Sci. Semicon. Proc.*, Vol. 21, pp. 104–110.
- [26] Guillen, C. & Herrero, J. 2006, "Stability of sputtered ITO thin films to the damp-heat test", *Surf. Coat. Technol.*, Vol. 201, pp. 309–312.
- [27] Thompson, C. et al. 2013, "The effects of device geometry and TCO/buffer layers on damp heat accelerated lifetime testing of Cu(In,Ga)Se<sub>2</sub> solar cells", *IEEE J. Photovolt.*, Vol. 3, No. 1, pp. 494–499.
- [28] Wennerberg, J. et al. 2000, "Degradation mechanisms of Cu(In,Ga)Se<sub>2</sub>-based thin film PV modules", *Proc. 16th EU PVSEC*, Glasgow, Scotland, pp. 309–312.
- [29] Klaer, J. et al. 2005, "Damp heat stability of chalcopyrite mini-modules: Evaluation of specific test structures", *Proc. 31st IEEE PVSC*, Lake Buena Vista, Florida, USA, pp. 336–339.
- [30] Kempe, M. et al. 2008, "Stress induced degradation modes in CIGS mini-modules", *Proc. 33rd IEEE PVSC*, San Diego, California, USA, pp. 1–6.
- [31] Coyle, D. 2013, "Life prediction for CIGS solar modules. Part 1: Modelling moisture ingress and degradation", *Prog. Photovoltaics Res. Appl.*, Vol. 21, No. 2, pp. 156–172.

## About the Authors



**Mirjam Theelen** received her M.Sc. in chemistry from Radboud University Nijmegen in the Netherlands in 2007, and her Ph.D. from Delft University of Technology in 2015 for her research work on stability testing of CIGS solar cells. Since 2007 she has been a research scientist at TNO/Solliance, where her main research areas are deposition and reliability of CIGS solar cells.

## Enquiries

TNO/Solliance  
High Tech Campus 21  
5656 AE Eindhoven  
The Netherlands

Tel: +31 6 46847434  
Email: Mirjam.theelen@tno.nl  
Website: www.solliance.eu

# PV Modules

Page 87  
News

Page 90  
Cell-to-module power loss/  
gain analysis of silicon wafer-  
based PV modules

Jai Prakash Singh, Yong Sheng Khoo,  
Jing Chai, Zhe Liu & Yan Wang, Solar  
Energy Research Institute of Singapore  
(SERIS), National University of  
Singapore (NUS), Singapore

Page 99  
Double-glass PV modules  
with silicone encapsulation

Shencun Wang<sup>1</sup>, Xiang Sun<sup>1</sup>, Yujian  
Wu<sup>2</sup>, Yanxia Huang<sup>2</sup>, Nick Shephard<sup>3</sup> &  
Guy Beaucarne<sup>4</sup>

<sup>1</sup>BYD, Shenzhen, Guangdong, China;  
<sup>2</sup>Dow Corning (China) Holding Co.  
Ltd., Shanghai, China; <sup>3</sup>Dow Corning  
Corporation, Midland, Michigan, USA;  
<sup>4</sup>Dow Corning Europe S.A., Seneffe,  
Belgium



87



99



## New EU trade duties start on certain PV firms in Taiwan and Malaysia

Punitive trade duties will now be applied to Chinese cells and modules shipped through Malaysia and Taiwan.

The new measures came into force on 12 February, following their publication in the official journal of the EU.

The commission decided, following an investigation, to impose anti-dumping and anti-subsidy duties of 53.4% and 11.5% to Malaysian and Taiwanese firms that were judged to be enabling Chinese manufactured products to enter the EU with an alternate origin.

National customs and revenue organisations can pursue backdated duties from May 2015 onwards.

Some estimates suggest that as much as 16% of all modules imported into Europe since that date could be impacted leaving a bill running into millions of euros.

Member states are taking differing approaches to recouping the monies with some only willing to invoice the first importer and others more aggressively pursuing the duties right along the value chain including the end customer.

Genuine manufacturers based in Malaysia and Taiwan will not be affected.



Credit: Hanwha Q CELLS

Hanwha Q CELLS was one of the companies exempted from the new rules.

News

## Trade disputes

### UK and Germany at loggerheads over China solar import deal

The UK and Germany appear to be increasingly at odds over the future of the solar price undertaking between the EU and China.

As the UK government published fresh evidence of the costs the minimum important price (MIP) is adding on to solar installations, the German government weighed in, attacking UK proposals to suspend the MIP as "incomprehensible".

The UK's energy secretary Amber Rudd

confirmed that DECC has collaborated with "lead-ing engineering consultants" to estimate the price differential caused by the pricing.

DECC estimates "an indicative 10 to 14% example for a drop in prices" if the MIP were re-pealed.

But the UK's position puts it at odds with that of the German government, which is known to be a supporter of the solar trade tariffs and MIP.

### EU withdraws Trina from solar panel MIP

The European Commission has officially withdrawn Chinese solar panel manufacturer Trina Solar and related companies from the EU-China price undertaking.

The Minimum Import Price (MIP) agreement allows Chinese firms to avoid anti-dumping duties in the EU in return for agreeing to annual import quotas and selling above a pre-determined price.

However, any exporting producer may voluntarily withdraw its undertaking at any time during its application. Thus, Trina announced plans to walk away from the undertaking in December last year.

At the time, Trina released a statement saying that the current interpretation of the undertaking "unfairly" limits the company's growth potential in the EU.

Trina will now sell into Europe from non-Chinese manufacturing facilities incurring no additional trade duties.

### Australia's solar anti-dumping investigations resurrected

The anti-dumping saga in Australia has been reignited after the Anti-Dumping Commission on 8 January overturned

last year's decision to terminate the investigation.

The inquiry began over alleged dumping of various crystalline silicon PV modules exported from China to Australia, but was ended on 6 October 2015 because, even though evidence of dumping was found, it was deemed as having a negligible effect on Australian industry.

This was partly due to the fact that Australia-based manufacturer Tindo Solar, which first lodged the complaint, manufactures AC modules, which are not in direct competition with the largely DC modules imported by Chinese suppliers.

At the time the Australian Solar Council said it welcomed this "common sense conclusion" to the case.

Nevertheless Tindo Solar asked for a review of the decision on 5 November 2015.

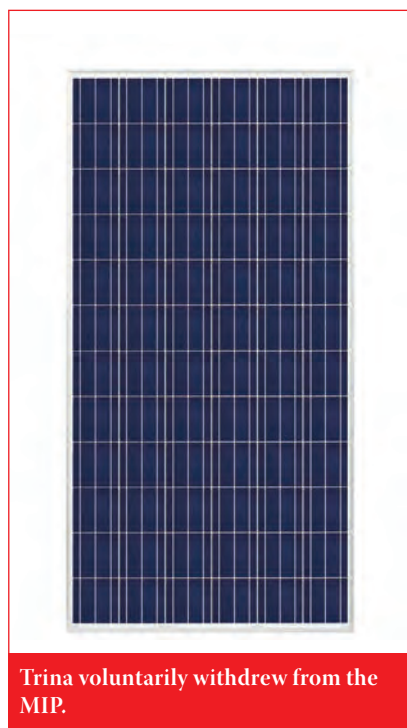
After the publication of a new Statement of Essential Facts as a result of this review, the commission has now decided to reopen the investigation.

### Top US official casts doubt on reports of imminent India WTO solar deal

Reports that the US and India are close to reaching an agreement in the trade dispute over India's local content rules for solar equipment were refuted by a top US trade official.

US Trade Representative Michael Froman said: "We're still engaged in conversations with them. It's too early to tell whether we're going to have an agreement or not."

India had also made a last minute proposal to shift its Domestic Content Requirement (DCR) rules for using domestically manufactured solar



Credit: Trina Solar

Trina voluntarily withdrew from the MIP.

equipment in certain Indian projects away from the private sector and into the public sector.

Froman declined to comment on the WTO's intentions in the case. However, he confirmed that it was a US decision to delay the announcements – adding: "It's at our discretion whether the WTO extends or not, based on how the conversations are going."

## The Market

### News

### Top-10 solar module manufacturers in 2015

The top five ranked PV module manufacturers in 2015 form the backbone of the key six-member 'Silicon Module Super League' (SMSL).

The Top-10 PV module manufacturers list for 2015 was based on actual module shipments through the first nine months of last year and guidance figures as well as analysis of over 45 leading manufacturers' expected shipments for the full year.

Yingli Green fell several ranking positions from initial shipment guidance at the beginning of the year and went from being ranked second in 2014 to seventh in 2015.

Separating the SMSL members from the top six ranking positions was CdTe thin-film leader, First Solar, which had

built shipment momentum through the year and later revised shipment guidance upwards to 2.8GW to 2.9GW. First Solar therefore climbed two ranking positions from 2014 and stopped its slow rankings fall over the last few years.

Competition for ranking positions in the next 10 lower positions has intensified over the last 12 months with a growing cluster of manufacturers with shipments in the 1GW region. The top-10 PV module manufacturers ranking list for 2015:

1. Trina Solar
2. Canadian Solar
3. JinkoSolar
4. JA Solar
5. Hanwha Q CELLS
6. First Solar
7. Yingli Green
8. SFCE
9. ReneSola
10. SunPower Corp

### NREL finalises new quality standard for PV module manufacturing

Researchers at the US National Renewable Energy Laboratory (NREL) in the US have finalised the development of a new international quality standard for PV module manufacturing.

The standard is intended to increase levels of confidence among investors, utilities and consumers in the safety and reliability of PV panels.

It marks the culmination of five years of work instigated under the PV Quality Assurance Task Force (PVQAT), spearheaded by NREL.

Module reliability is not defined or covered by the current IEC standards, so although modules may receive certifications under certain test conditions, those do not guarantee their reliability. The PVQAT set out to draw up new guidelines to deal with influences on a module such as raw materials and components, process control, testing regimes and staff training.

Once formally adopted by the IEC, the new standards will become the standard basis for audits of PV module manufacturers.

### PV Cycle achieves record 96% recycle rate for silicon-based PV modules

PV Cycle, a not-for-profit compliance and waste management programme for solar PV technology in Europe, has achieved a record recycling rate of 96% for silicon-based PV modules.

Previous recycling records for silicon-based modules stood at around 90%. Now one of PV Cycle's Europe-based recycling partners for silicon-PV modules is using a new process that combines mechanical and thermal treatment to recycle silicon flakes as well as recycling a combination of EVA laminate, silicon-based semiconductors and metals.

Previously there had not been viable solutions for the further recycling of silicon flakes. The silicon flakes could be used for the production of new products or materials, but could not be further recycled in an environmentally and economically sound manner, said a PV Cycle spokeswoman.

### PV cost decreases to ensure strong demand in 2016 and beyond

A projected 15% decrease in the installed cost of PV over the next two years will continue to drive demand worldwide, according to Taiwan-based EnergyTrend.

There have been significant ongoing decreases in PV system costs in the past year, a trend that is set to continue and to spur growing demand for solar.

Policies in major markets including the US, China and India will cause a gradual decline in module prices in 2016, in parallel with price declines for other components, such as inverters and other related consumables.

On modules, EnergyTrend highlights the incremental improvements in conversion efficiency rates of PV cells as a key driver and also the increasing power of modules, with mainstream multi-Si products



Credit: PV Cycle

Photo credit: © PV CYCLE

PV Cycle has achieved a 96% recycling rate in silicon modules .

expected to achieve a power output of 265W in the second half of 2016 and their mono-Si counterparts reaching 275-280W.

## Companies

### Chinese state-owned asset-management firm interested in Yingli's debt restructuring - reports

China Cinda Asset Management, a Chinese state-owned asset management company is reportedly interested in participating in the debt restructuring of struggling module manufacturer Yingli Green Energy Holding.

Yingli Green has not expanded capacity for several years due to its large debts and overall financial position, which led to curtailment of module production and a partial shift to OEM module sales to boost liquidity issues in the second half of 2015.

The company has fallen several ranking positions for global solar module manufacturers, having been ranked second in 2014 and tumbling to seventh in 2015.

### Spire to restructure and morph into turnkey solutions

PV module assembly equipment specialist

Spire Corporation will focus on the turnkey PV manufacturing segment after completing the sale of its sun simulator business to Eternal Sun.

Rodger W. LaFavre, president and CEO of Spire Corporation said: "Spire is able to take steps to restructure the company to concentrate its efforts to pursue opportunities in its solar turnkey business. The company will concentrate on improving its relationship with its vendors, and will re-brand its image to reflect its new focus towards solar manufacturing lines and away from the simulator business."

The company had previously been involved primarily in the turnkey PV module assembly sector along with automation expertise.

Spire plans to offer turnkey solutions across wafer, cell and module segments.

## Deals

### Horad to supply Xinneng Solar with 500MW automated turnkey module line

China-based module assembly automation specialist Suzhou Horad New Energy Equipment Co (Horad) has secured a new 500MW automated turnkey module line order from Xinneng Solar.

Xinneng Solar was said to be located in

Zhejiang Province, China. Further details were not disclosed.

Horad also recently secured a 200MW turnkey module assembly line order with major Tai-wanese cell producer, Motech Industries.

### Valoe secures €15.8 million automated back contact module assembly line order from Ethiopia

PV module assembly equipment supplier Valoe Corporation has secured its long-awaited first order for an automated turnkey back contact module assembly line from an unidentified customer in Ethiopia for €15.8 million.

Valoe, formerly Cencorp had developed conductive back sheet (CBS) technology and processes to enable lower-cost back contact solar cell modules, reducing cell to string losses and providing higher module conversion efficiencies.

The company said that the main financier for the production line was the Development Bank of Ethiopia, which is contributing €9.5 million of the sales price.

However, the rest of the sales price will be held in shares of the customer company by Valoe, equating to it having a 30% shareholding, making it a manufacturing partner.

The turnkey assembly line will be delivered sometime this year.

## News



Credit: Spire

Spire has sold its sun simulator business to Eternal Sun.

# Cell-to-module power loss/gain analysis of silicon wafer-based PV modules

Jai Prakash Singh, Yong Sheng Khoo, Jing Chai, Zhe Liu & Yan Wang, Solar Energy Research Institute of Singapore (SERIS), National University of Singapore (NUS), Singapore

## ABSTRACT

We are always hearing about champion cells demonstrating efficiencies of 24% or higher, yet only 20 or 21% can be obtained at the module level. Where are all these hard-earned electrons going? Moreover, why should every photon and electron be counted? Cell efficiency is important, but it is *module* efficiency that defines the bottom line of every solar project. This paper will highlight the different loss mechanisms in a module, and how they can be quantified. Once it is known where photons and electrons are lost, it is possible to develop strategies to avoid this happening. In-depth loss-analysis methods for studying various loss mechanisms in a PV module have been developed at SERIS. Using these methods, in combination with various characterization tools/techniques, such as external quantum efficiency (EQE) line scan, electroluminescence imaging, and IV testers, a detailed loss/gain analysis of the cell-to-module process has been carried out and is presented in this paper. The loss/gain analysis is demonstrated using two dominant cell technologies: p-type multicrystalline and n-type monocrystalline cells.

## Introduction

In conventional silicon wafer-based PV technology, solar cells are connected in series and encapsulated into PV modules. The interconnection increases the power and voltage, while the encapsulation provides environmental protection for the solar cells. The main purpose of a PV module is to protect the cells from the harsh environment throughout an expected lifetime of 20 to 25 years.

Although the modularization offers protection to the cells, it also induces loss mechanisms that affect module power and energy yield. When a solar cell is integrated into a module, its working environment is altered (e.g. the glass and encapsulant layers introduce additional optical parasitic absorption), which affects its optical performance. Furthermore, the interconnection ribbons introduce additional resistive losses that affect the electrical performance. Because of the various loss mechanisms associated with the modularization process, the module power is generally less than the total of the power of all the individual cells used to fabricate the module. This difference between total cell power and module power is termed *cell-to-module (CTM) power loss*. The losses in the CTM process can be broadly separated into optical, resistive and mismatch components.

An accurate characterization of the CTM power loss (or gain) allows a better evaluation of new designs and

materials in PV modules. The losses in the CTM process for wafer-based PV modules have been widely investigated by various researchers and module manufacturers [1–3]. To calculate the losses, solar cells and modules are typically measured using different *I–V* measurement systems, which consequently introduces uncertainty in the measurements [4].

“An accurate characterization of the CTM power loss (or gain) allows a better evaluation of new designs and materials in PV modules.”

To analyse the loss/gain in the CTM process more precisely, various measurement-based techniques are presented in this paper. These methodologies are easy to use and minimize the uncertainty in the CTM-loss/gain calculations. A quantitative analysis of the CTM loss/gain in silicon wafer-based PV modules is experimentally demonstrated.

## Optical loss/gain in PV modules

For the light-harvesting analysis, a glass/backsheets PV module can be broadly divided into two parts: the active module area (i.e. containing the solar cells) and the backsheets area (i.e. without the solar cells).

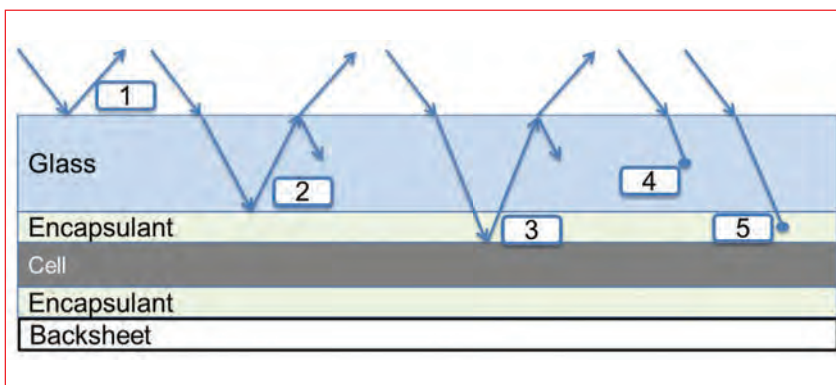


Figure 1. Optical losses in a silicon wafer-based PV module (active area). (Reflection: 1 = air–glass, 2 = glass–encapsulant, 3 = encapsulant–cell. Absorption: 4 = glass, 5 = encapsulant.)

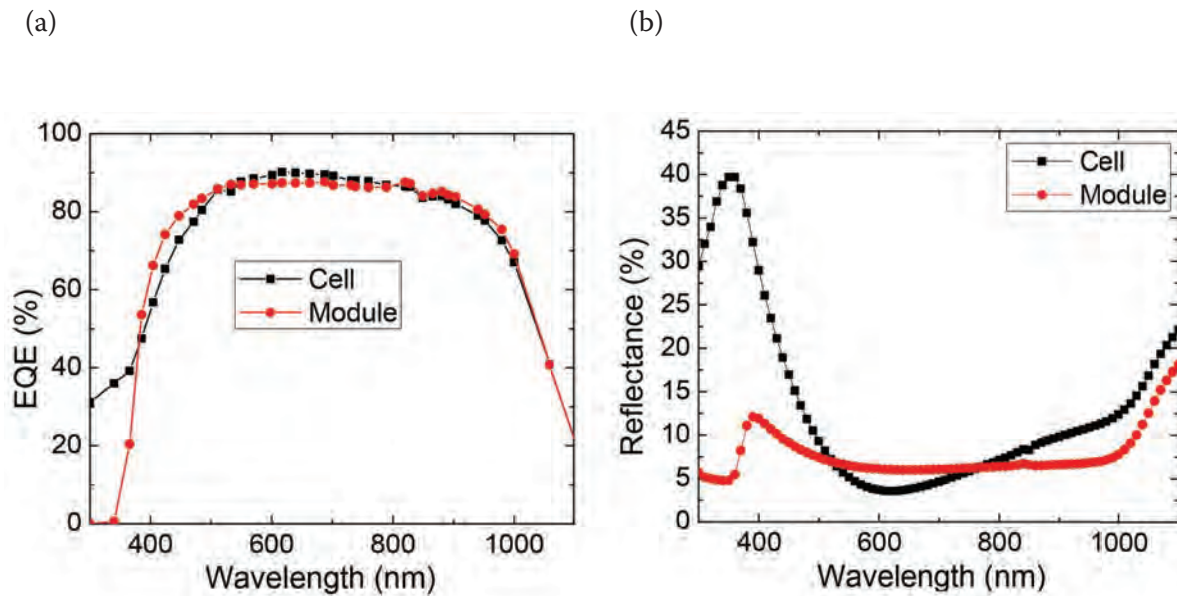


Figure 2. (a) Measured EQE of the cell and of the module with conventional EVA. (b) Corresponding reflectance measurements.

PV  
Modules

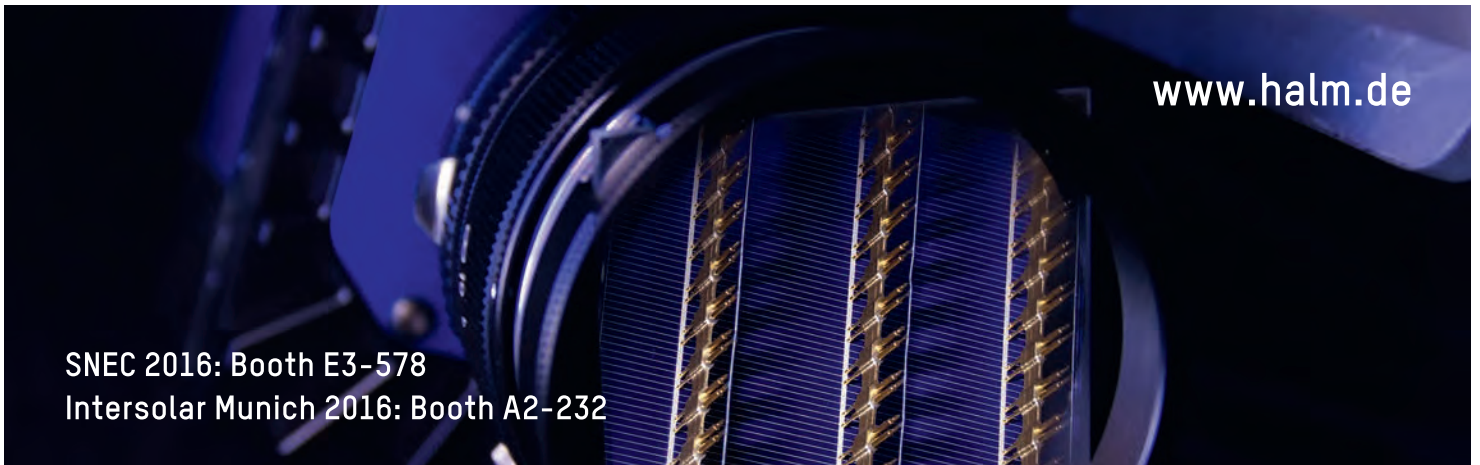
**Power loss/gain for the active module area**

Optical losses in the active module area occur because of the hemispherical reflectance at

various interfaces and the parasitic absorptance of the encapsulation layers (glass, encapsulant) used to fabricate the module [5–7]. Fig. 1 shows the various optical loss mechanisms in a

wafer-based PV module.

Besides the optical losses, there are also optical gains as a result of direct and indirect optical coupling. *Direct optical coupling* (reduced



SNEC 2016: Booth E3-578  
Intersolar Munich 2016: Booth A2-232

**cetisPV  
Product  
line**

High precision Class A+ A+ A+  
measurement systems  
for PV-cells and modules

**Step into the PV future:**

- High throughput manufacturing  
> 3600 cells/h and > 200 modules/h
- Universal solutions for  
highest efficiency cells and modules
- Highest precision in temperature coefficients  
and energy rating of PV modules
- Advanced inline quality and process control by  
EL-inspection and image analysis



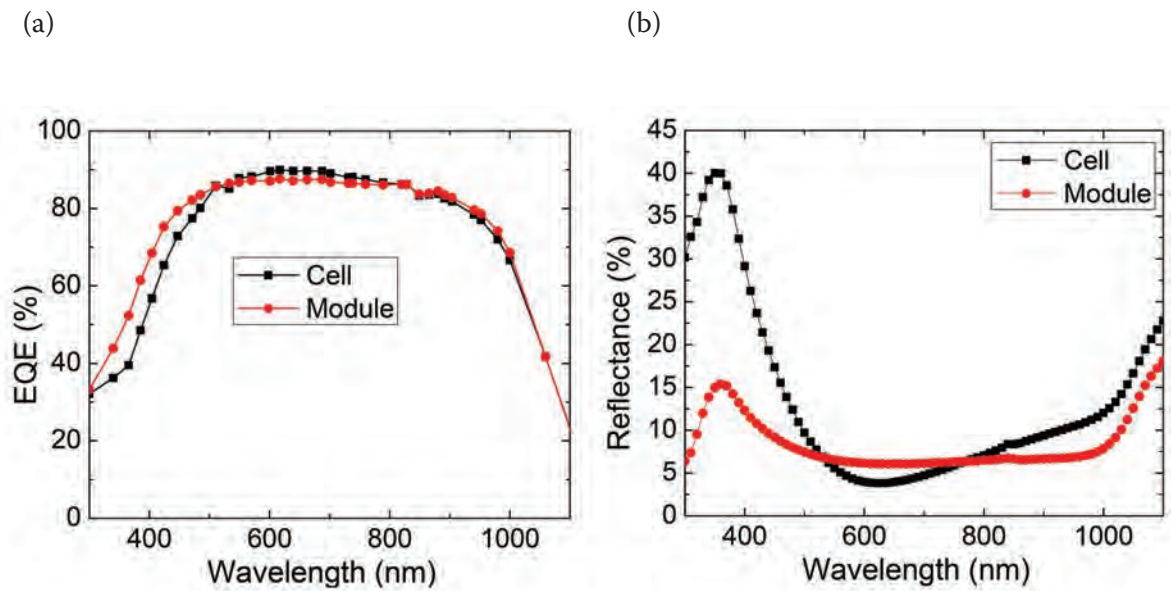


Figure 3. (a) Measured EQE of the cell and of the module with super-clear EVA. (b) Corresponding reflectance measurements.

reflectance) occurs because of the various encapsulation layers with monotonically increasing refractive indices [8–10]. *Indirect optical coupling* (reduced reflectance) occurs because of the total internal reflectance at the glass–air interface (from the contacting fingers and busbars), which redirects the light back onto the solar cell.

At SERIS, a method has been devised to experimentally quantify the optical loss resulting from parasitic absorption in the encapsulant materials (glass, EVA etc.), and the optical gain due to optical coupling [1]. The method requires the fabrication of single-cell mini-modules with a glass–glass configuration using processes and materials identical to those employed for large full-size modules. The glass–glass configuration can eliminate any edge effect caused by the backsheet around the cell area. The reflectance and the external quantum efficiency (EQE) of the bare solar cells and the mini-modules are measured using a UV-VIS and a full-area illumination EQE measurement system respectively.

**Example: Comparison of different EVAs**

To compare the parasitic absorptance losses in different EVAs, mini-modules with two different types of EVA were fabricated. The EQE and reflectance measurements were carried out on the solar cells before and after encapsulation, for two types of EVA, as shown in Figs. 2 and 3. With the

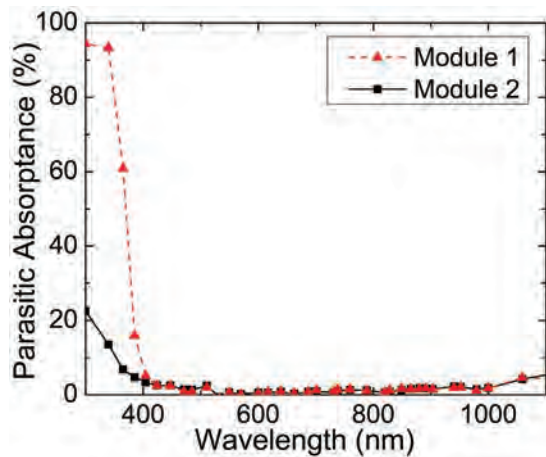


Figure 4. Parasitic absorptance for modules encapsulated with conventional EVA (module 1) and with super-clear EVA (module 2).

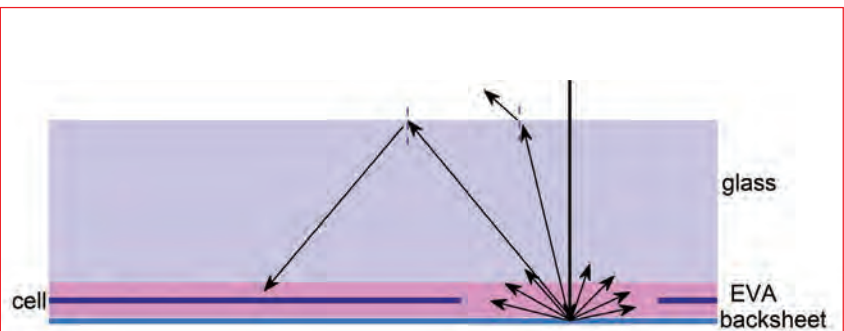


Figure 5. Schematic (not to scale) showing various light paths in a glass/backsheet PV module. Light incident on the cell-gap area of the backsheet is randomly scattered.

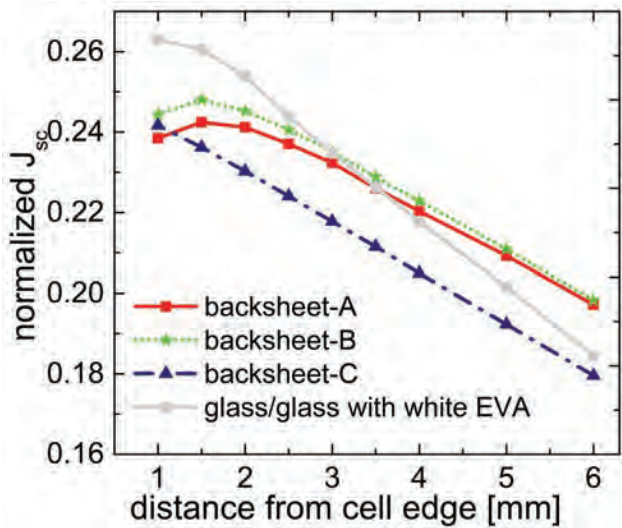


Figure 6. Normalized  $J_{sc}$  scans of mini-modules with different backsheets/EVA.

measurements taken from the bare cells and mini-modules, the parasitic absorptance  $A_{para}$  can be calculated [1] as:

$$A_{para} = 1 - R_{mod} - (1 - R_{cell}) \frac{EQE_{cell,mod}}{EQE_{cell}} \quad (1)$$

where  $R_{cell}$  and  $EQE_{cell}$  are the reflectance and EQE measured for the bare cell, while  $R_{mod}$  and  $EQE_{cell,mod}$  are the measurements for the mini-module. The parasitic absorptance for the two modules with different EVAs is shown in Fig. 4.

The loss/gain in short-circuit current density ( $J_{sc}$ ) can be calculated using

the reflectance, parasitic absorptance data, and AM1.5G photon flux, and is summarized in Table 1. From this table it can be seen that after encapsulation, the cells encapsulated with conventional EVA lose an average of 0.39% of their  $J_{sc}$ , whereas the cells encapsulated with the super-clear EVA gain an average of 0.27% of their  $J_{sc}$ . The reason for this is that the modules encapsulated with super-clear EVA suffer less current loss due to parasitic absorption.

#### Power gain from the backsheet in the cell-gap area

In a conventional glass/backsheet module, the power gain is mainly due to the backsheet static concentration effect. The light incident onto the gap between the cells in a glass/backsheet module is scattered back at different angles. A significant proportion of this light can be entirely internally reflected at the glass-air interface and redirected onto the cells, thus increasing the module current. Fig. 5 illustrates this backsheet static concentration effect in a module. The gain in module current due to the backsheet is mainly influenced by the geometry of the backsheet area (cell-gap region), and by the backsheet properties (reflective and angular backscattering).

PV  
Modules

# LEDs COPY THE SUN

To measure PV cell efficiency, you must copy the sun — flawlessly. Repeatedly. Rapidly. The SINUS-220 LED solar simulator from WAVELABS gives you faster and more accurate efficiency measurements — by using 21 different colors of LEDs instead of a xenon lamp. The more accurate your measurements, the higher you can rate your cells. That boosts your bottom line. Shorten production line cycle times and stop losing money to measurement tolerances — contact WAVELABS today and copy the sun. [www.wavelabs.de](http://www.wavelabs.de)

SNEC 2016  
Come visit us  
at JSun's booth  
#E3-550

 WAVELABS

WAVELABS is proud partner of



To quantify the current contribution due to the backsheet, an EQE line scan is performed on mini-modules (glass/backsheet). In this approach, EQE measurements are taken at several points (spaced at 0.5mm intervals) on the backsheet area, near the cell edge, using a small-area illumination source. The  $J_{sc}$  at each illumination point is then calculated from these EQE measurements and normalized with respect to the mini-module  $J_{sc}$  (measured on the cell area of the mini-module). An example of a plot of the normalized  $J_{sc}$  as a function of the distance of the illumination spot from the cell edge is shown in Fig. 6. The advantage of EQE line scan measurements is that the current gain for a module with a particular cell gap can be calculated directly, by integrating the normalized  $J_{sc}$  results.

**Example: Comparison of different backsheets and white EVA**

To evaluate the optical performance and associated current gain, three different types of backsheet and white EVA (glass/glass configuration) were compared. Mini-modules were fabricated using

the different backsheets/EVA, and EQE measurements performed on these mini-modules. Fig. 6 shows the normalized  $J_{sc}$  plots for four different samples: for a module with a cell gap of 3mm and a string gap of 5mm, the current gain is calculated to be 2.14% (backsheet A), 2.20% (backsheet B), 2.08% (backsheet C) and 2.38% (white EVA).

**Novel approach to quantifying light harvesting from the inactive area of a PV module**

Besides EQE and spectrophotometry to quantify the optical properties of PV modules, SERIS has developed a novel method to quantify the light harvesting from the inactive area of a PV module using luminescence imaging [11]. Luminescence imaging, including electroluminescence (EL) and photoluminescence (PL), is a versatile technique for spatially resolved analysis of the optical and electrical properties of solar cells and modules. At SERIS, luminescence imaging has been demonstrated to be useful for spatially

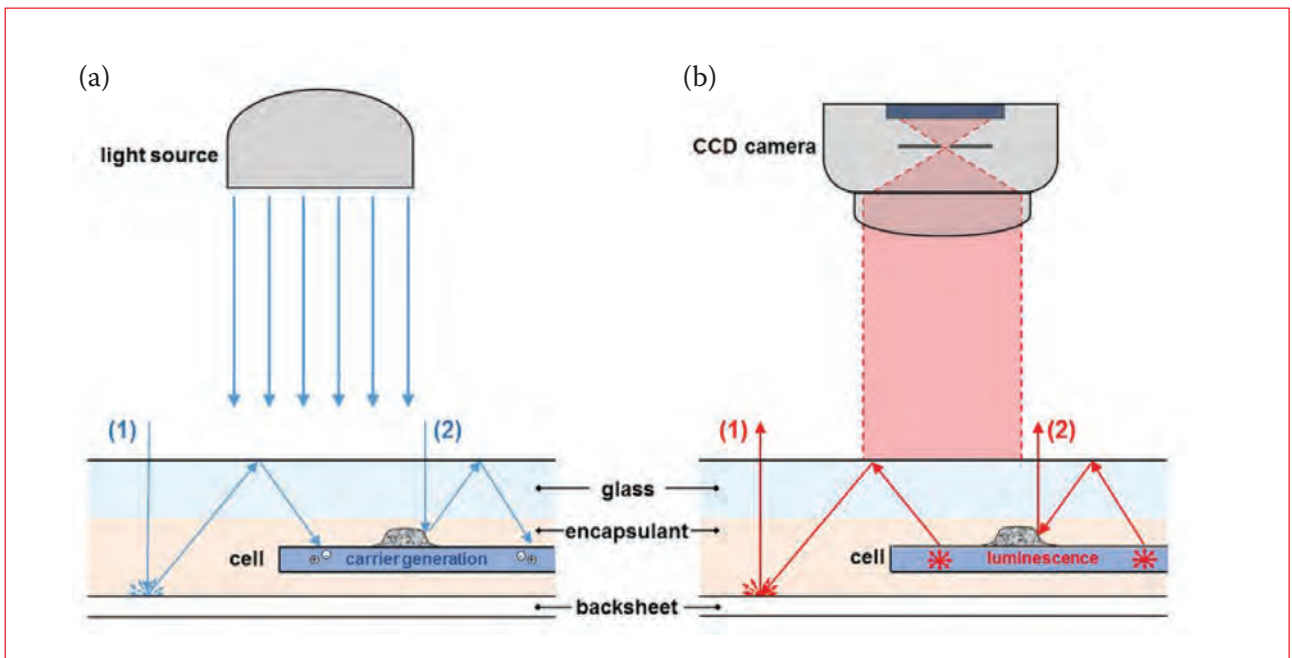
resolved optical characterization. This technique is used to access lateral variations of light harvesting in PV modules made of crystalline Si wafer solar cells. By exploiting the reciprocity theorem relating luminescence emission to EQE, a relative EQE map is extracted from a luminescence image of a PV module (see Fig. 7). In this way, the light-harvesting efficiency at the different inactive areas can be directly quantified.

**Example: Comparison of different backsheets and light-redirecting film**

To compare different backsheets and light-redirecting film using SERIS' new approach, several mini-modules were fabricated using different backsheets with and without light-redirecting film. Fig. 8(a) shows that for the mini-module with a white backsheet, more than 20% of the photons impinging on the backsheet near the cell edges are harvested. For the mini-module with the scattering tape, it can be seen that 45% of the photons impinging on the tape can be harvested. The scattering tape has the potential to be used in high-efficiency PV modules, as it is capable of harvesting

Module structure	Cell		Module			
	$J_{sc,R_{cell}}$ [mA/cm <sup>2</sup> ]	$J_{sc,cell}$ [mA/cm <sup>2</sup> ]	$J_{sc,R_{mod}}$ [mA/cm <sup>2</sup> ]	$J_{sc,A_{para,mod}}$ [mA/cm <sup>2</sup> ]	$J_{sc,mod}$ [mA/cm <sup>2</sup> ]	$\Delta J_{sc}$ [%]
1 Glass/Conventional EVA/Tedlar	3.46	33.60	2.68	0.905	33.47	-0.39
2 Glass/Super-clear EVA/Tedlar	3.44	33.50	2.72	0.636	33.59	0.27

**Table 1. Short-circuit current density and losses in short-circuit current density for modules with different types of EVA (AM1.5G spectrum).**



**Figure 7. Schematic (not to scale) of the reciprocity relationship of (a) EQE measurement and (b) luminescence imaging. The solid lines with arrows labelled as paths 1 and 2 indicate the paths of the incident photons that are harvested by the cell, as well as the reverse paths of the emitted photons that are detected by the camera. Path 1 shows light harvesting from the backsheet area, while path 2 shows light harvesting from a metal finger.**



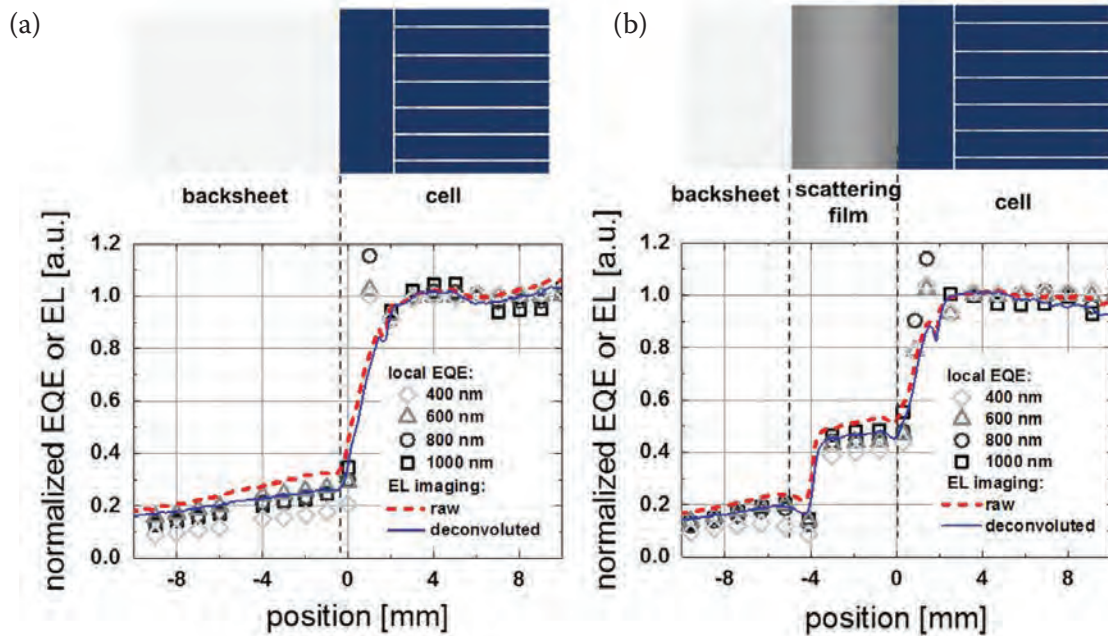


Figure 8. Line scan of the EL signal and local EQE near the cell edge of (a) a standard glass/backsheet mini-module, and (b) a glass/backsheet mini-module with additional scattering tape near the cell edge. Both EL and EQE data were normalized by the respective signals of the cell area. The EQE line scans are shown for 400, 600, 800 and 1000nm wavelengths.

PV  
Modules

more than twice the quantity of photons compared with the white backsheet. The light-harvesting efficiencies calculated using EL can then be translated to the relative gain in module current for a specific cell and string gap.

### Power loss due to cell mismatch

Mismatch losses occur because of the difference in maximum power point currents ( $I_{mp}$ ) of the individual series-connected solar cells [12]. If there

is a difference in the  $I_{mp}$  of the cells, then the cells connected in series do not perform simultaneously at their individual maximum power points; this results in a total output power that is less than the sum of the maximum

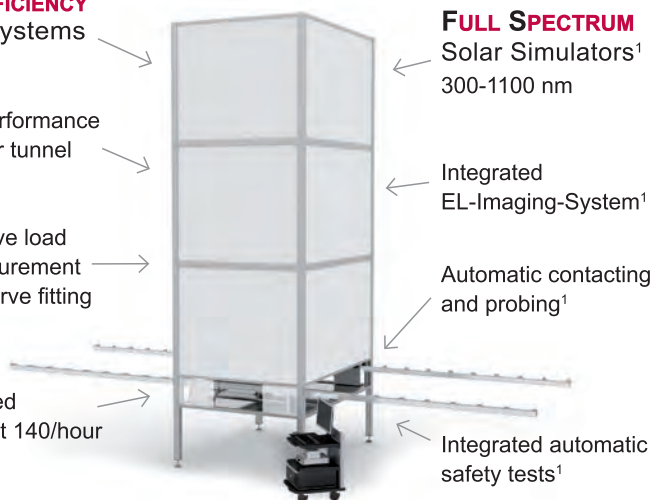
# BERGER Lichttechnik

## HIGH EFFICIENCY Tester Systems

A\*A\*A\* performance  
in tower or tunnel

Full passive load  
and measurement  
without curve fitting

High Speed  
throughput 140/hour



FULL SPECTRUM  
Solar Simulators<sup>1</sup>  
300-1100 nm

Integrated  
EL-Imaging-System<sup>1</sup>

Automatic contacting  
and probing<sup>1</sup>

Integrated automatic  
safety tests<sup>1</sup>

BERGER Lichttechnik A\*A\*A\* module testers measure all types of modules from high efficiency silicon solar cells to thin film with accuracy and repeatability in your facility at the rate of up to 140 modules an hour.

To see how we can help you test your modules faster and more accurately contact us:  
[info@bergerlichttechnik.de](mailto:info@bergerlichttechnik.de)

<sup>1</sup> optional feature

GERMANY  
BERGER Lichttechnik GmbH & Co. KG  
Wolfratshauer Str. 150  
D-82049 Pullach - Germany  
Phone +49 (0)89 793 55 266  
Fax +49 (0)89 793 55 265  
[www.bergerlichttechnik.de](http://www.bergerlichttechnik.de)

CHINA  
德国贝格光科技有限公司上海代表处  
上海市黄浦区蒙自路169号智造局2号楼206室  
邮编 200023  
Phone +86-21-6888-0306  
Fax +86-21-3390-8211  
Mobile +86-138-1655-9892

USA  
BERGER Lichttechnik  
1 West Exchange Street  
Unit 2704  
Providence, Rhode Island 02903, USA  
Phone +1 (401) 351 2222

TAIWAN  
BERGER Lichttechnik  
No.189, Sec. 1, Jhongsing Rd.,  
Wugu Dist., New Taipei City 248  
Taiwan (R.O.C.)  
Phone +886 928-854-669

**SNEC 2016**  
Hall E3  
Booth E3-388

powers of individual cells [3]. PV module manufacturers deal with the mismatch by measuring and binning the solar cells prior to module fabrication [13].

To calculate the mismatch loss in a PV module, the individual cell's maximum power points and the maximum power point of a series interconnection of these cells must be known. Since in a finished module it is not possible to measure the operating point without the inclusion of optical and resistive effects, a combination of curve-fitting and circuit-simulation tools can be used to calculate the mismatch loss. The inputs to the simulation are the  $I-V$  curves of the individual solar cells, measured under standard test conditions (STC). Using curve-fitting and standard circuit-simulation software, such as LTSpice, the module  $I-V$  characteristics are determined on the assumption that the interconnection of the solar cells is ideal (i.e. there are no resistive losses due to cell interconnection). In this way, the simulated module  $I-V$  curve will provide the maximum power that accounts for mismatch losses only. The mismatch loss  $P_{\text{mis}}$  can be calculated using:

$$P_{\text{mis}} = \sum_{i=1}^n P_{\text{cell}}^i - P_{\text{simu}} \quad (2)$$

where  $P_{\text{cell}}^i$  and  $P_{\text{simu}}$  are the individual solar cell power and simulated module power respectively.

The mismatch loss was determined for the 60-cell modules incorporating two types of solar cell, namely n-type mono and p-type multi. The loss was calculated to be 0.14% for the n-type mono cells and 0.20% for the p-type multi cells.

### Power loss due to resistive components

The resistive loss in a wafer-based PV module arises because of 1) the power losses in the various components used to interconnect the solar cells, and 2) the leakage currents at various points in the module. The main resistive components include the soldering ribbons, the bus ribbons, the contact resistance between the cell busbar and the soldering ribbons, the junction box and the cables; these are illustrated in Fig. 9, along with their relative contributions in a commercial 60-cell PV module. Resistive losses are a major concern for modules incorporating high-efficiency cells, particularly cells with improved current response [14].

To quantify the resistive loss in a 60-cell PV module,  $I-V$  measurements of individual cells are taken prior to module fabrication; the  $I-V$  characteristics of the finished module are then measured

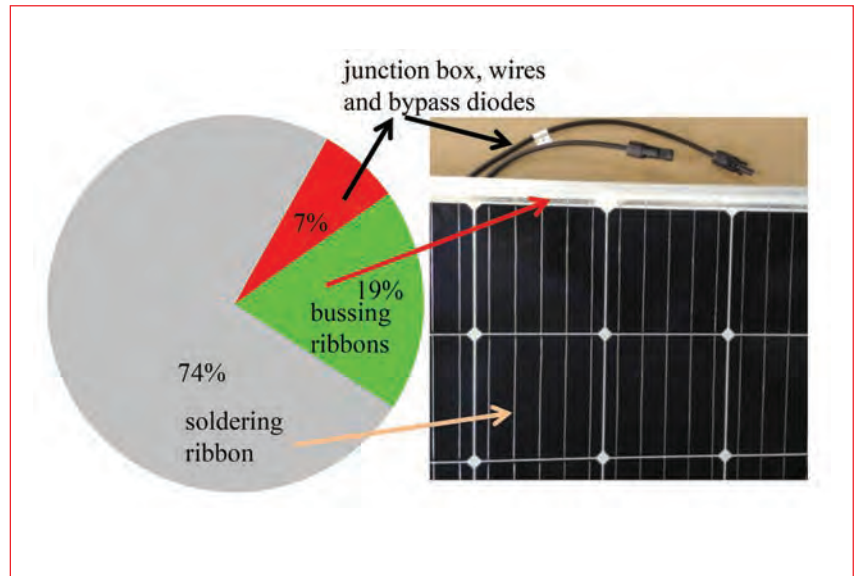


Figure 9. Additional resistive loss components in a PV module (over and above the solar cell series resistance).

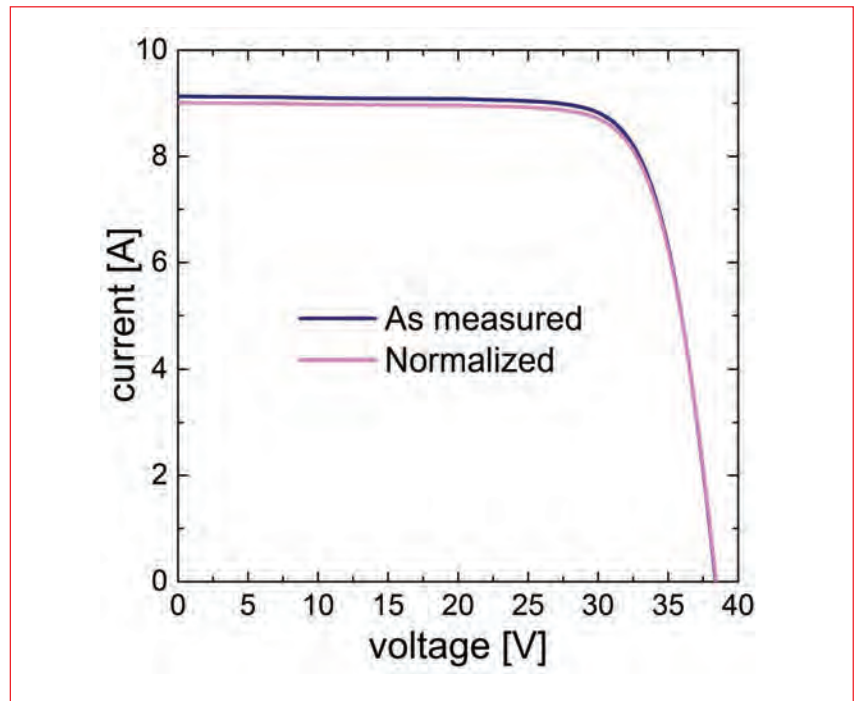


Figure 10. Module  $I-V$  curves: as-measured and normalized to solar cell measurements.

under STC. Because of the difference in cell and module measurement systems and their calibration standards, a certain amount of uncertainty is introduced in the measurements. To eliminate this uncertainty, the module  $I-V$  measurements are normalized with respect to the cell  $I-V$  measurements, or vice versa.

“Resistive losses are a major concern for modules incorporating high-efficiency cells.”

In a module with solar cells connected in series, the short-circuit current of the module will be equal to the minimum of the short-circuit currents among the group of cells, corrected for the optical loss/gain. Similarly, the module open-circuit voltage will be equal to the sum of the open-circuit voltages of all the cells, provided that no cells are damaged as a result of the modularization process. Using the relative optical gain/loss  $P_{\text{opt}}$  calculated in the previous section, the normalized short-circuit current  $I_{\text{sc.mod}}^{\text{cal}}$  and the normalized open-circuit voltage  $V_{\text{oc.mod}}^{\text{cal}}$  of the module with respect to the cell measurements are given by:

$$I_{sc,mod}^{cal} = (1 - P_{opt}) \min_{i=1} (I_{sc,cell}^i)$$

$$V_{oc,mod}^{cal} = \sum_{i=1}^n V_{oc,cell}^i \quad (3)$$

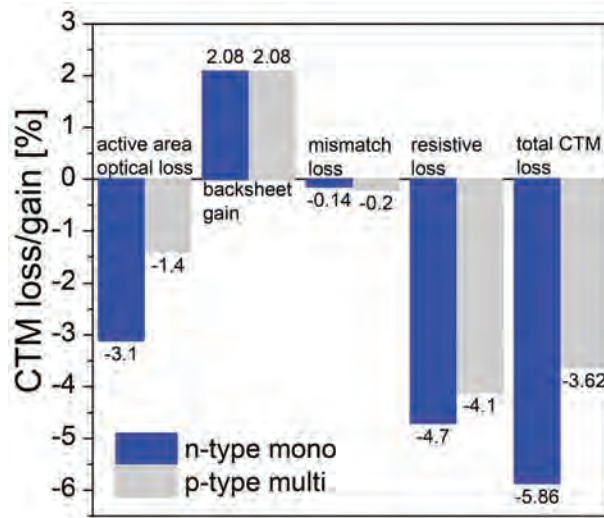
The module  $I-V$  curve normalized using Equation 3 will be free from the errors caused by the cell and module measurements using two different systems. Fig. 10 shows the  $I-V$  curves, both as-measured and normalized to the cell measurements, for a module. The difference between the sum of the individual cell powers and the maximum power  $P_{mod}^{norm}$  of the normalized module  $I-V$  curve will be the total electrical loss (mismatch and resistive). Now, using the mismatch loss calculated earlier, the resistive loss in the CTM process can be obtained using the expression:

$$P_{res} = \sum_{i=1}^n P_{cell}^i - P_{mod}^{norm} - P_{mis} \quad (4)$$

Using the above analysis, the calculation of the resistive loss components for two 60-cell modules with n-type mono and p-type multi cells works out to be 4.7% and 4.1% respectively.

Module type	$I_{sc}$ [A]	$V_{oc}$ [V]	Fill factor [%]	Power [W]
p-type multi	8.84	37.90	77.5	259.6
n-type mono	9.13	38.39	76.8	269.2

**Table 2. Measured electrical parameters for the two experimental modules.**



**Figure 11. CTM power losses for p-type monocrystalline and n-type multicrystalline PV modules.**

PV Modules



**KÖMMERLING**  
KÖMMERLING CHEMISCHE FABRIK GMBH

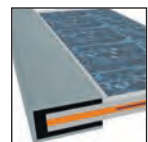
## HelioBond® & HelioSeal®

Adhesives & Sealants

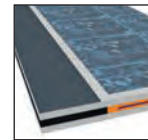
Moisture Vapour Barrier

Long term durability

Outer Sealing



Inner Sealing



Bonding and Potting of the J-Box



Headquarters: KÖMMERLING CHEMISCHE FABRIK GMBH | Zweibrücker Str. 200 | D-66954 Pirmasens | info-solar@koe-chemie.de | +49 6331 562626 Phone  
China Representative: KÖMMERLING CHEMISCHE FABRIK GMBH | 1007, Air China Plaza, 36 Xiaoyun Road, Chaoyang District | CN-100027 Beijing | +86 10 6461 9988 Phone

www.koe-chemie.de

## Discussion and conclusion

A CTM-loss calculation method has been demonstrated for two types of wafer-based module (60-cell) – one with monocrystalline cells and the other with multicrystalline cells. Table 2 lists the measured electrical parameters of the two types of module, while Fig. 11 shows a detailed chart of the CTM losses of the two module types.

In Fig. 11 it can be seen that mono cells have higher optical losses than multi cells when they are encapsulated into a module; the reason for this is that mono cells have better light absorption (less reflection) than multi cells, and hence the optical coupling gain is less for a mono cell. The mismatch losses do not contribute much to the total CTM loss and can therefore be neglected if a good cell-binning strategy is used. In the current experiments, the resistive losses are a major loss component: the losses obtained are on the high side, which indicates that the module interconnection process is not optimized. Some of the well-known technologies for reducing resistive losses in the CTM process are *half-cut cell* and *multi-busbar*.

**“The mismatch losses do not contribute much to the total CTM loss and can therefore be neglected if a good cell-binning strategy is used.”**

An estimation and understanding of CTM losses in wafer-based PV modules is important, since these losses affect the energy yield of a module, and hence the cost of generated electricity. In this paper, various methods and equipment for quantifying the CTM losses/gains in a PV module have been presented. The calculations of individual loss components have been explained by experimental examples and the fabrication of mini-modules and large full-size modules. The presented analysis of CTM losses is important in helping module manufacturers to reduce the losses and improve module performance by carefully selecting the materials and optimizing the processes used in module fabrication.

## References

- [1] Khoo, Y.S., Walsh, T.M., Lu, F. & Aberle, A.G. 2012, “Method for quantifying optical parasitic absorptance loss of glass and encapsulant materials of silicon wafer based photovoltaic modules”, *Sol. Energy Mater. Sol. Cells*, Vol. 102, pp. 153–158.
- [2] Biao, L. et al. 2012, “Effect of encapsulant on cell-to-module efficiency loss in PV modules with ion implant and  $\text{POCl}_3$  cells”, *Proc. 38th IEEE PVSC*, Austin, Texas, USA, pp. 2336–2341.
- [3] Wilson, K., De Ceuster, D. & Sinton, R.A. 2006, “Measuring the effect of cell mismatch on module output”, *Proc. 4th WCPEC*, Waikoloa, Hawaii, USA, pp. 916–919.
- [4] Spribille, A. et al. 2013, “HIP-MWT: Our approach for high performance ribbon based back contact MWT modules with low CTM losses”, *Proc. 7th SNEC Int. PV Power Gen. Conf.*, Shanghai, China.
- [5] Kang, M.H., Ryu, K., Upadhyaya, A. & Rohatgi, A. 2011, “Optimization of SiN AR coating for Si solar cells and modules through quantitative assessment of optical and efficiency loss mechanism”, *Prog. Photovoltaics Res. Appl.*, Vol. 19, pp. 983–990.
- [6] McIntosh, K.R. et al. 2009, “An optical comparison of silicone and EVA encapsulants for conventional silicon PV modules: A ray-tracing study”, *Proc. 34th IEEE PVSC*, Philadelphia, Pennsylvania, USA, pp. 544–549.
- [7] Peters, I.M., Yong Sheng, K. & Walsh, T.M. 2014, “Detailed current loss analysis for a PV module made with textured multicrystalline silicon wafer solar cells”, *IEEE J. Photovolt.*, Vol. 4, pp. 585–593.
- [8] Krauter, S. & Grunow, P. 2006, “Optical simulation to enhance PV module encapsulation”, *Proc. 21st EU PVSEC*, Dresden, Germany, pp. 2065–2068.
- [9] Haedrich, I. et al. 2013, “Minimizing the optical cell-to-module losses for MWT-modules”, *Energy Procedia*, Vol. 38, pp. 355–361.
- [10] Ballif, C., Dicker, J., Borchert, D. & Hofmann, T. 2004, “Solar glass with industrial porous  $\text{SiO}_2$  antireflection coating: Measurements of photovoltaic module properties improvement and modelling of yearly energy yield gain”, *Sol. Energy Mater. Sol. Cells*, Vol. 82, pp. 331–344.
- [11] Z. Liu et al. 2016, “Luminescence imaging analysis of light harvesting from inactive areas in crystalline silicon PV modules”, *Sol. Energy Mater. Sol. Cells*, Vol. 144, pp. 523–531.
- [12] Bishop, J. 1988, “Computer simulation of the effects of electrical mismatches in photovoltaic cell interconnection circuits”, *Solar Cells*, Vol. 25, pp. 73–89.
- [13] Field, H. & Gabor, A.M. 2002, “Cell binning method analysis to minimize

mismatch losses and performance variation in Si-based modules”, *Proc. 29th IEEE PVSC*, New Orleans, Louisiana, USA, pp. 418–421.

- [14] Guo, S. et al. 2013, “A quantitative analysis of photovoltaic modules using halved cells”, *Int. J. Photoenergy*, Vol. 2013.

## About the Authors



**Jai Prakash Singh** received his Ph.D. in electrical and computer engineering from NUS. He works as a research scientist at SERIS, where he focuses on characterization, loss analysis and optimization of c-Si solar cells and modules.



**Yong Sheng Khoo** has more than five years’ experience in PV module development and testing, and is the head of the module development group at SERIS. He obtained his Ph.D. from NUS, and also has a B.S. and an M.Eng. in mechanical and aerospace engineering from Cornell University, USA.



**Jing Chai** received his MEngSc in photovoltaics from the University of New South Wales (UNSW), Australia, in 2010. Since 2012 he has been a research assistant at SERIS, where his research focus is on high-efficiency and long-durability Si-based PV modules.



**Zhe Liu** received a B.Eng. in electrical engineering from NUS in 2012. Since 2012 he has been a Ph.D. student at SERIS, with a research focus on modelling and characterization of Si solar cells and modules.



**Yan Wang** is the director of the PV module cluster at SERIS. He received his Ph.D. in 2007 through a co-educated graduate student collaboration between Forschungszentrum Jülich, Germany, and Nankai University, China.

## Enquiries

SERIS  
National University of Singapore  
Block E3A, #06-01  
7 Engineering Drive 1  
Singapore

Tel: +65 660 11034  
Email: yongshengkhoon@nus.edu.sg

# Double-glass PV modules with silicone encapsulation

Shencun Wang<sup>1</sup>, Xiang Sun<sup>1</sup>, Yujian Wu<sup>2</sup>, Yanxia Huang<sup>2</sup>, Nick Shephard<sup>3</sup> & Guy Beaucarne<sup>4</sup>

<sup>1</sup>BYD, Shenzhen, Guangdong, China; <sup>2</sup>Dow Corning (China) Holding Co. Ltd., Shanghai, China; <sup>3</sup>Dow Corning Corporation, Midland, Michigan, USA; <sup>4</sup>Dow Corning Europe S.A., Seneffe, Belgium

## ABSTRACT

Double-glass PV modules are emerging as a technology which can deliver excellent performance and excellent durability at a competitive cost. In this paper a glass–glass module technology that uses liquid silicone encapsulation is described. The combination of the glass–glass structure and silicone is shown to lead to exceptional durability. The concept enables safe module operation at a system voltage of 1,500V, as well as innovative, low-cost module mounting through pad bonding.

## Introduction

Recently several double-glass (also called glass–glass or dual-glass modules) c-Si PV modules have been launched on the market, many of them by major PV manufacturers. These modules use a sheet of tempered glass at the rear of the module instead of the conventional polymer-based backsheet. There are several reasons why this structure is appealing. First, glass is completely impermeable to moisture and therefore degradation caused by water ingress is expected to be much slower than for a conventional glass–backsheet structure with the same encapsulant. Moreover, a glass–glass laminate is mechanically much more robust than a glass–backsheet laminate, even if thin 2mm glass is used. This is because the double sheet

of glass provides higher rigidity while the cells are placed in the ‘neutral plane’ of the laminate and therefore experience no compression or tension when the structure is bent; this greatly reduces fatigue stresses in the tabbing. The possibility of using thin glass for the front cover also enables a small efficiency increase thanks to the higher light transmittance relative to the thick front cover glass. Finally, a glass–glass structure enables a frameless installation and/or the implementation of rail or pad bonding instead of conventional module affixation.

Even more than for conventional modules, the bill of materials is critical for double-glass modules. In particular, the choice of encapsulant has a large impact on the module manufacturing process as well as on performance and

reliability [1]. Various encapsulant materials can be considered. Polyvinyl butyral (PVB) has been used for a long time for glass–glass PV modules, particularly for thin-film modules. For various reasons (it entails a longer, more complicated process, and comparatively high water uptake), this is not the preferred material for modern crystalline Si double-glass modules.

Several manufacturers have chosen to use the material that has become standard in the manufacturing of conventional glass–backsheet modules, namely ethylene vinyl acetate (EVA). This is challenging, as volatile organic compounds are generated as by-products of the peroxide cure initiation reactions and need to be fully evacuated before cure completion – otherwise voids are formed [1]. This is not easy to achieve for glass–glass structures, and very careful process tuning is necessary. Nevertheless, several EVA-encapsulated double-glass modules are now commercially available.

**“Silicone as an encapsulant material is extremely stable under thermal and UV stress.”**

Another family of materials that has been considered is thermoplastic or slightly cross-linking polyolefins (TPO) [2]. Finally, one can use silicone as an encapsulant material; this is known to be extremely stable under thermal and UV stress. The use of a liquid encapsulant, such as silicone, also reduces cell damage caused during the placement of the second piece of glass.

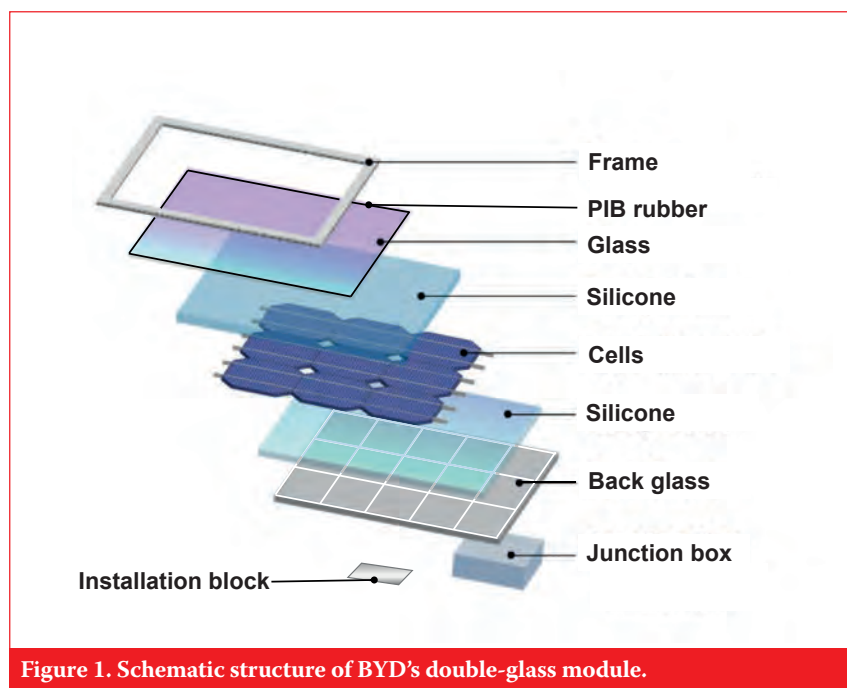


Figure 1. Schematic structure of BYD's double-glass module.

Early PV modules were often encapsulated with silicone, and have demonstrated outstanding stability in the field, with degradation rates over 20 to 30 years that are much lower than the typical degradation rates for EVA-encapsulated modules [3–5]. The silicone materials used at the time, however, were products that had been developed for electronics, and the manufacturing processes were not adapted to PV needs. A few years ago, renewed interest led to the development of dedicated silicones for modern PV modules [6,7], resulting in the recent launch of a new optimized silicone encapsulant [8]. Aiming for an extremely durable and reliable module, and on the basis of an assessment of the various encapsulation options for double-glass modules, it was decided to implement this new silicone encapsulation technology in BYD's double-glass PV module product. This paper describes the module concept and design, discusses the manufacturing implementation, and highlights module performance and very recent developments.

### Module concept

The structure of the BYD module is shown in Fig. 1. As in conventional modules, it consists of several layers laminated together, with the solar cell matrix in the centre; however, there are some major differences.

The rear outer layer is not a conventional polymer backsheet, but a sheet of toughened glass, providing an excellent barrier against water vapour and electrical breakdown protection. In order to capture the maximum possible amount of light, the glass is locally coated with a white reflective layer, which is applied in a grid pattern and is aligned with the area between the cells in the final module. As mentioned earlier, a silicone PV encapsulant was used instead of conventional EVA – this aspect is covered in more detail in the next section.

In order to prevent water vapour ingress through the edges of the laminate, a polyisobutylene (PIB) rubber seal is applied along the perimeter. This material demonstrates extremely low water vapour transport rate ( $< 0.2\text{mg}/\text{m}^2/\text{day}$ ) and extremely high volume resistivity ( $\sim 10^{16}\Omega\cdot\text{cm}$ ). The combination of this rubber seal with the rear glass sheet and the silicone encapsulation leads to exceptional environmental and electrical protection of the module.

The double-glass structure makes the module quite rigid compared with

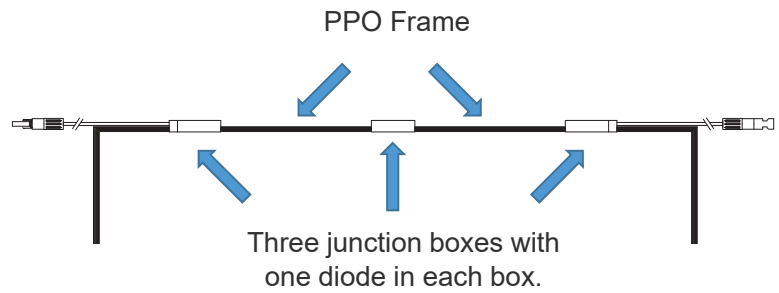


Figure 2. Detail of BYD's double-glass PV module design, highlighting the frame and the edge junction boxes.



Figure 3. Example of a PV system using BYD's double-glass modules.

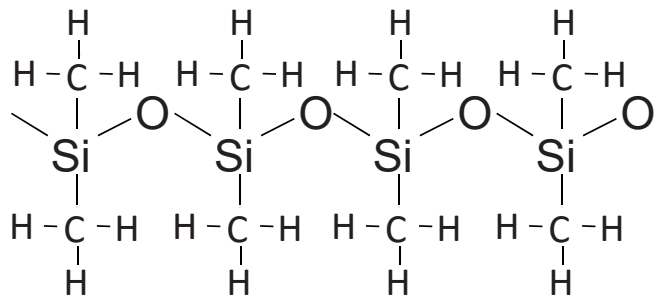


Figure 4. Chemical structure of polydimethylsiloxane silicone.

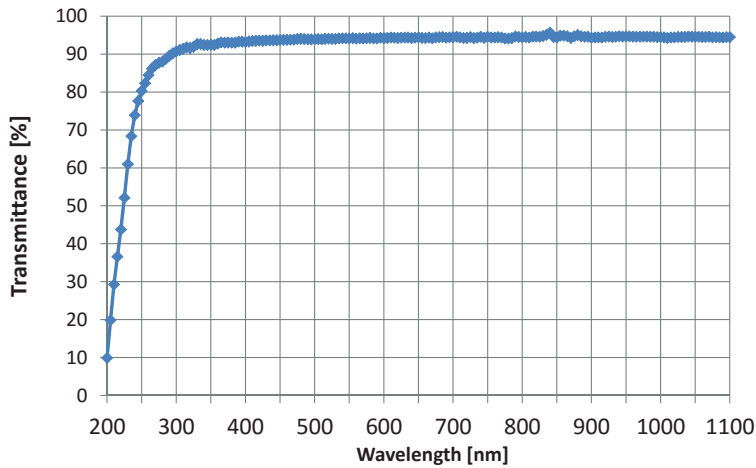


Figure 5. Transmittance of PV-6212 as a function of wavelength.

the sleek appearance of the module. Moreover, there is no need to make holes in the rear glass sheet. Finally, the resistance losses are lower because of shorter cables and bussing tapes.

To mount the module onto its support, a strong metal fixture is attached to the laminate. These rectangular pieces of stainless steel, referred to as *installation blocks*, are glued directly onto the rear glass sheet using structural silicone adhesive. The technology to bond glass to structural elements in order to create structures that can withstand large wind loads is commonly practised in the construction industry and benefits from decades of experience.

The installation blocks are designed and placed on the laminate in such a way that they can be bolted onto two brackets with a U-shaped cross section. Each pair of brackets will typically carry several modules, the number of which depends on the PV system design (Fig. 3). This module concept enables flexibility in system design as well as easy installation, with a low risk of module breakage, compared with the clamping systems that are typically used for frameless modules. Mechanical load tests with a module ‘hanging from’ or ‘lying on’ two brackets showed that the modules

standard laminates. As a result, a conventional aluminium frame is not necessary; instead, a light frame made of polyphenylene oxide (PPO) polymer, a high-temperature thermoplastic, is used to protect the glass edges from impact during transport. Because the frame is non-conductive, it does not need to (and cannot) be grounded. The whole front surface of the module is

electrically floating.

With regard to the junction box, the solution chosen consists of three separate edge junction boxes, each containing one bypass diode, instead of one central junction box containing three bypass diodes (see Fig. 2). This arrangement has several advantages. The individual junction boxes can be quite narrow and therefore maintain

## INNOVATIVE TECHNOLOGY 4U

[buerkle-technologies.com](http://buerkle-technologies.com)

# Be prepared for the coming PV REVOLUTION

### THE MOST VERSATILE LAMINATION SYSTEM

Reliable and flexible lamination system for high volume production of Glass-Glass and Glass-Backsheet modules

- Shortest possible lamination times with the patented Bürkle SL-Technology
- Highest production flexibility and module quality
- Fastest and smoothest lamination process for Glass to Glass Modules on the market

Bürkle PV Equipment for the best module quality with the longest life time.



ROBERT BÜRKLE GMBH  
Stuttgarter Straße 123 · D-72250 Freudenstadt  
E-Mail: [laminator@buerkle-technologies.com](mailto:laminator@buerkle-technologies.com)

**BÜRKLE** 

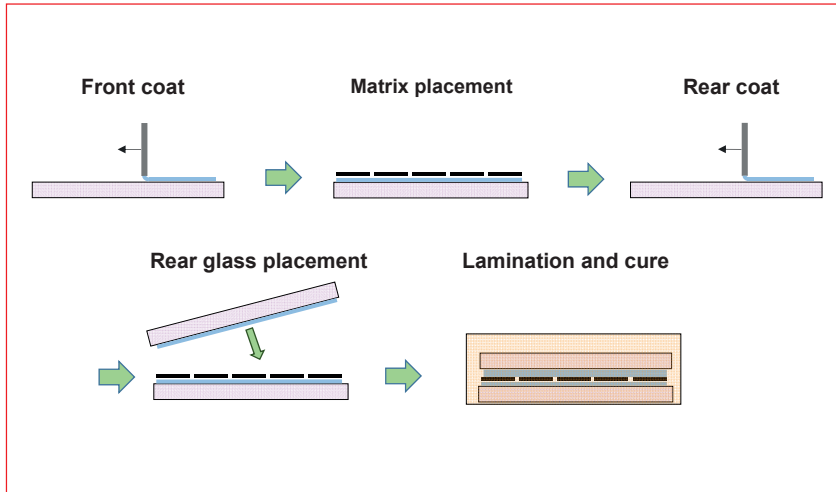


Figure 6. Encapsulation process using PV-6212 silicone encapsulant for glass-glass modules.



Figure 7. Front (a) and rear (b) of a fabricated BYD double-glass module.

remained intact during a wind load of 2,400Pa and a snow load of 5,400Pa, without any cracking of the cells or decrease in performance.

### Silicone encapsulation

The silicone encapsulant material selected for this work was *Dow Corning*<sup>®</sup> PV-6212 Cell Encapsulant. In contrast to most commercial PV encapsulants, this material is supplied as a liquid, not as a foil. It is dispensed in the liquid form and is cured into a solid by cross-linking during lamination. PV-6212 is a polydimethylsiloxane (PDMS),

consisting of molecules with a ‘Si-O-Si-O...’ backbone and two CH<sub>3</sub> groups on each Si atom (see Fig. 4), that uses an addition curing system; as a result, there is no by-product of the cross-linking reaction. PV-6212 is provided in two parts which need to be mixed just before application. The curing process results in a firm but fairly soft rubber (shore A hardness 11.5); this provides protection but still allows some movement of the encapsulated pieces, which is important for reliability in thermal cycling testing.

The Si-O bond in the silicone backbone is much stronger than the C-C bond in the backbones of organic

polymers (such as EVA), with a bond energy of 452KJ/mol vs. 346KJ/mol; this makes the material intrinsically more stable. Moreover, cured PV-6212 has a high transparency, including over the UV range, in which conventional encapsulants have reduced transmittance (Fig. 5). This is particularly important for new solar cell technologies which demonstrate improved response at short wavelengths. The transparency in the UV range also makes the silicone inherently more resistant to hardness and colour changes caused by UV degradation.

The encapsulation process is shown schematically in Fig. 6; it begins with the dispensing of PV-6212 onto the first glass panel. Next, the solar cell matrix is placed onto the silicone. Another glass panel is coated with the encapsulant and is then turned upside down and placed onto the first panel containing the cell matrix. The whole sandwich is then introduced into a laminator, where a vacuum is drawn and the laminate is heated up, thus beginning the silicone curing process.

### Implementation and manufacturing at BYD

A complete manufacturing process was designed on the basis of the module design, a preliminary silicone encapsulation process and an initial selection of other key components, such as the frame, junction box and PIB rubber. This process was first implemented, improved and fine-tuned on a pilot line. It was subsequently transferred to a manufacturing line, and high-volume production began; one of the fabricated modules is shown in Fig. 7.

### Module performance, durability and safety

The electrical performance of the BYD double-glass modules was as expected for multicrystalline cells, with power bins ranging from 245W to 265W for 60-cell modules, and from 295W to 315W for 72-cell modules.

### Accelerated ageing

The modules were subjected to numerous accelerated ageing tests. Table 1 shows the climate-chamber test data for damp-heat (DH), thermal-cycling (TC) and humidity-freeze (HF) tests. Only a small degradation can be observed, with at most around 1% after twice the duration of the standard tests prescribed by IEC-61215 (whereas this standard specifies a maximum permissible degradation of



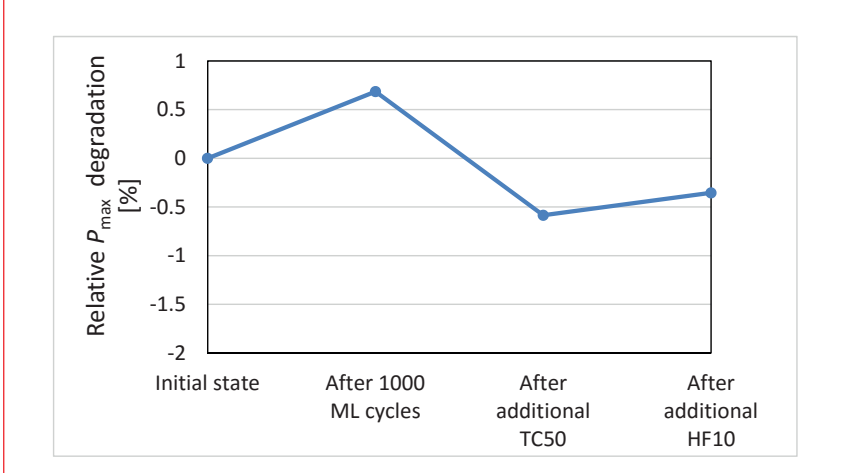
Test type	Test duration	Relative power change [%]
Thermal cycling	TC200	-0.1
	TC400	-0.8
Damp heat	DH1000	-0.5
	DH2000	-0.9
Humidity freeze	HF10	-1.2
	HF20	-1.0
	HF30	-1.4

**Table 1. Accelerated ageing test results.**

5% after 1×IEC). All the modules still comfortably passed wet leakage tests after accelerated ageing.

The results of a test combining dynamic mechanical testing (1,000 cycles, 1,440Pa), 50 thermal cycles and 10 humidity-freeze cycles are given in Fig. 8. As expected, the mechanical load has no negative impact on performance. The subsequent TC and HF tests reveal no significant damage to the strings, with a final degradation of less than 0.4% relative to the initial module power.

PV Modules



**Figure 8. Module power degradation during combined mechanical load, thermal cycling and humidity-freeze test procedures.**

**“The double-glass module is extremely PID resistant.”**

**Potential-induced degradation**  
Another ageing phenomenon that must be tested is potential-induced degradation (PID). Over the last few years, PID has become a very important topic as PV systems become very large, resulting in long module strings and high operating voltage. The standard PID test involves keeping modules with metallic foil on the front surface in 85% relative humidity and 85°C conditions (85/85) for 96 hours under a potential of -1,000V, with a permissible power loss of 5%. After

# WHITE EVA - HIUV G401W

## Double Glass Solutions



www.hiuv.net  
**HIUV**  
 Materials Technology

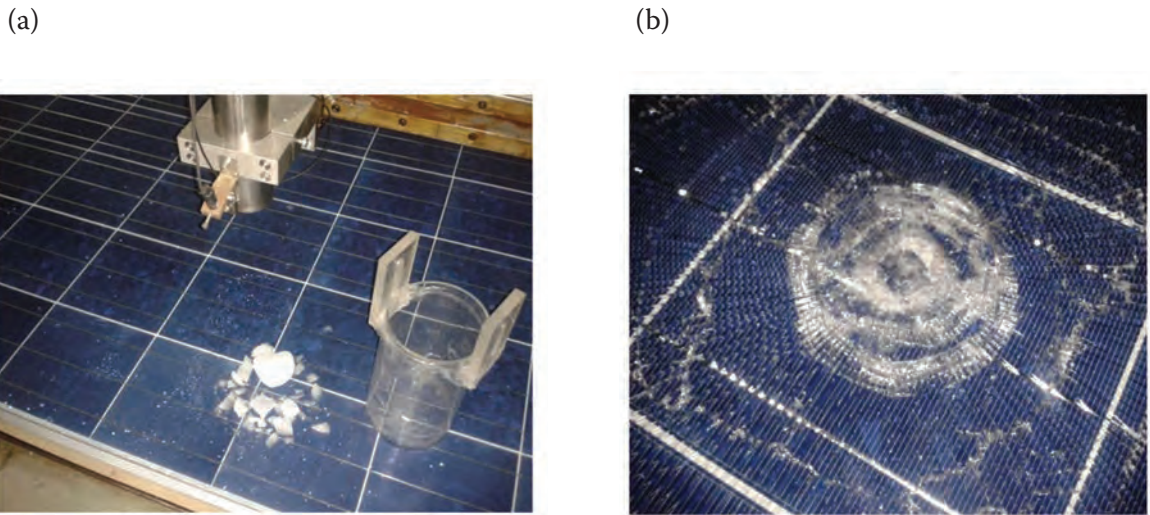
396, Minfeng Rd., Pudong, 201209 Shanghai, China

### Others EVA problematic

- White overflow on Cells & Ribbons
- White Wrinkles
- Bubbles & Unfilled edges



**Come to visit us at SNEC Solar Materials Hall W4 - Booth 575**



**Figure 9. Results of the hail test (5cm, 126km/h) on (a) a BYD double-glass module, and (b) a conventional module with glass, EVA and backsheets.**

192 hours of PID testing, however, the power loss of the tested module was only 0.6%. The voltage was then increased to 1,500V, and after an additional 96 hours, the power loss was still only 0.7%.

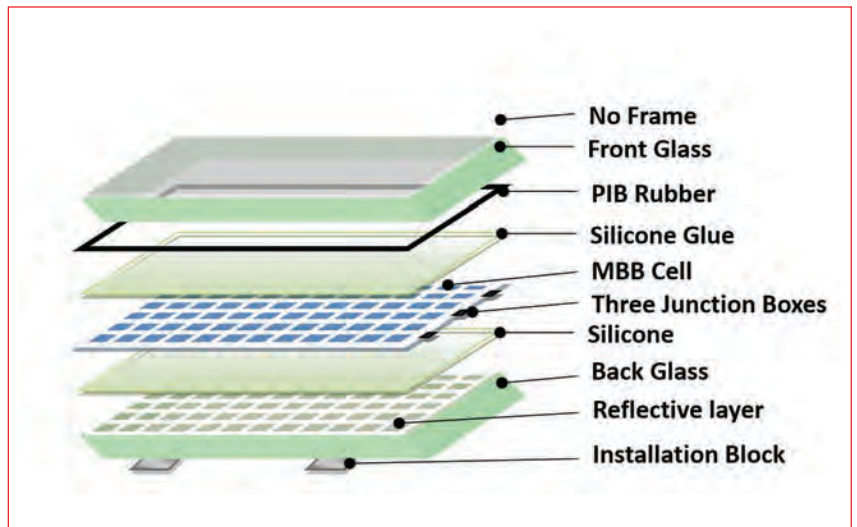
Another test involved applying 1,000V in 85/85 damp-heat conditions, but this time for 600h (both positive and negative bias). The power degradation was only 0.6% for +1,000V and 1.4% for -1,000V, which is an outstanding result for such a stringent test. It can therefore be concluded that the double-glass module is extremely PID resistant.

**Hail resistance**

The impact of hail was also investigated. This test consisted of projecting hailstones with a 5cm diameter at a velocity of 126km/h onto the module and observing the damage. As can be seen in Fig. 9, the double-glass module is intact, whereas the same test conducted on a conventional glass with EVA and backsheets results in substantial glass damage and module power reduction. The laminate rigidity, thanks to the double-glass structure, combined with the dampening effect to some degree of the silicone, appears to be very effective in preventing impact damage.

**Module certification**

A set of modules was submitted for certification to TÜV Rheinland: all the tests, carried out in accordance with IEC 61215, IEC 61730-1 and IEC 61730-2, were passed. Moreover, TÜV Rheinland did the electrical testing required for the new PV plant voltage standard of 1,500V. On the basis of the positive results obtained, for the



**Figure 10. Schematic of 'PV Module 2.0'**

first time for modules manufactured in China a certificate was issued confirming that these modules could safely be used in PV plants at operating voltages of up to 1,500V (compared with the current standard of 1,000V). The possibility of building systems that operate at higher voltages (i.e. more modules per string) allows significant PV system cost reduction, because fewer inverters are needed and the total cable length is decreased.

As a result of the outstanding reliability and durability data collected, the BYD double-glass module has been nicknamed the *430 module*. The first digit, '4', indicates that the products are estimated to work for 40 years. The middle digit, '3', means that the average annual power attenuation is as low as 0.3%. The last digit, '0', indicates that the module is PID free and exhibits no snail tracks.

**Next generation of glass-glass silicone modules**

In order to further increase performance and reduce cost, several innovations have recently been introduced, which have resulted in a new generation of glass-glass modules (Fig. 10). To reflect the momentous change that this type of module represents with respect to conventional modules, this technology has been named *PV Module 2.0*. The module is now totally frameless, and the interconnection ribbons have been replaced by 24 wires with a round cross section. The cells are 'multi-busbar' cells [9], featuring lots of very small solder pads instead of the three wide busbars conventionally used, onto which the wires are soldered.

This new structure allows a 25% reduction in silver consumption,



**SOLAR  
ENERGY  
UK**

 **Clean  
Energy**  
LIVE

# Solar and Storage leading the low carbon transition

THE NEC, BIRMINGHAM, UK | 4 – 6 October 2016

INCORPORATING:



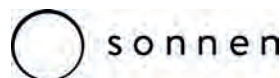
“ I found this year’s event extremely worthwhile, especially in the face of uncertainty caused by Government policy. It was good to hear a lot of resilience in the market and positive attitude to continue and diversify and the seminars were excellent for information gathering.”

**Drew Clough, Product Manager, Npower**



[uk.solarenergyevents.com](http://uk.solarenergyevents.com)

Some of 200+ exhibitors include:



as the total busbar area is less than that for conventional cells, and also because a lower finger cross section is permissible when the fingers are shorter. Moreover, because of the round shape of the interconnection wires, most of the impinging light is reflected onto the cell rather than back towards the sky, and therefore the short-circuit current and efficiency are increased. With this structure, a power of 275W has been obtained for a multicrystalline 60-cell module.

**“The combination of a glass–glass structure and silicone encapsulation leads to exceptional robustness, reliability and durability.”**

### Conclusion

A novel double-glass module technology has been developed that makes use of silicone encapsulation. The combination of a glass–glass structure and silicone encapsulation leads to exceptional robustness, reliability and durability. These modules are particularly well suited to applications in harsh conditions and/or where very long module lifetime is required. Recent changes to the design, including the use of a multi-busbar design, have led to further improvements in cost and performance.

### References

- [1] Perret-Aebi, L.-E. et al. 2010, “Insights on EVA lamination process: Where do the bubbles come from?”, *Proc. 25th EU PVSEC*, Valencia, Spain.
- [2] Cattaneo, G. et al. 2015, “Lamination process and encapsulation materials for glass–glass PV module design”, 27th edn, *Photovoltaics International*, pp. 82–90.
- [3] Skoczek, A., Sample, T. & Dunlop, E.D. 2009, “The results of performance measurements of field-aged crystalline silicon photovoltaic modules”, *Prog.*

*Photovoltaics Res. Appl.*, Vol. 17, p. 227.

- [4] Ketola, B. et al. 2008, “Silicones for photovoltaic encapsulation”, *Proc. 23rd EU PVSEC*, Valencia, Spain.
- [5] Lopez, J., Pozza, A. & Sample, T. 2015, “Analysis of crystalline silicon PV modules after 30 years of outdoor exposure”, *Proc. 31st EU PVSEC*, Hamburg, Germany.
- [6] Ketola, B. et al. 2010, “Demonstration of silicone encapsulation of PV modules in a large scale outdoor array”, *Proc. 25th EU PVSEC*, Valencia, Spain.
- [7] Powell, N. et al. 2010, “Improved spectral response of silicone encapsulated photovoltaic modules”, *Proc. 35th IEEE PVSC*, Honolulu, Hawaii, USA.
- [8] Dow Corning 2014, “Dow Corning to launch and showcase several novel silicone-based solutions at SNEC PV Power Expo 2014 – China” [[http://www.dowcorning.com/content/news/Solar\\_SNEC\\_2014.aspx](http://www.dowcorning.com/content/news/Solar_SNEC_2014.aspx)].
- [9] Braun, S., Micard, G. & Hahn, G. 2012, “Solar cell improvement by using a multi busbar design as front electrode”, *Energy Procedia*, Vol. 27, pp. 227–233.

### About the Authors



**Shencun Wang** received his master’s in 2010 from the Central South University of China. He joined BYD in 2010, where he leads a team involved in double-glass module application and process development. He has recently been appointed the production manager for double-glass modules.



**Xiang Sun** received his bachelor’s in 2000 from the University of Science and Technology of China. He joined BYD in 2000, where he has held the positions of quality manager, production manager and project manager, and is currently the manager of the PV technology R&D centre.



**Yujian Wu** joined Dow Corning in 2012 as the Asia Pacific Application Development Leader for PV. Before joining Dow Corning, Yujian gained 12 years’ experience in c-Si and thin-film solar, semiconductor IC fabrication and LED applications.



**Yanxia Huang** holds a Ph.D. in polymer Science from Tongji University, China, and worked for BASF and Henkel, focusing on acrylate adhesives, before joining Dow Corning in 2013. She is a senior product development chemist at Dow Corning China, working on materials for the construction and solar industries.



**Nick Shephard** joined Dow Corning in 1985, and has collaborated on products and processes for PV applications since 2004. He specializes in the field of surface science and adhesion durability, to which he has contributed patents, new products, new measurement techniques and global lectures.



**Guy Beaucarne** holds a Ph.D. from the University of Leuven, Belgium. After working as a PV researcher in Australia, he returned to imec, where he headed the Solar Cell Technology group for six years. In 2009 he joined Dow Corning, where he has been developing new materials and applications for PV, lighting and electronics.

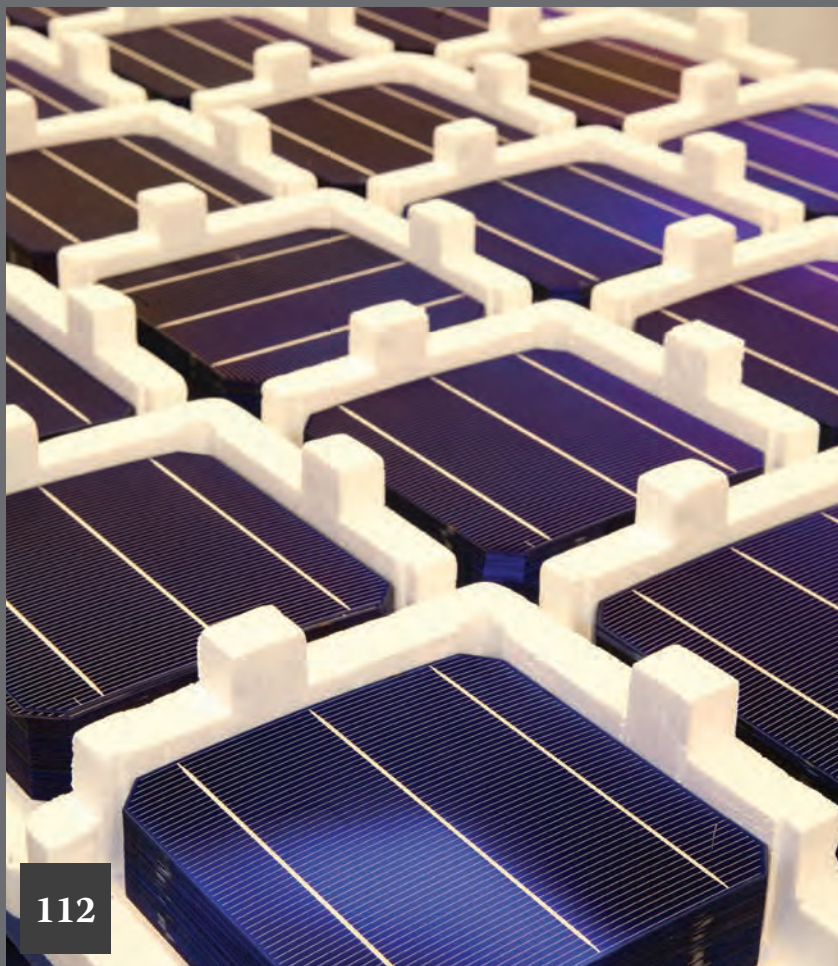
### Enquiries

Shencun Wang  
BYD  
Shenzhen, Guangdong  
China  
Email: wang.shencun@byd.com

Guy Beaucarne  
Dow Corning  
Seneffe, Belgium  
Email: guy.beaucarne@dowcorning.com

# Market Watch

---



Page 108  
News

---

Page 112  
**PV capital expenditure shifts  
from polysilicon to cell  
capacity additions**

Finlay Colville, Head of Market  
Intelligence, Solar Media Ltd.

---

## China displaces Germany as solar capacity leader

China has officially overtaken Germany as the world's leader in installed solar capacity after Beijing confirmed that 15.13GW was added in 2015.

The official figures now show that the country has 43.18GW of solar. The National Energy Administration (NEA) claims that 37.12GW is utility-scale and around 6GW is distributed PV. The figure is a 43% increase on 2014's tally of 10.6GW and a huge 54% boost in total installed from 28.05GW at the end of 2014.

Grid curtailment issues continue to plague some provinces with Gansu (31%) and Xinjiang (26%) particularly badly hit, according to the NEA statement.

Germany has a 2.5GW annual cap on solar deployment in place, which made China's ascension in the rankings inevitable.



Credit: GCL

China has now overtaken Germany as the country with the largest installed PV capacity.

News

## Europe

### UK could retain European PV deployment crown in 2016, says SolarPower Europe

The UK installed 3.5GW of Europe's 8GW of PV capacity in 2015, according to SolarPower Europe.

The trade group presented its first estimates in early February ahead of the final figures being revealed after *Photovoltaics International* went to press. The numbers, based on actual grid-connected projects, are up 15% on the previous year with the UK market contributing a significant chunk. SolarPower Europe has also estimated global installed PV capacity of 50GW.

With reductions in policy support continuing to kick in for the UK market, SolarPower Europe CEO James Watson expects the UK to remain among the leaders in 2016, if not retaining its position.

"A figure of 3.5GW makes the UK market the biggest market in Europe again," he said.

### Giving China market status would cut anti-dumping import cost by 19%

The cost of Chinese imports affected by European anti-dumping duties would fall 19% if the EU decides to treat China as a market economy at the end of this year.

An independent report commissioned by the EC said that the change could lead to the loss of 30,400-77,000 jobs in the affected sectors unless "mitigating measures" are put in place. The report was presented to the European Parliament and trade ministers of member states.

Conditions of China's ascension to the World Trade Organization expire on

11 December and as such China would be considered a market economy. The EC must decide whether to put forward legislation to reflect this in its anti-dumping regulations. To prove a case for dumping against a market economy, it must be shown that it is selling products overseas below its own domestic prices.

### France's output from PV installations grew 25% in 2015

The power output from PV systems in France grew by 25% last year to 7.4TWh, up from 5.9TWh, according to the latest figures from the French electricity transmission system operator.

The country now has a total of 6,191MW of PV deployed, having installed an additional 895MW in 2015.

One third of this increase came from the commissioning of Europe's largest solar park, the 300MW Cestas solar park, developed by Neoen.

At the end of 2014, total installations stood at 5,296MW overall with deployment during the year standing at 930MW, slightly up compared to 2015.

## Americas

### US installed 7.3GW of solar power in 2015, says report

The US installed 7.3GW of solar in 2015, according to new data published by GTM Research and the Solar Energy Industries Association (SEIA) in February.

The figure is more than 1GW up on the previous year's record of 6.2GW with residential and utility-scale solar making the biggest gains. It was also the first year the country installed more solar power generating capacity than natural gas. In total, solar counted for 29% of all the new additions in 2015.

With the investment tax credit (ITC) extended for solar beyond the original scheduled phase out at the end of 2016, Resch is confident that there is plenty more to come.

"Over the next few years, we're going to see solar continue to reach unprecedented heights as our nation makes a shift toward a carbon-free source of energy that also serves as an economic, job-creating engine," said



Credit: Neoen

Cestas, France. The country's PV power output grew 25% in 2015.

# SUBSCRIBE TODAY!

Technology and business solutions for commercial and utility-scale PV power plants – from the publisher of Photovoltaics International and [www.pv-tech.org](http://www.pv-tech.org)



### Highlights from the latest issue:

#### MARKET WATCH

- How solar can harness the momentum from Paris to become a global force
- MENA special – desert-proof hardware
  - strategies for PV O&M in the desert
- Japan looks for alternatives to mega solar

#### FINANCE

- Opening up the finance markets for merchant solar
- Reviving argument for self-consumption
- Corporate financing global trends in solar

#### SYSTEM INTEGRATION

- Technical briefings in –
  - Quantifying installation handling impact on power losses
  - Reliability of large-scale PV plants and inverters
  - Mega-scale plants with Japan's land restrictions

SUBSCRIBE AT:

[www.pv-tech.org/power](http://www.pv-tech.org/power)



Japan's solar feed-in tariff is in line for further cuts.

## News

Rhone Resch, president and CEO of the Solar Energy Industry Association.

### NREL: Solar tax credits to boost US deployment by up to 20GW

The extension of solar investment tax credits (ITC) will support steady growth in US PV deployment, according to a new study by the National Renewable Energy Laboratory (NREL).

The research group found that by 2022, 20GW of solar that would not have been installed without the ITC will be in the ground.

The ITC had been set to drop at the end of 2016 to zero for residential installs and 10% for all others. But an extension passed at the end of 2015 means it will remain at 30% until 2019 and then fall to 26% the following year and 22% in 2021 before remaining permanently at 10% thereafter.

The positive impact becomes harder to model with time, according to the NREL, which starts to see reductions in solar capacity between its models with and without the extension.

### Chile surpasses 1GW solar milestone

Chile's cumulative installed solar capacity has surpassed 1GW, according to the latest figures from Chilean renewable energy research institute (CIFES).

The amount of solar PV in operation in Chile reached 1,013MW as of the end of January 2016, up 165MW from 848MW at year end 2015. There are now 2,195MW of projects under construction, with 10,755MW approved and a further 4,016MW awaiting qualification.

A total of 279 renewables projects were registered in 2015. Solar PV plants requiring US\$28.9 billion investment are at various stages of development with the potential to generate 14,356MW of gross capacity, Chile's society for industrial development, Sofosa, said.

## Asia & Oceania

### Japan's FiT degression back to previous levels

Japan's FiT for the next financial year could be set at ¥24 (US\$0.21) per kWh. Japanese news outlets reported in late February that a panel advising the government's Ministry of Economy, Trade and Industry was recommending the new price, which would be applicable to power plants of over 10kW capacity.

This represents a drop from the current level of ¥27 of around 11%. The drop is in line with the more moderate degressions of the first couple of years of the policy than last year's cut, when it was slashed by an unprecedented 16%, following a period in which solar was drawn into wider discussions about Japan's energy policy.

Residential solar, generators smaller in scale than 10kW, would see a drop of ¥2 per kWh from this year's level. The proposed rates still need to be approved by minister Motoo Hayashi.

Japan is expected to stick to its course of targeting 22% to 24% of its energy to come from renewable sources by 2030, which according to previously issued documents and the Japan Photovoltaic Energy Association (JPEA) is equitable to around 64GW of PV, leading to speculation that the country's large-scale sector in particular could be restricted by the time an auction process is introduced to tender utility-scale projects in the 2017 financial year.

### Indian government expects to commission 3.8GW of solar this year

Solar projects commissioned under government of India and state policies are likely to reach 3,790MW within the year 2015/16, according to the latest figures from the Ministry of New and Renewable Energy (MNRE).

The Indian government expects 570MW to come online under its own initiatives and 3,220MW under state policies within this financial year, having already seen 1,504MW commissioned so far.

However, Jasmeet Khurana, associate director at consultancy firm Bridge to India said: "The government hopes that it will increase to 3.8GW by the end of March. However, we think that many of these projects will slip to the next financial year."

Even without taking Bridge to India's carry over into account, MNRE projects a vast increase in capacity additions in 2016/17 of 12,161MW. Overall, the total commissioned capacity in India under both government and private schemes has now reached 5,248MW as of 31 January 2016.

## Middle East & Africa

### Senegal plans 200MW solar via IFC 'Scaling Solar' programme

The government of Senegal plans to develop 200MW of solar power as part of the World Bank Group's initiative 'Scaling Solar', which aims to assist African countries in procuring renewable energy quickly and affordably power through private investment.

The International Finance Corporation (IFC), a member of the World Bank Group, signed an agreement with the Senegal government to help it conduct due diligence and tender the solar project; the IFC, the World Bank and the Multilateral Investment Guarantee Agency are expected to support the bidding phase.

Just over half the population of Senegal currently has access to electricity, according to World Bank data.

### Middle East has arrived as a multi-GW solar market

With around 3GW added to its pipeline in 2015 and another 4GW expected this year, the Middle East's arrival as a gigawatt-scale source of solar demand has been confirmed in a report by the Middle East Solar Industry Association (MESIA).

The 2016 MESIA Market Outlook anticipates the procurement to be led by 2GW in Algeria, 1,150MW by the UAE (800MW in Dubai, 350MW in Abu Dhabi) as well as a further 250MW in Egypt and 245MW in Morocco.

While conventional wisdom might suggest that plummeting oil prices would leave the region short of cash to develop projects, the reality on the ground is different. According to Dr. Raed Bkayrat, director of research at MESIA and author of the report, the fall in oil revenues has instead hastened fossil fuel subsidy reform.



# 2016 UK & INTERNATIONAL EVENTS



15 March | Manchester

16 March | Newcastle on Tyne

17 March | Edinburgh

5 April | Nottingham

6 April | Brighton

7 April | Cardiff

[ukroadshow.solarenergyevents.com](http://ukroadshow.solarenergyevents.com)



16 - 17 March 2016 | Kuala Lumpur, Malaysia

[celltech.solarenergyevents.com](http://celltech.solarenergyevents.com)



19 - 20 April 2016 | Accra, Ghana

[westafrica.solarenergyevents.com](http://westafrica.solarenergyevents.com)



Formerly:  
**LARGE-SCALE  
SOLAR UK**

26 - 28 April 2016 | Twickenham Stadium, UK

[summit.solarenergyevents.com](http://summit.solarenergyevents.com)

INCORPORATING:



LONDON | NEW YORK | SINGAPORE | INDIA | THAILAND

7 June 2016 | London, 1-2 November | Delhi

[financeindia.solarenergyevents.com](http://financeindia.solarenergyevents.com)

25-26 2016 October | New York

[www.solarenergyevents.com](http://www.solarenergyevents.com)



4 - 6 October 2016 | NEC, Birmingham, UK

**FREE to attend!**

[uk.solarenergyevents.com](http://uk.solarenergyevents.com)

INCORPORATING:



**BOOK NOW: [www.solarenergyevents.com](http://www.solarenergyevents.com)**

For speakers opportunities contact Jo-Anne Duff: [jduff@solarmedia.co.uk](mailto:jduff@solarmedia.co.uk)

For sponsorship opportunities contact Sylvester Gabriel: [sgabriel@solarmedia.co.uk](mailto:sgabriel@solarmedia.co.uk)

# PV capital expenditure shifts from polysilicon to cell capacity additions

Finlay Colville, Head of Market Intelligence, Solar Media Ltd.

## ABSTRACT

Capital expenditure by the solar PV industry continues to rebound from the lows of 2012, but the spending trends have now shifted from polysilicon expansions to cell capacity additions. In particular, the transition to cell capex has been driven mainly by the need for Chinese module suppliers to diversify manufacturing outside mainland China and especially to countries in Southeast Asia, coupled with the ongoing problems for polysilicon producers struggling to adapt to sales prices for goods produced.

Capital expenditure (capex) in technology sectors is notoriously cyclic in nature, reflecting the global aspirations of supply-based manufacturers to seek market-share gains when cash flow is positive and the climate for investment is attractive.

The solar PV industry certainly follows this generalisation, but the fine details of solar PV capex remain potentially more turbulent and harder to follow than complementary and adjacent technology sectors such as semiconductors and displays.

This article provides an overview of solar PV capex over the past few years, explaining the motives and outcomes arising from investments across the full value chain of the upstream manufacturing segment, spanning polysilicon production through to module assembly.

The conclusions point towards a shift in caution across the value chain towards committing capex to new expansion activities, with any new facilities governed by long build-out timelines being postponed due to uncertainty regarding the near-term evolution of the solar PV industry. This uncertainty is shown to be grounded in concerns related to end-market demand growth, raw material consumption levels, and the delicate balance between total in-house production costs and component average selling prices (ASPs).

## Understanding the drastic swings in solar PV capex

During the period 2006-2010, allocating capex to expand upstream operations was seen by almost every component producer in the solar industry as the default means of growing market share. This included standard crystalline silicon (c-Si) technologies that were proven in manufacturing and a host of competing options that had barely made it out of the research labs.

As a consequence, capex levels exploded to figures that prompted most capital equipment suppliers to urgently set up solar-specific business units. And capacity

levels, in particular across China, for c-Si p-type production grew to levels that could have met the entire global demand.

However, it was the collapse of component sales prices (from polysilicon through to modules) between 2011 and 2013 that truly ushered in austerity measures throughout the entire industry. Indeed, this forms the starting point for the analysis presented in this article, with decision-making on PV capex before 2013 being largely of academic interest only.

Figure 1 shows the first direct effect of the pricing collapse on solar PV manufacturing, where the market capitalization values of publicly listed companies hit a dramatic cliff edge. The graphic here – taken from Yahoo! Finance – shows the stock prices for three of the main c-Si manufacturers in the solar PV industry today: Canadian Solar (CSIQ), Trina Solar (TSL) & JinkoSolar (JKS).

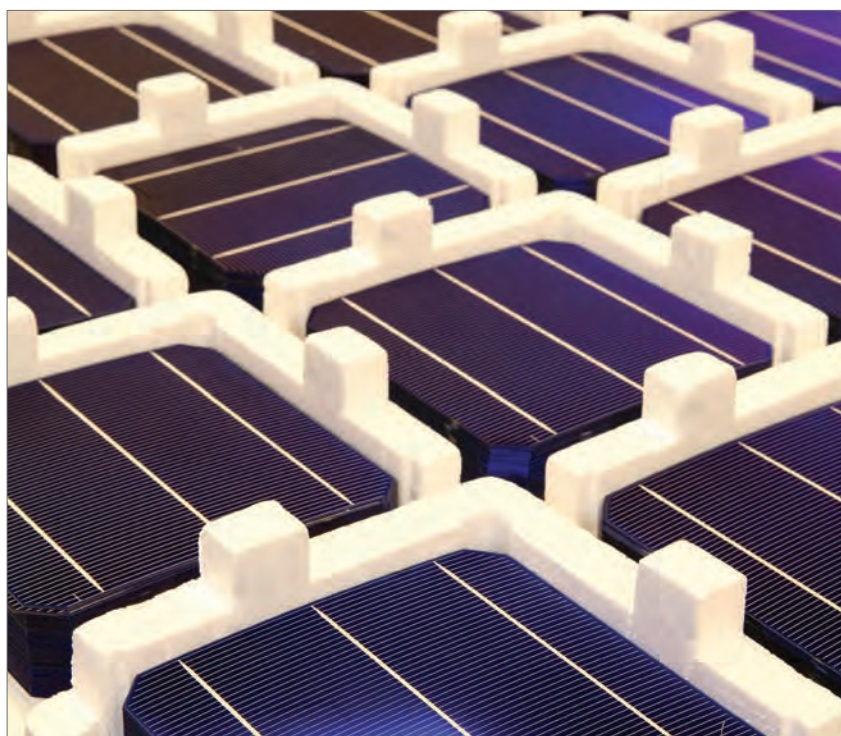
The downturn period can be seen to last

about 18 months, from Q4'11 to Q2'13. Yet, during this time, there was no slow up in end-market growth. Therefore, to remain solvent, everything turned to cash saving and cost reduction in manufacturing. Capex for upstream manufacturing was one of the first things to be removed, with most PV manufacturers operating on draconian maintenance-only capex models.

## Cost savings became the only option as cash remained elusive

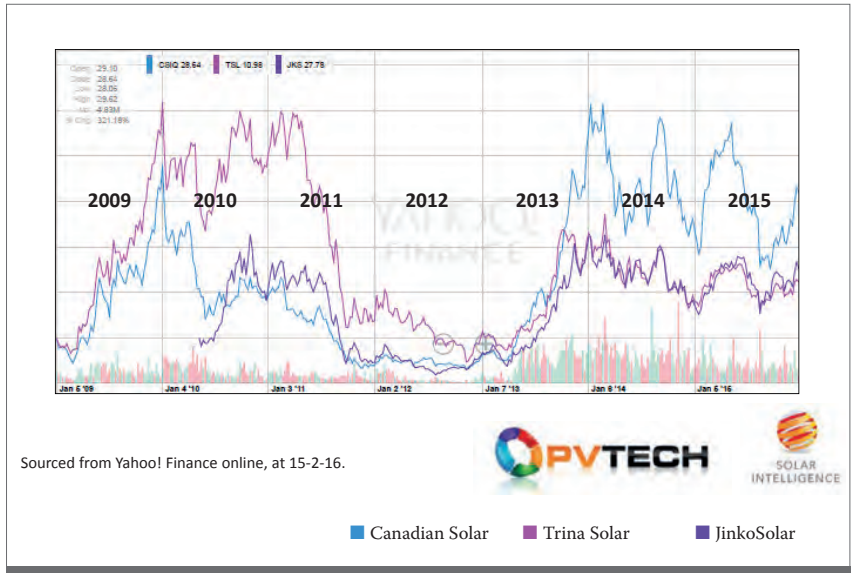
Any cash generated from ongoing operations, or from additional borrowings, was allocated to downstream projects business where return on investment remained healthy and was an option welcomed from the investor community that was attracted to vehicles that could guarantee a long-term revenue stream.

The ensuing lack of cash available for



The latest rebound in solar capex has seen investment increase in cell capacity additions.

Credit: Imnotech Solar



Sourced from Yahoo! Finance online, at 15-2-16.

Figure 1: The collapse of the market capitalization values of leading solar PV manufacturers at the end of 2011 led directly to PV capex being reduced to minimal levels across the industry during 2012 and 2013.

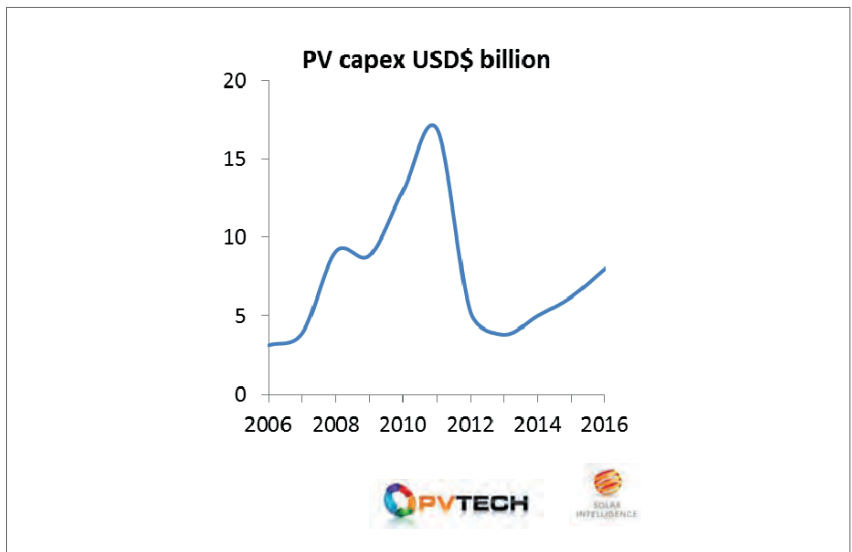


Figure 2: PV capex went through two growth peaks between 2007-2009 and 2010-2011, driving the industry into overcapacity, which in turn led to strong price declines across the whole PV value chain.

PV manufacturing also prevented any technology buy-cycle from occurring, with changes in PV production for c-Si components limited to improvements that did not require any process flow alterations to existing production lines. The only two exceptions to this rule in the industry at the time were First Solar and SunPower, each with in-house technology expertise and differentiation. These companies continued to invest heavily in R&D and capex through the downturn period to ensure that in-house production remained competitive when investments were restarted across China and other Southeast Asia manufacturing hubs.

In some ways, however, the focus on cost reduction did focus the attention on manufacturing processes, something that had largely been bypassed during the days of building new factories and installing

production lines as fast as possible. This was seen in particular at the ingot stage with casting furnaces for p-type multi block driving process optimization and wafer quality to efficiency levels that had not been considered possible for multi cells just a few years earlier.

In fact, several other changes during 2011-2013 can be grouped together as forming the basis of the PV technology roadmap at the time. These included multi-busbar forming in module production, the use of improved silver paste, higher aspect ratios for screen-printed fingers, diffusion furnace upgrades and the increased use of automation across China.

**Upturn in PV capex from 2013**

Confidence returned to the solar industry in the second half of 2013, and investments

for upstream manufacturing started to pick up again. This is shown clearly in Figure 2, derived from analysing the capex trends across a sample group of 100 leading PV manufacturers during the time period shown. The downturn phase shown here is an almost carbon copy of that in Figure 1 for the stock prices of the companies shown.

However, to many of the PV equipment suppliers that benefited during the boom phase of 2006-2011, the upturn from 2013 onwards will look very different on order books for tools. In fact, the two upturn phases should really be treated separately, as there are few similarities for PV capex.

First, a large portion of the PV capex during 2008 to 2011 is sitting mothballed today across the value chain, from polysilicon factories in China that failed to meet quality or cost targets to ambitious thin-film a-Si-based fabs that were struggling at the best time to reach double-digit percentage efficiency levels.

“To many of the PV equipment suppliers that benefited during the boom phase of 2006-2011, the upturn from 2013 onwards will look very different.”

However, in order to understand better what PV capex looks like from 2013 onwards, we need to examine spending in more detail across the value chain. The following section addresses this by examining the capex trends of the leading c-Si module suppliers to the industry today, and then looking at capex being allocated by the top-50 PV manufacturers across the whole manufacturing value chain.

**Silicon Module Super League focus on midstream capacity consolidation**

During the previous capex upturn phase, the main Chinese cell and module manufacturers had aspirations to expand across the full c-Si value-chain, with gigawatt-level capacities from polysilicon to module. What evolved mainly was expansion confined to ingot/wafering, cell and module production, leaving polysilicon to dedicated suppliers.

Indeed, capacity additions at the ingot and wafer stage were also curtailed, with GCL-Poly becoming the lead force in supplying multi c-Si wafers within China. Internal wafer supply to the main cell and module producers in China declined to below 50%, with many fully dependent on outsourcing wafers locally.

Looking at the Silicon Module Super League of 2015 – comprising Canadian Solar, JA Solar, JinkoSolar, Hanwha Q CELLS, Trina Solar and Yingli Green –

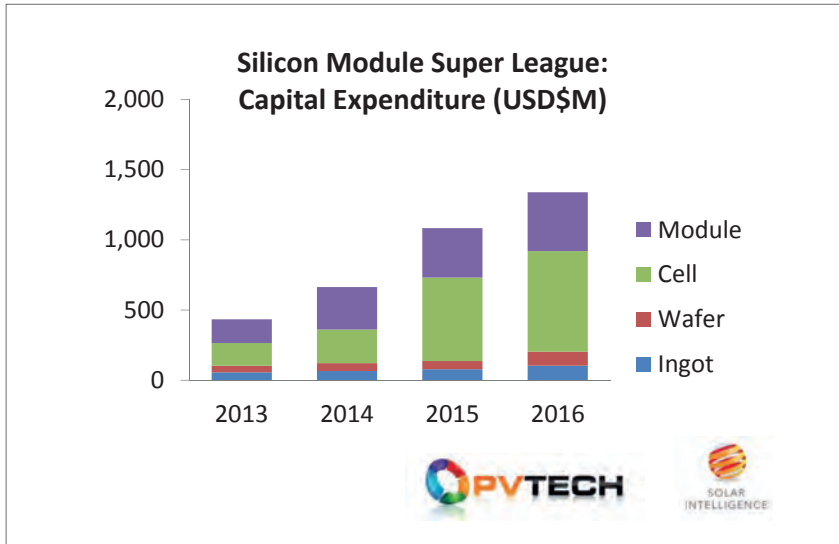


Figure 3: PV capex for the Silicon Module Super League shows the growing trend for new cell and module capacity located outside China, and the continued shift away from adding new ingot and wafer equipment.

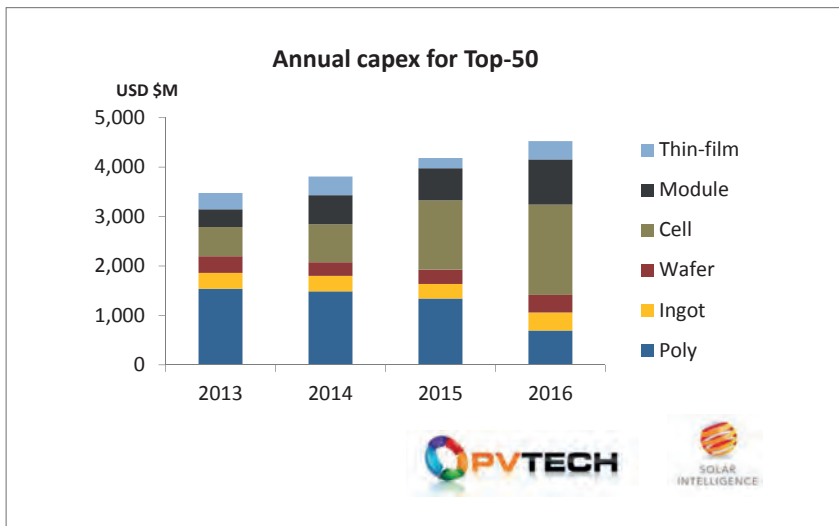


Figure 4: While PV capex rebounded in 2013 and has been growing each year since then, the contributions across the value chain have been shifting, with polysilicon investments falling and being replaced in particular by cell equipment purchases.

and extracting manufacturing capex for the period 2013-2016 reveals how the upturn in capex for these companies saw a continuation of this midstream manufacturing focus (see Figure 3).

Spending on ingot and wafering has been largely at maintenance-only levels, with limited new capacity brought online by this grouping of manufacturers. Rather, the focus has been on cell and module capacity additions, with cell capex dominating in part because of the larger \$/W capex for cell lines alongside the declining cost of new module tooling coming exclusively from Chinese module suppliers.

With the increased focus of these module suppliers on having a more diversified geographic spread of c-Si cell and module production, this trend is expected to continue. This will further act to segment out polysilicon and wafer supply to the PV industry, in the absence of any further

consolidation or acquisitions within China.

### Polysilicon capex surge halted as pricing shows no sign of rebound

A further level of detail on recent capex trends can be seen by looking at the capex of the top-50 PV manufacturers across the whole value-chain from polysilicon to modules, and including the contributions from the only two thin-film suppliers of note to the industry today (First Solar and Solar Frontier). This top-50 group of manufacturers produces in excess of 80-90% of components within the solar industry today, and the market share has been gradually increasing in the past few years.

The capex breakdown is shown in Figure 4, and shows clearly the shift from capex going into polysilicon plant build-outs to the c-Si cell stage. While the trends related to the Silicon Module Super League discussed

above are equally valid for the top-50 group, in regards to the ingot to module spending, the polysilicon capex changes from 2013 to 2016 tell an altogether different story.

Due to the multi-year build process associated with bringing new polysilicon factories online, most of the spending on polysilicon was authorised by companies as far back as 2009-2011. At this point, few had any idea about the rapid price declines that would impact on polysilicon producers, and this has been the most important factor driving the changes in polysilicon capex during 2013 to 2016.

The polysilicon capex is coming mainly from new plants being built with the prospects for some of these still at risk, as impairment charges (based on regular downward forecasts for polysilicon prices out to 2017) continue to have a crippling impact on the financial stability of the companies involved.

Other factors are driving polysilicon capex down, such as limited cash available in China to increase capacity levels to grab more market share within a US\$13-15/kg spot price environment. Furthermore, problems have arisen at several sites in starting operations with the prerequisite purity levels and quality needed ahead of mass production ramping.

### Conclusions

Capex to the solar PV industry for upstream manufacturing has gone through its prolonged downturn phase and has been growing each year since 2013. However, in contrast to the frantic spending that characterized the previous capex upturn phases from 2006 to 2011, spending in the past few years has been heavily weighted first to legacy decisions to construct new polysilicon plants, and then to cell production mostly outside China and Taiwan.

Beyond 2016, capex allocated to ingot and wafer stages will start to rebound, with polysilicon spending possibly still having to wait somewhat longer before seeing renewed investor confidence in the viability of particular polysilicon technologies or the strategies of the companies seeking to make further upstream investments in this sector.

### About the Author



**Finlay Colville** joined Solar Media as head of the new Solar Intelligence activities in June 2015, before which he was vice president and head of solar at NPD Solarbuzz until October 2014. Widely recognised as a leading authority on the solar PV industry, he has presented at almost every solar conference and event worldwide, and has authored hundreds of technical blogs and articles. He holds a Ph.D in nonlinear photonics.

ADVERTISER	WEB ADDRESS	PAGE NO.
Asys Solar	www.asys-solar.com	49
BERGER Lichttechnik GmbH & Co. KG	www.bergerlichttechnik.de	95
Centrotherm	www.centrotherm-pv.com	47
Clean Energy Live	uk.solarenergyevents.com	105
Clean Energy Summit	summit.solarenergyevents.com	41
Dow Corning Solar Solutions	dowcorning.com/solar.	3
h.a.l.m	www.halm.de	91
Heraeus Precious Metals	www.pvsilverpaste.com	67
Intersolar	www.intersolarglobal.com	13
JA Solar Holdings Co., Ltd.	www.jasolar.com	Inside Front Cover
KÖMMERLING CHEMISCHE FABRIK GMBH	www.koe-chemie.de	97
Meco Equipment Engineers B.V.	www.besi.com	65
Metallization Workshop 2016	www.metallizationworkshop.info	55
PV CellTech Conference Malaysia	celltech.solarenergyevents.com	27
PV Tech Power journal	www.pv-tech.org/power	109
RENA Technologies GmbH	www.rena.com	45
Renolit Belgium NV	www.renolit.reflexolar.com	5
ROBERT BÜRKLE GMBH	buerkle-technologies.com	101
Shanghai HIUV New Materials Co., Ltd.	www.hiuv.net	103
SNEC 2016	www.snec.org.cn	Inside Back Cover
Solar Media Events 2016	www.solarenergyevents.com	111
S'tile	www.silicontile.fr	69
Von Ardenne GmbH	www.vonardenne.biz	9
WAVELABS	www.wavelabs.de	93
Wuxi Suntech Power Co., Ltd.	www.suntech-power.com	Outside Back Cover

To advertise within Photovoltaics International, please contact the sales department: Tel +44 (0) 20 7871 0122

**NEXT ISSUE:**

- Heterojunction cell processing advances
- Process optimisation
- Half-cut solar cells

**THE INDISPENSABLE GUIDE FOR MANUFACTURERS IN SOLAR**

**Photovoltaics International** contains the latest cutting edge research and technical papers from the world's leading institutes and manufacturers.

Divided into six sections – Fab & Facilities, Materials, Cell Processing, Thin Film, PV Modules and Market Watch – it is an essential resource for engineers, senior management and investors to understand new processes, technologies and supply chain solutions to drive the industry forward.

An annual subscription to **Photovoltaics International**, which includes four editions, is available at a cost of just \$199 in print and \$159 for digital access.

Make sure you don't miss out on the ultimate source of PV knowledge which will help your business to grow!



**SUBSCRIBE TODAY.**

[WWW.PHOTOVOLTAICSINTERNATIONAL.COM/SUBSCRIPTIONS](http://WWW.PHOTOVOLTAICSINTERNATIONAL.COM/SUBSCRIPTIONS)

## Solar cell technology roadmap for 2016

New research undertaken by Solar Intelligence, part of Photovoltaics International's parent company Solar Media, can exclusively reveal the forecasted breakdown of production for the different technologies being used within the solar industry in 2016.

Using new proprietary methodology, developed over the past six months by the in-house research team at PV Tech, the findings reveal the continued push from a diverse range of cell architectures, with no sign of any significant push to consolidation across the different n-type or p-type, mono or multi, and standard or advanced cell processes being used in production today.

The main conclusion from our new research is the continuation of company strategies across different cell substrate types, with growth forecast across the board, and sustained optimism by wafer and cell suppliers to pursue in-house roadmaps and end-market supply tactics.

We have chosen to segment production data across established industry terminology that breaks out p-type mono and multi technologies into standard or advanced categories. This may appear at odds with some other long-term forecasts that are holding firm on PERC being a well-defined cell process that will be adopted widely throughout the industry.

With regards to PERC, we retain a degree of caution, as the announced capacity expansions using PERC are not translating directly into cell production yet, although the growth in p-type advanced groupings is clearly heavily weighted to adding rear-side passivation layers and using lasers for contact openings.

Caution is being applied, as the solar industry can be prone to knee-jerk reactions when forecasting technology changes for p-type manufacturing. One only has to recall the misplaced optimism over the past decade for laser-fired contacts, wrap-through variants, selective emitters and cast-mono substrate adoption; and not to mention legacy thin-film market-share projections or the dye-sensitized and organic solar cell aspirations of yesteryear. But perhaps the main reason for not applying PERC to the chosen cell technology groupings for now is that PERC is a very specific cell type, and the challenges in implementing widely into p-type multi lines are considerable.

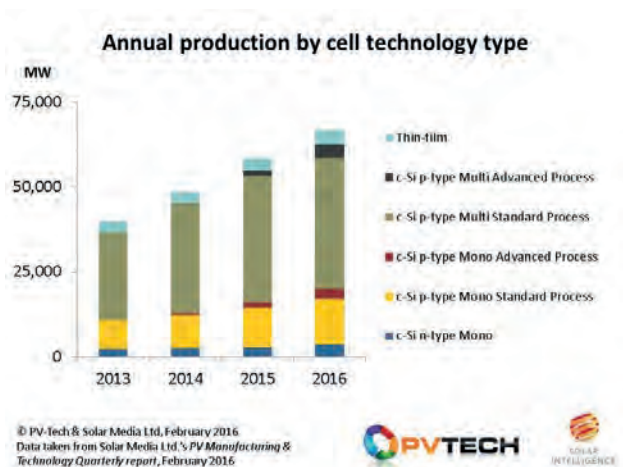
In the same way that improved front-side paste supply, multi-busbar forming and fine-line printing became the low barrier-to-entry routes to front-side cell improvements in the past few years, applying a passivation layer to the rear side of solar cells should probably be taken in isolation as one of several steps that could be used to enhance productivity going forward.

Therefore, assuming a mass migration to a PERC-specific architecture does seem somewhat simplistic, and acts somewhat as a smokescreen to other cell process improvements that may be undertaken in parallel or as additive changes.

As a consequence, we prefer to follow advanced cell process flows as a separate category for now, within which the PERC upgrades are included, or indeed any non-standard process flows within which adding rear passivation layers is one of the new process steps.

The results of our new research are shown in the figure, where we have taken historic activity back to 2013 to show the trends observed during the past few years.

The overall split in production output across p-type mono and multi categories is not expected to see any huge change in



2016, compared to 2015. This comes in spite of the ambitious mono ingot and wafer expansion announcements of the past six months, many of which are yet to show signs of coming to fruition.

It is interesting to note here that statements on the solar industry seeing rapid growth in p-type mono, compared to p-type multi, are coming mainly (and perhaps not surprisingly) from the supply side (ingot and mono producers) and not from the cell community. Furthermore, the calls for mono supply are even less visible from the segment of the solar industry that really matters here (developers and EPCs).

That said, p-type mono production (across wafer and cells) is forecast to grow in 2016, but this has to be viewed alongside the considerable expansions for p-type multi that tend to fly under the radar when it comes to company press releases.

Putting p-type aside and focusing on n-type, again there is growth year-on-year, but it will not be until 2017 before we know if SolarCity's Silevo plans can fulfil the ambitious plans to shift a legacy R&D operation into an effective GW-scale production site. Many have tried and failed in the past, and with meaningful production metrics not yet available from SolarCity, a high degree of risk still has to be assigned here.

The other company that has announced long-term n-type expansion plans is LG Electronics, but again, the output from this is not going to be visible until 2017 or whether the rooftop market can absorb the increased module supply at the continued premium ASP expectations.

Indeed, what will happen in 2017 is likely to be a key output from the forthcoming PV CellTech conference in Kuala Lumpur, Malaysia, 16-17 March 2016, where senior technologists from almost all the top-20 cell manufacturers in the industry are lined up to present on company manufacturing activities and plans.

Details on how to register for the event can be found at [celltech.solarenergyevents.com](http://celltech.solarenergyevents.com)

*This is an edited version of a blog that first appeared on [pv-tech.org](http://pv-tech.org)*

Finlay Colville is Head of Market Intelligence at Solar Media.



**SNEC 10th (2016) International Photovoltaic Power Generation Conference & Exhibition**

Gather worldwide PV industry leaders and enterprises.  
Grasp the newest trends in PV technologies and the PV industry.  
Build international co-operation and trade platforms for the PV industry.  
Attract tens of thousands of powerful buyers.

[www.snec.org.cn](http://www.snec.org.cn)

Welcome to Shanghai

**May 24-26**  
**2016**



**Shanghai New International Expo Center**  
(2345 Longyang Road, Pudong District, Shanghai, China)



**180,000m<sup>2</sup>**  
Exhibition Space

**1,800+**  
Exhibitors

**5,000+**  
Professionals

**150,000**  
Visits

Shanghai, China Tel: +86-21-64276991  
+86-21-33561099  
For exhibition: [info@snec.org.cn](mailto:info@snec.org.cn)  
For conference: [office@snec.org.cn](mailto:office@snec.org.cn)

California, USA Tel: +1-510-219-6103  
For exhibition: [Petersnec@gmail.com](mailto:Petersnec@gmail.com)



No matter where you are,  
together we **MASTER** the future.



24-26 MAY 2016  
SHANGHAI NEW INT'L EXPO CENTRE

*We sincerely invite you  
to visit our booth at Hall N1  
**#330***

**SUNTECH**  
BE UNLIMITED